R.M. Buitenhuis

Validation of CPT-based axial pile capacity design methods in signal matching analysis

TU Delft

Validation of CPT-based axial pile capacity design methods in signal matching analysis

Applicability of static design methods in dynamic soil models

By

R.M. Buitenhuis

in partial fulfilment of the requirements for the degree of

Master of Science

in Geotechnical Engineering

at the Delft University of Technology,

to be defended publicly on

Supervisor:	Prof. dr. ir. K. Gavin	TU Delft
Thesis committee:	Asst. Prof. dr. Ir. A. Tsouvalas,	TU Delft
	Ir. R. van Dorp	Allnamics BV

Abstract

Pile foundations have been utilized for centuries to support large structures in soft soils. Pile installation plays a critical role in foundation engineering, and historically, empirical formulas were employed to predict pile driving outcomes and bearing capacity. However, these formulas exhibited considerable variability in their predictions. In the 1960s, the application of stress wave theory gained popularity, accompanied by the introduction of stress wave measurement equipment and software. This theory provided a better understanding of the dynamic and static behaviour of the hammer-pile-soil system, enabling the development of reliable soil reaction models to estimate the mobilized pile capacity.

Within this context, the aim of this master's thesis is to investigate the accuracy and applicability of cone penetration test (CPT)-based axial pile capacity design methods for the static component of the mechanical system, as described by the TNO soil model. The TNO soil model aims to model the dynamic soil response during a dynamic load test after pile installation. In this mechanical system, the springs at the shaft and base represent the soil stiffness during dynamic loading, while the plastic sliders correspond to the local ultimate shaft friction and ultimate base stress, referred to as yield stresses in the TNO soil model. The objective is to verify whether design methods for static pile capacity can be applied to the static portion of the dynamic soil model through signal matching analysis.

The dynamic component, represented by a dashpot, is associated with theoretical solutions for shaft and base radiation damping. In the TNO model, damping is independent of static resistance, and viscous damping, which is part of the mobilized static friction, is neglected. The design methods utilized in this study are the unified methods for driven piles in sand and clay, which are employed to determine the local ultimate shaft friction and end bearing resistance, incorporating setup factors based on the time elapsed between the end of installation and pile testing.

The calculated local ultimate shaft friction obtained from the design methods serves as the starting point for the signal matching analysis, which is conducted after dynamic load testing to establish the mobilized pile resistance during a hammer impact. The mobilized end bearing resistance is derived through signal matching after a high quality match on the the shaft friction has been established. The obtained base stress is correlated with the ultimate base stress provided by the design methods to determine the degree of stress mobilization at the base in a dynamic load test. The ultimate base stress is typically established at a pile base displacement of 10% of the pile diameter, this amount of base displacement is often not reached after a single hammer blow.

The signal matching analysis aims to align the signals acquired from dynamic measurements (force and velocity) with a simulated signal generated by a user-dependent specific soil model that most likely represents the in-situ soil conditions based on the solution of the one-dimensional wave theory. AllWave-DLT is employed to conduct the signal matching analysis, where force and velocity measurements collected by a Pile Driving Analyzer (PDA) are utilized to derive the deep foundation forces, encompassing displacement-dependent static resistance and velocity-dependent dynamic resistance.

Overall, this thesis explores the application of CPT-based axial pile capacity design methods in the TNO soil model and at the same time the obtained radiation damping constants are correlated to geotechnical soil parameters derived from soil investigation.

List of Figures

List of Tables

Contents

1. Introduction

The determination of axial bearing capacity of driven piles in soft soils is still an issue in geotechnical engineering practice. In the past decades, several dynamic soil reaction models have been proposed by researchers to approach the problem of soil resistance during driving and static loading. In early times, estimating the pile bearing capacity was heavily based on empirical correlation and many formulas were proposed for different types of piles and soils. The first work on incorporating the stress wave theory into pile driveability was by E.A.L. Smith in the 1960's. The so-called discretized lumped mass model was the first mechanical model that was used to describe shaft and base friction in numerical wave equation programs developed by Smith. In this model, the pile was modelled as connected point masses with weightless springs and the soil friction through a series of springs with dashpots connecting the point masses. Until 1974, when friction was introduced, the solution to the partial differential stress wave equation could only be solved analytically if the soil friction was represented as an analytically function. To obtain the theoretical solutions for the wave equation in case soil friction is given as a numerical value instead of analytical form, the method of characteristics was usable and extended to analyse the stress wave propagation in piles with friction. The friction was concentrated at the interfaces of adjacent pile elements along the pile axis and the parts of the pile between these interfaces are not subjected to friction while the method of characteristics is still valid. Wave propagation within the pile is modelled exactly in which the time increment is directly proportional to the length of a pile element for an accurate solution. This development was part of the Hydroblok impact hammer and was later on the incorporated into TNOWAVE software. Several soil models based on mechanical models were proposed by researches to model soil response under dynamic loading and were implemented in wave equation application software. At the end of pile driving, different classes of test methods have been used by engineers to establish the pile capacity, through static, StatRapid and dynamic testing. The focus in this research is on dynamic load testing whereby the main objective of this testing method is to derive the mobilized static bearing capacity from the dynamic soil response after a hammer impact. Dynamic load testing includes the application of the one-dimensional wave theory in piles, pile dynamic test measurements/analyser (AllWave-PDA) and signal matching analysis software (AllWave-DLT). Signal matching analysis is performed in order to reproduce the reflected or upward travelling stress wave generated by soil friction with the measured stress wave in the field. Reproduction of the reflected signals are done by calculating the dynamic soil response of a user-defined soil model in the Wave Equation Analysis Program (WEAP) with as input into the model the measured downward travelling stress wave back-calculated from force and velocity measurements. The reflected stress waves are indirectly measured by strain sensors (force) and accelerometer (velocity) attached at the pile head. The reflected wave contains information about the soil friction that the downward travelling wave encounters while travelling downwards in the pile. The TNO soil model is used in the analysis as mechanical soil model, which consist of a linear spring with a plastic slider in combination with a radiation dashpot. The spring represent the static resistance of the soil and the dashpot the dynamic resistance to driving and together they form the total mobilized resistance that the hammer impact induces in the pile-soil system. The spring and dashpot are decoupled and the dynamic resistance is independent of the static resistance and vice-versa. The plastic slider maximizes the shaft friction and is based on values calculated from the new unified CPT-based axial pile capacity design methods for driven piles in sand and clay. In the TNO model the local ultimate shaft friction is denoted as the yield stress and limits the static resistance. Once the plastic slider is active, the pile-soil interface has exceed its elastic regime and plastic deformation occurs and the pile penetrates into the soil with permanent set. The purpose of this research is to validate the applicability of the CPT-based axial pile capacity design methods derived from static loading conditions in describing the yield stresses in the static part of the TNO soil under dynamic loading conditions. Besides the main objective related to mobilized static pile resistance, the second objective is to correlate the generated dynamic pile resistance, by means of radiation damping constants, to geotechnical site investigation data from different case studies both onshore and offshore with pile foundations related to windfarms. The onshore foundations consists of prefab concrete piles and offshore foundations are made up of large diameter monopiles.

1.2 Research questions

The main objective of this research is to validate how applicable CPT-based axial pile capacity design methods for driven piles in sand and clay are in predicting the yield stresses for the static part of the mechanical systems in the TNO soil model based on the results from signal matching analysis. The mechanical system, consisting of springs and dampers, models the total soil resistance to dynamic loading. The design methods provide estimates for local ultimate shaft friction and end bearing. An important assumptions in this research is that the maximum static resistance by means of a plastic slider strength in the static part of the mechanical system behaves similar under static and dynamic conditions. The static part, consisting of an elastic-plastic spring with a plastic slider, represent the generated static resistance to pile displacement. On top of that static resistance, dynamic resistance is proportion to pile velocity and is represented by a linear damper. The magnitude of the damping constants play a key role in the generation of dynamic forces.

Therefore the research question can be divided into the following main questions.

1. How applicable are the new Unified CPT-based axial pile capacity design methods for driven piles in sand and clay in predicting the local ultimate shaft friction and end bearing stresses compared to the derived yield stresses in the TNO soil model after signal matching analysis?

2. What is the strength of the correlations between the obtained shaft radiation damping constants in the TNO soil model based on the results from signal matching analysis with geotechnical soil parameters derived from site investigation data?

1.3 Approach to research

In order to answer the main research questions, the following method of working can be dedicated to each research question.

1. The input parameters used in the CPT-based design methods must be derived from site investigation. CPT-based correlations functions for geotechnical soil parameters are needed to calculate the local ultimate shaft friction and end bearing calculations. The focus of Chapter 4 is on the derivations of all the relevant geotechnical soil parameters. The soil layers are subdivided into sublayers based on CPT profile and each sublayer has a unique set of input parameters describing the static and dynamic part of the mechanical soil. Once the soil model parameters are quantified based on empirical correlation functions, the model parameters are refined for each individual sublayer by signal matching analysis in order to match the measured signals from a dynamic load test with the simulated stress wave signals by the user-defined TNO soil model in Allwave-DLT. After appropriate signal matching on pile head forces, displacement and velocity, the refined model parameters for each sublayer are compared with the initial calculated model parameters with the main focus is on the derived yield stresses. Quantification of the deviations between the obtained values and the theoretically calculated values is visualized in the first sections of Chapter 7.

2. Signal matching analysis built on finding the best soil model parameters that matches the dynamic soil response during an hammer impact with a simulated soil response by a user defined soil model in AllWave-DLT. The magnitude of yield stresses and radiation damping constants in the TNO soil model determines the shape of the simulated signal in terms of reflected stress wave, pile displacement and pile velocity. The matching quality on the shaft response mainly depends on the shaft yield stress and radiation damping constants, while the matching quality at the base depends mainly on the base yield stress and spring stiffness (quake value). The middle section of Chapter 7 deals with the derived radiation damping constants and pile-soil stiffness. The last section of Chapter 7 deals with the derived mobilized end-bearing and base stiffness. The radiation damping constants and pile-soil stiffness are compared with site investigation data and theoretical values based on analytically derived dynamic soil reaction models proposed by Simons and Randolph (1985) for dynamic shaft behaviour and Deeks and Randolph (1995) for dynamic pile base behaviour.

2. Pile driveability

2.1 Early empirical models

Pile driving formulas date back to the 1800's. Before computers were introduced in the field of pile driveability, empirical methods were developed to measure pile resistances during driving. The pile driving formulas were dependent on pile type and valid over certain range limits. At that time all impact hammers were actually free fall hammers with a fall height of about 1 m and the falling weight was related to the weight of the pile. The pile was regarded as a rigid body. For concrete and steel piles the weight of the block (W_{block}) was respectively calculated as follows

$$0.5\ W_{pile} < W_{block} < 1.0W_{pile} \tag{1}$$

$$0.25\ W_{pile} < W_{block} < 0.5W_{pile} \tag{2}$$

These empirical methods were mostly based on the principle that the energy that is needed to drive a pile over a certain distance is equal to the energy delivered by the impact hammer.

$$E_{hammer} = W_{block} \cdot h \cdot \mu = R_u \cdot s \tag{3}$$

The relation between static pile bearing capacity R_u, pile settlement s and driving resistance t_f was elaborated by T.K. Huizinga (1969) using several driveability formulas (Figure 1). Huizinga calculated the relation between pile bearing capacity and driving resistance expressed as pile settlement after the last hammer blow for a certain timber pile and falling weight. All the formulas were based on the simple energy concept in which the net energy transferred to the pile head should be equal to the work done by the total pile resistance on the measured pile displacement i.e. pile set.

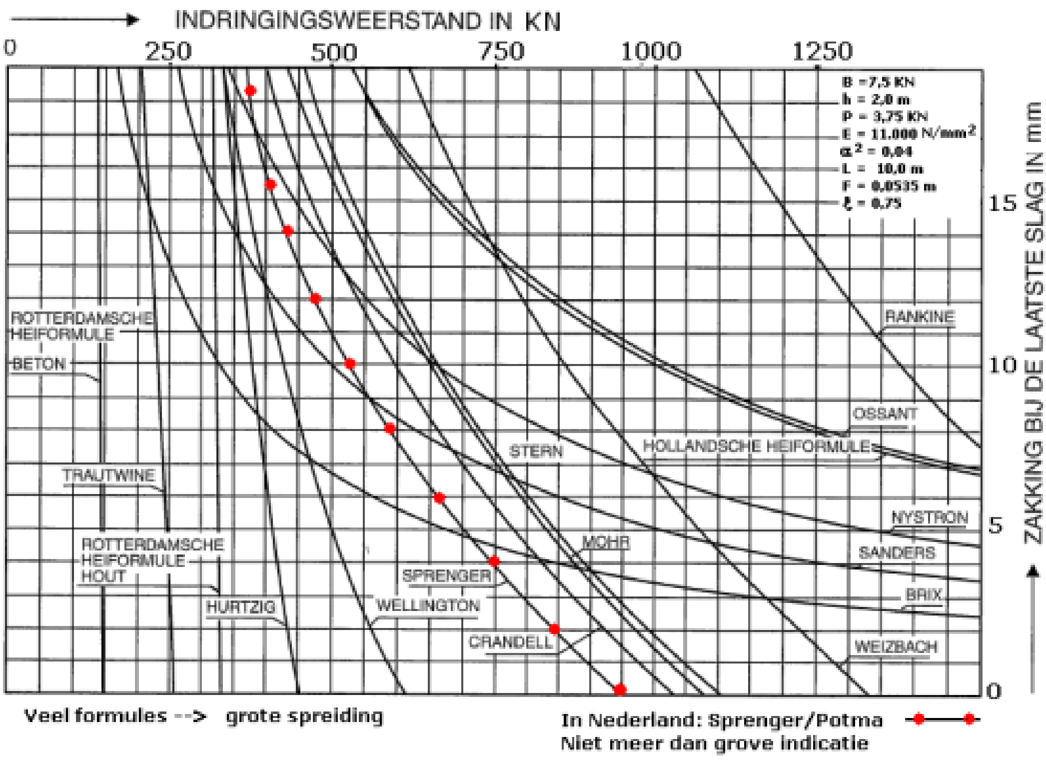

Figure 1: Calculated relation between pile bearing capacity and driving resistance as function of pile settlement at final blow *(Huizinga, 1969)*.

The results in Figure 1 show that there is a large variability in outcomes and that without calibration for a certain type of soil, hammer and pile the formulas are not that reliable.

2.2 One dimensional wave theory

The basic problem in dynamic load testing is to divide the total measured dynamic resistance in a contribution of mobilized static resistance and dynamic damping resistances. In the 1850's, the wave equation that was developed by A.J.C. Barre de Saint Venant and J.V. Boussinesq was able to indirectly assist in this problem, but the theory was based on longitudinal impact on long elastic rods, i.e. axial compressional waves (Middendorp & Verbreek, 2006). In 1931 and 1938 respectively, D.V. Isaacs suggested and the British Building Research Board demonstrated in a full scale test that the stress wave action was also applicable in pile driving and that pile driving did not follow the simple Newtonian impact that was assumed in traditional pile driving formulas (Isaacs, 1931). In 1938, E.N. Fox experimentally proved the existence of stress waves and published a simplified solution to the wave equation that was applicable to pile driving (Fox et al., 1938). No computers were available at that time so a number of assumptions had to be made. The simplifications did not give satisfactory accuracy so consequently the stress wave approach did not find widespread acceptance. In 1940 and 1941 A.E. Cummings discussed and provided a brief description of the wave theory approach of is foregoing researchers (Cummings, 1940). In the 1960's, when computers were introduced in the field engineering, it opened up new avenues for solving the complex mathematical wave equation problems. The wave equation was again proposed as being applicable to pile driving analysis by E.A.L. Smith. Smith created an algorithm that was able to make pile driving analysis suitable by solving the wave equation by numerical integration by a defining the pile and soil as a series of lumped masses. The wave theory did not involve dynamic pile driving formulas anymore, but the basis was the one-dimensional wave equation (Lowery et al., 1968). Smith adapted the wave theory of Cummings in a more realistic manner to meet actual conditions in pile driving. In the 1970's more wave equation computer programs were developed by researchers and companies to simulate the hammer impact force and the induced stress wave in piles during driving. The theoretical derivation of the one-dimensional wave equations was based on Newton's second law and Hooke's law.

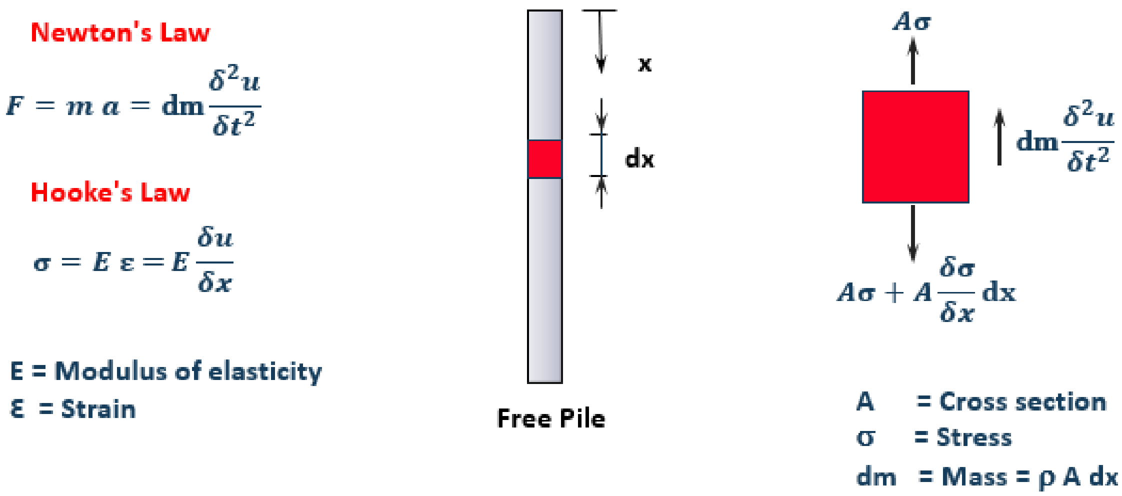

Figure 2: One-dimensional wave equation

The derivation of the wave equation can be demonstrated by drawing up the force balance of a small pile element as shown in Figure 2.

$$A\sigma + A\frac{\delta\sigma}{\delta x}dx = A\sigma + dm\frac{\delta^2 u}{\delta t^2} \tag{4}$$

In which stresses (σ), variation of stress along a pile element ($\frac{\delta\sigma}{\delta x}$) and the mass of an element (dm) can be rewritten as:

$$\sigma = E\,\varepsilon = E\frac{\delta u}{\delta x} \tag{5}$$

$$\frac{\delta\sigma}{\delta x} = E\frac{\delta^2 u}{\delta x^2} \tag{6}$$

$$dm = \rho A dx \tag{7}$$

Substitution of equation 5, 6 and 7 into equation 4 gives

$$EA\frac{\delta^2 u}{\delta x^2}dx = \rho A\frac{\delta^2 u}{\delta t^2}dx \tag{8}$$

The stress wave velocity (c) can be derived from the elasticity and density of a pile element.

$$c^2 = \frac{E}{\rho} \tag{9}$$

Substitution of equation 9 into equation 8 gives the general differential form of the one-dimensional wave equation without friction.

$$\frac{d^2u}{dx^2} - c^2\frac{d^2t}{dt^2} = 0 \tag{10}$$

The first driveability studies were made by using the solution of the one-dimensional stress wave theory, a second order partial differential equation, to predict impact stresses in a pile during driving and to estimate static and dynamic soil resistance on a pile. Due to embedment of the pile, the soil surrounding the pile generates resistance R due to pile motion during passage of the stress wave, in which the wave equation can be extended with a friction term.

$$\frac{d^2u}{dx^2} - c^2\frac{d^2t}{dt^2} + R = 0 \tag{11}$$

Solving this differential equations analytically is only possible when friction R depends on x, t and u. For the purpose of analysing the pile behaviour during an hammer impact, solving the differential equation analytically is not that usable in complex situations. The main problem is that the generated push of the ram is not defined beforehand and depends on the interaction between ram, hammer setup, dimensions and properties (i.e. cushion, helmet and striker plate), pile dimensions and friction. Another problem is that the boundary conditions at the pile base can't be defined analytically (Voites van Hamme, 1981). The most important boundary conditions at the pile base can be formulated as follows

"as long as the downward travelling stress wave is greater or equal to half of the base resistance, the magnitude of the generated upward travelling stress wave is the difference between the base resistance and downward travelling stress wave. If the downward travelling stress wave is smaller than half of the base resistance, an upward travelling stress is generated according to a fixed- or free-end condition if the downward travelling stress wave is respectively a compressive or tensional wave"

To solve the wave equation numerically and to find a solution to incorporate soil friction, the method of characteristics was applied to solve the stress wave propagation in piles. From experience, the method of characteristics proved to be a powerful method to solve the force interactions at different pile levels due to stress wave propagation when a pile is subjected to a dynamic load.

2.3 Method of Characteristics

The soil resistance during pile driving is modelled with a mechanical system consisting of static part and a dynamic part. The behaviour of the static part depends on pile-soil stiffness and yield stress and is represented by springs and plastic sliders. The dynamic part consist of dashpots with a damping constant and the dynamic force is a function of pile velocity. The dashpots can representing viscous, hysteretic and radiation damping. In the TNO model only radiation damping is considered and viscous damping is only considered at the pile base in the form of an exponent alpha to the pile velocity. The TNO soil model consists of linear springs whereby hysteric damping is neglected and thus soil nonlinearity due to gradual shear modulus reduction is not considered in the formulation. In Chapter 6.5 the formulation of the TNO model is discussed in more detail.

As mentioned before, the first wave equation software program was made by American engineer E.A.L Smith in the 1960's. Smith developed a mathematical model in which the effect of one hammer impact is calculated throughout the pile in very small timesteps. The idealized pile system by Smith is composed of a ram, cap block, pile cap, cushion block, pile and supporting soil (Smith, 1960). The pile is built up of a series of point masses and springs, in which the point masses are used to calculate the displacements and accelerations and the springs are used to calculate the forces inside the pile. In this approach the pile and soil are regarded as a lumped mass model. In this model the soil resistances are coupled to the point masses and the static and dynamic soil behaviour is simulated by elastic-plastic springs and dashpots, respectively. Smith used numerical integration to approach the wave equation, because no theoretical solution was possible due to the fact that soil friction was velocity and displacement dependent.

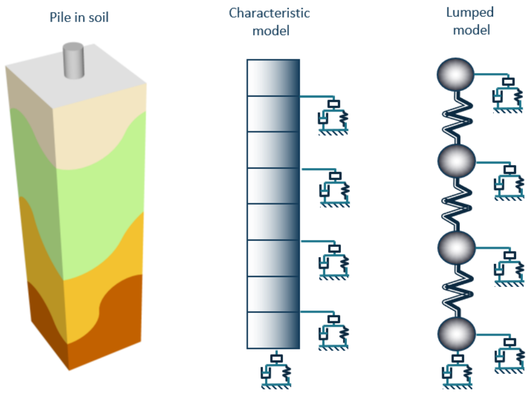

Figure 3: Pile-soil modelling: continuous (left) and lumped mass (right)

A comparable computer program was developed in the early 1970's to overcome instabilities in the lumped mass model and to generate a theoretical solution for the wave equation. This approach made use of the already existing theoretical solution for the one-dimensional wave equation, found by a French mathematician A.J.C. Barre de Saint Venant in the 1860's. The solution from Saint Venant resulted in two quasi-linear differential equation, the so-called Method of Characteristics. The theoretical solution produces a downward travelling wave and an upward travelling stress wave. The total displacement is a superposition of two mathematical disturbances in position and time.

$$u(x,t) = f^{\downarrow}(x-ct) + f^{\uparrow}(x+ct) \tag{12}$$

In which the total displacement at a specific pile level and time is a combination or superposition of two mathematic disturbances $f^{\downarrow}$ and $f^{\uparrow}$ related to the upward and downward travelling stress waves. In case of no soil friction, the value for $f^{\downarrow}$ in the solution does not change over time and position where $x - ct = \text{constant}$, the so called positive characteristic line. For example, $f^{\downarrow}$ can be considered as an undamped wave that travels along the $x - ct = \text{constant}$ line. Similarly $f^{\uparrow}$ can be considered as the undamped stress wave that travels along the negative characteristic line $x + ct = \text{constant}$. Figure 4 shows the propagation of the undamped stress wave along the positive characteristic line. The PDE of the wave equation is rewritten in equation 13. Verifying that $u = f(x + ct)$ is a solution for the PDE is given in the derivation scheme below and is confirmed in equation 17. The same holds for $u = f(x - ct)$

$$u_{tt} = c^2 u_{xx} \tag{13}$$

$$u(x,t) = f(x + ct) \tag{14}$$

$$f_{tt} = c^2 f''(x + ct) = u_{tt} \tag{15}$$

$$f_{xx} = f''(x + ct) = u_{xx} \tag{16}$$

$$c^2 f''(x + ct) = c^2 f''(x + ct) \tag{17}$$

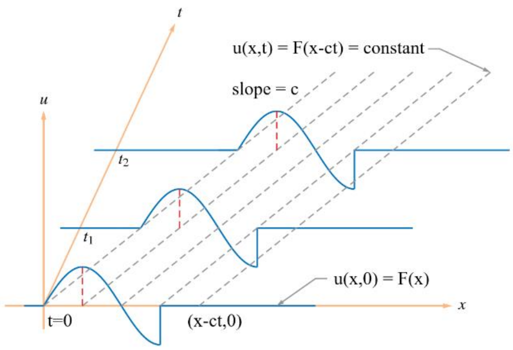

Figure 4: Visualization of positive characteristic line

Imagine an hammer impact on a pile head at time zero giving a disturbance with the shape of $u = f(x, o)$. At first instance, when no friction acts on the pile, only the downward travelling wave has a value (Figure 5) and maintains that initial shape and the solution to the PDE is only $u = f(x - ct)$.

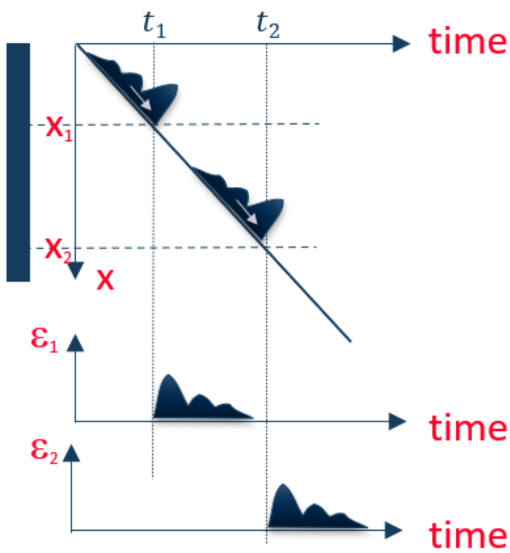

Figure 5: Initial disturbance travelling down the pile with no friction

Once soil friction acts on the pile and time passes ($t > 0$), waves are reflected at different pile levels and reduced in amplitude of the disturbance and the other solution $u = f(x + ct)$ becomes nonzero and both $f(x - ct)$ and $f(x + ct)$ are solutions for the wave equation (Figure 6).

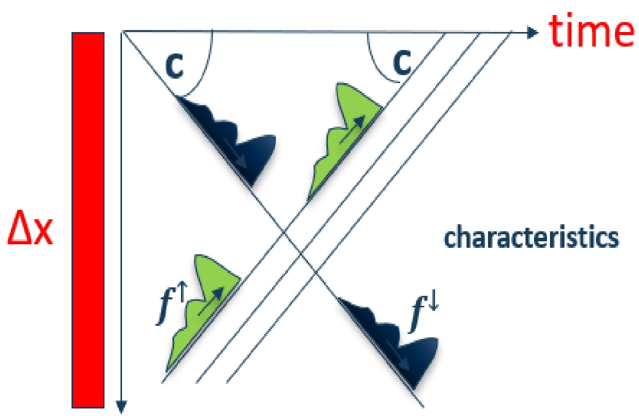

Figure 6: Zooming in on one pile element in which the total disturbance or displacement is made up of two functions

2.3.1 Main variables

The first main variable for setting up the solution for the one-dimensional wave equations is force and can be calculated at a pile level using Hooke's Law.

$$F = -EA\varepsilon = -EA\frac{du}{dx} \tag{18}$$

The solution to the wave equation (6) can be differentiated with respect to x to obtain strains $(\frac{du}{dx})$.

$$F = -EA\frac{df^{\downarrow}}{d(x-ct)} - EA\frac{df^{\uparrow}}{d(x+ct)} \tag{19}$$

Adding the downward and upward travelling stress wave together, the force at a certain level in the pile and at a certain moment in time $F(x,t)$ becomes

$$F = F^{\downarrow} + F^{\uparrow} \tag{20}$$

The second main variable is pile velocity and can be obtained by differentiating the solution of the wave equation with respect to time $(\frac{du}{dt})$

$$v = -c\frac{df^{\downarrow}}{d(x-ct)} + c\frac{df^{\uparrow}}{d(x+ct)} \tag{21}$$

The first part is the downward travelling velocity wave. The second part is the upward travelling velocity wave. Adding them together gives the pile velocity at a certain level in the pile and at a certain moment in time $v(x,t)$

$$v = v^{\downarrow} + v^{\uparrow} \tag{22}$$

The downward and upward travelling stress wave can also be written in terms of the corresponding downward and upward travelling velocity wave. Combining (19), (20) and (21) gives

$$F^{\downarrow} = \frac{EA}{c}v^{\downarrow} = Zv^{\downarrow} \tag{23}$$

$$F^{\uparrow} = \frac{EA}{c}v^{\uparrow} = -Zv^{\uparrow} \tag{24}$$

In which Z is the impedance of the pile and is related to the physical properties of the pile in terms of pile cross section area, elasticity and stress wave speed. Typical values for stress wave speed are 5100 m/s for steel and 3300 to 4100 m/s for concrete.

In a dynamic load test (DLT), the total force (F) and total pile velocity (v) are measured as function of time at the pile head by means of a strain sensor and accelerometer. By rewriting the equations (23) and (24) the measured total stress wave and pile velocity can be distinguished in a contribution from the upward and downward travelling stress wave. The upward travelling stress wave is relevant in signal matching analysis because it contains information about the wave reflection generated by soil friction.

$$F^{\downarrow}(t) = \frac{F(t) + Zv(t)}{2} \quad (25)$$

$$F^{\uparrow}(t) = \frac{F(t) - Zv(t)}{2} \quad (26)$$

2.3.2 Pile-soil friction

In pile driving prediction (PDP) the force (F_0) and velocity (v_0) are defined by the hammer specifications (rated impact energy) and on the basis of these initial boundary conditions at the pile head, the stress waves are simulated throughout the pile given a specific soil model acting along the shaft and base. Once there is soil friction along the pile, the partial differential equation in (11) must be expanded by a resistance term. The magnitude of soil resistance depends on the pile displacement and velocity. A method to implement friction is proposed by Voitus van Hamme (1981). In this method the continuous soil friction is discretised and only acts at the interface of two pile elements as shown in Figure 7. Between two interfaces the soil resistance is zero. At the interface between two elements the influence of soil resistance on the propagating stress wave can be calculated by using the equilibrium conditions and continuity conditions at the element interfaces.

$$F = F_1^{\downarrow} + F_1^{\uparrow} = F_2^{\downarrow} + W \quad (27)$$

$$v = v_1^{\downarrow} + v_1^{\uparrow} = v_2^{\downarrow} + v_2^{\uparrow} \quad (28)$$

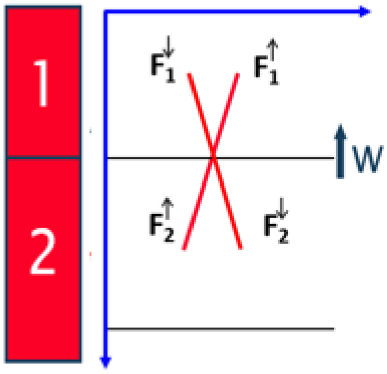

Figure 7: Stress wave interaction with local shaft friction

Assuming that $F_1^{\downarrow}$ (incident downward travelling stress wave) and $F_2^{\uparrow}$ (incident upward travelling stress wave) are known, solving both equations for reflected stress wave $F_1^{\uparrow}$ and transmitted downward stress wave $F_2^{\downarrow}$ gives

$$F_1^{\uparrow} = F_2^{\uparrow} + 0.5W \quad (29)$$

$$F_2^{\downarrow} = F_1^{\downarrow} - 0.5W \quad (30)$$

It can be observed that for the downward transmitted stress wave ($F_2^{\downarrow}$), the incident downward travelling stress wave ($F_1^{\downarrow}$) is reduced by half of the soil friction (W). For the reflected stress wave ($F_1^{\uparrow}$), the incident upward travelling stress wave ($F_2^{\uparrow}$) is increased by half of the soil friction (W). After calculation of the reflected and transmitted stress wave at interface i at time t, the same procedure applies for the subsequent pile elements in which the reflected stress wave from element i becomes the incident upward travelling stress wave for element $i-1$ and the transmitted stress wave becomes the incident downward travelling stress wave for element $i+1$ at time $t+1$. In practice, large offshore piles have changing wall thickness due to economical and structural reasons. A change in wall thickness and thus pile cross sectional area results in changes in the pile impedance and affects the reflected and transmitted stress waves in additional to friction at the element interfaces.

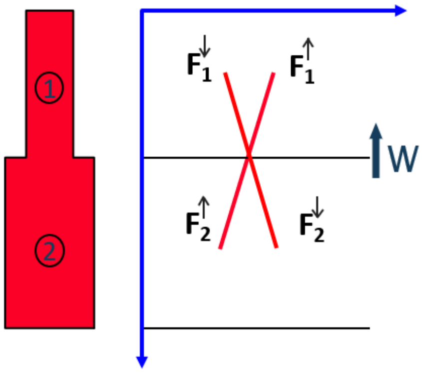

Figure 8: Stress wave interaction with local shaft friction and pile discontinuities

Using force equilibrium and continuity conditions, the reflected and transmitted stress wave for both pile discontinuity and friction can be calculated with the following algorithm.

$$F_{n,i}^{\uparrow} = -F_{n-1,i-1}^{\downarrow}\left(\frac{Z_n - Z_{n+1}}{Z_n + Z_{n+1}}\right) + \left(2F_{n+1,i-1}^{\uparrow} + W_{n,i}\right)\left(\frac{Z_n}{Z_n + Z_{n+1}}\right) \tag{31}$$

$$F_{n,i}^{\downarrow} = F_{n+1,i-1}^{\uparrow}\left(\frac{Z_n - Z_{n+1}}{Z_n + Z_{n+1}}\right) + \left(2F_{n-1,i-1}^{\downarrow} - W_{n,i}\right)\left(\frac{Z_{n+1}}{Z_n + Z_{n+1}}\right) \tag{32}$$

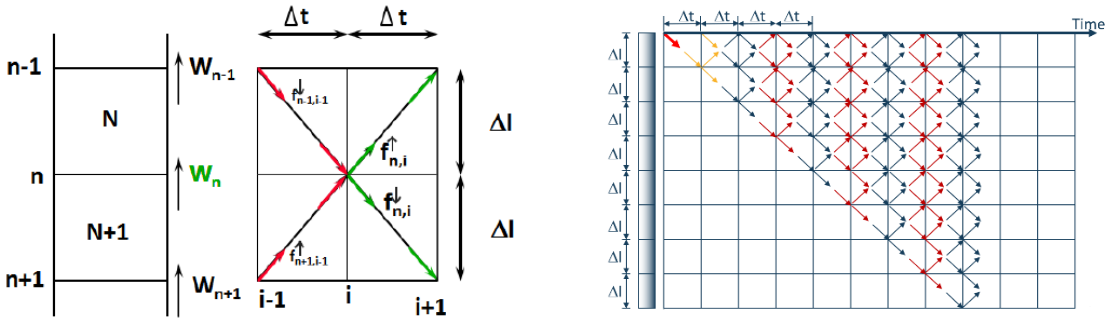

Figure 9: Discretization of the stress wave propagation in pile level and time

From the calculated downward and upward travelling stress wave, the corresponding downward and upward travelling velocity wave can be calculated by

$$v_{n,i}^{\downarrow} = \frac{F_{n-1,i-1}^{\downarrow}}{Z_n} \tag{33}$$

$$v_{n,i}^{\uparrow} = -\frac{F_{n+1,i-1}^{\uparrow}}{Z_{n+1}} \tag{34}$$

For driven piles, a complex interaction exists between the pile and the soil. First, the problem is three dimensional (or two dimensional if axial symmetry is used). Secondly, soil is a complicated material, with cohesion, friction, damping, elasticity, water pressures and complex stress state. In most dynamic soil reaction models, the pile-soil interaction is modelled by springs and dashpots, and if plugging occurs an additional mass is added to the mechanical system to account for inertia effects. The general formula for calculating the friction force $W(u, v)$ at a specific pile level and time in equation (31) and (32) at pile-soil interface is given by combining the static and dynamic resistance

$$W_{n,i} = K\int\left(v_{n,i}^{\downarrow} + v_{n,i}^{\uparrow}\right)dt + C\left(v_{n,i}^{\downarrow} + v_{n,i}^{\uparrow}\right)^{\alpha} \tag{35}$$

The scope of this thesis is to dive into the TNO soil model to find the best model parameters that matches with measured signal and thus resistances at different pile-soil elements in time and space ($W_{n,i}$).

2.3.3 Reflections at the pile base

As mentioned before, the upward travelling stress wave contains information about the mobilized soil resistance along the pile shaft and at the pile base. The soil conditions at the pile base have a major effect on the sign and magnitude of the upward travelling stress wave measured at the pile head. Three pile base conditions can be distinguished; free-end, fixed-end and base resistance.

2.3.3.1 Free-end condition

A pile with a free-end conditions reflects the stress wave with an opposite sign and the total fore at the pile base is zero ($F = F^{\uparrow} + F^{\downarrow} = 0$). The pile velocity becomes twice the magnitude as the downward travelling stress wave (F_{max}). In a free-end conditions the measured upward travelling stress wave at sensor level shows a large negative force due to a tensional wave.

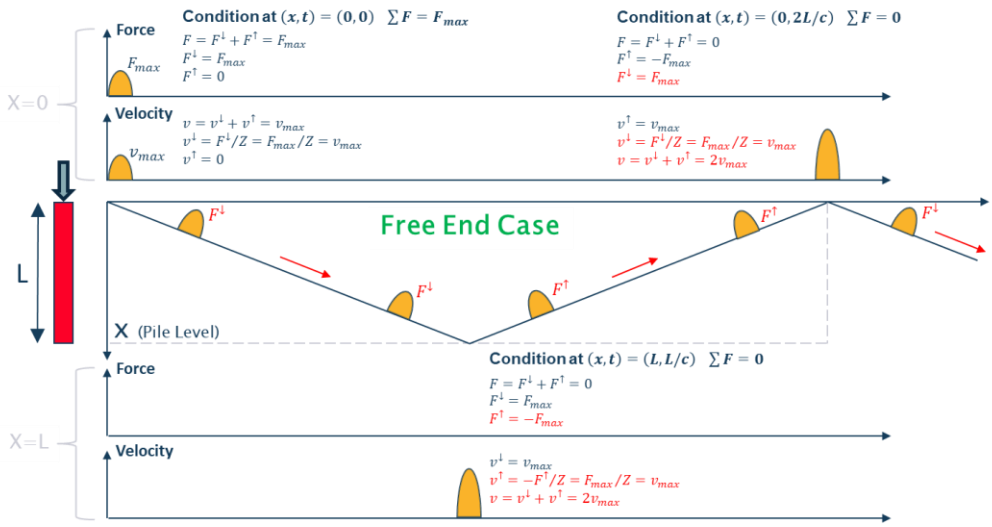

Figure 10: Free-end condition

2.3.3.2 Fixed-end condition

A fixed-end conditions reflects the downward travelling or incoming stress wave (F_{max}) with equal sign and a compressive wave is reflected. The pile base is not able to move and the pile velocity is zero. The reflected compressional stress wave at the pile top might damage pile head and equipment.

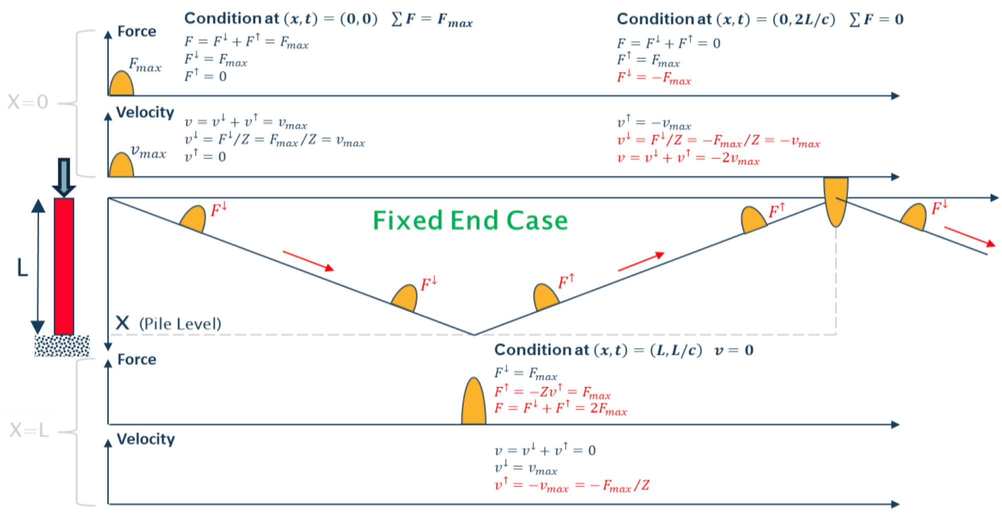

Figure 11: Fixed-end condition

2.3.3.4 Pile base resistance

For a pile with base resistance, it is assumed that the pile base can mobilized a maximum resistance of F_g. In case the downward travelling stress wave $F^{\downarrow}$ arrives at the pile base (F_{max}), an upward travelling stress wave must be generated, $F^{\uparrow}$, such that $F^{\uparrow} + F^{\downarrow} = F_g$ (Newtons third law: action-reaction). As long as $v \geq 0$ at the pile base ($F^{\downarrow} \geq 0.5F_g$), the characteristics of the stress waves are valid as shown in Figure 12. If $F^{\downarrow} < 0.5F_g$, the pile velocity at the base is negative and the pile should move up. This is restricted and in this case the pile base will not move. As long as $F^{\downarrow} < 0.5F_g$ is positive (compressional stress wave from hammer impact) the pile will not move and the pile base velocity should become zero, such that $F^{\uparrow} = F^{\downarrow}$. The total force balance at the pile base becomes $F = F^{\downarrow} + F^{\uparrow} = 2F^{\downarrow} < F_g$. The base reaction is then equal to twice the downward traveling stress wave. In case $F^{\downarrow}$ is negative (tensional stress wave), the pile base displaces such that $F^{\uparrow} = -F^{\downarrow}$ and the pile base velocity becomes $\frac{2F^{\downarrow}}{Z}$, which is positive what means that the pile base moves upwards and bounce back from the base.

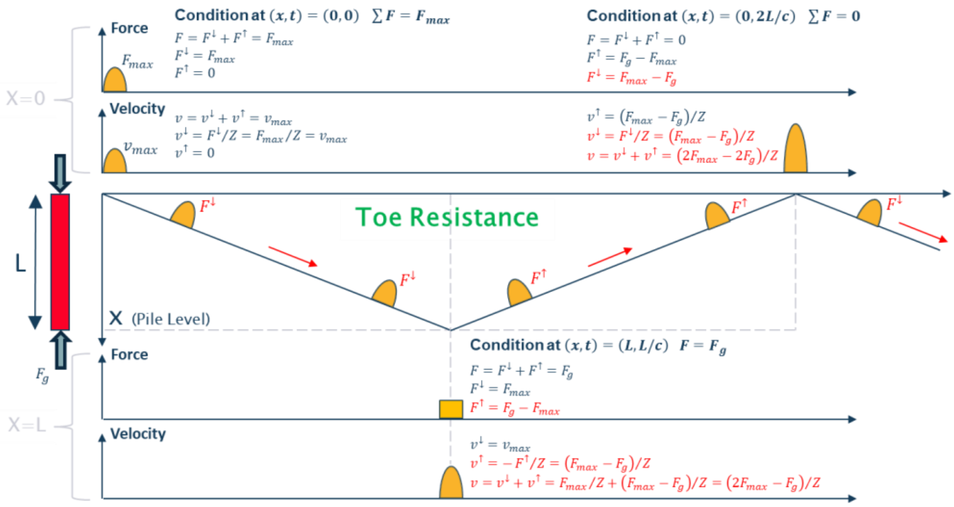

Figure 12: Intermediate pile base resistance

2.4 Wave Equation Analysis Programs (WEAP)

Starting in the 1930's, several scientist used a graphical approach of the method of characteristics in early pile driving analysis. The original method of characteristics was applicable to a rod with no interaction with shaft friction and base resistance. In 1956, the Dutch scientist G. de Josseling de Jong proposed a model to incorporate base resistance into the method of characteristics and in 1974 the Dutch company HBG (Hollandse Beton Groep) extended the method of characteristics by also incorporating the theoretical solution for piles with shaft friction. The approach by HBG enables to generate a valid theoretical solution when friction was concentrated at element interfaces of the pile. The parts of the pile in between two interfaces are not subjected to friction (Middendorp & Verbeek, 2006). The HBG computer program PILEWAVE was released a few years before the WEAP program was released in the USA and TNOWAVE was released in The Netherlands. Late 1970's the Dutch Organization of Applies Scientific Research (TNO), HBG and Heerema intensified the research in stress wave application to piles because of increasing pile driving activities in the North Sea oil fields. After the PILEWAVE release, TNO developed its own wave equation software program based on the method of characteristics in 1978. The TNOWAVE software program was extended to perform signal matching techniques, similar to CAPWAP. In the 1980's TNO extended the TNOWAVE with vibratory pile driving predictions, VDPWAVE in 1988 and later on with pile integrity tests in SITWAVE. VDPWAVE proved that not only relative short piles could be installed with vibro-hammers, but also long offshore piles.

Stress wave software programs are versatile and widely applicable in the field of pile testing and driveability studies, but the weakest link, soil modelling, can never be overlooked.

3. Soil resistance to driving

3.1 Mechanical soil model

The soil resistance during driving is made up of shaft resistance and base resistance. The total soil resistance during driving (R_{tot}) is divided into a static part (R_{stat}) and a dynamic part (R_{dyn}) and is defined as

$$R_{tot} = R_{stat} + R_{dyn} \quad (36)$$

In case of plugging of an open ended pile, the mass of the soil plug causes an additional inertia force that increases the total soil resistance by

$$R_{inertia} = m_{plug} \cdot a_p \quad (37)$$

The inertia force is calculated by using the mass of the soil plug and the acceleration of the pile. During pile driving and during dynamic load testing, plugging is not likely and for large offshore monopiles the inertia force is neglected and the soil reaction model is simplified to a spring and dashpot system without a mass. The setup of the first and simplest mechanical soil reaction model to pile driving is visualized in Figure 13 which has similarities with the TNO soil model.

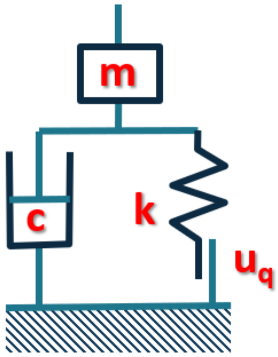

Figure 13: Visualisation of the static resistance (spring and plastic slider) and dynamic resistance (dashpot)

During pile driving, the ram of the hammer impacts the pile head and induces stress waves which travels throughout the pile and interacts with the soil around the pile shaft and base. The soil around the pile can store the energy by elastic deformation and absorb the energy by plastic deformation and hysteretic damping due to nonlinear soil behaviour from small to large shear strains. Part of the driving energy is radiated outwards into the surrounding soil in the form of waves and vibrations which carry away energy from the pile-soil system, contributing to energy dissipation. This specific mechanism is referred to as radiation damping and it's the form of damping that is present in the TNO soil model. Plasticity occurs at the highly deformed zone adjacent to the pile shaft and base. During pile driving, the pile penetrates into the soil and induces shear stresses along the pile shaft. In static load tests the maximum or ultimate shaft resistance is reached within relative small pile shaft displacement of about 10 mm for a driven soil displacement pile (Figure 14). The ultimate base resistance is fully mobilized at a pile base displacement of about 10% of the equivalent pile diameter.

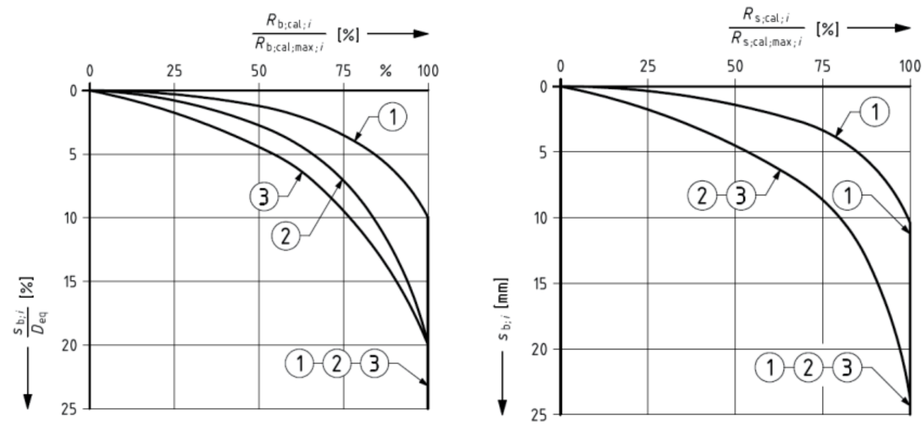

Figure 14: Displacement of the pile head due to force on the pile base (left) and shear force on the pile shaft (right) in % of the maximum force for ground displacement piles (1), auger piles and piles with little soil disturbance (2) and bored piles (3) (NEN 9997-1, 2012)

In AllWave-DLT software the maximum achievable static shaft friction is denoted as the shaft yield stress. The pile shaft displacement to reach the maximum shaft friction during dynamic loading is even smaller compared to static loading. Pile shaft displacement of less than 1% (~2.5 mm) of the equivalent pile diameter is usually needed to fully mobilise the ultimate shaft friction and up to 2% (>2.5 mm) for pile base displacement to reach maximum pile base resistance, because of short stress wave lengths occurring at the pile-soil interface (Loukidis et al., 2008). A thin shear band is formed around the pile shaft during pile driving when the maximum shaft resistance is reached. The thickness of the shear band depends on the mean particle diameter of the soil and the roughness of the pile material. In a couple of soil reaction models, the shear band is represented mechanically by springs with a plastic slider in combination with a viscous dashpot. The soil outside the thin shear band, so-called near field undergoes vertical cyclic shearing. The magnitude of the cyclic shear stress and angular distortion of the soil reduces in radial distance from the pile axis and can be expressed in hyperbolic form in the more advanced nonlinear soil models including hysteric damping. In some soil reaction models the near field is mostly represented by a linear or nonlinear spring. The remaining driving energy is dissipated into the far field, represented with a dashpot. Depending on the complexity of the soil models, all the types of damping could be defined by individual dashpots or included into one lumped dashpot (Chapter 5) which combines viscous and radiation damping or only radiation damping.

The static part of the soil resistance is built-up according to an elastoplastic soil model, in which the soil is regarded as a spring. The simplest soil model is the linear elastic perfectly plastic soil model (Figure 15). The linear elastic part is limited by the quake value ($\mathrm{u_q}$) and the maximum shear stress that can appear between pile and soil is the yield stress (F_y). With the yield stress and pile dimension the maximum static resistance ($\mathrm{R_{stat}}$) can be obtained. A plastic slider in series with the spring represents the yield stress and limits the generated shear stress during static loading. Once the plastic slider is active, plasticity causes slippages and relative displacement between pile and soil. The quake value determines the pile displacement (u) to which the soil behavior remains elastic and what the maximum mobilizable soil resistance can become at the end of that elastic limit once plasticity starts. As long as the pile displacement does not exceed the quake value, the pile will not penetrate the soil and rebounds to its original position.

$$R_{stat} = K \cdot u \tag{38}$$

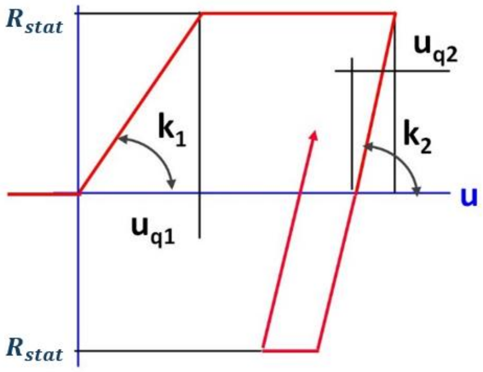

Figure 15: Linear elastic perfectly plastic soil model

After reaching the yield stress and exceeding the quake value the soil behaves perfectly plastic. The static soil resistance remains constant over increasing pile displacement while dynamic forces can still generate a higher total resistance due to velocity dependent damping. In the unloading phase the soil can have a different quake value and unloading stiffness than in the loading phase. When driving continues and the number of blows increases over time for a specific soil horizon, the yield stress decreased due to friction fatigue which is incorporated in the CPT-based axial pile capacity design methods and implemented in the TNO soil model for the situation end-of-driving (EOID) when the dynamic load test is performed. The dynamic part of the soil resistance (R_{dyn}) depends on the damping characteristics of the soil. Several methods have been developed to describe the generated damping forces as function of pile velocity. There are two ways in which the damping is modelled in the soil models. An empirical global damping factor (J) in which the dynamic resistance is linked to the static resistance and an analytical derived damping constant (C) based on mechanical soil properties (stiffness) and independent on mobilized static resistance. In stiffer soils, stress waves tend to travel faster, and less energy is absorbed by the soil, resulting in lower radiation damping. In contrast, in softer soils, stress waves travel more slowly, and more energy is absorbed, leading to higher radiation damping.An exponent (α) can be added to the velocity to make the damping force nonlinear.

$$R_{dyn} = J \cdot R_{stat} \cdot v \text{ or } J \cdot R_{stat} \cdot v^{\alpha} \tag{39}$$

$$R_{dyn} = C \cdot v \text{ or } C \cdot v^{\alpha} \tag{40}$$

Figure 16: Soil damping models with linear (left) and exponential (right) relation to pile velocity

Simons and Randolph (1985), stated that the spring component of static soil resistance contributes typically only 20 - 40 % of the total resistance during the passage of a stress wave and the remaining resistance can be attributed to dynamic resistances. In the Smith model (1960), the damping resistance is also a function of the static soil resistance. An empirical damping parameter, J, is multiplied to the yield stress used in the Smith model to define a sort of lumped damping resistance (equation 34). In the analytical soil models a damping constant C is used at which the damping constant is derived from geotechnical soil parameters describing theoretical solutions (equation 29). An exponent α determines if the dynamic resistance is linear or exponential with pile velocity. The pile velocity in exponential form was introduced in soils models because it was observed that soil in rapid motion generated more resistance than in slow motion (Coyle & Gibson, 1970). In the years after the publication of Smith's method, more research was done to improve the velocity dependent damping model. Smith model parameters are essentially empirical and not based on conventional soil characteristics that could be measured in the laboratory or evaluated theoretically. Scattered values for quake and damping constants were reported and by calibration with dynamic field tests various values were proposed for different soil types with large variability. All the energy lost in Smith's model is included in a lumped viscous dashpot and neglects hysteric and radiation damping. In the analytical soil models the shaft model is essentially based on theoretical studies by Novak et al. (1978) and later improved by Deeks and Randolph (1995). The first analytic base model was proposed Lysmer and Richart (1966) and later on improved by Deeks and Randolph (1995).

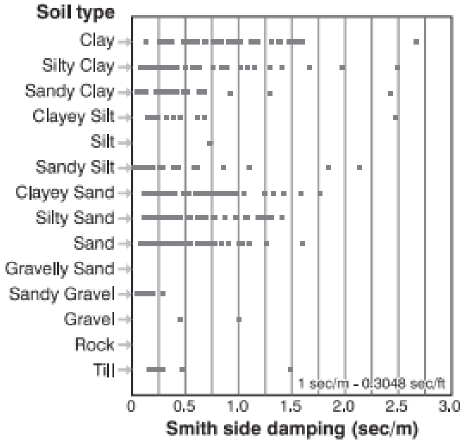

Figure 17: Variety of Smith shaft damping values per soil type (Paikowsky et al., 1994)

3.2 Soil damping

Soils exhibit strong time-dependent behaviour, which can be translated in terms of strain-rate effects. The degree of this behaviour varies with soil type, stress history and soil structure. During pile driving and dynamic load testing, high impact velocities on the pile head causes loading rate effects leading to significant increase of pile resistance. Kraft et al. (1981) reported that the ultimate bearing capacity of piles in clay can increase between 40% and 75% when the loading rate is increased by a factor 3. Figure 18 shows the experimental results of a Constant Rate of Penetration test (CRP) on model piles in sand (Fleming, 1958) and Smith (1965) developed the first practical soil-pile model that could be used for numerical analysis of pile driving and pile bearing capacity predictions of driven piles. Smith introduced a lumped or generalized viscous damping factor J included all the types of damping: viscous, radiation and hysteretic damping. Other researchers quantified each damping term with their individual contributions to the total dynamic resistance. In dynamic loading, all the damping forces adds to the static forces and increases the total soil resistance during pile motion.

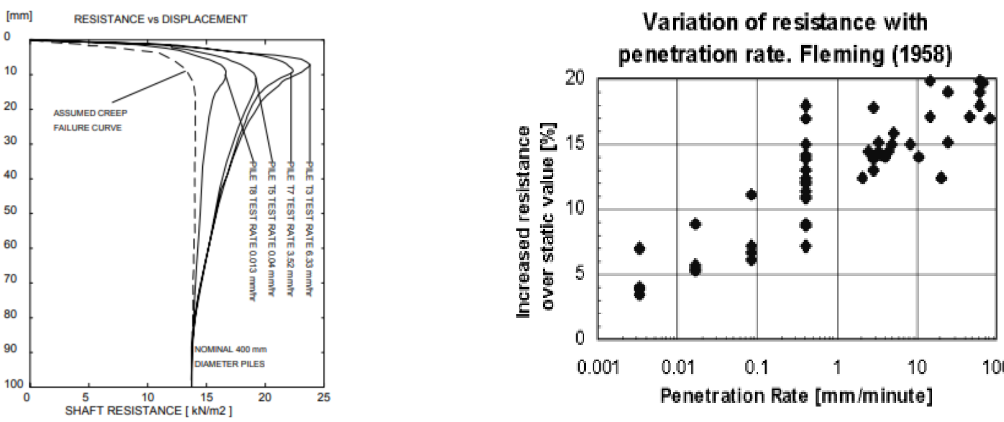

Figure 18: CRP test (left) and pile resistance vs penetration rate (right) *(Fleming, 1958)*

3.2.1 Hysteretic damping

In hysteretic damping or material damping, energy in the system is dissipated due to friction by repetitive deformation and restoration of the soil to its original shape during pile driving (Iwasaki et al., 1978). Pile-soil interaction is governed by a stress-strain relationship and soil does not follow the same stress path for loading and unloading process, because of nonlinear soil response at small to pre-failure strain levels. This results in gradual plastic deformation and energy loss. Hysteretic damping is related to cyclic stress-strain behaviour and not to the rate of loading and pile velocity. The energy dissipation is equal to the enclosed area of the hysteresis loop. The damping ratio is the ratio of the area enclosed by the secant or average shear modulus G_{sec} (W) divided by the area enclosed by the hysteresis loop (ΔW) and resembles the percentage of input energy absorbed in the soil every full stress cycle. The area beneath the secant modulus curve represent the theoretical energy from a single loading cycle. The area within the hysteresis loop represent the energy loss in the soil by friction and particle interaction. At small strains the operational shear modulus is equal to the maximum shear modulus G_{max} or G_0. When the cyclic strain amplitude increases along the shaft due to pile penetration, the stiffness of the soil fabric decreases and the damping ratio increases. The shear modulus reduction curve is shown in Figure 19 and this can be used to estimate the soil stiffness degradation along the pile axis as function of relative depth.

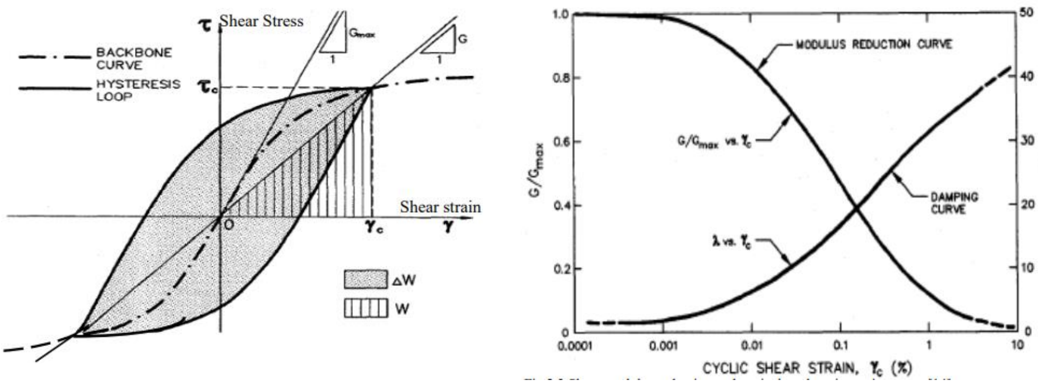

Figure 19: Stress-strain hysteresis (left), modulus reduction curve and damping curve (right) (Kavazanjian et al., 1997)

3.2.2 Viscous damping

Viscous damping is dependent on the rate of loading and unloading. In saturated soils, water is captured in the pores of the soil skeleton and induce a viscous damping force during dynamic loading. The magnitude of the viscous damping force is related to the pile velocity, but also on soil properties. The viscous damping in sand is lower than for clays because of well drainage conditions. In sands, viscous damping is generally lower compared to clays due to the coarser particle size and the generally lower water content. Sands exhibit more elastic behaviour and lower energy dissipation under cyclic loading. In clays, especially highly plastic and sensitive clays, viscous damping can play a more significant role due to their fine particles and ability to retain water. The water content and pore water pressures in clays contribute to increased viscous interactions between particles. In the context of pile driving, viscous damping refers to the dissipation of energy that occurs as a pile is driven into the ground. When a pile is subjected to dynamic loading, such as the impact from a pile hammer, it undergoes cyclic vibrations and deformations. These vibrations cause the soil particles around the pile to move relative to each other, generating internal friction and interactions with the pore present in the soil pores. This interaction between soil particles and pore fluid creates resistance to the motion of the pile and results in the conversion of mechanical energy into heat energy. This energy dissipation due to the internal friction and viscous interactions is referred to as viscous damping. In other words, as the pile moves up and down during pile driving, the energy of these motions is gradually transformed into heat within the soil. Viscous damping in pile driving can significantly influence the behaviour of the pile-soil system during dynamic loading. It affects the rate at which energy is transferred to the soil and the rate at which vibrations attenuate over time. The presence of viscous damping tends to reduce the amplitudes of pile vibrations and can also lead to a phase shift between the applied forces and the resulting pile displacements. In some soil models the viscous damping force is neglected or generalized into a lumped damping mechanism (Smith, 1960), because of the relative small contribution to the total energy loss, but other soil model incorporate the viscous damping term individually, such as Nguyen et al. (1988) and Simons and Randolph (1985). In the TNO soil model the viscous effect is decoupled from the static resistance. Unlike hysteretic damping, viscous damping is velocity and frequency dependant but does not depend on the strain level and loading history (Aasen et al., 2017).

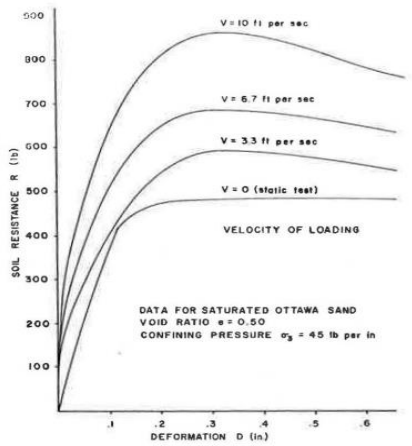

Figure 20: Increase of soil resistance due to viscous damping with increasing pile velocity

3.2.3 Radiation damping

Radiation damping or geometric damping is energy dissipation by stress waves spreading out in the surroundings from the pile-soil interface. Radiation damping is frequency dependent. Radiation damping is an important factor in dynamic loading and is responsible for most energy loss during pile driving. Radiation damping has a larger effect on the pile shaft than on the pile base resistance (Nguyen, 1987). The impact of the hammer generates a downward travelling stress wave in the pile and the soil reacts against the pile motion. In hysteretic and viscous damping the energy dissipation occurs at the interface or shear band between the pile and soil, but also energy radiates outwards in the surrounding soil by inducing soil motion in the form of radiation damping what can be experience on the job site. The magnitude of soil motion depends on soil type, pile diameter, pile volume, pile shaft roughness and soil stiffness.

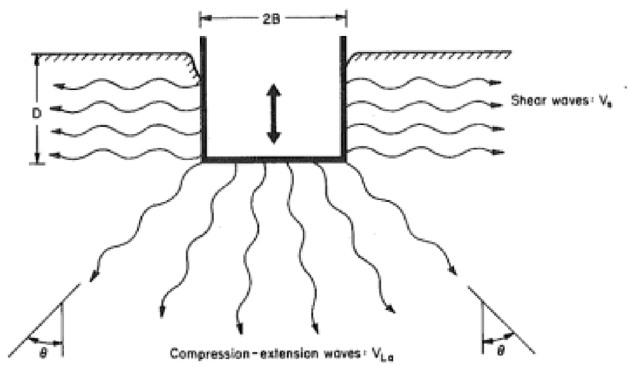

Figure 21: Radiation damping during pile driving (Gazetas et al., 1985)

The relationship between radiation damping and soil stiffness can be counterintuitive, especially when comparing different soil types like soft clay and sand. The radiation damping can be higher in soft clay, even though its soil stiffness is lower than that of sand, the following reasons can explain this

1. Propagation Speed of Stress Waves: In dynamic loading scenarios such as pile driving, stress waves are generated and propagate through the soil. The speed at which these stress waves travel is related to the square root of the ratio of the soil's elastic modulus (a measure of stiffness) to its density. Soft clay typically has a lower elastic modulus (stiffness) compared to sand, making the stress waves travel more slowly in clay.
2. Energy Absorption: Radiation damping is essentially the dissipation of energy as stress waves propagate through the soil. Softer soils like clay, while having lower stiffness, tend to dissipate more energy because the slower-moving stress waves result in more significant wave dispersion and scattering. This leads to a higher degree of energy absorption in clay.
3. Effective Mass: The density of the soil also plays a role. Softer soils often have a lower density than denser soils like sand. This lower density effectively increases the "mass" that the stress waves encounter as they propagate through the soil. This increased effective mass contributes to greater energy dissipation, thus higher radiation damping.
4. Damping Mechanisms: Different soil types have different mechanisms for energy dissipation. Soft clays may contain water, organic matter, or other materials that can lead to additional damping effects. Sand, being denser and composed of larger grains, may have fewer mechanisms for energy dissipation.

In summary, while soft clay has a lower soil stiffness than sand, its higher radiation damping can be attributed to the slower propagation of stress waves, the characteristics of the soil matrix, and the effective mass encountered by the waves. These factors collectively contribute to the higher energy dissipation observed in soft clay during dynamic loading, leading to higher radiation damping.

4. CPT based soil model parameters

The relationships between the pile motion and the soil reactions are not based on rigorous analysis of dynamic soil behavior. Smith soil model parameters, quake and damping are not fundamental soil properties and cannot be measured directly by standard geotechnical investigation techniques in the field. A stiffness based quake value and damping constants suggested by the analytical models attempting to relate them to fundamental soil properties. Shear modulus (G), Poisson's ratio (ν), soil density (ρ) and yield stress (τ_{sf}) are the most common fundamental soil properties that are used in the analytical soil reaction models to quantify static and dynamic components. Usually the Smith model parameters are based on experience from signal matching analysis for different types of soils. On the basis of cone penetration tests (CPT), standard penetration tests (SPT) and laboratory tests it is possible to link the Smith's approach in a comprehensive manner to improved realistic fundamental values what can be used in the analytical models. In the Netherlands, CPT is a commonly used soil investigation test to obtain engineering parameters and based on CPT data various correlation between cone resistance and sleeve friction can be made to derive the fundamental geotechnical soil parameters that functions as input for the analytical soil models.

4.1 Soil density

Cohesionless soils

In a couple of analytical models, the soil density is used to quantify soil damping constant. An estimate of the overburden pressure at depth can be made from (Robertson & Cabal, 2010) which uses the saturated unit weight as approach.

$$\frac{\gamma_{sat}}{\gamma_w} = 1.236 + 0.27 \cdot \log(R_f) + 0.36 \cdot \log\left(\frac{q_t}{P_{atm}}\right) \tag{41}$$

The function is based on the sleeve friction (f_s) and the net cone resistance (q_t) and is limited to clays and sands with a saturated unit weight above 15 kN/m^3 and with a specific gravity (G_s) between 2.6 to 2.7. Soils with different specific gravity can be multiplied by $G_s/2.65$. The corrected cone resistance (q_t) for pore pressure effects is set equal to the measured cone resistance (q_c) in case of insufficient data. Alternatively, Mayne (2014) proposed two equations for a wider range of soil types, including silts and soft clays. The calculated saturated densities have a minimum density of 12 kN/m^3. The equations are solely based on sleeve friction.

$$\gamma_{sat} = \left[1.22 + 0.153 \cdot \ln\left(\frac{100 f_s}{P_{atm}} + 0.01\right)\right] \cdot \gamma_w \tag{42}$$

$$\gamma_{sat} = \left[26 - \frac{14}{1 + (0.5 \cdot \log(f_s + 1))^2}\right] \cdot \gamma_w \tag{43}$$

Organic peats are largely overestimated and fall not within the desired ranges (Mayne, 2014). The total vertical stress is calculated by summation of the saturated unit weight γ_{sat} and layer thickness (ΔH_s) over depth profile.

$$\sigma_{v0} = \sum \gamma_{sat} \cdot \Delta H_s \tag{44}$$

In fine grained soils pore pressure effects has its influence on the measured cone resistance. After correction for pore pressure the corrected cone resistance becomes:

$$q_t = q_c + u_2(1 - a) \tag{45}$$

In sandy soils and for simplicity $q_t \approx q_c$. The correction factor a is the net area ratio and typically between 0.7 and 0.85 and is related to the dimension of the cone.

$$a = \frac{A_N}{A_T} \tag{46}$$

In which A_N is the load transfer are behind the cone tip and A_T is the cross sectional area a the base of the cone tip.

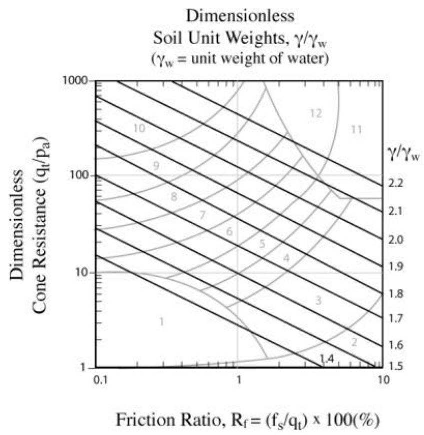

Figure 22: Relationship between CPT results and soil unit weight *(Robertson & Cabal, 2010)*

Cohesive soils

For soft to firm clays, the cone resistance q_t shows a linear trend with depth. The resistance to depth ratio can be represented by the parameter m_q

$$m_q = \frac{\Delta q_t}{\Delta z} \approx \frac{q_t}{z} \tag{47}$$

From observations the resistance-depth ratio is limit to $80\ \mathrm{kN/m^3}$ for soft to firm clays. In order to capture variations in unit weight with depth a more sophisticated method uses q_t and m_q (Mayne & Peuchen, 2012)

$$\frac{\gamma_{sat}}{\gamma_w} = 0.886 \cdot \left(\frac{q_t}{P_{atm}}\right)^{0.072} \cdot \left[1 + 0.125\frac{m_q}{\gamma_w}\right] \tag{48}$$

In clays, (partially) undrained conditions are present and can influence the CPT measurements. In normal and lightly over-consolidated clays, a simplified conversion can be applied to the cone resistance to get a corrected cone resistance (Schnaid et al., 2004).

$$q_t = 1.14 q_c \qquad \frac{q_c}{\sigma'_{v0}} < 6 \tag{49}$$

$$q_t = q_c \qquad \frac{q_c}{\sigma'_{v0}} < 6 \tag{50}$$

The corrected cone resistance is based on a pore pressure ratio (B_q) of 0.6 and a cone area ratio (a) of 0.8. For stiff clays (q_c > 1 MPa), $q_t = q_c$ (Lehane et al., 2020).

4.2 CPT Material Index

The CPT material index (I_c) is useful to screen for soil types in the Robertson chart. The index separates the zones 2 to 7 in the SBTn chart (Soil Behaviour Type) in which I_c is. The type of soil is necessary to choose which design method must be used to do the calculations for shaft and base friction.

$$I_c = \sqrt{(3.47 - \log Q_t)^2 + (\log F_r + 1.22)^2} \tag{51}$$

In which the normalized cone resistance in non-dimensional form Q_t and friction ratio F_r respectively are

$$Q_t = \left(\frac{q_t - \sigma_{v0}}{\sigma'_{v0}}\right) \tag{52}$$

$$F_r = \left(\frac{f_s}{q_t - \sigma_{v0}}\right) \cdot 100\% \tag{53}$$

A rough estimate of exponent n is normally n=1 for clay, n=0.75 for silt and 0.5 for sand. The value of n can also be calculated as follows:

$$\mathrm{n} = 0.381 \cdot \mathrm{I_c} + 0.05 \cdot \left(\frac{\sigma'_{v0}}{\mathrm{P_{atm}}}\right) - 0.15 \tag{54}$$

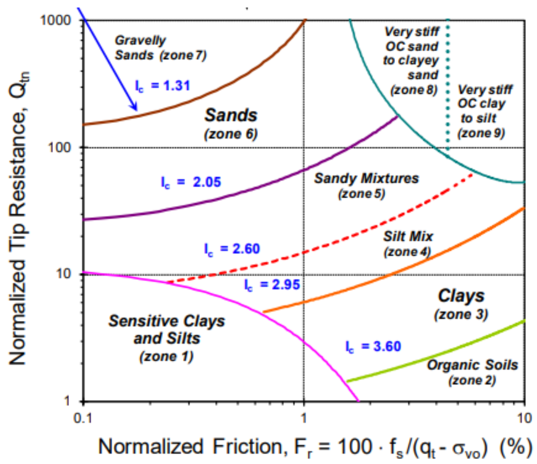

Figure 23: Soil behaviour index chart *(Robertson, 2009)*

In zone 2 to 7 the boundaries of the soil behaviour type in Figure 23 can be approximated by concentric circles. The radius of every circle represent the a soil behaviour type index (Jefferies & Davies, 1993).

4.3 Local ultimate shaft friction

In the pile design process, there is a distinction between ultimate and limit soil resistance. Upon pile loading the soil resistance increases with increasing pile displacement, but the increment of this rate decreases once the pile displacement continues. The soil resistance remains at a maximum value once the pile has displaced beyond a certain level of pile displacement. In order to mobilize the maximum shaft friction (τ_{sf}) a relatively small pile displacement is required and therefore the maximum shaft friction is equal to the ultimate shaft friction in the design methods ($\tau_{s,ult} = \tau_{sf}$). A pile displacement of about 10 mm or 1% of the pile diameter is often sufficient under static conditions to reach the ultimate limit state for the pile shaft (ULS). Base stress mobilization up to the limit pile base resistance (q_{bL}) needs much more pile displacement than the resistance that is obtained by a 10% pile base displacement according to ULS design methods ($q_{b,ult} = q_{b0.1}$). In order to design a pile in ULS with ultimate capacity, the ultimate shaft resistance will be quickly mobilized, but the limit base resistance will not always be reached at 0.1D and base resistance increases with additional settlement.

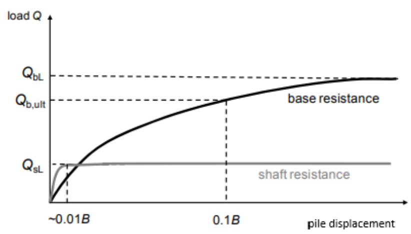

Figure 24: Definition of τ_{sL}, q_{bL} and $q_{b,ult}$ on the load-displacement curve

Predicting the ultimate shaft friction that can be mobilised along the shaft of a driven pile is subjected to changes due to installation effects, equilibrium of excess pore pressure and loading rate of the pile. During installation the surrounding soil undergoes distortion and changes to the soil fabric (Bond & Jardine, 1991). The soil ahead of the pile base will move outwards with a strain field that resembles spherical cavity expansion theory. Soil adjacent to the pile shaft resembles cylindrical cavity expansion.

The design methods for shaft friction given in section 4.3.1 and 4.3.2 are based on the stress state at 2 weeks after pile installation in which also friction fatigue and soil relaxation is included. The time duration between installation and dynamic load test is relevant for the calculated shaft friction because a setup factor is necessary to correct for the setup effects. Pile capacity is after all also a function of time.

4.3.1 Cohesive soils

The shaft resistance of a driven pile in clay depends on the in situ conditions and the complex changes that take place during installation, excess pore pressure dissipation and subsequent loading. The ultimate shear strength sets the maximum shear stress that the soil can provide against the pile shaft. For determining the shear strength, the intact and remoulded shear strength of soils can be used. During pile driving the soil around the pile is remoulded and the sleeve friction of a CPT measurement is a quick approach for determination of the ultimate shear strength. Lunne et al. (1997) have shown that the sleeve friction values are often similar to the remoulded undrained shear strength of fine grained soils. The sleeve friction is in general less accurate than the cone tip resistance. Lack of accuracy is mostly due to pore pressure effects on the end of the sleeve, surface roughness of the sleeve and load cell design and calibration (Lunne & Andersen, 2007). A rough estimate of the ultimate shaft resistance is based on the sleeve friction.

$$\tau_{sf} \approx f_s \tag{55}$$

Early works on estimating the ultimate shaft resistance was made by using the cone resistance in combination with a correction factor (c_s) as shown in Table 1 (Aoki & Velleso, 1975).

$$\tau_{sf} = c_s \cdot q_c \tag{56}$$

Pile type	c_s		c_b	
Displacement piles	Pure clay	0.017	Soft to lightly OC clays	0.9-1.0
	Silty clay	0.011	Stiff OC clays	0.35
	Silty clay with sand	0.0086		
	Sandy clay with silt	0.008		
	Sandy clay	0.0069		

Table 1: Summary of recommended values for c_s and c_b for calculating base resistance and shaft resistance from cone resistance in clayey soils (Aoki & Velleso, 1975)

Based on CPTu data Eslami and Fellenius (1997) correlated the shaft resistance to effective cone resistance (q_t or q_E) by using a correlation coefficient (C_{se}) and varies per soil type. The effective cone resistance includes the effect of pore pressure generation on the measured cone resistance during cone penetration.

$$\tau_{sf} = C_{se} \cdot q_t \tag{57}$$

The approximation of the shaft resistance based on direct sleeve and cone measurements do not include the effects from installation, friction fatigue, equalisation and loading.

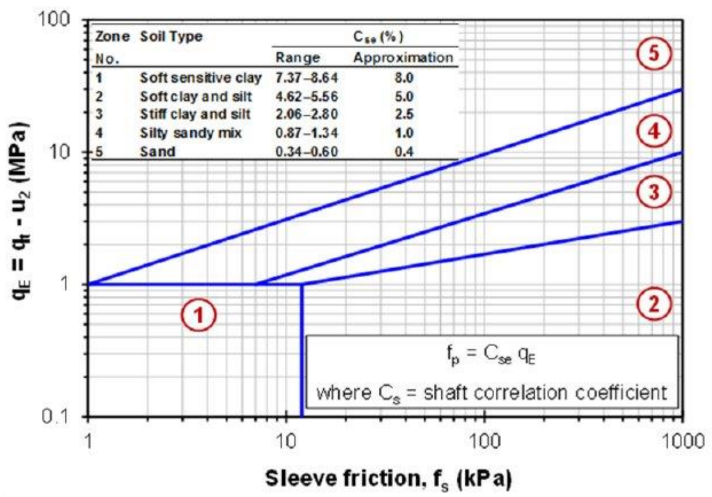

Figure 25: Chart for soil type and shaft coefficient (Eslami & Fellenius, 1997)

Randolph (2003) noted that a scientific approach to determine the local shaft resistance of a driven pile should consider the complex stress-strain history. The complex stress-strain history includes 1) initial in situ soil conditions, 2) pile installation, 3) equalisation and 4) loading. Field testing was done on instrumented piles (ICP) which was installed in a wide range of clay types. Chow (1997) proposed a conventional earth pressure approach to calculate the equalised radial effective stress along the pile shaft by

$$\sigma'_{rc} = K_c \sigma'_{v0} \tag{58}$$

In which K_c is

$$K_c = (2.2 + 0.016\text{YSR} - 0.87\log_{10}S_t)\text{YSR}^{0.42}\frac{h}{R}^{-0.2} \tag{59}$$

The radial effective stress accounts for the effect of friction fatigue along the pile. The yield stress ratio (YSR) relaced the over consolidation ratio (OCR). The yield stress ratio is calculated by

$$\text{YSR} = \frac{\sigma'_{vy}}{\sigma'_{v0}} \tag{60}$$

In which σ'_{vy} is calculated by equation (44). The local ultimate shaft friction at failure is then calculated by

$$\tau_{sf} = f_L K_c \sigma'_{v0} \tan(\delta_f) \tag{61}$$

The loading factor f_L is 0.8 for loading and δ_f is the interface friction angle at failure. For open ended piles the radius R can be adapted to $R^* = \sqrt{R_o^2 - R_i^2}$. The sensitivity ($S_t$) is the ratio of the undisturbed undrained shear strength over the remoulded undrained shear strength and are accurately obtained by lab testing. A CPT based estimate is given by (Mayne, 2007).

$$S_t = \frac{0.073(q_t - \sigma_{v0})}{f_s} \tag{62}$$

The most recent development of an empirical method for pile shaft capacity in clay is given by Lehane et al. (2020) as the unified method for piles in clay. The method was established after a Joint Industry Project (JIP) under the management of the Norwegian Geotechnical Institute to create a unified database for driven piles in sand and clay (Lehane et al., 2017, Liu et al., 2019). The method defines the dependence of the equalised shaft friction (τ_{eq}) on the corrected cone resistance (q_t), relative pile depth (h), friction fatigue (h/D). This method is applicable for clays in the SBT Zones 2,3 and 4 (Lehane et al., 2022).

$$\tau_{eq} = 0.07 q_t \left(\max\left(\frac{h}{D^*}, 1\right)\right)^{-0.25} \tag{63}$$

Depending if it is an open or closed ended pile, for open-ended piles the radius R must be changed by R^*. The factor 0.07 in the equation is an average value to incorporate important features such as over-consolidation ratio and clay sensitivity. The equalised shaft friction for piles in clay calculated by the unified method is based on a database of instrumented piles with aging period ranging from 21 to 130 days with an average of 60 days. Only piles which has undergone a degree of excess pore pressure dissipation of about 80% were included in the database. A setup factor must be applied to calculate the shaft friction at a specific time after installation (Chapter 4.6).

4.3.2 Cohesionless soils

In the past, several methods were proposed to calculate the local ultimate shaft friction based on CPT measurements for piles in cohesionless soils. Aoki and Velleso (1975) proposed a correction factor (c_s) for ultimate shaft friction in sandy soils. In a similar equation as (56) and Table 3 the ultimate shaft friction for sandy soils is estimated. A more extensive CPT based method was developed by Jardine et al. (1998). This method is part of the Imperial College Project (ICP-05) method and calculates the local shaft friction of driven piles in sand. The method incorporates complex stress-strain history which includes, initial in-situ conditions, friction fatigue, equalisation and loading. The local ultimate shaft friction obeys Coulomb's law.

$$\tau_{sf} = \sigma'_{rf} \tan(\delta_{cv}) \tag{64}$$

Where σ'_{rf} is the effective radial stress at peak friction and δ_{cv} is the ultimate constant volume interface friction angle. The effective radial stress is a combination of the stationary radial effective stress (σ'_{rc}) and an increase of radial effective stress due to dilatancy during pile loading ($\Delta\sigma'_{rd}$). The ICP-05 method is given as

$$\tau_{sf} = a\left(0.029bq_c\left(\frac{\sigma'_{v0}}{P_{atm}}\right)^{0.13} \cdot \max\left(\frac{h}{R^*}, 8\right)^{-0.38} + \frac{4G_{max}\Delta t}{D}\right)\tan(\delta_{cv}) \tag{65}$$

Jardine et al. (2015) stated that the ICP-05 method predicts the axial pile capacity more or less after 100 days after installation. In equation (65), h is the distance of a certain horizon above the pile tip at the end of driving. The last term inside the brackets is the post horizontal effective stress change denoted as $\Delta\sigma'_{hd}$. The horizontal effective stress on the shaft at the end of pile installation is given in the first term. During pile loading in dense sand, the soil tends to dilate and this is shear band thickening Δt and is equal to 0.02 millimetres. D is the diameter of the pile and the shear modulus G_{max} is given in Section 4.5.1. The parameter a is 0.9 for open-ended piles in tension and 1.0 for all other cases. The parameter b is 0.8 for piles in tension and 1.0 for piles in compression. R^* is the equivalent radius, which is R for circular closed ended piles and for a non-circular closed ended pile it has a pile radius equivalent to circular pile with same end area. For an open ended pile the equivalent radius is $R^* = \sqrt{R_0^2 - R_i^2}$.

Another CPT-based method was developed by Lehane et al. (2005) from pile load tests and centrifuge test to obtain τ_{sf} for displacement piles in sand. This method, so-called University of Western Australia (UWA-05) has similarities to the IC method. The ultimate shaft friction is given by

$$\tau_{sf} = \frac{f_t}{f_c}\left(\frac{0.03q_c A_{r,eff}^{0.3}}{\sqrt{\max\left(\frac{h}{D}, 2\right)}} + \frac{4G_{max}\Delta t}{D}\right)\tan(\delta_{cv}) \tag{66}$$

The ratio $\frac{f_t}{f_c}$ is 1.0 for piles in compression and 0.75 for piles in tension, due to Poisson effect (Lehane et al., 2020). Both equations (65) and (66) are valid for unplugged piles in which the effective pile area becomes $A_{r,eff} = 1 - \text{PLR}\frac{D_i^2}{D_o^2}$. $A_{r,eff}$ is 1 for closed ended pile. The penetration of an open ended, compared to a closed-ended pile, leads to less soil volume displacement and therefore lower stress level. It is assumed that the short duration of the stress wave generated by a hammer impact will not induce plugging in an open ended pile.

A new unified CPT based method for axial pile capacity for driven piles in siliceous sands was developed to improve all the key features of the previous proposed CPT based methods (Lehane et al., 2020). The method provides more reliable predictions of the capacities than the methods in the API and ISO guidelines. The JIP database of pile load tests has a typical set-up time of between 1 week and 2 months with a median of 14 days. The proposed Unified CPT-based method is intended to provide an estimate of shaft friction available at around a setup time of 14 days after driving. The method is likely to under-estimate the capacities in very silty sands and over-estimate the capacities in gravelly sands. The operational shear modulus was updated in the method and became less than the small strain stiffness because of non-linear relationship with strain increments. The increase in radial stress during pile loading becomes

$$\Delta\sigma'_{rd} = \left(\frac{q_c}{10}\right)\left(\frac{q_c}{\sigma'_{v0}}\right)^{-0.33}\left(\frac{d_{CPT}}{D}\right) \tag{67}$$

In which d_{CPT} is the diameter of a standard CPT probe ($d_{CPT} = 35.7\text{mm}$). Different formulations were made for estimating the stationary radial effective stress (σ'_{rc}). The best fit to data from instrumented piles gave the following formulation (Lehane et al., 2020).

$$\sigma'_{rc} = \left(\frac{q_c}{44}\right)A_{r,eff}^{0.3}\left(\max\left(1,\frac{h}{D}\right)\right)^{-0.4} \tag{68}$$

The interface friction angle (δ_{cv}) can be obtained by laboratory tests. In absence of ring shear interface tests a mean value of 29 degrees is reasonable for steel piles. The local ultimate shaft friction becomes

$$\tau_{sf} = \left(\frac{f_t}{f_c}\right)(\sigma'_{rc} + \Delta\sigma'_{rd})\tan(\delta_{cv}) \tag{69}$$

The effective piles radius $A_{r,eff}$ in the unified method is slightly different than in the ICP-05 and UWA-05 method for open ended piles, due to a change in formulation for the plug filling ratio

$$PLR \approx \tanh\left(0.3\sqrt{\frac{D_i}{d_{CPT}}}\right) \tag{70}$$

For full scale offshore open ended piles ($D < 3\text{m}$) with full coring ($PLR = 1$) the dilatancy effect in effective radial stress can be ignored. The equation for local ultimate shaft friction becomes:

$$\tau_{sf} = \left(\frac{f_t}{f_c}\right)\left(\frac{q_c}{80}\right)\left(\max\left(1,\frac{h}{D}\right)\right)^{-0.4}\left(1-\left(\frac{D_i}{D}\right)^2\right)^{0.3} \tag{71}$$

For the shaft resistance, the friction angle δ_{cv} is related to critical state friction angle φ_c mobilized along the shaft. The shear modulus is calculated by equations in Section 4.5.1. In Table 2 an estimate is given for different pile types.

Pile type	δ_{cv}
Steel	$0.85 \cdot \varphi_c$
Precast concrete	$0.95 \cdot \varphi_c$

Table 2: Different pile types and values for $\boldsymbol{\delta}$ (Salgado, 2008)

In absence of testing, the interface friction angle can be estimated by using CPT based correlations. The interface friction angle, as stated in Table 2, uses the critical state friction angle. The critical state friction angle φ'_c can be calculated by an empirical equation that relates the mobilized friction angle φ' with the dilation angle ψ by

$$\varphi'_c = \varphi' - 0.8\psi \qquad \varphi'_c$$

The mobilized friction angle is given by Uzielli et al. (2013) with an $R^2 = 0.92$

$$\varphi' = 25\left(\frac{\frac{q_t}{P_{atm}}}{\sqrt{\frac{\sigma'_{v0}}{P_{atm}}}}\right)^{0.10} \tag{72}$$

The dilatancy angle can estimated by using the relative density (D_r) of the soil

$$\psi = -2 + \frac{12.5D_r}{100} \tag{73}$$

In which the relative density can be roughly approximated by (Jamiolkowski et al., 2001).

$$D_r(\%) = 100\left(0.268\ln\left(\frac{\frac{q_t}{P_{atm}}}{\sqrt{\frac{\sigma'_{v0}}{P_{atm}}}}\right) - 0.675\right) \tag{74}$$

The empirical equation is proposed for clean sands with less than 15% fines and at medium compressibility. For pre-consolidated sands, Mayne (2009) suggest to multiply the 0.675 by $OCR^{0.20}$ in equation (74).

In general it is assumed that the ultimate shaft resistance is identical under both dynamic compressive and tensile loading. Experimental research (De' Nicola & Randolph, 1993) has shown that the ultimate shaft resistance is significantly lower for tensile loading compared to compressive loading. The main cause of lower tensile ultimate shaft resistance is due a Poisson's ratio effect leading to changes in radial effective stress in the soil around the pile. From full scale test the ratio between the ultimate tensile and compressive shaft resistance varies between 0.44 and 0.85 with an average of 0.65. In the unified methods for piles in sand and clay an average ratio of 0.75 is sufficient.

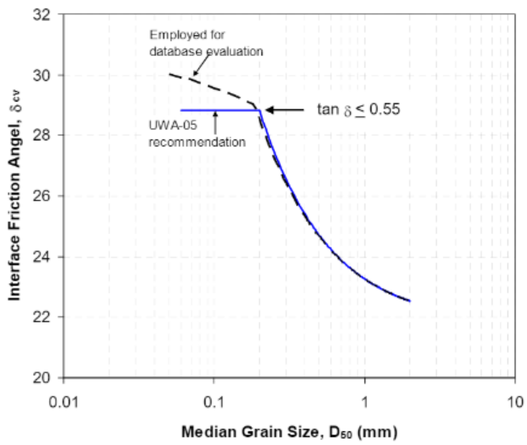

Figure 26: Variation of interface friction angle with median grain size (D50)

4.4 Ultimate base stress

In simple methods for end bearing capacity determination, it is assumed that the cone tip resistance (q_c) gives a good estimate of the limit base resistance of a deep circular foundation. In design methods such as UWA-05, IC-05 and unified method-20, the ultimate base resistance is defined at a base settlement of 10% of the pile outer diameter. These methods give values to base resistances that are lower than the cone resistance during steady penetration. Values of $\frac{q_{b0.1}}{q_c} < 1$ can be attributed to partial mobilisation of base resistance. During pile driving, often the pile mobilises a fraction of the ultimate base capacity linked to a settlement of 0.1D according to the failure criteria for static loading. A pile base stress which has a fraction of the ultimate base stress is still able to penetrate the soil (q_{bf}). When exceeding the failure settlement criterion of 0.1D, penetration increases and the base resistance q_b increases and ultimately it reaches the cone resistance which is roughly equal to the limit or plunging failure base resistance for driven piles. The main difference between a large diameter pile and cone penetrometer is the effect of a larger influence zone around the pile base and stress changes due to pile penetration. From instrumented piles in sand, data show that the maximum or limit base resistance at plunging, q_{bL} of open ended and close ended piles are close to the measured cone resistance (75). For piles in clays, piles a similar relationship between cone resistance was observed an no distinction was made between end bearing resistance of open or closed ended piles. The direct relation between q_c and q_b was based on the LCPC method in which q_c was averaged over 1.5D above and below the pile base.

$$q_{bL} \approx q_c > q_{bf} \tag{75}$$

$$q_{b0.1} = c_b q_{c,1.5D} \tag{76}$$

In which $q_{c,1.5D}$ is calculated by

$$q_{c,1.5D} = \frac{\int_{L-1.5D}^{L+1.5D} q_c(z)dz}{3D} \tag{77}$$

The $q_{c,1.5D}$ is used as $q_{c,avg}$ in determination of end bearing. The value of c_b is 0.45 or 0.65 for undrained or drained loading of plugged piles and 1.0 or 1.6 for undrained or drained loading of unplugged piles. In Figure 27, a value c_b of 0.5 is reasonable for closed ended piles in sand using LCPC method (Figure 27). The LCPC method shows a clear trend as pile diameter increases. In the Dutch averaging method, $q_{c,Dutch}$, used in UWA-05 method, a value of $c_b = 0.6$ is proposed. The Dutch averaging method shows no clear trend as pile diameter increases. Measured pile base capacity contains uncertainties related to residual loads (Lehane et al., 2020).

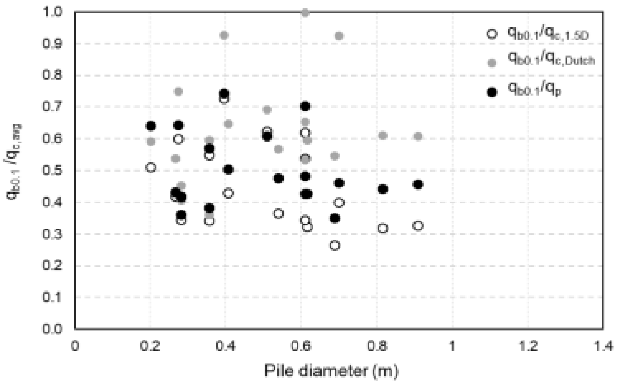

Figure 27: $q_{b0.1}$ values compared with 3 q_c averaging techniques of end bearing measurements (Lehane et al., 2020)

Figure 28 shows the ratio between the average cone resistance and ultimate base capacity in relation to the effective area ratio for piles in sand. For large offshore monopiles the effective area ratio is close to zero resulting and a ratio of $q_{b0.1}/q_{c,avg}$ of about 0.15 can be taken (Lehane et al., 2020).

$$q_{b0.1} = q_{c,avg}(0.12 + 0.38A_{re}) \tag{78}$$

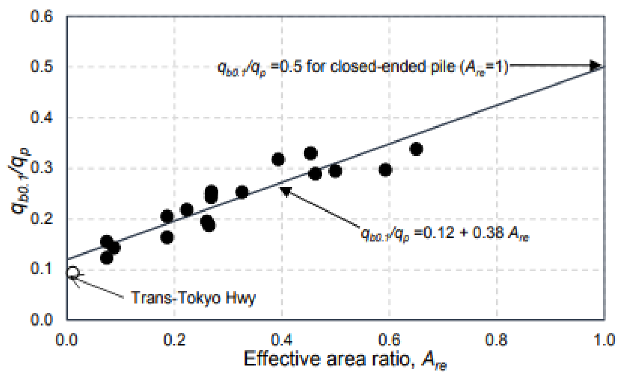

Figure 28: Ratio of $\frac{q_{b0.1}}{q_c,avg}$ as function of the effective area ratio for open-ended piles (Lehane et al., 2020)

A distinction between soil displacement and soil removal piles is necessary because driven piles induce larger stresses in the surrounding soil during installation than bored in cast in situ piles. Loading a closed-ended pile resembles the expansion of a spherical cavity in an infinite medium. Open-ended piles experience higher compression of soil in the core and plug and below the pile tip. Both phenomena increases the mean stresses around the pile tip and could lead to higher base resistance than expected from measured cone resistances. Early correction factors for a direct relation between the cone resistance q_c and ultimate pile base and shaft friction by means of c_s and c_b are given in Table 3 for different types of soils.

Pile type	c_s		c_b
Displacement piles	Clean sand (Aoki & Velleso, 1975)	0.004	0.35 – 0.5 (Chow, 1997)
	Silty sand	0.0057	0.4 (Randolph, 2003)
	Silty sand with clay	0.0069	
	Clayey sand with silt	0.008	(1.02 – 0.0051)Dr (Foye et al., 2006)
	Clayey sand	0.0086	
	Silty clay	0.011	
	Pure clay	0.017	
Open-ended pipe piles	IFR ≤ 60% (Lee et al., 2003)	0.0015 – 0.003	
	60% < IFR ≤ 100%	0.0015 – 0.004	
Closed-ended pipe piles	D_r ≤ 50% (Lee et al., 2003)	0.004 – 0.006	
	50% ≤D_r ≤ 70%	0.004 – 0.007	
	50% ≤D_r ≤ 90%	0.004 – 0.009	

Table 3: Summary of recommended values for $\mathbf{c_s}$ and $\mathbf{c_b}$ for calculating base resistance and shaft resistance from cone resistance in sandy soils (Aoki & Velleso, 1975)

Regarding a pile base in clay, the formulation for the ultimate base resistance changes to (Lehane et al., 2022).

$$q_{b0.1} = q_{t,avg}(0.2 + 0.6A_{re}) \tag{79}$$

Equation (79) implies that in case of undrained end bearing capacity the ultimate base resistance of a large offshore pile ($A_{re} \approx 0$) is approximately $0.2q_{t,avg}$, in which the cone resistance is corrected for pore pressure effects. The end-bearing for a closed-ended pile in clay with A_{re} equal to 1 becomes $0.8q_{t,avg}$.

4.5 Elastic stiffness parameters

4.5.1 Shear modulus

The shear modulus is a recurring soil properties that is used in the calculation of the quake and damping parameters in pile driving analysis. During pile driving and dynamic load tests, the pile displaces with reference to the surrounding soil and a shearing zone is formed. The shear modulus is not a constant soil property but strongly dependents on the amount of shear strain and shearing cycles the soil has experienced during driving (Figure 29). The impact of the hammer and with that the shear strain amplitude is the highest near the pile head and decreases over depth because of decreasing stress wave amplitude due to pile friction.

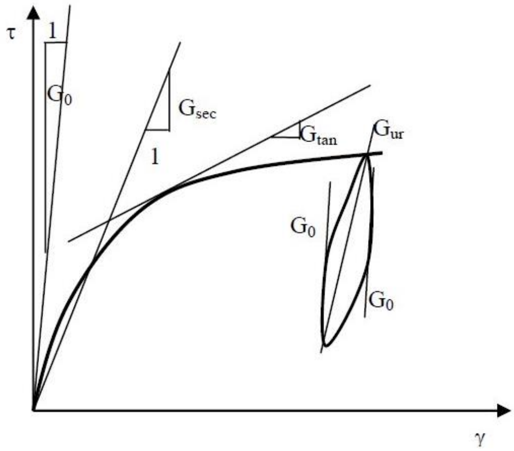

Figure 29: Degradation of shear modulus under cyclic loading

Eslaamizaad and Robertson (1997) showed that an accurate prediction of the soil shear wave velocity V_s could be obtained from the load displacement curves of both shallow and deep foundations. Direct measurements of the shear wave velocity are preferred above correlations, however direct shear wave velocity measurements are not often performed in low-risk geotechnical projects. Throughout the years, many correlations were made between q_c and V_s because of the similarities in cone resistance and shear wave velocity. The shear wave velocity depends strongly on the area and number of the grain-to-grain contacts and therefore cementation, aging, relative density, effective stress state and arrangement of the particles have a large impact. The value for q_c strongly depends on relative density and stress state, but less dependent on amount of cementation and degree of aging of the soil. A good correlation between q_c and V_s is possible with some variability. Subsequently V_s has a direct relationship with the small strain shear modulus G_{max} and therefore q_c can also be used in the determination of the soil stiffness parameters. A correlation between the normalized cone resistance and the normalized shear wave velocity for drained cohesionless soils is given by (Robertson, 2009).

$$V_s = \left[\frac{a_{vs}(q_t - \sigma_{v0})}{P_{atm}}\right]^{0.5} \tag{80}$$

Where a_{vs} is the shear wave velocity cone factor. The value for a_{vs} (in $\left(\frac{m}{s}\right)^2$) can be estimated by using the soil behaviour index type, I_c

$$a_{vs} = 10^{0.55 \cdot I_c + 1.68} \tag{81}$$

At low shear strain levels, less than 10^{-4}%, the shear modulus is denoted as the small strain shear modulus G_{max} and has a maximum and constant value in the elastic zone. The G_{max} can be calculated by using the stress wave velocity V_s and the soil density ρ_s

$$G_{max} = \rho_s V_s^2 \tag{82}$$

Robertson (2009) was able to correlate cone resistance with the small strain shear modulus (G_{max}) for drained coarse-grained soils. The equation is less reliability for fine grained soils and cemented soils.

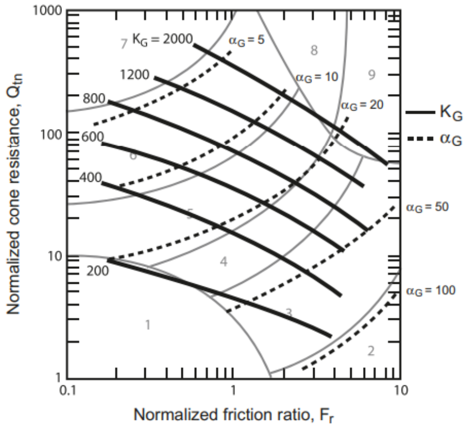

Figure 30: Contours of small strain shear modulus for uncemented Holocene and Pleistocene aged soils *(Robertson, 2009)*

Figure 30 provides an estimate for the small strain shear modulus. Equation (83) provides an simplified estimate for G_{max} over a wide range of soils. The equation is less reliable for fine-grained soils ($I_c >$ 2.6), because sleeve friction is strongly influenced by soil sensitivity.

$$G_{max} = \frac{\rho_s}{P_{atm}} \cdot [(10^{0.55 \cdot I_c + 1.68}) \cdot (q_t - \sigma_{v0})] \tag{83}$$

With ρ_s in $\frac{g}{cm^3}$ and P_{atm} is atmospheric pressure (100 kPa). Kawaguchi and Tanaka (2008) proposed a formulation of the elastic shear modulus for natural sedimentary clay soils. Existing formulations were mainly based on void ratio but difficult to apply for reconstituted soils and in the field. The new formulation consist of three other parameters: liquid limit w_L, current mean effective stress p' and maximum mean consolidation pressure p'_{max}. In order to apply this to the field, the equation is adapted for using the in-situ effective overburden pressure σ'_{v0} and OCR.

$$G_{max} = 20000 \cdot w_L{}^{-0.8} \cdot f(OCR) \cdot \sigma'_{v0}{}^{0.8} \tag{84}$$

$f(OCR)$ is a function that converts p' into σ'_v and is expresses by

$$f(OCR) = \left(\frac{2}{3} OCR\right)^{0.2} \cdot \left(\frac{1 + OCR^{0.5}}{3}\right)^{0.6} \tag{85}$$

Liquid limit and plasticity index increases with an increase in sleeve friction and at the same time cone resistance decreases. In the case no values are given for the liquid limit a comprehensive method is proposed by Cetin and Ozan (2009). The liquid limit can be calculated by using the following formulas:

$$w_L = 10^{1.506 + 0.31 \cdot \log(F_r) - \frac{\log(q_{tn})}{2.526}} \tag{86}$$

The normalized net cone resistance (q_{tn}) is calculated

$$q_{tn} = \frac{q_t - \sigma_{v0}}{\left(\frac{\sigma'_{v0}}{P_{atm}}\right)^c} \tag{87}$$

The exponent c can be calculated in an iterative procedure. The starting value of c is 1.0 and can be repeated until a difference of Δc is 0.01. The final value for c can be implemented in (87).

$$c = \frac{\sqrt{\left(\frac{q_t - \sigma_{v0}}{\left(\frac{\sigma'_{v0}}{P_{atm}}\right)^c} - 233.52\right)^2 + (\log(F_r) + 55.42)^2 - 272.38}}{275.19 - 272.38} \tag{88}$$

For alluvial site characterized by clay layers, which are weakly organic alternating with silt and sands the elastic shear modulus can be calculated from q_c and σ'_v (Togliani et al., 2015).

$$G_{max} = \rho_s[(277q_c^{0.13}(\sigma'_v)^a]^2 \quad (89)$$

In which a is 0.22 for $\sigma'_v \leq 100$ kPa and otherwise 0.17.

4.5.2 Poisson ratio

The Poisson's ratio is a common soil property that appears in the equations for spring and dashpot constants. A rule of thumb is that for most soils $v_s = 0.3$ is a good value and for saturated clays $v_s = 0.48$ can be considered. For drained loading the Poisson's ratio of the soil v_s can be approximated by

$$v_s = 0.1 + 0.3(\varphi' - 25) \quad (90)$$

The formula is applicable for soil with friction angles φ' between 25 and 45 degrees. More refined values are given in Table 4 for both quick loading during pile driving and static loading (Poulos et al., 2000)

Soil type	Quick loading	Slow loading
Gravel	0.30	0.30
Sand	0.35	0.30
Silt and silty clay	0.45	0.35
Stiff clay	0.45	0.25
Plastic clay	0.50	0.40
Compacted clay	0.45	0.30

Table 4: Poisson's ratio for different types of soil

In a couple of soil models, like the hardening soil model, also a unloading/reloading Poisson's ratio appears. For most soils a characteristic value for the elastic unloading/reloading ranges between $v_{ur} = 0.1$ and $v_{ur} = 0.2$ (Figure 31) at low mobilization ratio's ($\frac{q}{q_{max}}$). A consequence of a lower Poisson's ratio during unloading/reloading is that the shear modulus is higher and the soils acts stiffer according to

$$G_{ur} = \frac{E}{2(1 + v_{ur})} \quad (91)$$

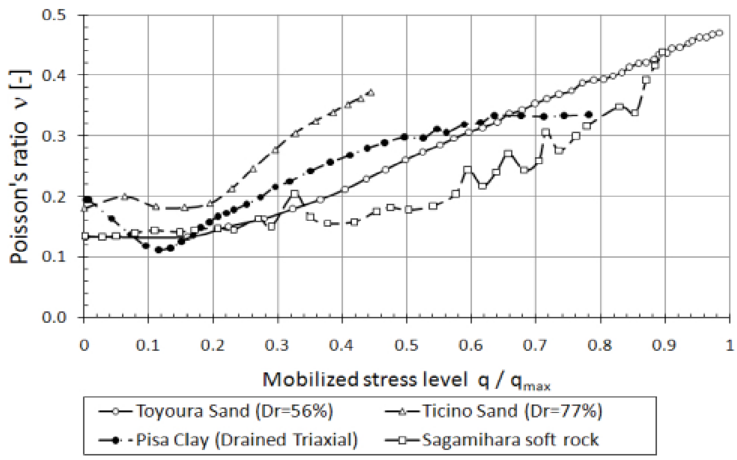

Figure 31: Poisson's ratio vs mobilized stress level for sand, clay and soft rock (Mayne et al., 2009)

4.6 Pile setup effect

The pile capacity of a driven pile changes with time after installation. A process of equalisation starts in which excess pore pressure generated during pile driving dissipates and consolidation starts in the pile-soil interface zone accompanied by an increase in pile capacity. The magnitude of positive or negative excess pore pressure depends on the contractive or dilative behaviour of the soil. The excess pore pressure is mainly positive in normal consolidated soils, but can be negative in dilative and over-consolidated stiff clays. The setup effect is due to changes in the effective stress acting on the pile and therefore it changes the stress conditions around the shaft. In less permeable soils like clays the equalisation process can take months. In silts and sands the changes can be significant in the first minutes after end of initial pile driving (Randolph & Gourvenec, 2011). The CPT based design methods in Chapter 4.3 and 4.4 are calibrated to approach pile capacity calculations for piles in sand after 2 weeks of driving and for clays with a minimum of 80% of consolidation. The set up effects is mainly affected by 1) the time required to achieve equilibrium conditions depend on soil properties 2) type of soil and 3) slenderness ratio. Despite the uncertainties of the magnitude of the setup effect and lack of insightful understanding of the mechanisms, a first correlation was proposed to quantify the set up effect based on the elapse time in the form of (Svinkin & Skov, 2000)

$$\frac{\tau_{\mathrm{ref}}}{\tau_{\mathrm{i}}} = \mathrm{A}\log\left(\frac{\mathrm{t}_{\mathrm{ref}}}{\mathrm{t}_{\mathrm{i}}}\right) + 1 \tag{92}$$

Often a dynamic load or restrike test is performed one day after installation. The time for restrike is taken as 1 (24 hours) to use the logarithmic time scale. The shaft friction at restrike is unknown, but the calculated shaft friction at 14 days ($\mathrm{t}_{\mathrm{ref}}$) is equal to the values ($\tau_{\mathrm{ref}} = \tau_{\mathrm{sf}}$) obtained by the design methods. The objective is to back-calculate the shaft resistance at a specific time (t) using equation . Values for factor A are given in Table and varies per soil type and obtained from 2219 datapoints from different sites in the world (Lee et al., 2019).

Type of soil		Factor A
Fine-grained soil	Upper bound	0.990
	Best fit	0.404
	Lower bound	0.104
Coarse-grained soil	Upper bound	0.691
	Best fit	0.365
	Lower bound	0.207

Table 5: Summary of proposed empirical factor A for correlations

Any restrike can be calculated by changing t to $\mathrm{t} = 14 - \mathrm{t}_{\mathrm{RSTR}}$ in days. The setup effect can be divided into three main parts, a nonlinear rate of excess pore pressure dissipation, a linear rate of excess pore pressure dissipation and aging effect. In the first and second phase the effective horizontal stress increases. The third phase is independent of effective stress and has a more frictional and mechanical cause, resulting in an increase in soil stiffness (van Komurka et al., 2003). Setup effect primarily takes place along the pile shaft while the pile base capacity remains relatively constant after driving (Herrington, 2018).

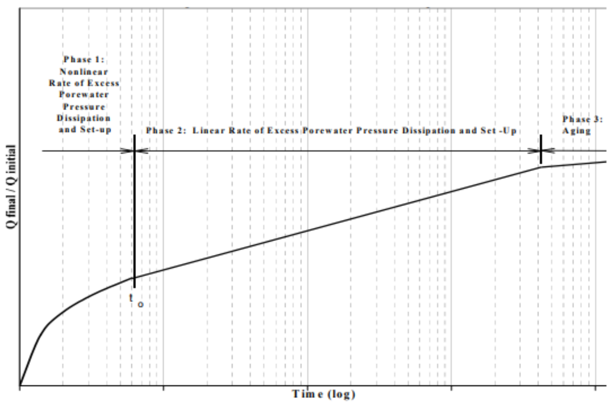

Figure 32: Idealized setup phases after pile installation

The pile capacity is not only based on stresses and soil characteristics, it's also a function of time. None of the proposed design methods contains the variable time to account for time setup effects on pile capacity in sand and clay. Time correction factor must be applied to calculate shaft capacity at a specific target pile age after installation. Based on observations of aging effects, a more sophisticated and improved best fit trendline was proposed for different design methods for piles in sand for the time correction factor F_{time} (Lehane et al., 2017) which is

$$F_{time} = \frac{1}{e^{-0.1t^{0.68}} + 0.45} + d_{offset} \tag{93}$$

The d_{offset} differs per design method and is -0.1 for ICP-05 and -0.2 for UWA-05 and zero for the unified method for driven piles in sand.

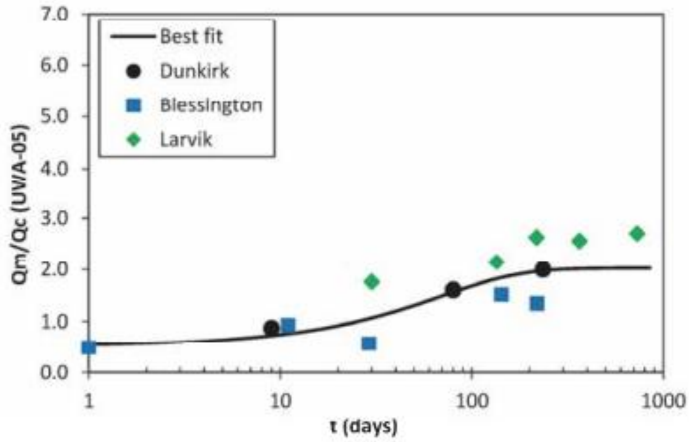

Figure 33: Observations of pile ageing in sand at three sites and best fitting curve for UWA-05 design method

A median ageing period for piles in the database was about 14 days and the CPT based methods for piles in sand were calibrated such that F_{time} was equal to 1 at 14 days after installation. The offset in equation (93) was set to zero. The shaft friction, corrected for setup effects at a specific time ($\overline{\tau_{sf}}$), can be calculated as follows

$$\overline{\tau_{sf}} = \left(\frac{1}{e^{-0.1t^{0.68}} + 0.45}\right) \cdot \tau_{sf} \tag{94}$$

In which t is the number of days after installation. At $t = 14$, $\overline{\tau_{sf}}$ is equal to τ_{sf} obtained from the design methods UWA-05 and ICP-05. In UWA-13 and later on the unified method for piles in clay was used to estimate the fully equalised shaft friction (τ_{eq}). Lim & Lehane (2017) proposed a formula to estimate the shaft friction for partially equalised conditions after certain days after installation.

$$\overline{\tau_{sf}} = \max\left(0.4\tau_{eq}, 0.32\tau_{eq}\log\left(\frac{t}{{R_{eff}}^2}\right)\right) \tag{95}$$

In which the equalised shaft friction τ_{eq} is obtained from the design method for piles in clay in equation (63). It can be seen that when $t = 1350R_{eff}^2$, $\overline{\tau_{sf}}$ is equal to τ_{eq}. The minimum value for pile shaft friction in clay is 40% of the equalised shaft friction. The effective pile radius R_{eff} can be calculated with the pile dimensions as follows

$$R_{eff} = \sqrt{\frac{{D_0}^2 - PLR \cdot {D_i}^2}{4}} \tag{96}$$

The plug length ratio PLR is calculate by

$$PLR = \min\left(\left(\frac{D_i}{2.5}\right)^{0.2}, 1\right) \tag{97}$$

Usually plugging does not occur in large diameter piles during a dynamic load test and a full coring pile has a PLR equal to 1.

4.7 Friction fatigue

Friction fatigue, the progressive reduction in shaft resistance at a certain soil horizon upon penetration of the pile, for sandy soils is related to the relative penetration and the cyclic nature of pile driving. As for sand and clay, the shaft resistance of a driven pile depends on the in-situ soil conditions and complex stress changes that take place around the pile during driving and loading. Installation and loading of a driven pile can be divided into a number of different stages. Normally in sands, drainage is sufficient such that excess pore pressure generated during driving dissipates rather quickly. In contrast to piles in clay, an equalisation period is negligible and removes the need to wait for a period of set-up before piles can be loaded. As mentioned in Chapter 4.3 shaft friction is governed by Coulomb's law in which τ_{sf} is estimated from the horizontal effective stress at failure, σ'_{hf} and the pile-soil interface friction angle, δ (Randolph & Gourvenec, 2011). The horizontal effective stress at rest changes due to pile installation effects, friction fatigue and reloading to a horizontal effective stress at failure. The framework of the pile-soil behaviour at each stage is used in the unified method (Lehane et al., 2020).

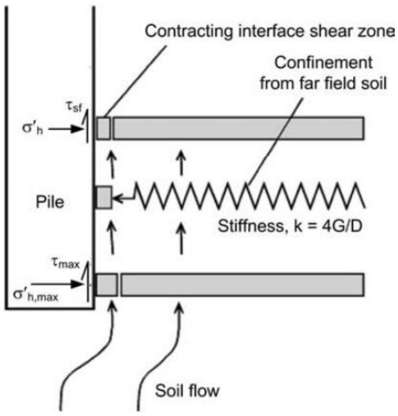

Figure 34: Friction fatigue mechanism *(White & Bolton, 2002)*

During installation the pile tip moves downwards and the stress level around a soil element rises significantly to push the soil radially outwards from the pile tip. As the soil passes the pile tip and reach the pile shaft the stress reduces behind the tip. The degree of radial displacement depends on the soil volume that has to displaced which is related to the pile diameter. In that way an open-ended pipe pile creates a smaller amount of radial displacement than a closed-ended pile. Large diameter pipe piles displace a minimal volume of soil compared to their gross area, leading to only a small increase of stress in the surrounding soil. An open-ended pile penetrating the soil in a plugged manner show similarities with a closed-ended pile. The pile effective area ratio takes into account the influence of the displaced soil for both shaft and end bearing capacity.

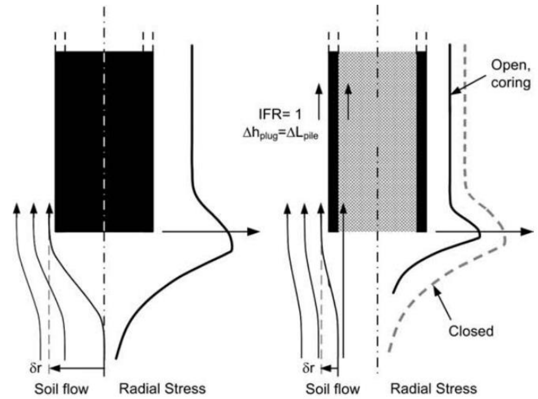

Figure 35: Streamlines of soil flow and radial stress development around the tip and shaft of a closed- and open-ended pile (White et al., 2005)

The more hammer blows, the more the soil is cyclically sheared back and forth. Cyclic shearing leads to a contraction of soil particles. Volume change causes relaxation in the surrounding soil cylinder causing unloading of the normal stress on the pile shaft. Relaxations leads a reduction in horizontal stress acting on the pile shaft. In Figure 36 this process of friction fatigue is shown. Friction fatigue leads to a reduction in unit shaft resistance once the distance between a certain soil horizon and pile tip increases.

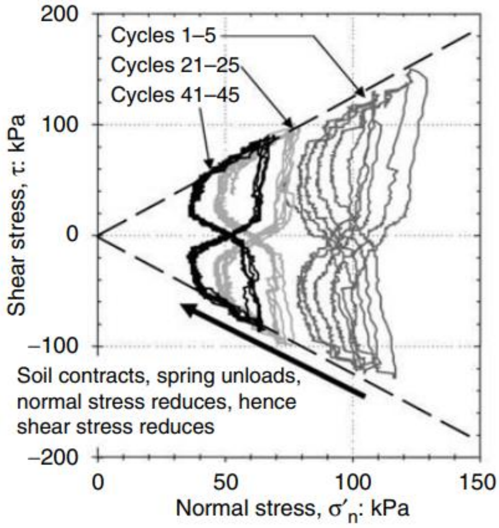

Figure 36: Friction fatigue modelled in a shear box test (de Jong et al., 2003)

In linear-elastic perfectly plastic modelling of the pile-soil interaction, the effective horizontal stress at failure divided by the spring stiffness results in the quake value. A quake value of 2.5mm is usually applied. This value is reasonable because a quick hammer blow must force the surrounding soil at the pile-soil interface to move under the effect of friction forces. The unit shaft friction at the interface between the contracting interface shear zone and the pile has to exceed to effective horizontal stress at failure, obtained from calculations by the unified methods in order to displace the pile permanently.

4.8 Residual loads

Residual loads can remain at the pile base after the complete removal of the installation load after reaching target penetration. Following a hammer blow the pile moving downwards and penetrates the soil. Subsequently the pile recovers partly in an upward movement with a rebound. A compression wave travels from the hammer along the pile shaft to the pile base. After reflection of the compression wave at the pile base, the pile tends to recover to its original length. The soil decompresses and the pile rebounds till it reach its final position (Lopes et al., 2011). An incomplete rebound from the soil at the pile base causes residual stresses and can lead to inaccurate interpretation of dynamic test results. Elastic soil behaviour at the pile base causing a rebound which adversely affects pile driveability and compilates bearing capacity assessment. The rebound induces a 'locked-in' compressive stress at the pile base which is balanced by negative skin friction at the upper pile of the pile shaft. The compressive stress generated by rebounding due to decompression of the soil beneath the pile base after unloading is the so-called residual loads ($q_{b,res}$). Residual loads can lead to a underestimation of the base resistance and an over-estimation of the shaft resistance in a compressive load test. Residual loads a typically in the range of 5% - 25% of the average cone resistance, $q_{c,avg}$ for closed-ended piles (Xu et al., 2008).

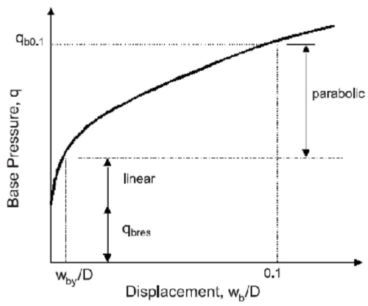

Figure 37: Idealized base load transfer curve (Gavin & Lehane, 2007)

Residual loads can be measured by reading off the strain values from strains gauges after removal of driving force. Test results in Figure 38 show the relevance of different pile cross sectional area on soil compaction around pile base, therefore residual loads for closed-ended piles are greater than for open-ended piles.

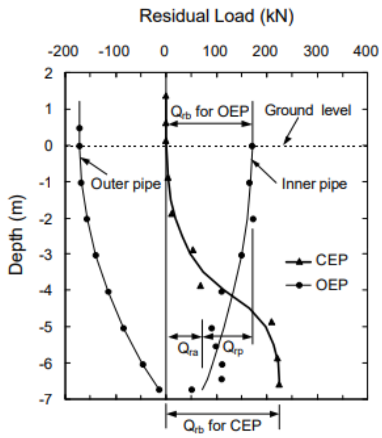

Figure 38: Load distribution curves for residual loads (Paik et al., 2004)

Residual loads do not affect the total bearing capacity of piles. The summation of residual forces must equal zero, but ignoring the effect of residual loads can lead to mispredictions of the contribution of shaft and base resistance on the total bearing capacity. In the TNO soil model the soil is modelled with linear elastic springs in which plastic deformation starts after the quake value has been reached. Figure 39 illustrates the case of no residual stress present at the pile base. The plastic deformation or final set at a certain pile level is the maximum displacement minus the quake value. During unloading, the elastic displacement reduces and becomes zero when the pile base is fully unloaded.

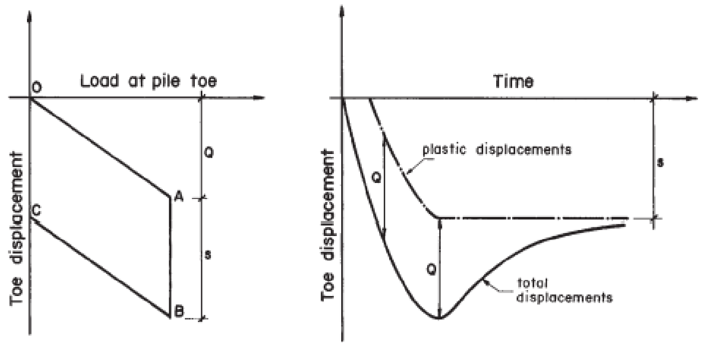

Figure 39: Load-displacement diagram at the pile base without residual stress (Lopes et al., 2011)

In case of residual stresses (Figure 40), the final base displacement is higher than the maximum displacement subtracted with the elastic displacement i.e. quake value. The reason for this difference is that a residual stress, locked in a compressive stress at the pile base during unloading at the pile base. During unloading the elastic displacement at the base reduces but does not reach a zero value after complete unloading of the pile after a hammer blow. In this situation, the plastic deformation is a sum of the plastic deformation that would occur in case of no residual stress and an elastic residual displacement. The elastic residual displacement can be calculated by dividing the residual stress by the unloading stiffness.

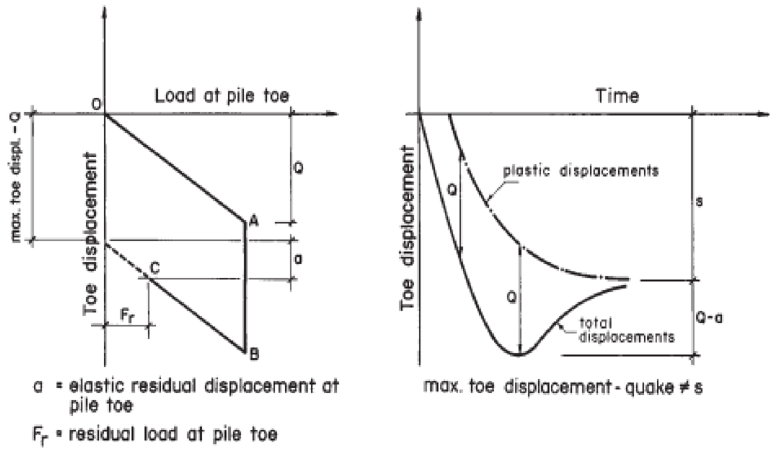

Figure 40: Load-displacement diagram at the pile base with residual stress (Lopes et al., 2011)

In reality one hammer blow produces successive loading and unloading cycles at the pile base. In Figure 41 a series of peaks and stress wave reflections at the pile base are shown. In signal matching the first loading and unloading cycle is most important in the analysis. If residual stresses are present at the pile base, a hammer blow what is in essence a reloading of the pile, does not change the yield stress of the soil at the pile base. Residual stresses influence the elastic displacement and reduces the retrieved quake value. In a dynamic load test it is difficult the determine the residual stress present at the pile base.

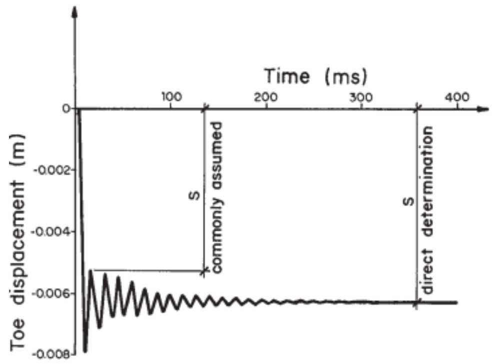

Figure 41: Pile base displacement over time during and after a hammer blow (Lopes et al., 2011)

In dynamic load testing and afterwards signal matching analysis, the magnitude of the residual stress not known beforehand and can only be deducted by outcomes of signal matching analysis. In case of negative shaft friction in the lower pile parts, the springs around the shaft are in tension. The relative high elastic displacement that the pile has to overcome to move from a state of tension to a state of compression to reach the compressive yield stress during reloading of the pile might indicate the presence of residual forces that leads to a higher loading quakes in the lower parts of the pile. A direct lock-in of residual stresses after a hammer blow, might be deduced if the unloading quakes are very low, meaning that the unloading phase cannot be fulfilled resulting in an incomplete rebound of the pile. Residual stress specifically at the pile base might be indicated be a relative low loading quake, because the pile base is already in a state of compression and needs a fraction of the default loading quake value to reach the yield stress, but a default loading quake value for the pile base is difficult to determine and the pile base quake varies per soil type and pile diameter. In equation (97) a quick approach is given to derive a compressive residual force F_r concentrated at the pile base, in which the difference between a default unloading quake value (U_{unl}) is subtracted with the derived unloading quake value ($U_{unl,der}$) from signal matching analysis is multiplied with the unloading stiffness of the soil. In case the derived unloading quake is equal to the default unloading quake the residual stress is zero.

$$\mathrm{F_r} = \mathrm{K_{unl}}\left(\mathrm{U_{unl}} - \mathrm{U_{unl,der}}\right) \tag{98}$$

Figure 42 shows two examples in which there are indications if residual loads are present. In case no residual loads are present, the assumptions is that the pile will rebound to its original shape after the hammer blow has dissipates and the final displacement of the pile head should be equal to the pile base. The upper chart in Figure 42 shows no deviation between the final pile head and base displacement. For comparison, the lower chart shows a difference in final pile head and base displacement indicating that residual loads might be present close to the pile base. Quantifying the residual loads present at the pile base is difficult in signal matching analysis, but it does not change the overall bearing capacity of the pile.

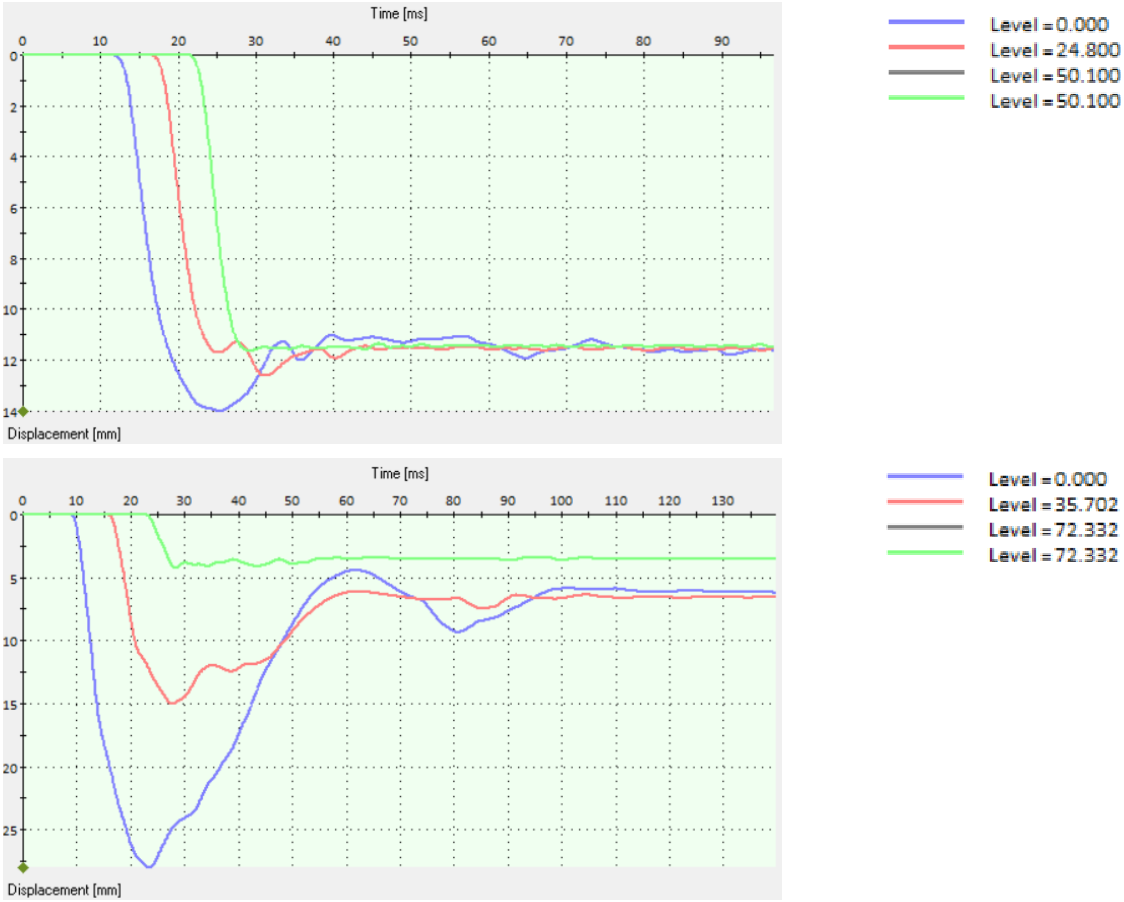

Figure 42: Examples of no indication (top) and a possible Indication of residual loads (bottom) present at the pile base

5. Analytical soil reaction models

The rapidly increase of stress wave measurements on pile foundations or deep foundations have led to many analytical soil reaction models for driveability studies in order to study the mobilized shaft and end-bearing resistance since the 1960's. Several wave equation analysis programs were developed (WEAP) and made use of the Smith soil model. The Smith model is simple and mathematically well founded. The input parameters for the model are straightforward and intensively ground investigation is not necessarily needed to establish these parameters. However the soil parameters in this model are empirical derived and not theoretically defined. Efforts to overcome this weakness of the Smith soil model are proposed by several researchers and based on better rheological soil models and appropriate soil parameters. Improved analytical soil reaction models make use of conventional geotechnical soil parameters for determining damping and stiffness. Chapter 5 outlines existing mechanical soil models that describes the dynamic behaviour for the soil-structure interface.

5.1 Shaft and base model by Smith (1960)

The first soil model that was used in numerical simulation of pile driving was the model proposed by Smith (1960). The soil resistance model is based on pile displacement (u) and pile velocity (v). The classic Smith model consist of a spring with a plastic slider in parallel with a dashpot (Figure 44). In the classic model the damping force depends on the static force. In general the soil shaft friction and total soil shaft resistance in the Smith model can be written as follows

$$\tau_s = \min(K_s \cdot u, \tau_{sf}) + \min(K_s \cdot u, \tau_{sf})\, J_s \cdot v \qquad (99)$$

$$R_t = R_s + R_s J_s \cdot v \qquad (100)$$

The magnitude for base friction and total base resistance occur in a similar manner by replacing the local ultimate shaft friction (τ_{sf}) to the limit bases stress (q_{bL}) and the Smith shaft damping factor (J_s) to a base damping factor (J_b) which varies per soil type. In the Smith model it is possible that the sustained shaft and base force is well above the static failure load due to the fact that the plastic slider is in series with the spring. This phenomena is often observed during pile driving because loading rates effects generates an addition force in the viscous dashpot. The Smith model give rise to some fundamental concern regarding to total soil resistance. The model calls into question if the damping force is linear proportional to static force, but investigation has shown that viscous damping is more a power function of pile velocity. The ultimate shaft friction (τ_{sf}) is determined from soil investigation. The soil stiffness K and global soil damping factor J are empirically determined parameters and are not based on fundamental soil properties, but obtained from experience and back-analysis for driven piles in different types of soils. This back-analysis is done by signal matching analysis. The soil stiffness, represented by the spring, can be calculated after the quake value (U_q) per soil layer is defined. The quake (in millimetres) is the pile displacement at which elastic limit is reached and perfectly plasticity starts, what occurs at the defined yield stresses in the TNO model. Once the plastic slider is active the spring force does not increase any further. The pile shaft soil stiffness ($\mathrm{kN/m^3}$) is calculated by the shaft quake ($U_{q,s}$)

$$K_s = \frac{\tau_{sf}}{U_{q,s}} \qquad (101)$$

The dashpot, representing the viscous damping force for the pile shaft is calculated by using an empirical damping parameter (J_s)

$$C_s = J_s \tau_{sf} \qquad (102)$$

The soil resistance at the pile base (q_b) is written in a similar manner as for the shaft ($q_{bf} = q_{bL}$).

$$q_b = \min(K_b \cdot u, q_{bf}) + \min(K_b \cdot u, q_{bf})\, J_b \cdot v \qquad (103)$$

The soil base stiffness and base damping coefficient are respectively

$$K_b = \frac{q_{bf}}{U_{q,b}} \tag{104}$$

$$C_b = J_b q_{bf} \tag{105}$$

The soil quake and damping coefficient are not fundamental soil parameters. In general a shaft quake of 2.5mm is often proposed, but the base quake can vary widely. Damping factors for clays and silts are generally higher than for sandy soils. Values for the dynamic soil parameters in the Smith model do not rely on strong correlation and show large scattering. Furthermore, Aoki and de Mello (1992) noticed that values for quake and damping also related to the hammer energy. Hanning et al. (1998) also stated that the damping factor can vary with time and higher dynamic parameters are appropriate for analysis in End of Initial Driving (EOD) to Beginning of Restrike (BOR). Advantages of the Smith soil model is that is simple and straightforward but has some limitations. In the soil model there is one lumped viscous soil damping coefficient and no distinction is made between viscous, radiation and hysteretic damping. In laboratory tests it has been shown that viscous soil damping is a power function of the static soil resistance and is not linear proportional as in the Smith soil model. However, due to increasing amount of dynamic pile measurements and quantitative analysis Weng and Sritharan (2013) concluded that:

1. Dynamic soil parameters are not constant along the pile depth, but vary for different soil types and properties. In cohesive soils at EOD, J_s increases with SPT N-values as Q_s decreases with SPT N-values. Empirical equations were developed to establish to quantify the dynamic soil parameters with SPT N-values (Figure 43).
2. In cohesionless soils at EOD, J_s decreases with SPT N-values, while Q_s increases with SPT-values.
3. Higher dynamic soil parameters for cohesive soils over time (EOD vs BOR) due to pile setup.
4. No clear relationship observed between CPT friction ratio and shaft quake.
5. No clear relationship was established between both SPT N-value or CPT values and dynamic soil parameters for the pile base.

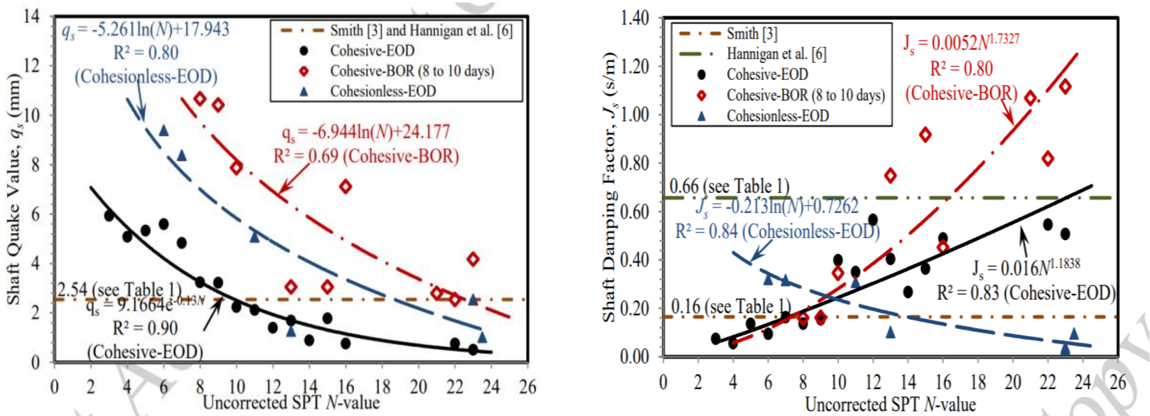

Figure 43: SPT N-value correlations for quake and damping *(Weng & Sritharan, 2018)*

A summary of empirical relationships for shaft dynamic soil parameters based on SPT and CPT results and the associated coefficient of determination (R^2) is given in Table 6. A high degree of scatter is observed at BOR probably due to complexity of pile setup. Uncorrected SPT N-values include the effect of overburden soil in the correlation analysis (Weng & Sritharan, 2018).

In-situ Soil Test	Soil type	EOD/ BOR	Parameter	Unit	Relationship	R^2
SPT	Cohesive	EOD	J_s	s/m	$J_s = 0.16N^{1.1838}$	0.83
	Cohesive	EOD	Q_s	mm	$Q_s = 9.1664e^{1.1838 \cdot N}$	0.90
	Cohesive	BOR	J_s	s/m	$J_s = 0.0052N^{1.7327}$	0.80
	Cohesive	BOR	Q_s	mm	$Q_s = -6.944\ln(N) + 24.177$	0.69
	Cohesionless	EOD	J_s	s/m	$J_s = -0.213\ln(N) + 0.7262$	0.84
	Cohesionless	EOD	Q_s	mm	$Q_s = -5.261\ln(N) + 17.943$	0.80
CPT	Dense clay (N>9)	EOD	J_s	s/m	$J_s = -0.286\ln(F_r) + 0.8426$	0.64
	Soft clay (N≤9)	EOD	J_s	s/m	$J_s = 0.08$	-
	Dense silt (N>9)	EOD	J_s	s/m	$J_s = -0.286\ln(F_r) + 0.8426$	0.64
	Soft silt (N≤9)	EOD	J_s	s/m	$J_s = 0.08 - 0.30$	-
	Sand	EOD	J_s	s/m	$J_s = 0.10 - 0.30$	-
	All soils	EOD	Q_s	mm	$Q_s = 0.2 - 8.4$	-

Table 6: Suggested empirical relationships between SPT/CPT and shaft dynamic soil parameters

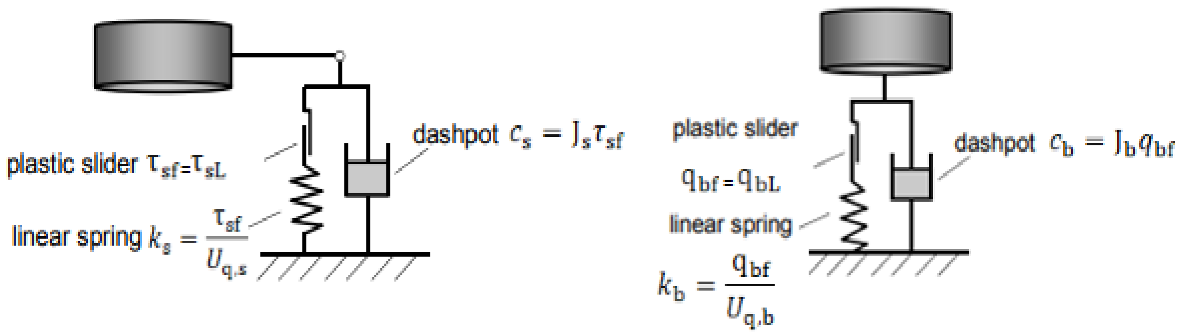

Figure 44: Smith soil model for shaft (left) and base (right)

Suggested and commonly used dynamic soil properties proposed by Coyle et al. (1973) and Hannigan et al. (1998) are listed in Table 7.

Reference	Soil type	Damping factors [s/m]		Quake values [mm]	
		Shaft (J_s)	Base (J_b)	Shaft (Q_s)	Base (Q_b)
Smith (1960)	All	0.16	0.49	2.54	2.54
Coyle et al. (1973)	Clay	0.66	0.03	2.54	2.54
	Sand	0.16	0.49	2.54	2.54
	Silt	0.33	0.49	2.54	2.54
Hannigan et al. (1998)	Cohesive soil	0.66	0.49	2.54	D/120 (dense and hard soil)
	Cohesionless soil	0.16	0.49	2.54	D/60 (soft soil)

Table 7: Dynamic soil properties

Liang (2000) conducted a statistic analysis with CAPWAP signal matching results on 611 driven piles. The analysis resulted in values for EOD and BOR for both sand and clay soils. Results show that quakes varies minimally with soil type and timeframe within the dynamic test compared to soil damping.

Soil type	Parameter	Statistical summary	EOD	BOR
Sand	J_s	Mean	0.53	0.67
		Standard Deviation	0.53	0.53
	Q_s	Mean	3.0	3.0
		Standard Deviation	4.6	3.8
Clay	J_b	Mean	0.43	0.73
		Standard Deviation	0.40	0.53
	Q_b	Mean	2.8	3.0
		Standard Deviation	1.3	1.5

Table 8: Statistically obtained values (Liang, 2000)

Fellenius and Massarsch (2008) argued that the damping factor at the pile base is not solely related to soil properties, but also on dynamic properties of both the soil and the pile.

$$J_b = 2\frac{Z_P}{Z^P} = 2\frac{A_t^P c_P \rho_s}{A^P c^P \rho^P} \tag{106}$$

In which A_t^P is the contact cross sectional area of the pile base, c_P the P-wave velocity in the soil, ρ_s the soil density, A^P pile cross sectional area above the pile base, c^P P-wave velocity in the pile and ρ^P the density of the pile. In case of an open-ended pipe pile $A_t^P = A^P$, however for and closed-ended pipe pile this is not the case, because the area of the shaft closely to the base is lower.

5.2 Base model by Lysmer (1965)

Lysmer (1965) investigated the dynamic behaviour of a rigid circular footing resting on a homogeneous linear elastic half-space which is subjected to a steady-state vertical oscillation. The steady-state solution can be used to describe the response of the pile base to a transient pulse-type vertical loading i.e. impact force (Lysmer, 1965). The model stated that a single degree of freedom system (one spring and one damper) can reproduce the harmonic behaviour of a rigid footing subjected to vertical time dependent force. In the new analogy the spring and dashpot are independent of the frequency of the vibration. The spring stiffness of a rigid circular foundations is written as:

$$K_b = \frac{4G_{max}r_0}{1 - v_s} \tag{107}$$

Lysmer's base model uses the Boussinesq's theory for the spring stiffness. In Figure 47 a linear approach of the load-pile base displacement envelop is shown with the initial slope equal to the spring stiffness given by Lysmer (1965).

In case of a non-circular footing, the equivalent pile radius is used $\left(r_0 = \sqrt{A/\pi}\right)$. The radiation damping constant is given by:

$$C_b = \frac{3.4r_0^2\sqrt{\rho_s G_{max}}}{1 - v_s} \tag{108}$$

The dashpot represents radiation or geometric damping in Lysmer's model. Due to wave propagation of shear, Rayleigh and compressive waves into the elastic subsoil, all footings-soil systems are strongly damped and radiation damping gives a higher loss of energy out of the mechanical system than damping by material damping or viscous damping. Lysmer reduced the problem of determining the vertical motion of a footing-soil system into a problem of determining the motion of a simple damped oscillator defined by the following equation of motion:

$$m \cdot a + \frac{3.4r_0^2\sqrt{\rho_s G_{max}}}{1 - v_s} \cdot v + \frac{4G_{max} r_0}{1 - v_s} \cdot u = Q(t) \tag{109}$$

Soils are elastic in the small strain domain and therefore the small strain shear modulus (G_{max}) is used, although cyclic loading and strain amplitude varies with distance from the pile head to the pile base due to energy loss along the pile shaft by friction and damping thus changing shear modulus. In order to set a limit to the elastic deformation a plastic slider represent the pile displacement at which plasticity starts. The static force exerted by the spring does not increase any further and has reached the limit base friction of the soil and only damping forces can increase the soil resistance. Figure 46 visualizes Lysmer's model in which the radiation dashpot is always active. The equations for spring stiffness and damping at the pile base proposed by Lysmer (1965) are mainly applicable for closed-ended pipe piles or solid concrete piles. In the offshore industry open-ended pie piles are mainly used. For simplicity the radius r_0 can be changed into the equivalent radius R^*. A similar equation for spring stiffness is given by Egorov (1965)

$$K_b = \frac{2G_{max} r_0}{(1 - v_s)\Omega(\eta)} \tag{110}$$

In which $\Omega(\eta)$ is a function of the ratio of the inner to outer radius of the pile, defined as $\eta = \frac{r_i}{r_0}$ with values given in Figure 45, reaching a value for η close to 0.65 for large diameter offshore piles. The damping coefficient for a pipe pile is approximated by Gazetas and Dobry (1984) and is given by

$$C_b = \frac{3.4(r_0^2 - r_i^2)\sqrt{\rho_s G_{max}}}{1 - v_s} \tag{111}$$

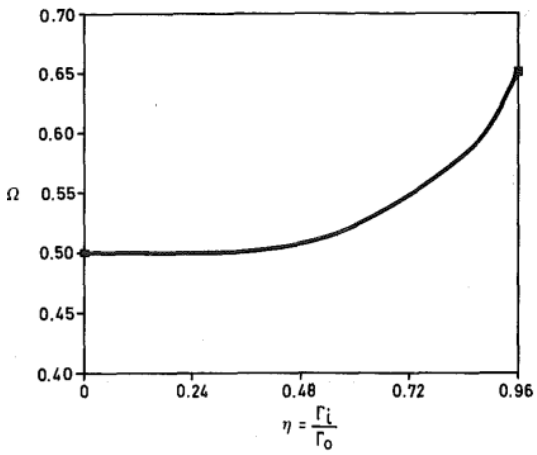

Figure 45: Variation of function Ω(η) with the ratio of inner to outer pile radius (Gazetas et al., 1985)

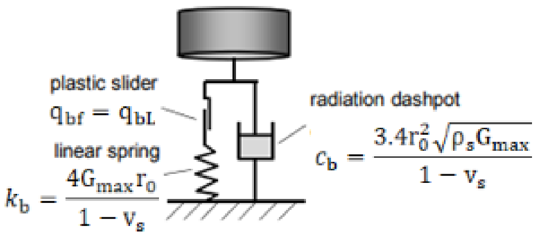

Figure 46: Base model from Lysmer's analogy

From the static stiffness by Lysmer (1965) there can be made a simple analogy with the base quake in millimetres, in which the mobilized base resistance is used (q_{bf})

$$U_{q,b} = \frac{q_{bf}}{K_b} = \frac{q_{bf}}{\frac{4G_{max} r_0}{1 - v_s}} \tag{112}$$

Due to its simplicity Lysmer's analogy and the use of G_{max} the base stiffness is often overestimated. Furthermore it is not directly suitable for heterogeneous and non-linear soils, only if secant shear modulus G_{sec} is applied in combination with a certain strain amplitude.

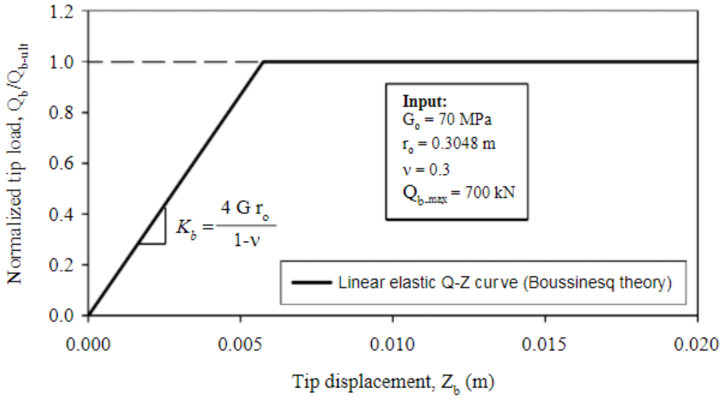

Figure 47: Pile base stiffness based on Lysmer's approach

5.3 Shaft model by Holeyman (1985, 1988)

The soil reaction model by Holeyman (1985, 1988) is based on the linear elastic behaviour of the shaft friction and rest on the fundament analysis of an embedded cylinder in a semi-infinite medium (Randolph & Wroth, 1978). The static model by Holeyman was improved by making use of a hyperbolic non-linear stress-strain relation for the static case (Randolph & Wroth, 1978). Randolph and Wroth (1978) assumed that the pile is rigid and shaft displacement is the integral of angular distortions of concentric cylinders surrounding the pile. The soil elastic medium was divided into a half space taking care of the pile base resistance and one layer taking care of the pile shaft friction (Figure 48). Holeyman (1985) extended the model for de dynamic case by proposing shaft friction that consist of a non-linear spring (hysteretic damping), a viscous dashpot and a radiation dashpot all connected in parallel (Figure 51). When the sum of all the forces has reached the slider strength (τ_{sL}), which is equal to the ultimate shaft friction in static loading (τ_{sf}) plus viscous damping, the slider becomes active what results in slippage between the pile shaft and soil.

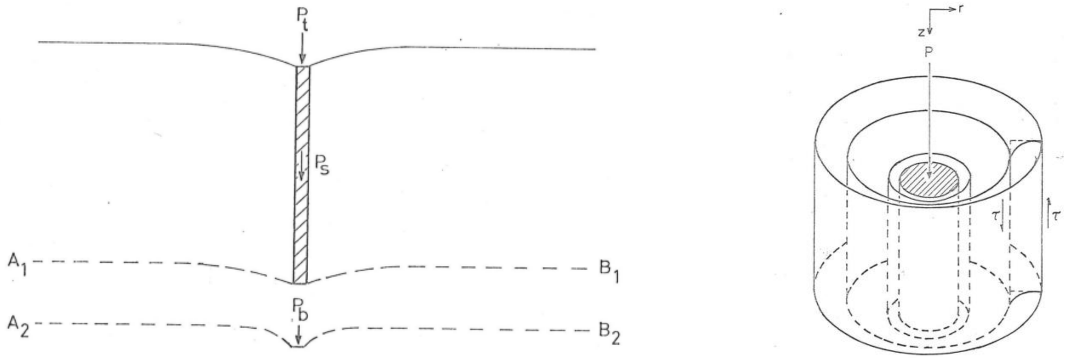

Figure 48: Uncoupled model Randolph and Wroth (1978)

The displacement of the pile as function of the shear stress (τ_s) in the static case is written by Randolph and Wroth (1978) as follows:

$$\tau_s = \frac{G_{max} \cdot u}{r_0 \ln\left(\frac{r_m}{r_0}\right)} \tag{113}$$

The obtained soil secant stiffness along the shaft becomes then:

$$K_s = \frac{\tau_s}{u} = \frac{G_{max}}{r_0 \ln\left(\frac{r_m}{r_0}\right)} \tag{114}$$

In which r_m is the empirical pile influence radius. Beyond r_m it is assumed that the shear stress becomes negligible (Cooke, 1974). When variation of r_m with depth is ignored (Figure 49) and an averaged value is taken, r_m becomes

$$r_m = 2.5L(1 - v_s) \tag{115}$$

In case of heterogeneous soil profile the equation of r_m can be extended by (Fleming et al. 1992):

$$r_m = \left(0.25 + \left(2.5(1 - v_s)\frac{G_{max,L/2}}{G_{max,L}} - 0.25\right)\frac{G_{max,L}}{G_{max,b}}\right)L \tag{116}$$

In which $G_{max,L/2}$, $G_{max,L}$ and $G_{max,b}$ are respectively the shear modulus halfway the pile, immediately above the bearing layer and of the bearing layer. The parameter r_m can be considered as a sort of pile movement to strain ratio.

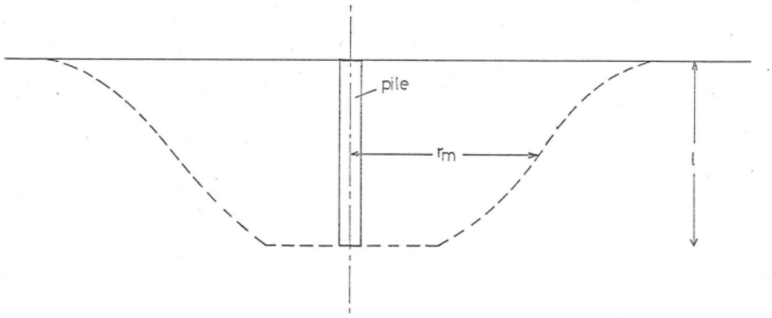

Figure 49: Hypothetical variation of r_m in the influence zone of the pile shaft (Randolph, 1977)

Figure 50 shows the linear elastic perfectly plastic t-z curve according to Randolph and Wroth (1978). The equation can be extend for the dynamic case by including viscous damping ($C_{s,V}$) and radiation damping ($C_{s,R}$). According to Holeyman (1988) the total soil resistance becomes

$$\tau_s = \frac{G_{max}}{r_0 \ln\left(\frac{r_m}{r_0}\right)}(1 + J_s \cdot v^n) \cdot u + \frac{G_{max}}{V_s} \cdot v \leq \tau_{sL} \tag{117}$$

The values for J and n are similar input parameters as used respectively in Smith (1960) and Simons and Randolph (1985).

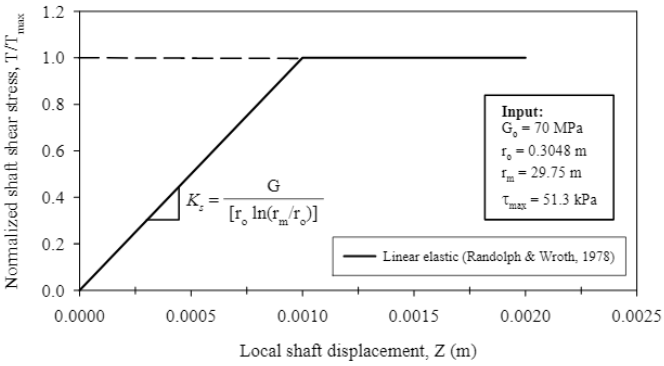

Figure 50: Soil stiffness static case (Randolph and Wroth, 1978)

Kondner (1963) proposed a functional form based on hyperbolic law to describe the stress-strain characteristics of soils, which was further improved by Duncan & Chang (1970) for static and quasi-static behavior of soil.

The stress-strain curves approximated in the hyperbolic form for soil during shear is given in equation (117).

$$\tau_s = \frac{u}{\frac{1}{G_{max}} + \frac{u}{\tau_{sL}}} \tag{118}$$

Holeyman (1988) adapted the hyperbolic function for the shaft displacement by a iterative process.

$$\tau_s = \frac{G_{max}}{r_0 \ln\left(\frac{\frac{r_m}{r_0} - \frac{\tau_s}{\tau_{sf}}}{1 - \frac{\tau_s}{\tau_{sf}}}\right)} (1 + J_s \cdot v^n) \cdot u + \frac{G_{max}}{V_s} \cdot v \tag{119}$$

Holeyman (1988) stated that hysteretic damping depends on the stress path and is therefore not associated with pile velocity. Nonlinear springs represent the nonlinear soil model in which a hyperbolic function relates the shaft shear stress to the pile displacement.

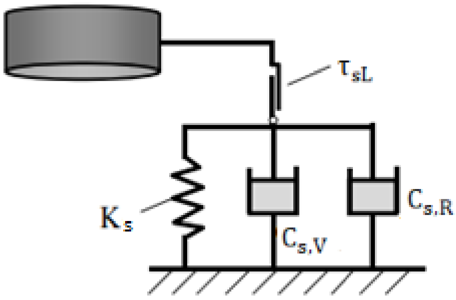

Figure 51: Shaft model (Holeyman, 1985)

The strength of the plastic slider depends on both a static component and a viscous component based on the rate of loading as in Randolph and Simons (1986). A value of $n = 0.2$ is commonly used. The strength of the plastic slider is the sum of the static resistance and the viscous damping using Smith empirical damping factor J. Pile penetration occurs when $\tau_s > \tau_{sL}$ with an active plastic slider.

$$\tau_{sL} = \tau_{sf}(1 + J_s \cdot v^n) \tag{120}$$

Faley and Carter (1993) and Faley et al. (1994) observed a much faster rate of shear modulus degradation for normally and over consolidated sands than suggested by the hyperbolic model of Kondner (1963). Randolph (1994) pointed out that the secant shear modulus of soils rapidly decays with increasing shear stress. To capture this faster degradation of the secant shear modulus with respect to the initial shear modulus (G_{max}), Faley and Carter (1993) proposed a modified hyperbolic model.

$$u = \frac{\tau_s r_0}{G_{max} g} \ln\left(\frac{\left(\frac{r_m}{r_0}\right)^g - f\left(\frac{\tau_s}{\tau_{sf}}\right)^g}{1 - f\left(\frac{\tau_s}{\tau_{sf}}\right)^g}\right) \tag{121}$$

In which f and g are empirical curve fitting parameters. The same modified hyperbolic model could be applied at the pile base. The hyperbolic model is expressed as (Chow, 1986)

$$u = \frac{q_b(1 - v_s)}{4G_{max} r_0 \left(1 - f\left(\frac{q_b}{q_{bf}}\right)^g\right)} \tag{122}$$

Values for f ranges from 0.9 to 1 and g can be taken 0.25 for natural soils and 0.7 to 1 for remoulded soils (Fahey & Carter, 1993) . Comparing a non-linear hyperbolic analysis with an equivalent linear analysis the secant shear modulus at one-third of the maximum shear strength can be used (Randolph & Wroth, 1978).

$$G_{1/3} = G_{max}(1 - \frac{R_f}{3}) \tag{123}$$

In which R_f is an empirical constant which is the ratio between the failure shear stress and the asymptotic shear strength. Values for R_f ranges from 0.5 and 1.0.

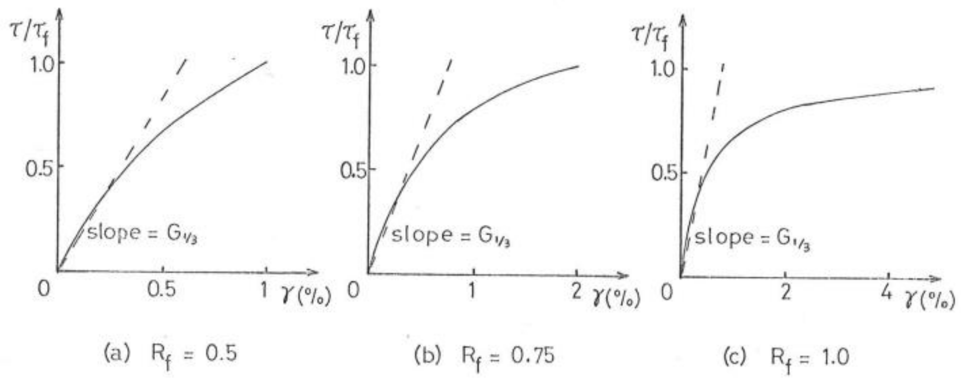

Figure 52: Hyperbolic shear stress-strain curves with different R_f

As shown in Figure 53, the linear elastic perfectly plastic model, conventional hyperbolic model and modified hyperbolic model have the same initial stiffness, but the proposed model by Fahey and Carter (1993) degrades at a much faster rate than the conventional hyperbolic model (Pando et al., 2006).

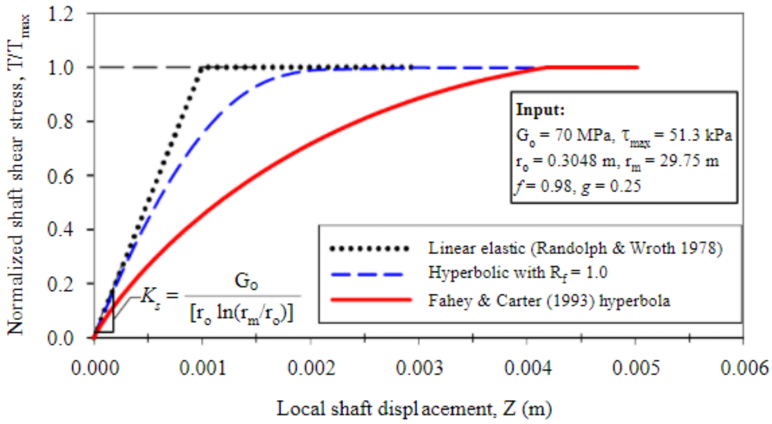

Figure 53: Theoretically derived T-Z curve using concentric cylinders, and the modified hyperbola from Fahey and Carter (1993)

5.4 Shaft model by Simons and Randolph (1985)

The proposed model by Simons and Randolph (1985) can be divided into two parts connected in series (Figure 54). The first part represent a narrow zone in which slippage, plasticity and large deformation occurs and representing the ultimate shaft resistance and viscous damping with a non-linear relationship with pile velocity (Gibson & Coyle, 1968). The second part is beyond the narrow zone and behaves elastically representing radiation damping in outer field. The first part consist of a plastic slider and a viscous dashpot in parallel. The dashpot represent viscous damping and considers the loading rate effect and is related to the mobilized static resistance. The plastic slider has a strength equal to the local ultimate shaft friction (124) and only slippage occurs when the mobilized static shear stress in the system is larger than the local ultimate shaft friction ($\tau_s \geq \tau_{sf}$). The viscous dashpot is only activated when the strength of the plastic slider has been exceeded and pile displacement and thus a velocity dependent force is generated by the viscous dashpot. The stress development in the upper system (τ_{s1}) is given by equation (126) in which the total shaft resistance is sum of static resistance (τ_{sf}) and a strength gain due to viscous rate effects (τ_{visc}).

$$\tau_{sL} = \tau_{sf} \tag{124}$$

$$\tau_{visc} = m_s \cdot v^{n_s} \tag{125}$$

$$\tau_{s1} = \tau_{sf} + m_s \tau_{sf} \cdot v^{n_s} \tag{126}$$

In which m_s and n_s are input parameters for the viscous dashpot and representing the rate effect. A value for the exponent n_s ranges from 0.2 to 0.5 for all soils and m ranges from 0.3 to 0.5 for sands and 2.0-3.0 for clays. Several researchers came up with values for m and n after laboratory experiments for both shaft and base for piles in clay and sand. Dayal and Allen (1975) and Heerema (1979) did not observe any rate effects on the interface between steel and sand.

Reference	Soil type	$\mathrm{m_s}$	$\mathrm{m_b}$	$\mathrm{n_s}$	$\mathrm{n_b}$
Flemming (1958)	Sand	0.25		0.12	
Coyle & Gibson (1970)	Sand	0.34-0.56	0.34-0.56	0.18-0.26	0.18-0.26
	Clay	0.95-1.55	0.95-1.55	0.11-0.25	0.11-0.25
Dayal & Allen (1975)	Sand	1	1	1	1
	Clay	0.93	0.49	0.34	0.23
Heerema (1979)	Sand	1	1	1	1
	Clay	0.6-1.9		0.2	
Litkouhi & Poskitt (1980)	Clay	0.78-2.1	0.44-1.0	0.16-0.57	0.17-0.37
Randolph (2003)	All soil types			0.2	0.2
Brown (2004)	Clay	1.26		0.34	

Table 9: Proposed values for $\mathbf{m}$ and $\mathbf{n}$ after several experiments

Values for $\mathrm{m_b}$ and $\mathrm{n_b}$ are applicable to the Deeks and Randolph (1995) soil base model in Chapter 5.7. Lee et al. (1988) collected all the experimental data from previous researchers and found relatively good correlation between the shear strength of the soil and the parameters $\mathrm{m_s}$ and $\mathrm{m_b}$. The empirical parameters $\mathrm{m_s}$ and $\mathrm{m_b}$ are lower for stiff and high strength soils. Lee et al. (1988) proposed a value for both $\mathrm{n_s}$ and $\mathrm{n_b}$ of 0.2 and independently of soil type. Values for $\mathrm{m_s}$ and $\mathrm{m_b}$ can be calculated by the following correlation for clays

$$\mathrm{m_s} = 1.65 - 0.75\left(\frac{\tau_{\mathrm{sf}}}{\mathrm{P_{atm}}}\right) \tag{127}$$

$$\mathrm{m_b} = 1.2 - 0.63\left(\frac{\tau_{\mathrm{sf}}}{\mathrm{P_{atm}}}\right) \tag{128}$$

And for sands the following correlation

$$\mathrm{m_b} = 1.5 - 0.083(\varphi - 30°) \tag{129}$$

In which φ is the peak friction angle of sand. The multiplier $\mathrm{m_s}$ could be ignored according to Lee et al. (1988) and set to 1. In general, $\mathrm{m_b}$ is lower than $\mathrm{m_s}$ for piles in clay, indicating that the pile shaft is more subjected to rate effects than the pile base. Furthermore, both values are higher in clays than in sands because of the higher viscosity and plasticity of clays compared to sands. The parameters $\mathrm{m_s}$ and $\mathrm{m_b}$ are similar to the Smith global damping factors $\mathrm{J_s}$ and $\mathrm{J_b}$, with the difference that loading rate is highly nonlinear and better fits with measured soil stresses in the field during driving using a power law on the pile velocity. On top of that, most research propose values for $\mathrm{n_s}$ and $\mathrm{n_b}$ of 0.2 for all soil types.

The second part consist of a spring and a dashpot in parallel. The spring is related to the purely elastic behaviour and the dashpot represent radiation damping. The second part represent the soil outside the shearing zone which has not reached a fully plastic state and remains elastic. Novak et al. (1978) derived an analytical solution for the soil reaction on the shaft of a vertical vibrating rigid pile assuming a thin elastic soil disk acting on a harmonically oscillating pile shaft.

$$\tau_{\mathrm{s2}} = (\mathrm{K_s} + \mathrm{iC_s}) \cdot \mathrm{u} = \frac{\mathrm{G_{max}}}{2\pi \mathrm{r_0}}(\mathrm{S_{\omega 1}} + \mathrm{iS_{\omega 2}}) \cdot \mathrm{u} \tag{130}$$

The terms $S_{\omega 1}$ and $S_{\omega 1}$ are functions of a dimensionless frequency $a_0 = \frac{\omega r_0}{V_s}$ with angular frequency ω of a vibrating pile. Simons and Randolph (1985) found that $S_{\omega 1}$ and $S_{\omega 1}$ can be approximated by respectively π and $2\pi a_0$. The simplified spring constant k_s and dashpot constant c_s can be written as

$$K_s = \frac{\pi G_{max}}{2\pi r_0} \tag{131}$$

$$C_s = \frac{G_{max}}{V_s} \tag{132}$$

$$\tau_{s2} = \frac{\pi G_{max}}{2\pi r_0} \cdot u + \frac{G_{max}}{V_s} \cdot v \tag{133}$$

In the case that the sum of the resistances in the second part of the mechanical system do not exceed the local ultimate shaft friction, represented by the plastic slider, the soil and pile move together. However, when the mobilized resistance is larger than the local ultimate shaft friction, slippage occurs between the thin interface shear band around the pile shaft and the outer field. Slippage is controlled by the plastic slider and the viscous dashpot. A disadvantage of this model is that hysteretic damping is not considered into the formulation.

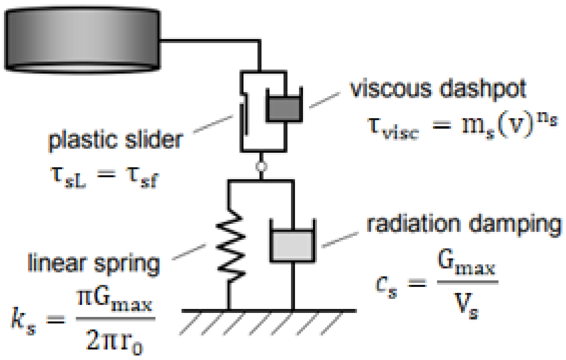

Figure 54: Shaft model proposed by Randolph and Simons (1986)

In 1985, Randolph and Simons used the soil reaction model at the pile base proposed by Lysmer (1965).

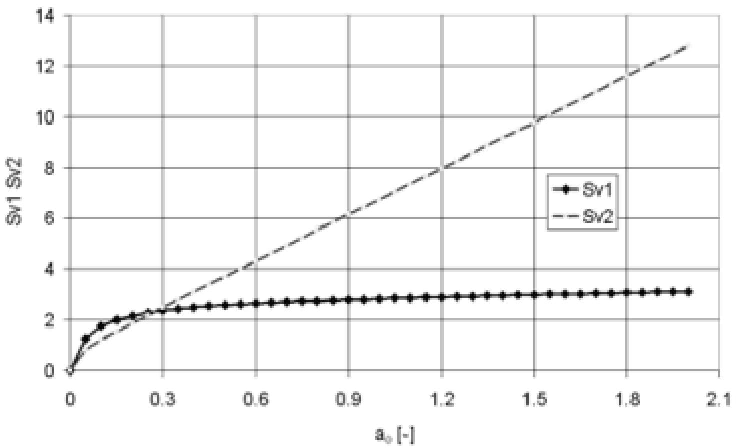

Figure 55: Parameters $S_{\omega 1}$ and $S_{\omega 1}$ of a homogenous elastic soil medium under plane strain conditions (Novak et al., 1978)

5.5 Shaft and base model by Nguyen et al. (1988)

Nguyen et al. (1988) proposed a similar set up for a soil model in terms of springs and dashpots for the shaft resistance as in the soil model by Holeyman (1985). The shaft model has one adaptation compared to Holeyman (1985), whereby the plastic slider is not connected in series with the spring and all the dashpots, but only connected with the spring ($\tau_{sL} = \tau_{sf}$). The setup of the base model is identical to the shaft model. The shaft stiffness and radiation damping ($C_{s,R}$) are the same as in Randolph and Simons (1986) in equation (131) and (132). The radiation damping at the base ($C_{b,R}$) is equal to Lysmer's analogy and disjoints from the system when τ_{sf} or q_{bf} is reached. In addition to all, a second dashpot is added and combines the hysteretic damping and viscous damping in the soil and regroups it into one hysteretic dashpot ($C_{s,H}$ and $C_{b,H}$). The hysteretic dashpot considers energy loss due to interparticle shearing (hysteresis) and the viscous dashpot the loading rate effects. Only pile velocity is used in the model and does not take the relative velocity between pile and soil into account. Hysteretic damping in the model is derived from the radiation damping constant multiplied with a relevant damping ratio.

$$C_{s,H} = \zeta_s \frac{G_{max}}{V_s} = \zeta_s C_{s,R} \tag{134}$$

$$C_{b,H} = 4r_0\zeta_b \cdot \left(\frac{\pi G_{max} L \rho_p}{1 - v}\right) \tag{135}$$

In which ζ_s and ζ_b are the damping ratios for the shaft and base (Hardin & Drnevich, 1972). In the soil model the soil shear modulus varies with shear strain amplitude, using a relationship derived by Hardin and Drnevich (1972). L is the pile length, G_{sec} is the shear modulus for a certain strain amplitude and ρ_p is the pile material density. The radiation damping for the pile shaft and base are given by

$$C_{s,R} = \frac{G_{max}}{V_s} \tag{136}$$

$$C_{b,R} = \frac{3.4 r_0^2 \sqrt{\rho_s G_{max}}}{1 - v_s} \tag{137}$$

Viscous damping is merely based on the empirical parameter and can be written in terms of Smith damping factor, spring stiffness and quake values as (Table 6 & Table 7) and adds up to the plastic slider strength.

$$\begin{aligned} C_{s,V} &= \tau_{sf} J \cdot v^n \\ C_{b,V} &= q_{bf} J \cdot v^n \end{aligned} \tag{138}$$

The effect of viscous damping is sometimes also incorporated in the hysteretic dashpot by increasing the damping ratio ζ (Poulos et al., 2000). In the hysteretic dashpot at the pile base the maximum shear modulus is replaced by the secant shear modulus. The secant shear modulus can be calculated by

$$\frac{G_{sec}}{G_{max}} = \frac{1}{1 + \gamma_h} \tag{139}$$

With γ_h representing the hyperbolic strain

$$\gamma_h = \frac{\gamma}{\gamma_r}\left(1 + ae^{-b\left(\frac{\gamma}{\gamma_r}\right)}\right) \tag{140}$$

In which γ_r is the reference strain,

$$\gamma_r = \frac{\tau_{max}}{G_{max}} \tag{141}$$

and γ the strain amplitude:

$$\gamma = \frac{V_p}{V_s} = \frac{V_p}{\left(\frac{G_{max}}{\rho}\right)^{0.5}} \tag{142}$$

A simplified approach of the strain amplitude is based on the average velocity V_p of a pile element and the shear wave velocity V_s in the soil (Nguyen et al., 1988). The pile velocity is obtained from the numerical solution of the one dimensional stress wave in piles (Chapter 2) and shear wave velocity is based on soil stiffness properties (Chapter 4).

The two curve fitting parameters a and b are soil type dependent and varies with blow count number (N) during pile driving.

Soil type	Value of a	Value of b
Clean dry sand	-0.5	0.16
Clean saturated sands	$-0.2\log(N)$	0.16
Saturated cohesive soils	$1 + 0.25\log(N)$	1.3

Table 10: Values of soil constant a and b for hyperbolic shear strain γ_h related to shear modulus (Hardin & Drnevich, 1972b)

The damping ratio ζ used in the formulation of the hysteretic damping is related to the shear modulus by

$$\frac{\zeta}{\zeta_{max}} = \frac{\gamma_h}{1 + \gamma_h} \tag{143}$$

The values a and b in γ_h in the damping ratio formulation are calculated as follows:

Soil type	Value of a	Value of b
Clean dry sand	$0.6N^{-\frac{1}{6}} - 1$	$1 - N^{-\frac{1}{12}}$
Clean saturated sands	$0.54N^{-\frac{1}{6}} - 0.9$	$0.65 - 0.65N^{-\frac{1}{12}}$
Saturated cohesive soils	$1 + 0.2\sqrt{f}$	$0.2f[e^{-\bar{\sigma}'_0}] + 2.25\bar{\sigma}'_0 + 0.3\log(N)$

Table 11: values of soil constant a and b for hyperbolic shear strain γ_h related to damping ratio (Hardin & Drnevich, 1972b)

In which f is the frequency of the blow counts and $\bar{\sigma}'_0$ is the mean effective stress. The mean effective stress can be calculated by using the coefficient of lateral earth pressure K_0.

$$\bar{\sigma}'_0 = \frac{\sigma'_v + 2\sigma'_h}{3} = \frac{\sigma'_v + 2K_0\sigma'_v}{3} = \frac{\sigma'_v + 2\left(\frac{v_s}{1 - v_s}\right)\sigma'_v}{3} \tag{144}$$

The maximum damping ratio ζ_{max} is soil and stress state dependent and decreases with increasing blow count number.

Soil type	Value of ζ_{max}
Clean dry sand	$33 - 1.5\log(N)$
Clean saturated sands	$28 - 1.5\log(N)$
Saturated cohesive soils	$31 - (0.3 + 0.003f)\sqrt{\bar{\sigma}'_0} + 1.5\sqrt{f} - 1.5\log(N)$

Table 12: Maximum damping ratio for different types of soils (Hardin & Drnevich, 1972b)

The shear strain during pile driving exceeds the limits of the small strain domain and therefore the damping ratio increases significantly by a rapidly decreasing shear modulus. To incorporate the damping ratio into hysteretic damping, the initial maximum damping ratio is used as shown in Table 12. The damping ratio for cohesionless and cohesive soils are taken respectively as $\zeta_{max} = 28\%$ and $\zeta_{max} = 31\%$.

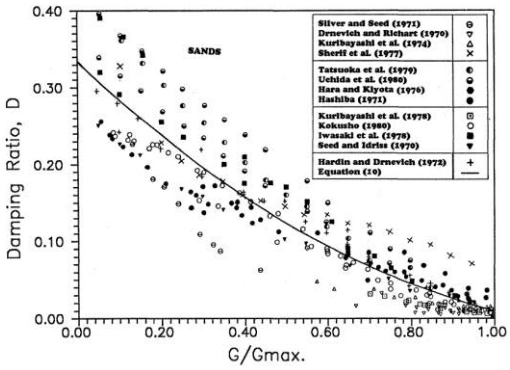

Figure 56: Damping ratio versus G/G_{max} for sands

Figure 56 shows that the damping ratio as function of the normalized shear modulus. As $\frac{G}{G_{max}}$ tends to zero, the hysteretic damping ratio increases. A relative stiff soil will exhibits very low damping or energy dissipation when subjected to dynamic loads.

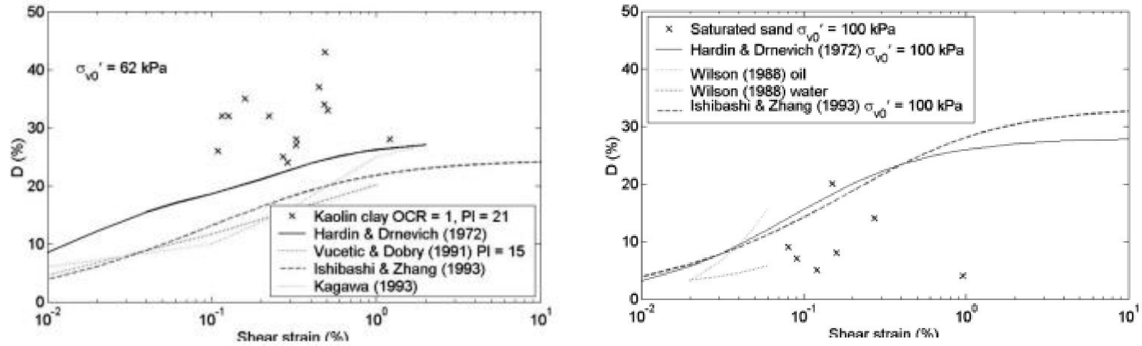

Figure 57: Damping ratio versus shear strain for NC clays and sand (Brennan et al., 2005)

The spring stiffness for the shaft is the same as in the model of Simons and Randolph (1985), but the secant shear modulus is considered to account for soil non linearity

$$K_s = \frac{\pi G_{sec}}{2\pi r_0} \tag{145}$$

The spring stiffness for the base is the same as in the model of Lysmer (1965)

$$K_b = \frac{4 r_0 G_{sec}}{1 - v_s} \tag{146}$$

The generalized total soil resistance during dynamic loading for the shaft and base are respectively:

For $\tau_s < \tau_{sf}$ (or q_{bf})

$$\tau_s = \min\,(K_s \cdot u, \tau_{sf}) + (C_V + C_H + C_R) \cdot v \tag{147}$$

and for $\tau_s \geq \tau_{sf}$ (or q_{bf})

$$\tau_s = \min\,(K_s \cdot u, \tau_{sf}) + (C_V + C_H) \cdot v \tag{148}$$

Once the ultimate shaft friction has been reached in plastic slider, slippage occurs and the radiation damping dashpot disjoints from the system.

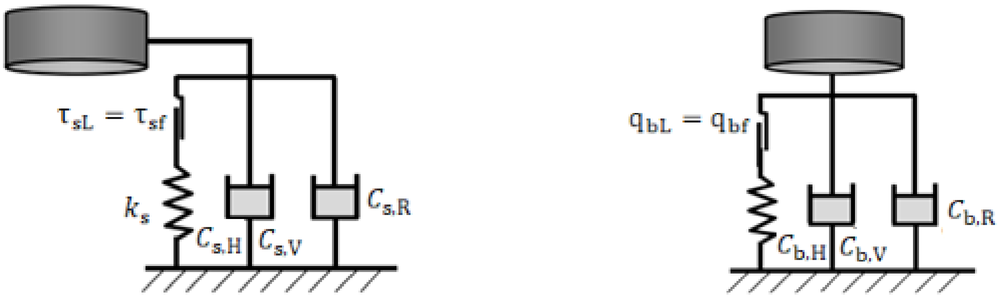

Figure 58: Shaft and base soil reaction model by Nguyen et al. (1988)

5.6 Shaft and base model by Liang and Sheng (1992)

Liang and Sheng (1992) developed a theoretical expression for Smith quake and damping at the pile base based on dynamical spherical cavity expansion theory and punching failure. The Smith shaft quake was derived from the concentric cylinder model what was developed for static loading of piles. Shaft damping was derived by using a semi empirical rate effect law. The damping and quake at the pile base per unit pile length are respectively

$$J_b = \frac{2r_0\rho_s}{3q_{bL}\pi r_0^2}\frac{v_{pd}}{v_{pd}} + v_{pd} \tag{149}$$

$$Q_b = \frac{1+v}{2E}q_{bL}r_0 \tag{150}$$

In which ρ_s is the soil density, τ_{sf} and q_{bf} are the ultimate shaft friction and limit base resistance in static conditions, v_{pd} and v_{pd} are the pile penetration acceleration and velocity under dynamic conditions. Young's modulus is related to the shear modulus by $E = 2G(1+v)$. The base damping coefficient increases when the pile penetration rate (velocity) and pile diameter increases. The damping coefficient decreases when the static soil resistance increases. The shaft damping and quake are respectively

$$J_s = \frac{K_L}{v_{pd}}\log_{10}\left[\frac{v_{pd}}{v_{ps}}\right] \tag{151}$$

$$Q_s = \frac{\tau_{sf}r_0}{G_{max}}\ln\left[\frac{r_m}{r_0}\right] \tag{152}$$

In which τ_{sf} is the soil shear strength, G the soil shear modulus, r_0 is the radius of the pile-soil interface and r_m is the radius of influence. K_L is the soil viscosity coefficient, v_{pd} and v_{ps} is the pile penetration rate under dynamic and quasi static conditions. The quasi-static penetration rate, v_{ps}, can be determined by using results from static load tests in which the Davisson's failure criterion is used for a pile with a diameter less than 600 mm

$$v_{ps} = \frac{x}{t} = \frac{3.81 + \frac{D}{120}}{t} \tag{153}$$

For a pile with a greater diameter than 600 mm the equation can be written as

$$v_{ps} = \frac{x}{t} = \frac{0.033D}{t} \tag{154}$$

The pile diameter D and the pile displacement x are in millimetres. The Davisson failure criterion defines to the ultimate pile capacity by using the Offset Limit Method. The method defines the ultimate load that corresponds with a displacement that exceeds the elastic compression line of the pile. The ultimate load is regarded as the point in where the pile load-displacement curve meets the elastic compression line of the pile.

5.7 Base model by Deeks and Randolph (1995)

Deeks and Randolph (1995) improved the elastic base model proposed by Lysmer (1965) for plasticity mechanism using a finite element analysis (FEA). Soil nonlinearity and hysteresis are not incorporated in the soil model. The FEA was used to improve the rheological model. The base model is shown in Figure 59. The base model is subdivided into three parts. The first and second part has similarities with the shaft model of Simons and Randolph (1985). The base model also contains two masses what represent soil mass inertia effects during failure mechanism.

The spring constant is the same as in Lysmer's model

$$K_b = \frac{4r_0 G_{max}}{1 - v_s} \tag{155}$$

The radiation dashpot constants C_0 and C_1 are respectively

$$C_0 = \frac{4r_0^2\sqrt{\rho_s G_{max}}}{1 - v_s}\beta_0 \tag{156}$$

$$C_1 = \frac{4r_0^2\sqrt{\rho_s G_{max}}}{1 - v_s}\beta_1 \tag{157}$$

With β_0 ranging from 0.75 to 0.87 and β_1 ranging from 0.3 (for $v_s = 0$) to 0.83 (for $v_s = 0.45$). The masses (m_0) and (m_1) are respectively

$$m_0 = \frac{4r_0^3\rho_s}{1 - v_s}\alpha_0 \tag{158}$$

$$m_1 = \frac{4r_0^3\rho_s}{1 - v_s}\alpha_1 \tag{159}$$

Values for α_0 and α_1 ranging from 0.16 to 0.25. The masses never co-exist at the same time and depends on the Poisson ratio v_s. In case of undrained conditions ($v_s = 0.5$) in saturated clays, $m_1 = 0$ and in drained or partially undrained situation ($v_s < 0.5$) $m_0 = 0$. In this elastic-perfectly plastic soil model once perfect plasticity starts, the radiation dashpot C_0 diminishes to zero, but C_1 remains active after the static base capacity has been reached ($q_{b0.1}$). In part 2, a viscous dashpot is placed parallel with a plastic slider representing the loading rate effect. The viscous part is equal as in the shaft model from Simons and Randolph (1985).

$$q_{bf} = q_{b0.1} \tag{160}$$

$$q_{b2} = q_{bf} + m_b q_{bf} \cdot v^{n_b} \tag{161}$$

The parameters m and n are similar as in Randolph and Simons (1986). Once the sum of radiation damping and static resistance are larger than the ultimate base stress, slippage occurs. During slippage the behaviour of the soil is controlled by the plastic slider and the viscous dashpot with an additional inertial effect in part 3.

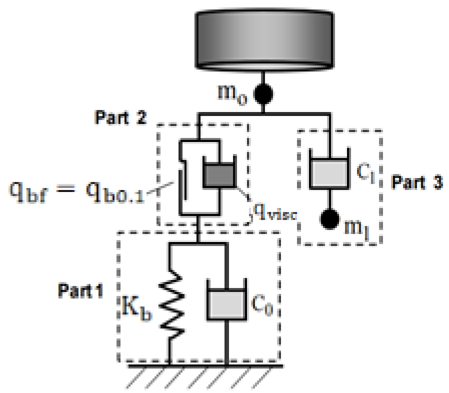

Figure 59: Base model by Deeks and Randolph (1995)

5.8 Shaft model by El Naggar and Novak (1994)

To overcome the limitations of the soil model by Simons and Randolph (1985) regarding linear soil behaviour, El Naggar and Novak (1994) added soil nonlinearity and hysteresis to the model. The shaft model is divided into 3 influence zones: a thin shear band, inner zone, and outer field. The thin shear band and linear outer zone are similar as in Simons and Randolph (1985). The inner zone is similar to the stress-strain behaviour described by Kondner (1963). In the thin shear band, loading rate effects (τ_{visc}) are present and slippage can occur between pile and soil. Slippage occurs when the ultimate shaft friction is reached $\tau_{sL} = \tau_{sf}$. Viscous damping is similar to Randolph and Simons (1986). The total mobilized resistance in the shear band can be written as

$$\tau_{s1} = \tau_{sf} + \tau_{sf} J_s \cdot v^{n_s} \tag{162}$$

The inner zone is the zone where nonlinear soil behaviour by means of hysteretic damping occurs and is represented by a nonlinear spring and additional dashpot (C). The additional dashpot is not further specified by El Naggar and Novak (Poulos et al,. 2000), but can be taken as equal to the radiation dashpot in the outer field (El Naggar & Novak, 1994).

$$\tau_{inner} = \frac{G_{max}}{r_o} \frac{u}{\ln\left(\frac{\frac{1.1r_o}{r_0} - \frac{\tau_{inner}}{\tau_{sf}}}{1 - \frac{\tau_{inner}}{\tau_{sf}}}\right)} + C \cdot v \tag{163}$$

During unloading the spring acts linear with a constant spring stiffness of

$$K_s = \frac{G_{max}}{r_0 \ln\left(\frac{1.1r_o}{r_o}\right)} \tag{164}$$

The spring stiffness in the linear outer zone is similar to Simons and Randolph soil model (1985).

$$K_s = \frac{\pi G_{max}}{2\pi r_0} \tag{165}$$

The total resistance, including radiation damping in the outer field can be formulated as

$$\tau_{outer} = \frac{\pi G_{max}}{2\pi r_0} \cdot u + \frac{G_{max}}{V_s} \cdot v \tag{166}$$

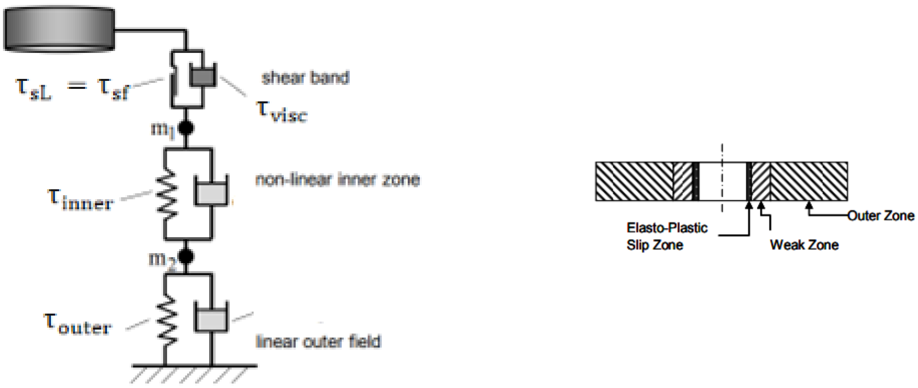

Figure 60: Shaft model by El Naggar and Novak (1994)

5.9 Shaft model by Michaelides et al. (1998)

The proposed shaft model by Michaelides et al. (1998) is an extension to the shaft model proposed by Novak et al. (1978) and more focused on vibratory driving. The model by Novak et al (1978) assumed constant shear modulus and Michaelides et al. (1998) improved this by implementing the secant shear modulus and a hysteretic damping ratio in the model due to shear modulus degradation during cyclic loading of the soil. The cyclic strain amplitude decreases with radial distance from the pile and therefore shear modulus and hysteretic damping is a function of radial distance from the pile. The spring stiffness and one dashpot including both radiation and hysteretic damping. The spring stiffness becomes (Michaelides et al., 1998).

$$K_s = \left(\frac{1.8G_{max}}{2\pi r_0}\left(1 + 0.5\sqrt{\frac{\omega r_0}{V_s}}\right)\right)\frac{1 - \frac{0.6\Lambda}{1-\Lambda}\left(\frac{\omega r_0}{V_s}\right)^{-0.5}}{1 - 1.2\Lambda} \tag{167}$$

The parameter Λ represents the effect of the amplitude of the shear stress on the soil damping and stiffness and ω is the angular frequency of the vibratory hammer. The total damping constants becomes

$$C_s = \left(\frac{1.2\rho V_s}{\left(\frac{\omega r_0}{V_s}\right)^{0.25}} + \frac{\zeta_{min} 1.8G_{max}\left(1 + 0.5\sqrt{\frac{\omega r_0}{V_s}}\right)}{\omega \pi r_0}\right) \cdot \left(1 - 0.84\,\Lambda\left(1 + 0.66\log\sqrt{\frac{\omega r_0}{V_s}}\right)\right) \tag{168}$$

In which the first terms between brackets in equation (157) represents radiation damping and the second term hysteretic damping. ζ_{min} is usually between 0.5% and 1%. Λ depends on the plasticity index PI, ultimate shaft friction and initial shear modulus (Figure 61)

$$\Lambda = 600\frac{\tau_{sf}}{G_{max}}e^{\left(-1.39\frac{PI}{125}\right)} \tag{169}$$

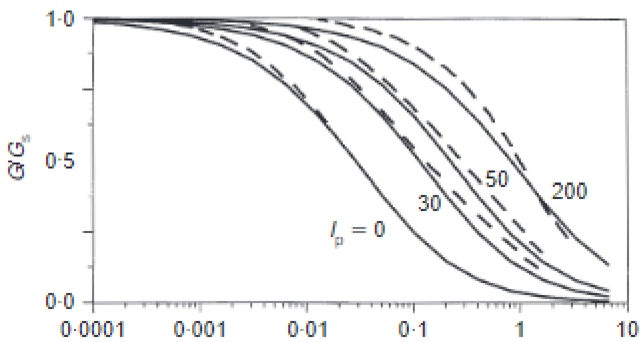

Figure 61: Effect of plasticity on shear modulus degradation with strain amplitude

The soil model is complex and the plastic slider is limited to the ultimate shear strength at the pile soil interface, τ_{sf} . In first instance, Michaelides et al. (1998) proposed that the plastic slider strength is independent of pile velocity (only static resistance (τ_{sf}), but this can be changed to make it a function of pile velocity as done by Simons and Randolph (1985) as in equation (126).

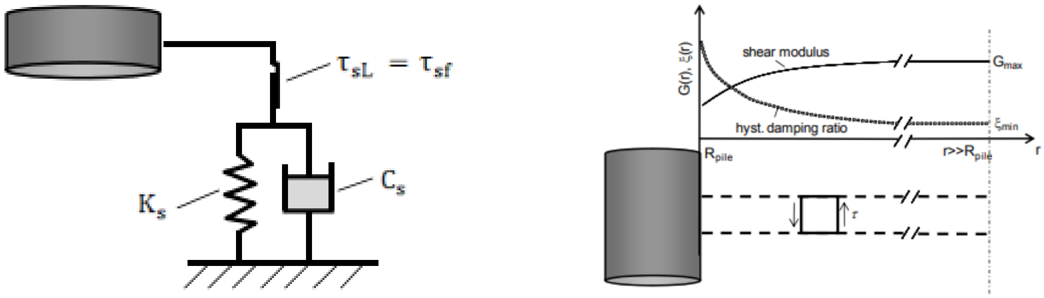

Figure 62: Shaft model by Michaelides et al. (1998) (left) and shear modulus and damping ratio as function of radial distance (right)

5.10 Analytically derived quake values

The quake values are related to the linear elastic part of the elastic perfectly plastic soil models. Once the quake value is exceed, plasticity starts. The spring stiffness is the yield stress divided by the quake values. In the equations obtained by several researchers the following quake values were obtained. The quake can only be related to the linear perfectly plastic soil models. In the analytically derived soil models the quake value is also depended on pile dimensions.

5.10.1 Smith (1960) shaft and base quake

According to Smith the quake values is determined based on the maximum static soil resistance and the stiffness of the soil. The quake is an empirically value and is differs per soil type. The stiffness of the soil K_s is not based on geotechnical properties. The quake values were states as 2 to 2.5 mm for both pile shaft and base quake in sandy soil, but with large variation to these values for piles in clay.

5.10.2 Randolph and Wroth (1978) shaft quake

Randolph and Worth (1978) proposed for the calculation of the shaft quake.

$$U_{q,s} = \frac{r_0 \tau_{sf}}{G_{max}} \ln\left(\frac{r_m}{r_0}\right) \tag{170}$$

The radius of influence r_m is calculated according to equation (116).

5.10.3 Simons and Randolph (1985) shaft quake

The proposed shaft quake according to Randolph and Simons (1986) can be evaluated as follows

$$U_{q,s} = \frac{2 r_0 \tau_{sf}}{G_{max}} \tag{171}$$

The quake value is not dependent of a pile influence radius.

5.10.4 Nguyen et al. (1988) shaft and base quake

The shaft and base quake according to Nguyen et al. (1988) becomes

$$U_{q,s} = \frac{r_0 \tau_{sf}}{2G_{max}} \left[\ln\left(\frac{r_m}{r_0}\right) + 2\right] \tag{172}$$

$$U_{q,b} = \frac{q_{bL}}{K_b} \tag{173}$$

In which K_b is the stiffness at the pile base according to Lysmer (1965).

5.10.5 Deeks and Randolph (1995) base quake

The elastic limit of the base spring in the Deeks and Randolph base model (1995) is similar to Lysmer's spring model (1965) and the quake value can be written as

$$U_{q,b} = \frac{q_{bf}(1 - v_s)}{4 G_{max} r_0} \tag{174}$$

6. Signal matching analysis

6.1 Signal matching procedure

When a hammer strikes on the top of a foundation pile, a compressive stress wave is induced and travels down along the pile shaft to the pile base. As mentioned in Chapter 2, a displacing pile induces friction at the pile-soil interface and the downward travelling stress wave is partly reflected. The magnitude of the reflected upward travelling stress wave depends on the mobilized resistance. In dynamic load testing, the upward travelling stress waves are indirectly measured at the pile head by strain transducers and accelerometers. Based on the stress wave theory and method of characteristics, the time at which the upward travelling stress wave arrives at the pile head can be related to the location of the soil resistance and its distribution along the shaft and pile base based on the solution of the one-dimensional wave theory and characteristic lines (Figure 4) based on stress wave velocity and travel time in the pile. In signal matching analysis, the reflected upward travelling wave is derived from the total measured force at the pile head according to equation (26). Signal matching analysis is performed between the measured and simulated upward travelling stress wave generated by the response of the TNO soil model and the match must be underpinned by a proper match on both upward stress wave, pile displacement and pile velocity. To mimic the blow of the hammer, the force in the downward travelling stress wave is used as signal input for the simulated hammer blow in the signal matching software, AllWave-DLT, according to equation (20), (25) and (26). Different soil models and input parameters generate varying mobilized soil friction and the objective is to choose the best soil model parameters for the analytical TNO soil model that matches field measurements with WEAP simulations. In signal matching the soil is modelled as a dynamic system with springs and dashpots and in case of pile plugging an additional soil mass. By an iterative process the software calculates the dynamic response of the soil by changing the soil model parameters and calculates the signal matching quality between the measured and generated upward travelling stress wave. The point of focus in this research is on the TNO soil model and its parameters (Chapter 6.5) which has several parallels with the shaft model from Simons and Randolph (1985) and the base model from Deeks and Randolph (1995) in which viscous damping is neglected. The procedure of signal matching analysis is given in Figure 63.

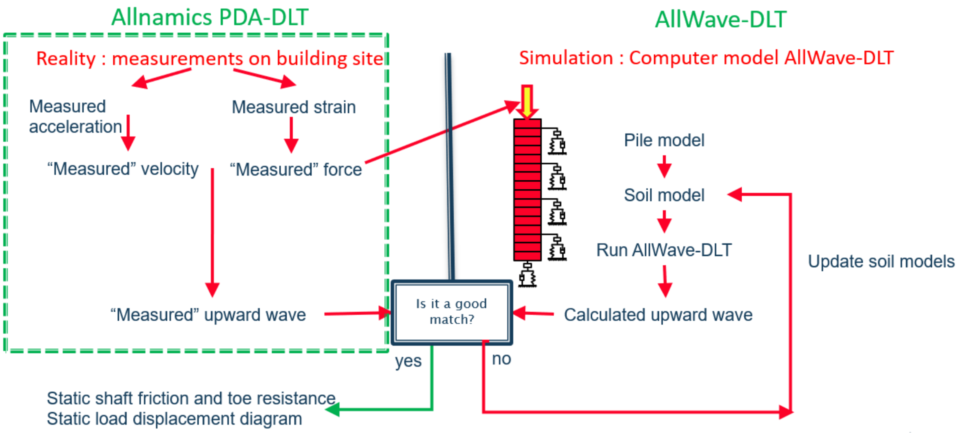

Figure 63: Overview of the DLT and signal matching procedure

The fundamental reason why a downward travelling stress wave is reflected is because of impedance changes. Impedance changes can be caused by changing soil friction, pile dimensions or discontinuities. To get a clear picture about real soil behaviour, the upward travelling stress wave must be analysed with knowledge of the pile dimensions to extract the influence of the impedance change by soil friction from impedance change from changing pile dimensions.

6.2 Automatic signal matching theory

In signal matching analysis, relevant soil model parameters are changed iteratively until the simulated soil response matches the measured response in the field during a dynamic load test. Automatic matching is often used to obtain satisfied results in a much faster way than manual matching, but a requirement is that the starting points of the soil model parameters in the TNO soil model are realistic to soil investigation data. Automatic signal matching has three requisites. The first premise is that a mathematic soil model must describe the pile-soil interaction with appropriate parameterization such as a mechanical model consisting of springs, dashpots and masses. In AllWave-DLT and other WEAP the method of characteristics and several analytical soil reaction models can be used. In this research, the TNO soil model is chosen because of the mechanical model is based on theoretical formulations for springs and dashpots in an linear elastic medium, compared to the empirical Smith soil model parameters. Secondly an accurate and efficient computation algorithm must solve the boundary value problems in the mathematical model whereby the model parameters are not allowed to deviate more than the initial maximum and minimum value for a soil model parameter. In Allwave-DLT this is the so called “forward” model (Esposito et al., 1998). At last realistic parametric values from site investigation must be available, such as CPT(u) or SPT data, to start the automatic signal matching in a proper direction. Given these conditions, a method was developed that would determine unknown or uncertain soil parameter values in the model giving a good agreement between the forward model and the measured signal. One of the premises of automatic signal matching theory is that it needs a priori knowledge about the probable soil parametric values and predefined variability of those in a specific soil layer. The starting values for soil model parameters for each layer can be estimated from soil investigation data in combination with reasonable values for local shaft and base friction. One of the objectives in this research is to verify if CPT-based axial pile capacity design methods (Chapter 4) give realistic values for the initial starting values for local shaft and base friction in the TNO soil model for signal matching analysis. A Kalman filtering is an optimal estimation algorithm which is used to update the soil parametric values and their reliability each iteration. The method is schematically shown in Figure 64. With the known downward travelling stress wave from the measured total force by the sensors and initial soil parameters given by the user, AllWave-DLT calculates a simulated upward travelling stress wave via a forward model. The derived upward travelling stress wave from measurements and the simulated upward travelling wave are feed in the Kalman filter and based on their difference, partial derivatives of the responses with respect to the soil parameters and covariances concerning measurement errors and parametric values, a proper gain is calculated to update the initial soil parameter values (Bielefeld & Courage, 1992). The procedure is repeated until a predefined convergence criteria is met. This criterion can be a maximum amount of iterations, a specific difference between measured and simulated upward response or small update of soil parametric values.

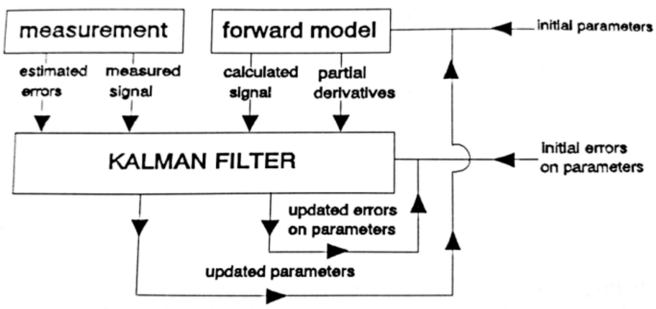

Figure 64: Schematic flow chart for automatic signal matching

There is not a unique solution in signal matching analysis (Figure 65), but the goal is to obtain from a range of solutions the best model parameters that matches the response of the soil model with field measurements in terms of upward travelling stress wave in which both have the same downward travelling stress wave as input into the soil model.

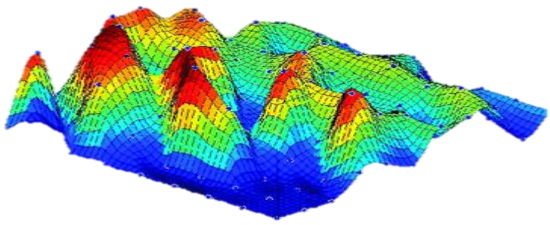

Figure 65: Finding the best optimum in range of several solutions

6.3 Data acquisition PDA

Dynamic load testing is extensively performed throughout the world and embedded in Eurocode 7. The method is recognized as a cost-effective and quick test for assessing pile capacity and load-displacement behaviour. The reliability is lower compared to static and rapid loading, but ideal for bulk testing and offshore monopiles. In DLT, the standard set-up is an instrumented pile head with two strain transducers and two accelerometer at opposing sides of the pile. Caution is needed in data acquisition to obtained workable data in which no eccentricity of the impact force is desired. Different type of strain transducers and accelerometer are used, depending on the site conditions (Figure 66). The impact on the pile head is provided by a drop weight or pile driving hammer. A downward travelling stress wave is induced in the pile and sensors measure indirectly the upward and downward travelling stress waves over time from the total stress recorded at the pile head. In case of very low mobilized shaft friction in the upper part of the pile, the downward travelling stress wave is almost equal to the total stress wave generated by the impact shown in second diagram in Figure 69.

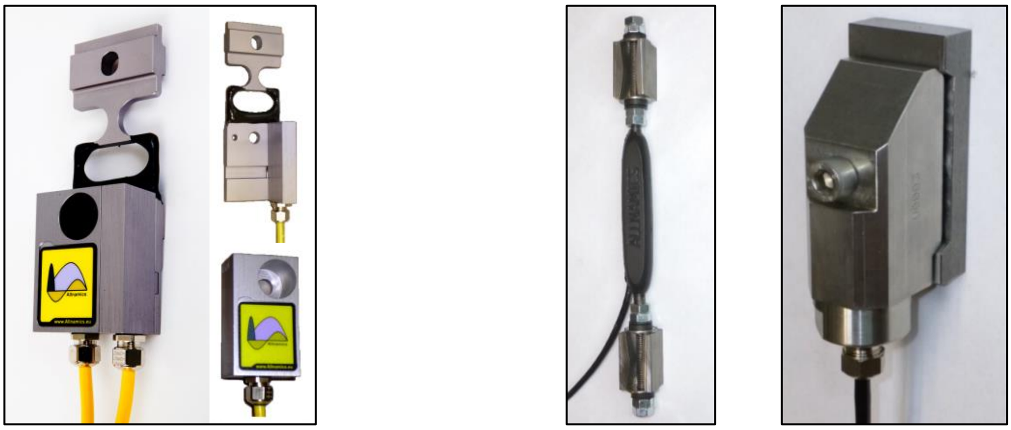

Figure 66: Test set-up dynamic load test onshore (left) and offshore (right)

From the sensor recordings (Figure 67), strain and acceleration, the force and pile displacement can be calculated by the equations (175) to (177).

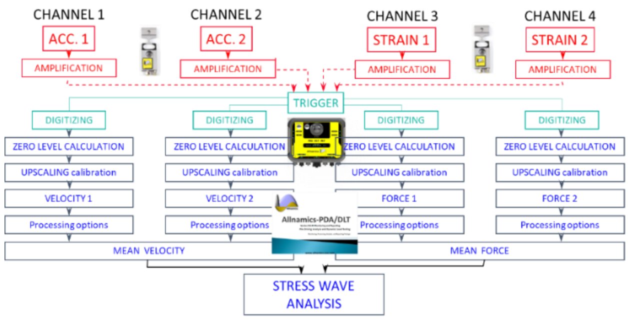

Figure 67: From sensor recording to stress wave analysis in AllWave-DLT

$$F(t) = E \cdot A \cdot \varepsilon(t) \tag{175}$$

$$v(t) = \int a(t)\,dt \tag{176}$$

$$u(t) = \int v(t)\,dt = \iint a(t)\,dt \tag{177}$$

The stress wave velocity and force in a pile are related to pile characteristics by means of so-called the impedance, which is a function of pile dimensions and material properties of the pile. Variation in pile shape can have a large effect on stress wave propagation throughout the pile (178) and thus on quality of the reflected stress waves for signal matching analysis. Figure 68 shows an example of a pile with changing impedance due to varying diameter and wall thickness over its length. Once the pile has been installed and a dynamic load test is performed on the pile, not only reflected due to soil friction are measured, but also reflections generated by impedance variations due to changing pile dimensions.

$$Z = \frac{E \cdot A}{c} = A \cdot \sqrt{E \cdot \rho} \tag{178}$$

Figure 68: Pile impedance changes over its length

From the recorded stress wave, the upward and downward travelling stress wave are separated from the measured signal according by equation (20), (25) and (26). In Figure 69 the result of separating the downward travelling stress wave and the upward travelling wave from the total measured stress wave over time is shown. Pile displacements are calculated by double integration of the measured accelerations at pile head level. The blue line in the top figure is the total force measured at the pile head according equation (175). The red line is the measured velocity multiplied with the known impedance of the pile at sensor level. The velocity is obtained by single integration of the acceleration according to equation (176). As long as there is no friction or impedance changes along the pile, the downward travelling stress wave is not hindered and no reflections are generated. The total force lies on top of the impedance times velocity line ($Z \cdot v$) because the upward travelling stress wave is zero. Once the two lines diverge it’s a sign of change in impedance due to soil friction or pile shape.

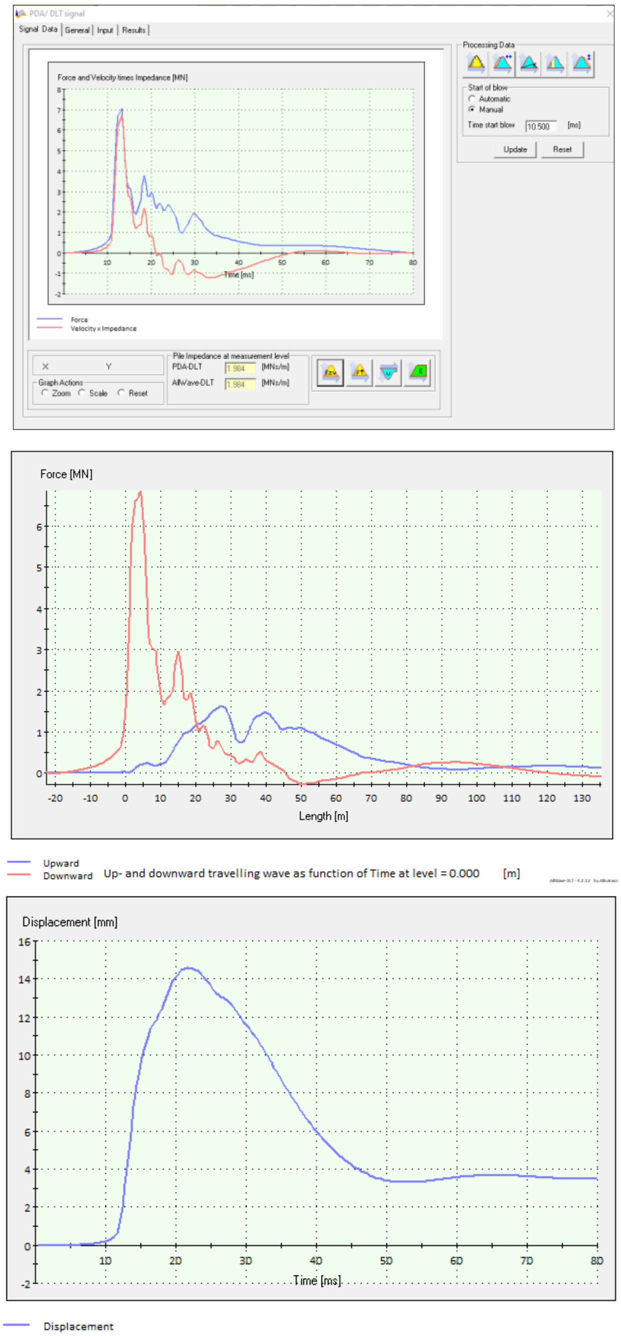

Figure 69: Retrieving relevant graphs from signal data for signal matching analysis

6.4 Pile modelling

Strain transducers are mounted to the pile head and converts the measured strains to stresses and forces. The characteristics of the pile are important to related strains to forces and therefore the modulus of elasticity is needed. The modulus of elasticity is mostly given by pile manufacturers. Concrete behaves in a linear manner up to 40% of its ultimate strength. During static loading, the static modulus of elasticity is slightly lower than the dynamic modulus of elasticity during dynamic loading. Piled foundations are mostly made of prestressed concrete in which the pile is a combination of steel and concrete. A typical stress-strain curve for concrete is shown in Figure 70. For steel piles the modulus of elasticity is close to 210 GPa, but for pre-cast concrete piles it can vary around 40 GPa, depending on several factors. The modulus of elasticity depends on the quality of the concrete, age of the concrete, loading rate and temperature. The modulus of elasticity can be estimated by back-calculating the stress wave velocity from the time elapse between the impact and a clear base reflection and pile length.

$$c = \frac{2L}{\Delta t} \tag{179}$$

$$E = c^2 \rho \tag{180}$$

Calculation of the modulus of elasticity depends strongly on the determination of the stress wave velocity and material density. Table 13 shows the commonly used moduli for different types of foundation piles.

Material	Modulus of elasticity	Density
	MPa	Kg/m^3
Steel	210.000	7.850
Old pre-cast concrete (prestressed)	40.000 >	2.500
New pre-cast concrete (prestressed)	40.000	2.500
Compacted cast-in-situ concrete	35.000	2.500
Uncompacted concrete	30.000	2.300
Poor quality concrete	20.000	<2.300

Table 13: List of pile materials and elastic moduli

To prevent pile fatigue risk, the induced stress wave by the hammer blow must be within the elastic range and below the yielding point in the stress-strain curve for steel and (prestressed) pre-cast concrete, as shown in Figure 70.

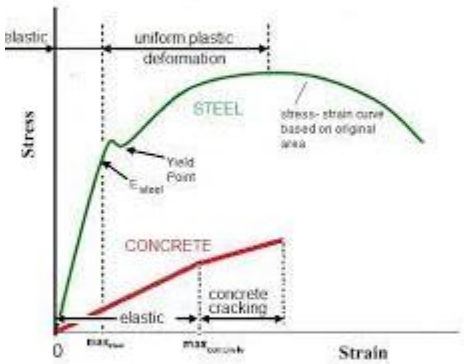

Figure 70: Stress-strain diagrams for concrete and steel

The procedure to model the pile in AllWave-DLT is shown in Figure 71. The length of the pile in AllWave-DLT is the length between the sensors at the pile head and the pile base.

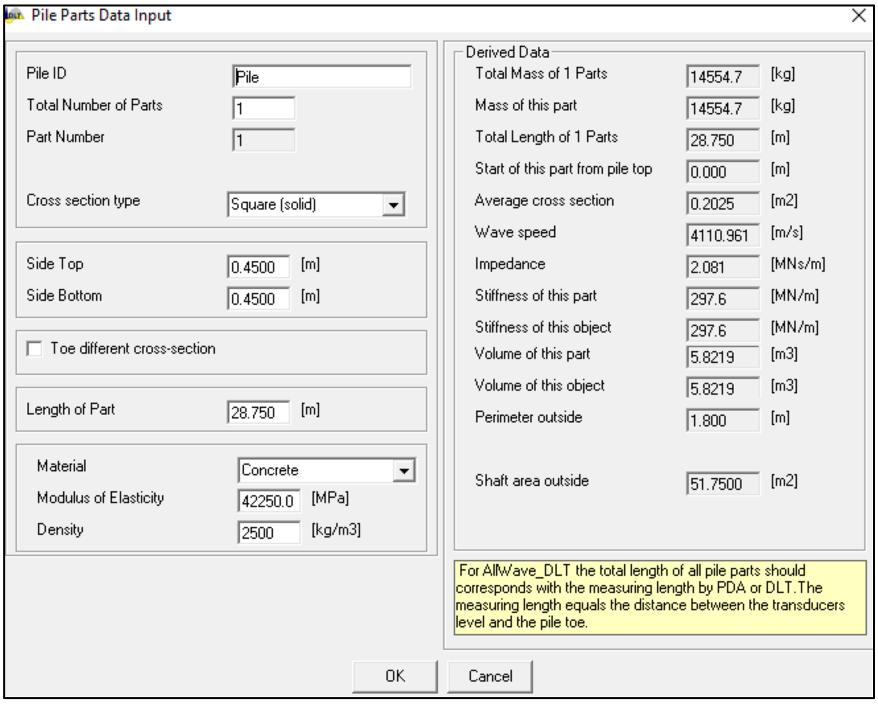

Figure 71: Input parameters for a (prestressed) pre-cast concrete pile modelling in AllWave-DLT

6.5 Soil modelling: TNO soil model

The TNO soil model is able to simulate the soil behaviour during dynamic loading in which the input parameters in the soil model are based on mechanical parameters that can be related to geotechnical soil properties. The general form the total resistance is a combination of the shaft and base resistance and can simply be simply as

$$R_t = K \cdot u + C \cdot v^{\alpha} \tag{181}$$

In the TNO model, the spring and dashpot are decoupled and damping resistance solely depends on the pile velocity. The TNO model written in a more comprehensive manner to indicate the geotechnical model parameters, gives for the total shaft resistance for both closed- and open-ended piles

$$\tau_s = \frac{\pi G_{max}}{2\pi r_0} \cdot u + \frac{G_{max}}{V_s} \cdot v^{\alpha} \tag{182}$$

The spring stiffness and plastic slider strength is similar to the spring model in Simons and Randolph (1985). The exact formulation for the base resistance in the TNO model depends on the type of pile. In generalized form, the total base resistance is given by

$$q_b = \frac{4G_{max}R}{1 - v_s} \cdot u + \frac{3.4R^2}{1 - v_s}\sqrt{\rho G_{max}} \cdot v^{\alpha} \tag{183}$$

In which for the open-ended piles, the radius R or diameter D changes to equivalent values R^* and D^*. For the static resistance, calculated by the linear spring by means of stiffness (K) and pile displacement (u), the shaft friction is limited to the local ultimate shaft friction calculated by the design methods and is denoted as yield stress in the TNO model. The dynamic part is described by radiation damping constant (C_s and C_b). A specific formulation for viscous damping related to static resistance is neglected in the TNO soil model and is replaced by only a decoupled radiation damping constant with power alpha. The spring in the TNO model is linear, what means that hysteric or material damping is also missing in the formulation and nonlinear soil behavior is excluded. In general α is set to 1 for the shaft because of its minor impact on the damping resistance. No signal matching is performed on the radiation damping constant at the base (C_b) and is fixed to the theoretical value by Deeks and Randolph (1995) as mentioned in Chapter 5.7. The exponent α is set to 0.2 for the base radiation damping constant according Deeks and Randolph (1995). The TNO soil model is a linear model in which the model parameters can be quantified by geotechnical soil parameters. Geotechnical properties of the soil can be obtained from relevant soil investigation data such as cone penetration tests (CPT). The soil investigation data from CPT's is converted into basic soil model parameters (Chapter 4). In all the soil models in Chapter 5, the soil is represented by a mechanical system of springs and dashpots and in case of a plugged pile an additional mass. The relevant parameters that define the behaviour at pile-soil interface in the TNO model are the yield stress, loading/unloading quakes, yield factor and a dashpots with a radiation damping constant combined with exponent α. The objective is to relate the obtained quake and damping in the soil model after signal matching analysis to soil stiffness parameters and radiation damping parameters related to geotechnical soil parameters derived from CPT based correlation functions. Based on obtained quake values, back-analysis is done on the soil stiffness degradation (G_s/G_{max}) during dynamic loading based on initial spring stiffness formulation by Simons and Randolph (1985) for the shaft (Chapter 5.10.3) and for the base (Chapter 5.10.5) by Deeks and Randolph (1995). The obtained radiation damping constant is a dynamic property of the soil and is related to its initial theoretical value (G_{max}/V_s) based on site investigation data. After pile driving and during loading the stress state in the soil has changed. A difference is expected to be observed between the initial theoretical values based on CPT data prior to installation and the back-calculated values for the geotechnical soil parameters quantifying the stiffness and damping in the mechanical soil model. For the stiffness in the spring model, the initial shear modulus G_{max} based on CPT based correlations is expected to reduce to a secant or operational shear modulus G_s. The yield stresses along the pile shaft and pile base, as described in Chapter 4, are in first instance respectively similar to the calculated local ultimate shaft friction and ultimate base stress from the unified method for driven piles in sand and clay, but refined during signal matching analysis. A yield factor specifies the relation between the yield stress in compressional and tensional loading. The design methods propose values around 0.75 for sand and clay, but this value is refined during signal matching analysis and can slightly differ from values obtained from statically loaded piles. In Allwave-DLT the soil surrounding the pile is subdivided into individual layers and for each layer soil model parameters can be assigned based on geotechnical soil properties described in Chapter 4.

Shaft Model | Toe Model | Toe Layer Only

		Shaft Model Data									
Layer Point [-]		Depth [m]	Thick nesss [m]	Yield Stress [KPa]	Quake Value 1 [mm]	Quake Value 2 [mm]	Yield Factor [-]	Damping Constant 1 [kNs/m3]	Power Alpha [-]	Added Mass [kg/m2]	Outside Factor [-]
	Constant			☐	☐	☐	☐	☐	☐	☐	☐
	Factor			1	1	1	1	1	1	1	1
1	Top	1.500	0.720	1.0	2.0	2.0	0.741	1.0	1.000	0.0	1.000
	Bottom	0.780		9.6	2.0	2.0	0.746	2.6	1.000	0.0	1.000
2	Top	0.780	1.950	9.6	2.0	2.0	0.715	2.6	1.000	0.0	1.000
	Bottom	-1.170		3.1	2.0	2.0	0.491	2.0	1.000	0.0	1.000
3	Top	-1.170	2.500	3.1	2.0	2.0	0.489	2.0	1.000	0.0	1.000
	Bottom	-3.670		4.1	2.0	2.0	0.490	2.5	1.000	0.0	1.000
4	Top	-3.670	2.190	4.1	2.0	2.0	0.487	2.5	1.000	0.0	1.000
	Bottom	-5.860		5.1	2.0	2.0	0.488	2.2	1.000	0.0	1.000
5	Top	-5.860	2.330	5.1	2.0	2.0	0.484	2.2	1.000	0.0	1.000
	Bottom	-8.190		8.8	2.0	2.0	0.485	4.5	1.000	0.0	1.000
6	Top	-8.190	3.080	8.8	2.0	2.0	0.471	4.5	1.000	0.0	1.000
	Bottom	-11.270		10.6	2.0	2.0	0.671	7.7	1.000	0.0	1.000
7	Top	-11.270	0.140	10.6	2.0	2.1	0.742	7.7	1.000	0.0	1.000
	Bottom	-11.410		17.4	2.0	2.1	0.744	26.0	1.000	0.0	1.000
8	Top	-11.410	0.790	17.4	2.0	2.0	0.709	26.0	1.000	0.0	1.000
	Bottom	-12.200		12.0	2.0	2.0	0.722	26.0	1.000	0.0	1.000
9	Top	-12.200	0.270	12.0	2.0	2.0	0.734	26.0	1.000	0.0	1.000
	Bottom	-12.470		20.0	2.0	2.0	0.738	26.0	1.000	0.0	1.000
10	Top	-12.470	0.790	20.0	2.0	2.0	0.692	26.0	1.000	0.0	1.000
	Bottom	-13.260		22.8	2.0	2.0	0.708	30.3	1.000	0.0	1.000
11	Top	-13.260	0.340	22.8	2.0	2.0	0.726	30.3	1.000	0.0	1.000
	Bottom	-13.600		21.1	2.0	2.0	0.731	39.0	1.000	0.0	1.000
12	Top	-13.600	1.300	21.1	2.0	2.0	0.696	39.0	1.000	0.0	1.000

Figure 72: An example of initial soil model parameters in the TNO soil model for the pile shaft in Allwave-DLT

6.6 Limitations TNO soil model

The one-dimensional mass-spring-damper system, often used in stress wave analysis for pile drivability studies, has several limitations. These limitations stem from its simplified approach to modeling the complex phenomena involved in pile driving. Key limitations are:

Simplification of pile-soil interaction

The model typically assumes a linear, elastic interaction between the pile and the soil. However, in reality, pile-soil interaction is highly non-linear and depends on various factors like soil type, pile material, and driving method. The TNO model may not accurately capture complex behaviors such as soil yielding, plastic deformation, or changes in soil properties due to repeated loading. Although, experience shows that the simplified models, such as Smith and TNO, are capable of describing the complex soil behavior during dynamic loading in a simple way.

Oversimplified damping representation

The damping in the model is typically represented by a single value, which is an oversimplification. A physical parameter based on the shear modulus and wave velocity of the surrounding soil. In reality, damping is a complex phenomenon influenced by factors like soil type, moisture content, and frequency of the applied load. In elastic perfectly plastic soils, energy dissipation in the form of damping occurs, but the mechanism and efficiency of this dissipation can be quite different compared to other soil types The efficiency of the damping is discussed in Chapter 7.6.

Three-dimensional wave propagation

The TNO model typically considers only one-dimensional wave propagation along the pile's axis. However, in reality, for large offshore monopiles and prefab concrete piles, wave propagation is a three-dimensional phenomenon, with energy radiating outward from the pile in all directions. Radiation damping is just one of several damping mechanisms in soils (others include material or hysteresis damping, viscous damping, etc.). The interaction and coupling between these different types of damping are not typically considered in the (mass)-spring-damper model. In the TNO model, radiation damping is represented as a type of lumped damping constant, where the viscous effects are characterized through an exponent that is related to the velocity of the pile.

Assumption of linear material behavior

The model typically assumes that both the pile and the soil behave linearly and elastically, which is not always the case, especially under high strain rates during pile driving. Next to that, in case of high internal damping of the stress waves in the pile, wave analysis based on method of characteristics should be adapted for that. But in general, the time duration in which the signal matching analysis is performed, mainly $2L/c$, is that short than internal damping has a very minor effect on the stress wave propagation and therefore wave analysis by means of method of characteristics.

6.7 Upward travelling stress wave

In signal matching analysis, the upward travelling stress wave is the underlying fundamental for pile capacity estimations. The upward travelling stress wave contains the reflections from both shaft friction and base resistance. In general the shape of the upward travelling stress wave, measured at the pile head over time, can be divided into 5 relevant intervals as shown in Figure 73. In each interval a specific part of the pile has its dominance in the signal.

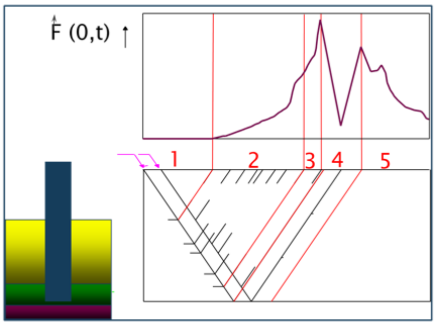

Figure 73: Effect of soil characteristics changes on upward travelling waves

Interval 1
In the first interval, no shaft friction acts on the pile and no reflections are generated. The first interval represent the part of the pile above ground level or a very loose soil stratum.

Interval 2
The second interval reflections are visible due downward pile movement and increasing shaft resistance. The stiffer and stronger the soil layer, the steeper the upward travelling wave. The shaft resistance can be calculated by using information from the upward travelling wave. The derivation of shaft friction (τ_s) at a specific time (t) and soil layer ($x_2 - x_1$) along the pile measured at the pile head can be calculated as follows:

$$F^{\uparrow}(t_2) = F^{\uparrow}(t_1) + \Delta F^{\uparrow} \tag{184}$$

$$\Delta F^{\uparrow} = \tau_s \cdot 2\pi R \cdot (x_2 - x_1) \tag{185}$$

$$\tau_s = \frac{F^{\uparrow}(t_2) - F^{\uparrow}(t_1)}{2\pi R \cdot (x_2 - x_1)} \tag{186}$$

Since

$$t_1 = \frac{2x_1}{c} \tag{187}$$

$$t_2 = \frac{2x_2}{c} \tag{188}$$

$$(x_2 - x_1) = \frac{c}{(t_2 - t_1)} \tag{189}$$

$$\tau_s = \frac{2(t_2 - t_1) \cdot F^{\uparrow}(t_2) - F^{\uparrow}(t_1)}{2\pi R \cdot c} \tag{190}$$

In which $F^{\uparrow}(t_2)$ is the force of the upward travelling stress wave at the end of change in slope, $F^{\uparrow}(t_1)$ is the force of the upward travelling stress wave at the start of a change in slope. $\Delta F^{\uparrow}$ is the force change in upward travelling stress wave between time of start t_1 and end t_2 of the slope. The starting depth of a specific layer is x_1 and the layer ends at a depth of x_2. The stress wave velocity is c and can be back-calculated or estimated by using Table 13.

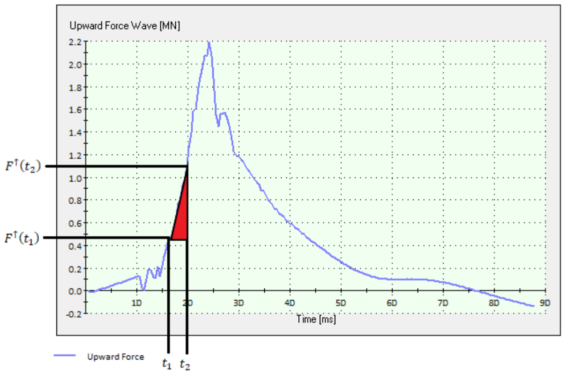

Figure 74: Relationship between mobilized resistance and force of the upward travelling stress wave

Interval 3
In the third interval, the shaft friction causes also and upward movement of the pile because of reflections generated along the pile shaft. The start of the upward movement of the pile head is determined when the velocity changes sign.

Interval 4
In the fourth interval the base resistance starts to contribute to the upward travelling stress wave. A reflection in the form of a tension wave can be seen as a dip in the upward travelling stress wave, while a compressional stress wave gives a peak.

Interval 5
The last interval is a combination of reflections from the shaft friction and base resistance. The influence of the damping constant and unloading quake in the soil models are relevant in this interval. In interval 1,2 and 3 ($\mathrm{t} = 0$ to $\mathrm{t} = \frac{2\mathrm{L}}{\mathrm{c}}$) for most cases a more or less perfect match can be obtained. In interval 4 is a good match more difficult because the base reflection are also present in the upward travelling stress wave and some deviation is acceptable. From interval 5 ($\mathrm{t} = \frac{3\mathrm{L}}{\mathrm{c}}$) the calculated signal should generally follow the measured signal, but more deviations are acceptable. In case the shaft and base damping are too low, less energy is dissipated and strong reflections are still visible in the beginning of interval 5. Increasing the radiation damping constants will results in more energy dissipation and less strong stress wave reflections.

6.8 Validation of signal matching results

In a dynamic load test it is important that at least the soil resistance along the pile shaft has been fully mobilized during the hammer blow. In general, the elastic limit or quake value of the soil around the pile shaft is easily exceeded during an impact because of its relative low value and therefore small pile displacements are needed to exceed that quake value. The quake value at the pile base can be much higher and has to be exceeded to get permanent pile displacement. The criterium in signal matching analysis is that the permanent pile displacement measured at the pile head must be underpinned by a pile base displacement that exceeds the pile base quake, otherwise no permanent pile displacement is possible. When the lower parts of the shaft springs are in tension and residual loads might be present at the base, once the hammer blow has fade away the pile does not rebound to its original shape and can lead to uncertainty in signal matching analysis. Residual loads are difficult to detect and quantify by signal matching analysis and often a complete rebound is assumed. AllWave-DLT is able to calculate the pile displacement at any pile level over time. The pile displacement at the pile base is lower than at pile head, what is reasonable because the energy of the downward travelling stress wave reduces due to soil friction and damping.

7. Results and analysis

The purpose of signal matching analysis is to determine the bearing capacity of piles during a dynamic load test and separate the mobilized capacity into contribution of shaft resistance and base resistance. The hammer blow induces a downward travelling stress wave in the pile that travels along the pile shaft to the pile base and once the stress wave experience static friction, damping or pile impedance changes stress wave reflection occurs and an upward travelling stress wave is generated which travels to the pile head again. Strain and accelerometers at the pile head measures indirectly the total force via summation of the downward and upward travelling stress wave and the pile displacement over time. Because stress wave reflection is caused when pile displacement dependent static soil friction and pile velocity dependent damping acts along the pile-soil interface. The reflected stress wave contains information about total generated resistance distributed along the shaft and base. As described in Chapter 6, signal matching analysis attempts to match a simulated soil response by means of a upward travelling stress wave with user depended soil model parameters with the back-calculated upward travelling stress wave obtained from a PDA measurement. In this chapter, the results of signal matching analysis are compared with CPT-based axial pile capacity design method calculations and soil investigation data which form the basis how the main research questions are addresses. Chapter 7.1 and 7.2 describe the case studies used in this research and the signal matching results on the closed-ended prefab concrete piles and the open-ended offshore monopiles. The focus in the first part of the results from Chapter 7.3 to 7.5 is on the accuracy of the yield stress in the static part of the TNO model in comparison to the calculated local ultimate shaft friction defined by the unified method for driven piles in sand and clay with consideration of the setup effect. Subsequently, the spring model is reviewed in terms of shear modulus reduction ($\mathrm{G_s/G_{max}}$) along the shaft which is back-calculated from the initial soil stiffness based on CPT correlations for G_{max} and initial pile-soil interface stiffness approach according to Randolph and Simons (1985) to derive the reduced operational shear modulus and pile-soil interface stiffness based on obtained quake values ($\mathrm{U_{q,s}}$). In the second part of the results in Chapter 7.6, shaft damping is considered in terms of the obtained radiation damping constant ($\mathrm{C_s}$) from signal matching analysis and is related to cone resistance value ($\mathrm{q_t}$), initial theoretical radiation damping values calculated by using mechanical soil properties based on soil investigation data ($\mathrm{C_i}$) and relative pile depth (h) and vertical effective stress (σ'_v). Finally in Chapter 7.7 and 7.8, the base resistance is discusses in which the mobilized static base resistance derived from signal matching analysis is compared to the calculated ultimate base resistance from the design methods. Subsequently the base loading stiffness is defined by considering the obtained pile base loading quake in the TNO soil model ($\mathrm{U_{q,b}}$) which is compared to its initial pile base-soil stiffness based on the pile base model by Deeks and Randolph (1995). The loading quake at the base is compared with the failure criterion defined for a pile base displacement of $0.1\mathrm{D}$ ($\mathrm{U_{b0.1}}$). which is needed to achieve the ultimate base capacity ($\mathrm{q_{b0.1}}$). The main focus of the last part of Chapter 7 is to verify how applicable and till what extend the linear spring model approach in TNO soil model is for dynamic pile loading is in order to match a by nature nonlinear pile base behaviour in static loading.

7.1 Case studies

Signal matching analysis is performed on both dynamic load tests on closed- and open-ended piles. The dynamic load tests are performed on 8 closed-ended prefab concrete onshore piles and 10 open-ended steel offshore monopiles. The prefab concrete closed-ended piles are located at the Nieuwesluisweg in Rotterdam and are part of the foundation for a series of onshore wind turbines. The open-ended piles are located on three locations in the North Sea; one monopile in the German territory, one monopile in the Dutch and eight monopiles in the United Kingdom part of the North Sea. The tested piles are all part of major offshore windfarms. The pile in the German territory is part of the DolWin wind farm, the Dutch one is part of Hollandse Kust Noord (HKN) and the monopiles in the UK territory are part of the East Anglia One offshore wind farm.

7.1.1 Site description

From site investigation a general soil profile for the closed-ended piles in Rotterdam is given in Table 14.

Level	Description	Consistency/Compactness
+2.0 to -2.0	Backfill, heterogenous, mainly SAND	Loose to dense
-2 to -10.5	CLAY and PEAT, with sandy interlayers	Very soft to loose
-10.5 to -25.5	Clayey SAND with local peat or clay layers	Loose to dense
-25.5 to -40	SAND with local silt or clay layer	Medium dense to very dense

Table 14: General soil stratification closed-ended piles in Rotterdam.

The open-ended monopiles in the Dutch and German territory of the North sea are largely located in dense sands over the entire installation length. The soil profiles in the UK part of the North sea have a larger variety with alternating sand and (stiff) clay layers. An approximate soil profile for the monopiles located in the UK territory is described in Table 15. The deepest layers on the project site, from -39 to 60 meters, can differ per location in which sand or clay is the dominant soil type. The installation depth of the monopile varies per location and the pile base can be situated in the deepest sand or stiff clay layer.

Level	Description	Consistency/Compactness
mudline to -11	SAND	Dense to very dense sand
-11 to -30	SAND with closely spaced beds of clay and silt	Loose to medium dense sand with very high strength to extremely high strength clays
-30 to -39	SAND	Very dense sand
-39 to -47	SAND with beds of clay / CLAY	Medium dense to dense sand with very high strength to extremely high strength clay
-47 to -60	CLAY with thin to medium beds of sand / SAND with medium beds of clay	Extremely high strength to ultra-high strength clay.

Table 15: General soil stratification for open-ended piles in UK territory.

Figure 75: Onshore wind turbine foundations at Nieuwesluisweg in Rotterdam (M1P25, M1P7, M3P23, M4P2, M4P13, M5P19, M8P17 and M8P24)

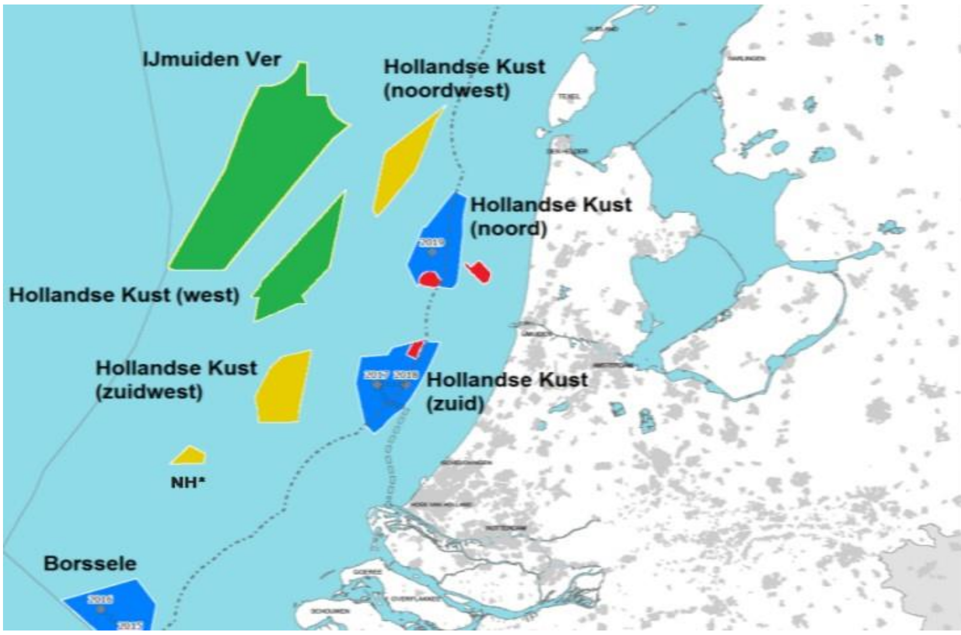

Figure 76: Wind turbine location NZ NL part of OWF HKW

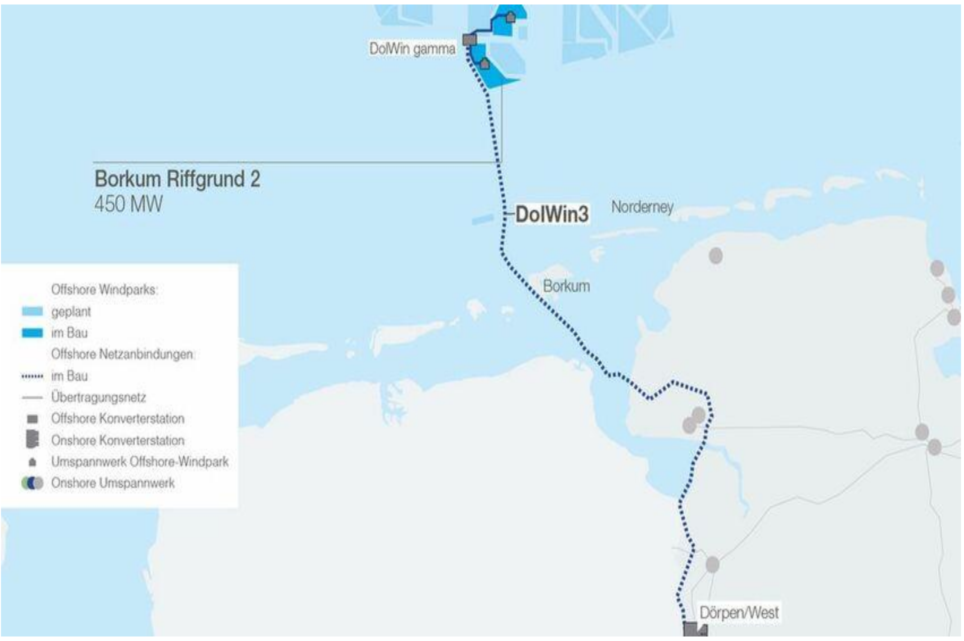

Figure 77: Offshore converter station foundation location NZ GE part of DolWin Gamma OWF

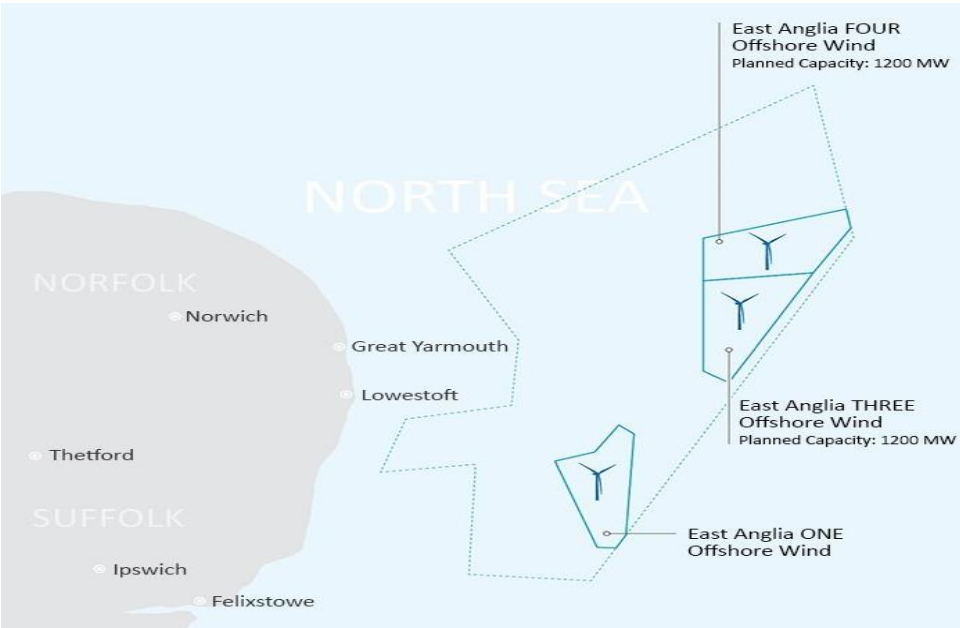

Figure 78: Offshore wind turbine foundations part of East Anglia One OWF (NZ UK B04, C01, C11, D11, D14, D15, F23 and F24)

7.1.2 Soil investigation data

Figure 79 shows the CPT based soil profiles for the prefab concrete closed-ended piles. Based on the cone resistance and sleeve friction, the soil behavior type index I_c is defined. An I_c value below 2.95 simplifies the soil type to sand for which the unified method for driven piles in sand is used (SBTn zone 4-7). An I_c value between 2.95 and 3.6 indicates a clay soil and the unified method for driven piles in clay is considered (SBTn zone 1-3). Values of I_c above 3.6 indicates organic soils and values for local ultimate shaft friction are estimated based by signal matching procedure. Appendix A shows the soil classification over depth for all the piles.

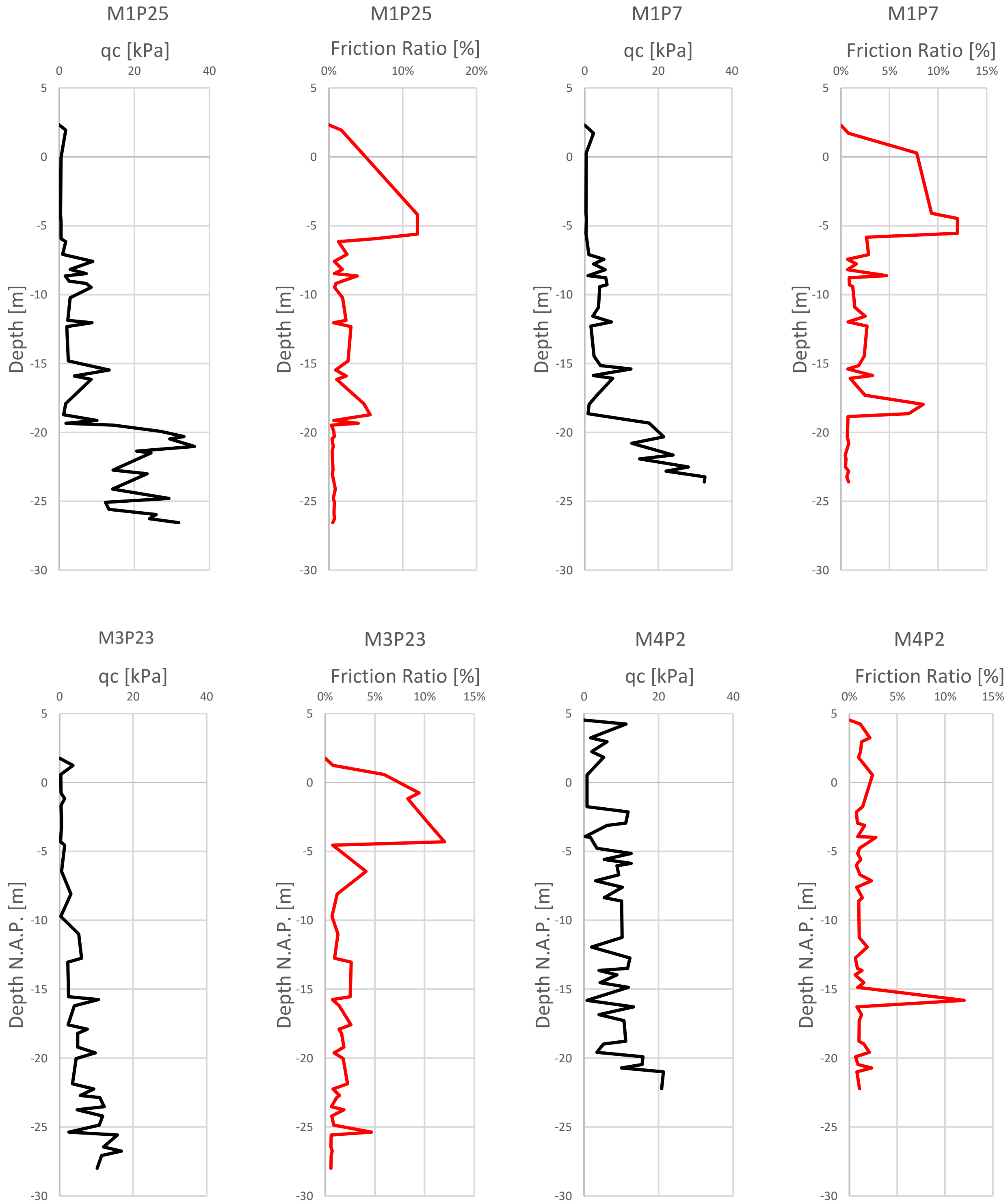

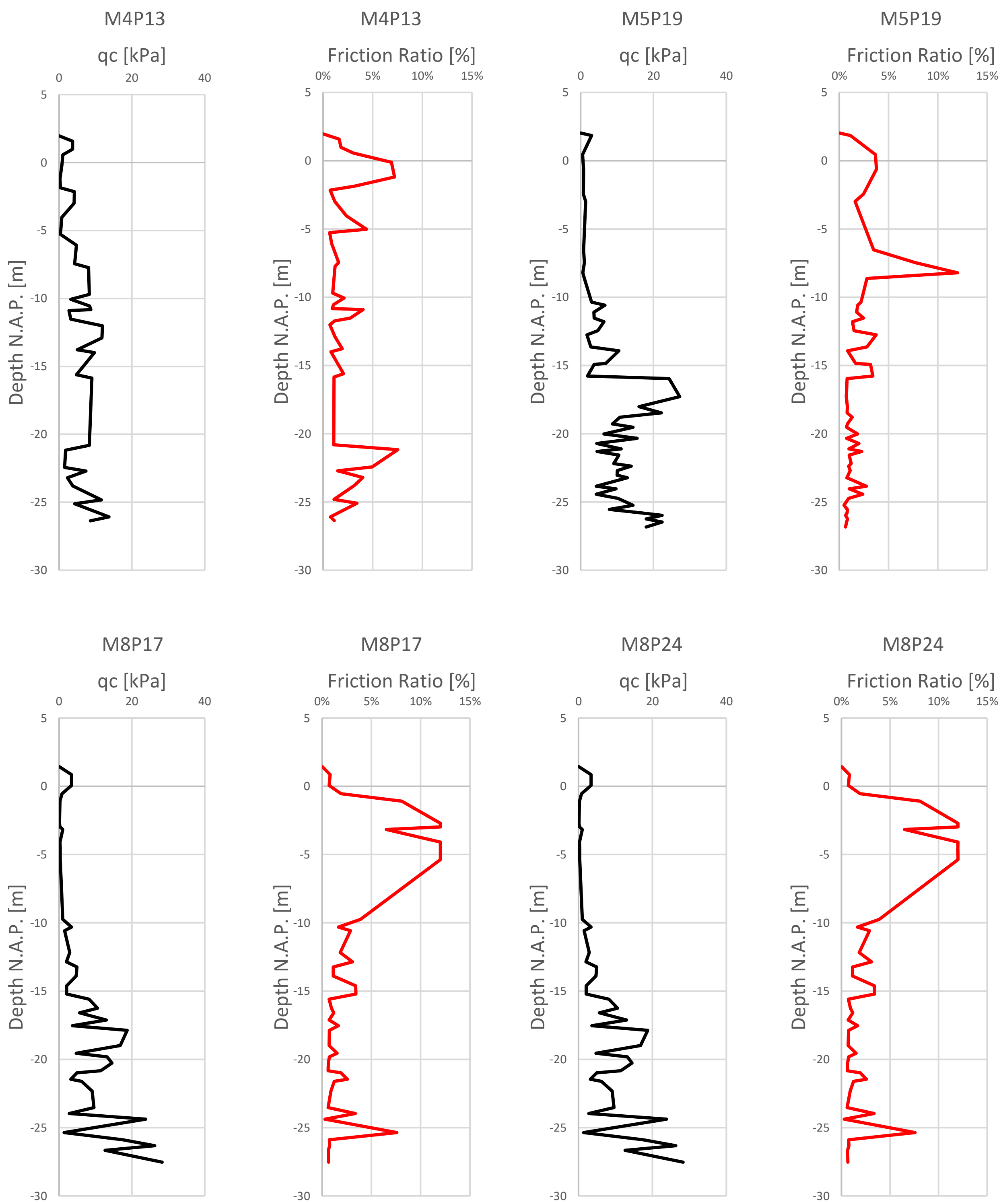

Figure 79: CPT profiles for closed- and open-ended piles

The soil profiles based on CPT data related to the 10 offshore steel open-ended monopiles are shown in Figure 80. The location NZ NL refers to monopile in the Dutch territory of the North Sea. NZ GE refers to the monopile in the German territory and NZ UK B04, C01, C11, D11, D14, D15, F23 and F24 refers to the monopiles in UK territory of the North Sea.

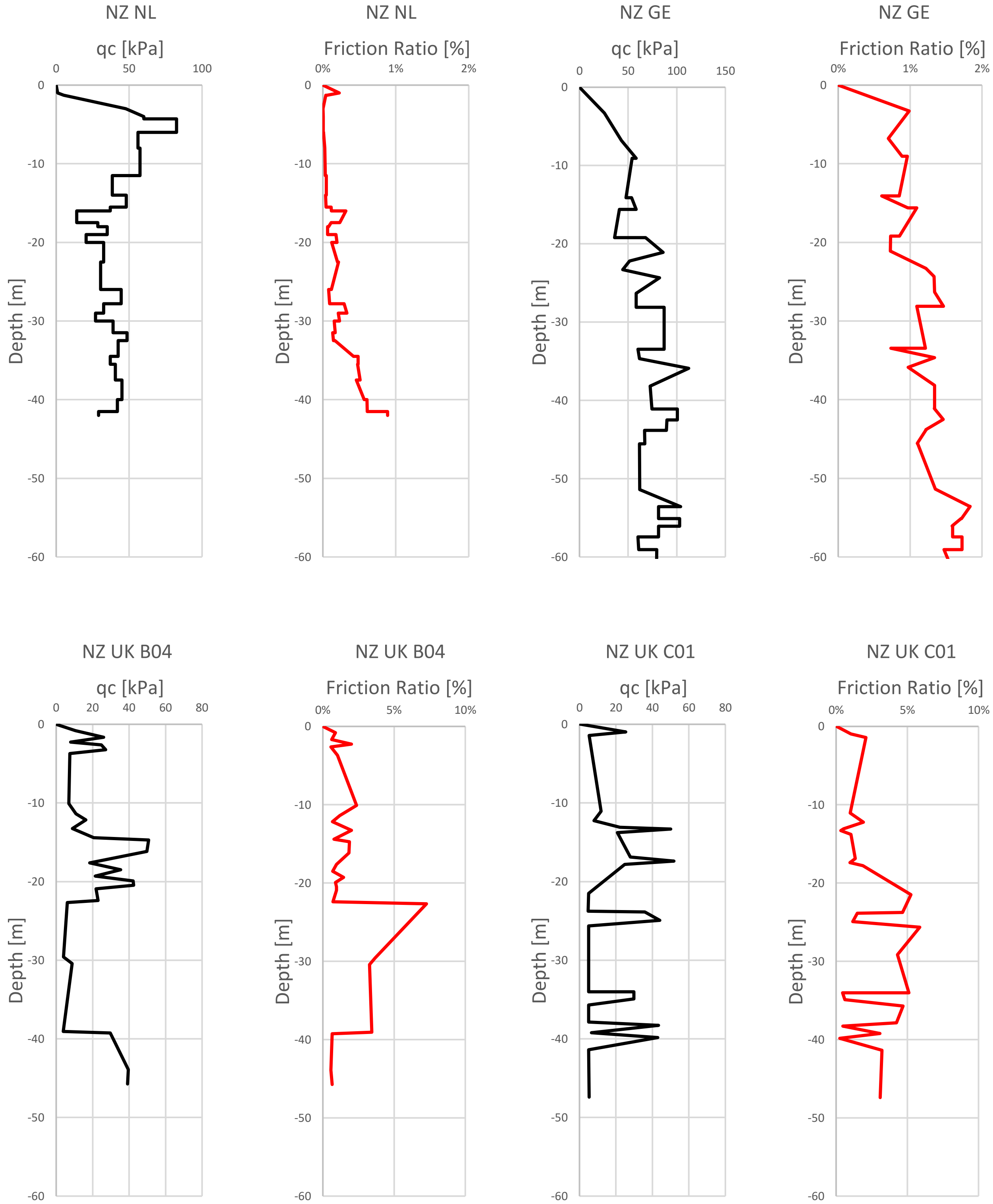

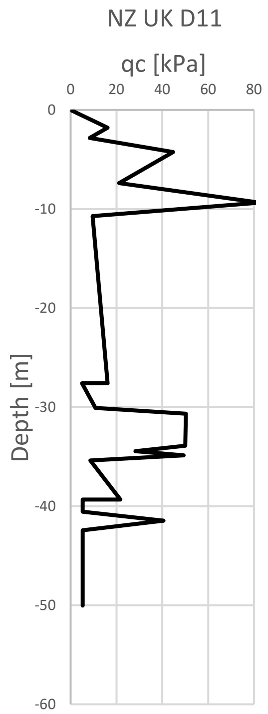
NZ UK D11
qc [kPa]
0 20 40 60 80
Depth [m]
0 -10 -20 -30 -40 -50 -60

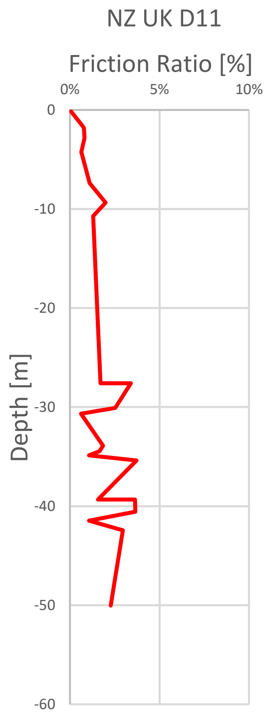
NZ UK D11
Friction Ratio [%]
0% 5% 10%
Depth [m]
0 -10 -20 -30 -40 -50 -60

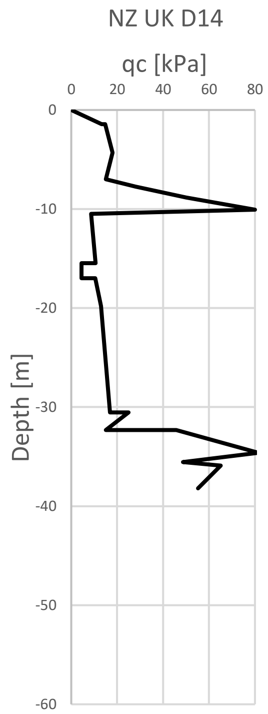
NZ UK D14
qc [kPa]
0 20 40 60 80
Depth [m]
0 -10 -20 -30 -40 -50 -60

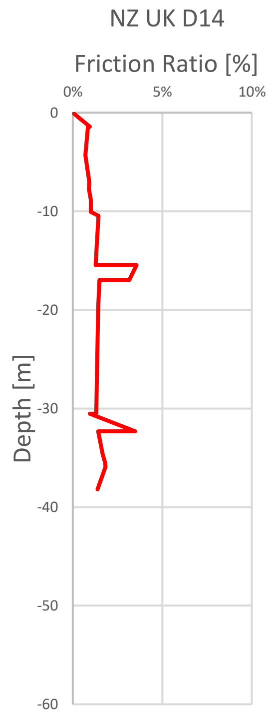
NZ UK D14
Friction Ratio [%]
0% 5% 10%
Depth [m]
0 -10 -20 -30 -40 -50 -60

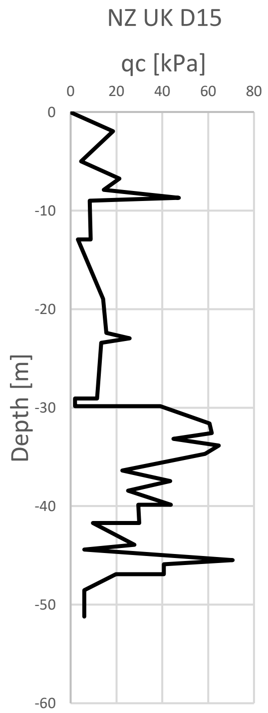
NZ UK D15
qc [kPa]
0 20 40 60 80
Depth [m]
0 -10 -20 -30 -40 -50 -60

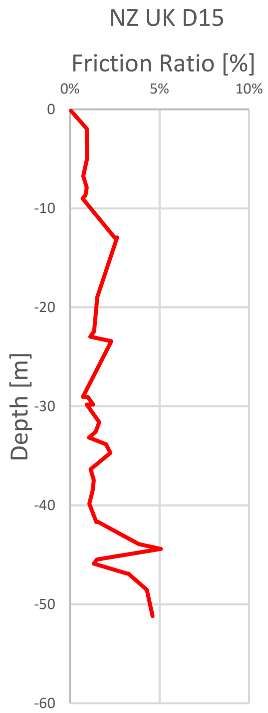
NZ UK D15
Friction Ratio [%]
0% 5% 10%
Depth [m]
0 -10 -20 -30 -40 -50 -60

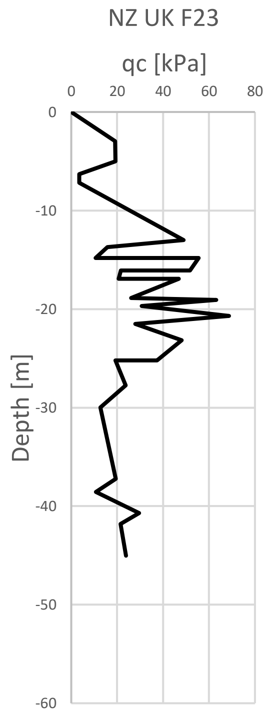
NZ UK F23
qc [kPa]
0 20 40 60 80
Depth [m]
0 -10 -20 -30 -40 -50 -60

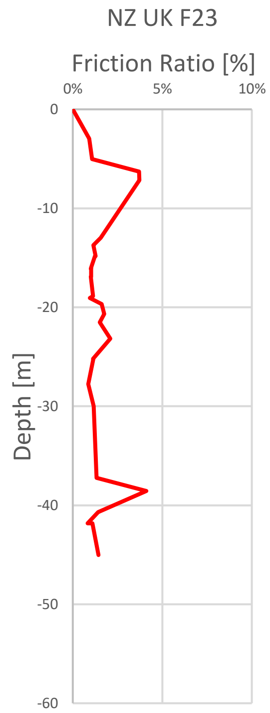
NZ UK F23
Friction Ratio [%]
0% 5% 10%
Depth [m]
0 -10 -20 -30 -40 -50 -60

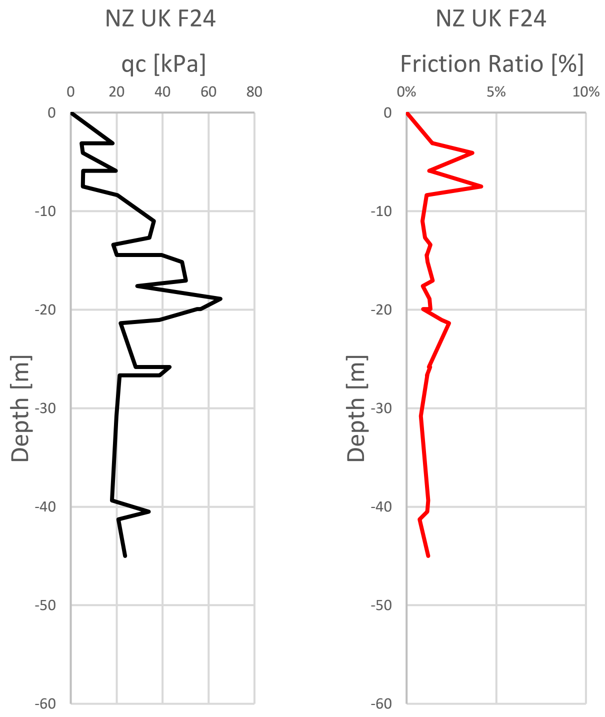

Figure 80: CPT profiles for open-ended piles

7.1.3 Pile dimensions and test dates

The closed-ended piles are prefab concrete piles vary in length from 23.25 to 29.25 meter with a constant diameter of 450x450 mm. The elastic stiffness of the piles vary from 42 MPa to 43.5 MPa, back-calculated from stress wave velocity and the duration of the stress wave for a clear pile base reflection. Table 16 summarizes all the pile information, installation depth and measurement dates for each pile. The restrike date for the majority of the piles is after 1 day of installation, but for a few piles the setup times are 4, 5 or 57 days. The tested piles are part of onshore wind turbine foundations and each wind turbine is supported by around 36 piles.

Pile name	Base level [m N.A.P.]	Penetration below ground level [m]	Setup time [days]
M1P25	-25.5	27.8	1
M1P7	-22.5	24.8	1
M3P23	-27.0	29.3	1
M4P2	-20.5	22.3	57
M4P13	-25.5	27.8	1
M5P19	-26.0	28.5	1
M8P17	-26.0	28.3	5
M8P24	-26.6	27.8	4

Table 16: Pile dimension for closed-ended piles in Rotterdam

The pile dimensions of the open-ended monopiles vary per project and location due to design optimization. The variety can be assigned to outer diameter, number of steel sections and wall thicknesses. At target depth, a dynamic load test is performed directly after end of initial driving (EOID) and the restrike (RS) after a couple of hours. A summary of all the tested piles are shown in Table 17.

Pile name	Base level below mudline [m]	Outer diameter ⌀ [m]	Steel sections Top to bottom [m]	Steel sections wall thickness Top to Bottom [mm]	Setup time EOID [days]	Setup time RS [days]
NZ NL	-38.80	2.438	17.1/33	65/55	0.01	1.0
NZ GE	-57.25	2.5	49.332/3/20	80/75/70	0.01	1.0
NZ UK B04	-43.22	2.5	8.775/6/29.225	54/44.5/38	0.01	0.17
NZ UK C01	-43.06	2.5	8.775/6/30.225	54/45/40.5	0.01	0.25
NZ UK C11	-46.93	2.5	8.775/6/32.725	54/44.5/38	0.01	0.22
NZ UK D11	-49.25	2.5	8.775/6/34.725	54/45/40.5	0.01	0.37
NZ UK D14	-36.12	2.5	7.775/6/21.725	54/45/40.5	0.01	0.33
NZ UK D15	-50.93	2.5	8.775/6/35.725	54/45/40.5	0.01	0.47
NZ UK F23	-41.59	2.5	8.775/6/27.725	54/44.5/38	0.01	0.42
NZ UK F24	-41.90	2.5	8.775/6/28.225	54/44.5/38	0.01	0.23

Table 17: Pile dimension for open-ended piles in North Sea sectors

In the design methods, the diameter of an open-ended monopile is converted to an equivalent diameter in which an open-ended monopile has the same soil displacement during installation as an equivalent closed-ended pile. For large offshore monopiles, in which full coring occurs, the equivalent diameter becomes

$$D^* = \sqrt{D_o^2 - D_i^2} \tag{191}$$

For a squared prefab concrete closed-ended pile the outer diameter is set equal to a circular pile with equal pile toe area as a squared pile.

$$D^* = D_o = 2 * \sqrt{\frac{LxB}{\pi}} \tag{192}$$

7.2 Signal matching analysis

In the TNO soil model the most important soil model parameters are the yield stress, quake value and damping constant. For shaft radiation damping, the exponent of the velocity is set to unity for the pile shaft and 0.2 at the pile base for both piles in sand and clay as proposed by Deeks and Randolph (1995). Unity for the shaft velocity exponent has been chosen from experience and to reduce the number of parameters in the signal matching process. In addition, the radiation damping constant at the pile base is also fixed to the theoretical value according to Deeks and Randolph (1994) and because of that merely the shaft radiation damping constant is varied in the signal matching procedure. In the TNO soil model, the yield stress at the pile shaft is set equal to the local ultimate shaft friction obtained from CPT-based design methods at the start of matching. The objective is to match the parameters of the TNO model with the yield stresses as close as possible to calculations from the design methods and with realistic values for the loading and unloading quake, yield ratio and damping such that a good match is achieved between the simulated and measured upward travelling stress wave supported with a fairly accurate match on velocity and displacement at pile head level. A relative small deviation between the simulated and measured pile displacement is allowable because of integration errors with double integration of measured accelerations.

7.2.1 Signal matching results of closed-ended piles

In Figure 82 the best obtained signal matches are shown for each location. The first column shows the force of the upward travelling stress wave which contains information about the mobilized soil resistances and the second column shows the pile head displacements. The displacements are calculated by double integration of the accelerometer mounted at the pile head. The pile head displacement diagram plays a key role in determining a reasonable quake value for the pile base model. A nonzero permanent pile displacement is only reached if the displacement at the pile base has exceed the elastic limit or quake value at the pile base, when assuming complete rebound of the pile at rest when the impact force has fully dissipated after hammer blow.

M1P25

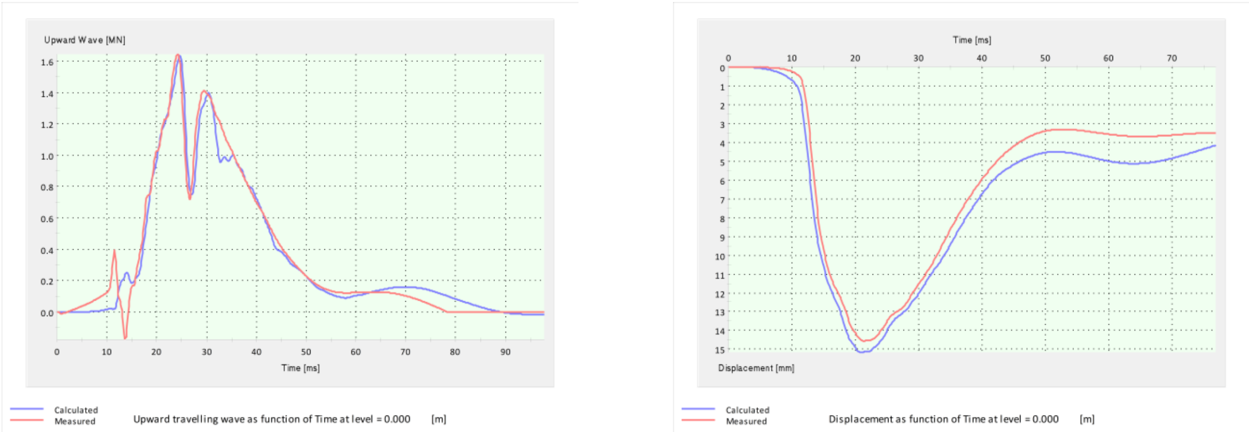

M1P7

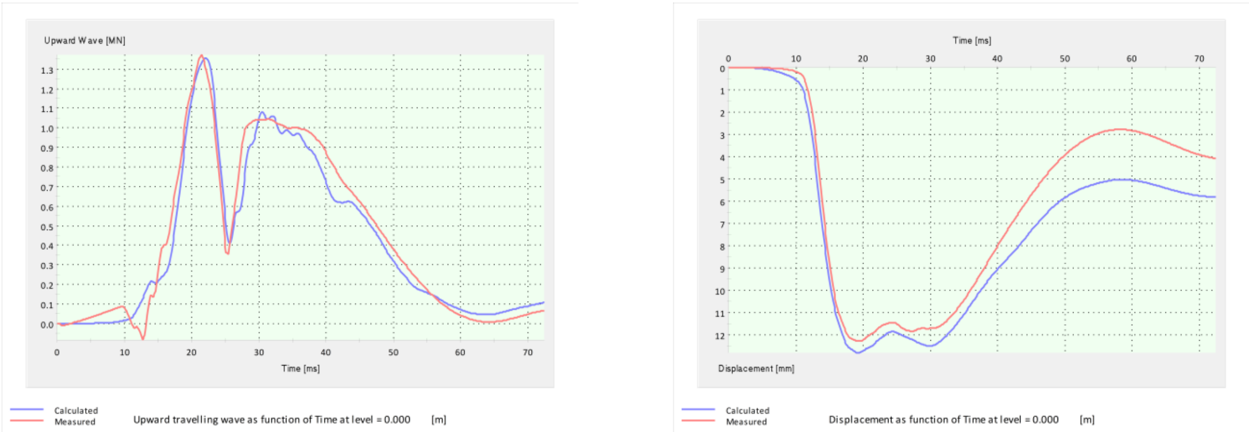

M3P23

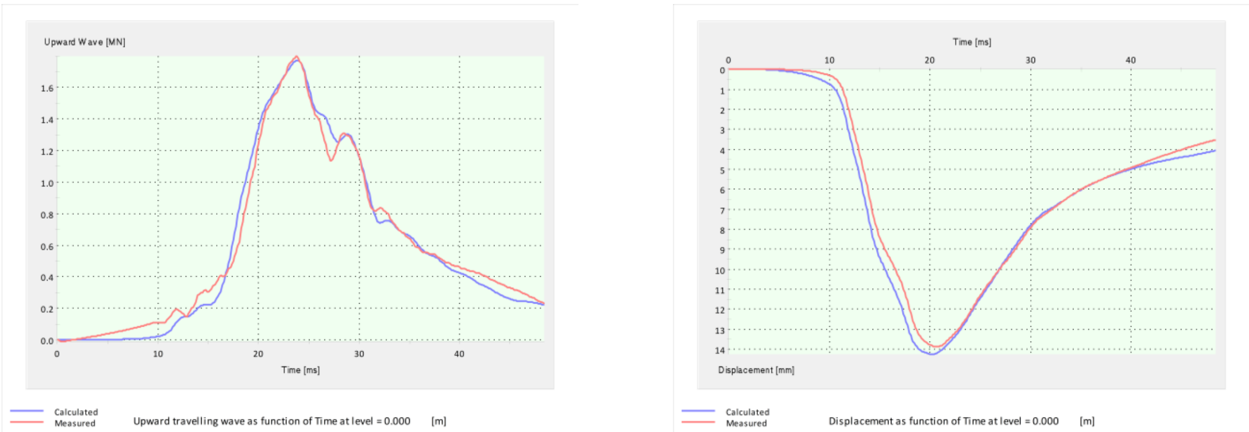

M4P2

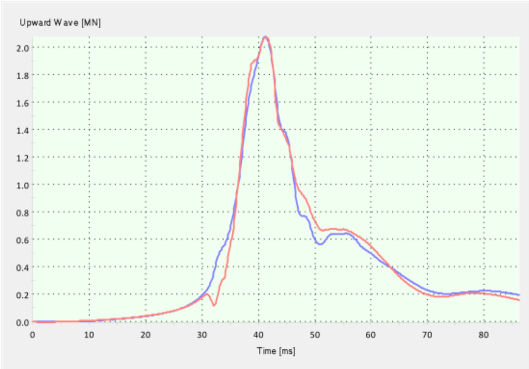

Calculated
Measured
Upward travelling wave as function of Time at level = 0.000 [m]

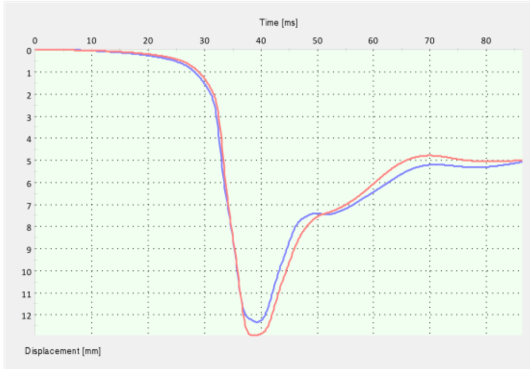

Calculated
Measured
Displacement as function of Time at level = 0.000 [m]

M4P13

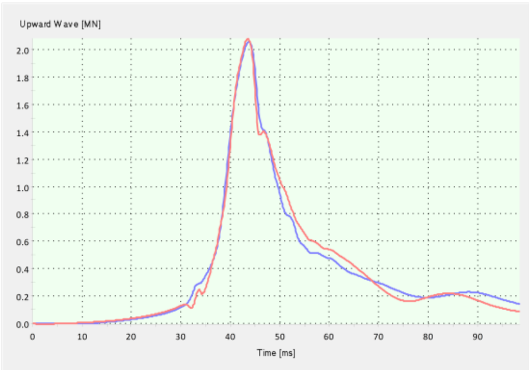

Calculated
Measured
Upward travelling wave as function of Time at level = 0.000 [m]

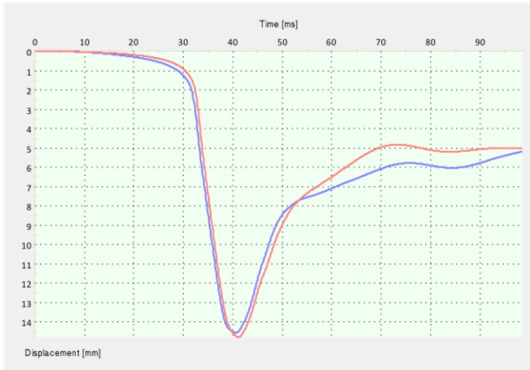

Calculated
Measured
Displacement as function of Time at level = 0.000 [m]

M5P19

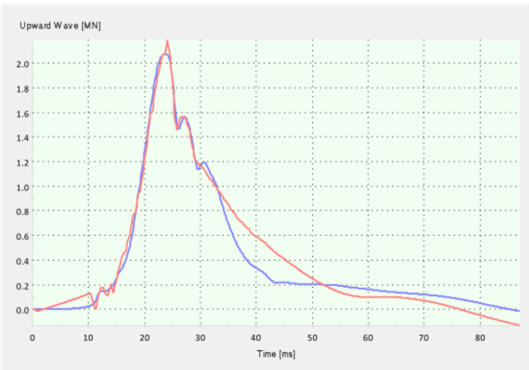

Calculated
Measured
Upward travelling wave as function of Time at level = 0.000 [m]

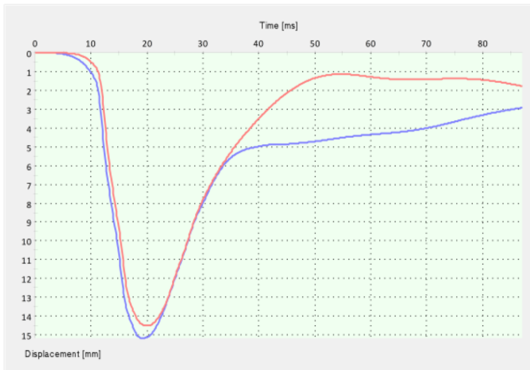

Calculated
Measured
Displacement as function of Time at level = 0.000 [m]

M8P17

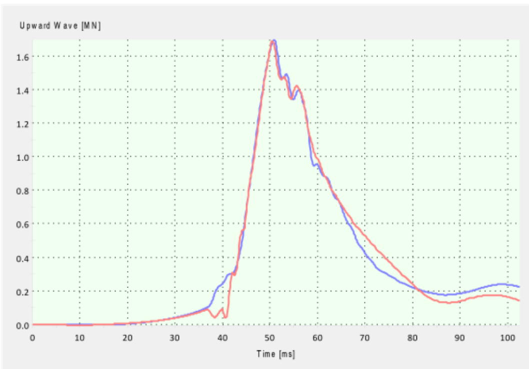

Calculated
Measured
Upward travelling wave as function of Time at level = 0.000 [m]

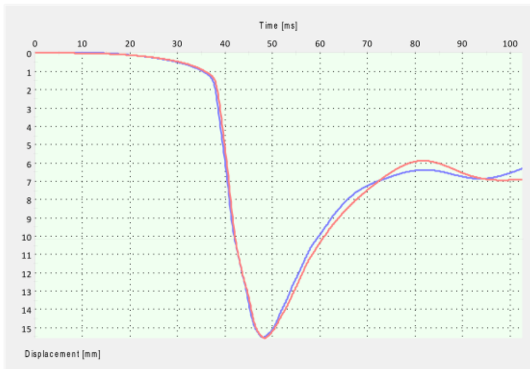

Calculated
Measured
Displacement as function of Time at level = 0.000 [m]

M8P24

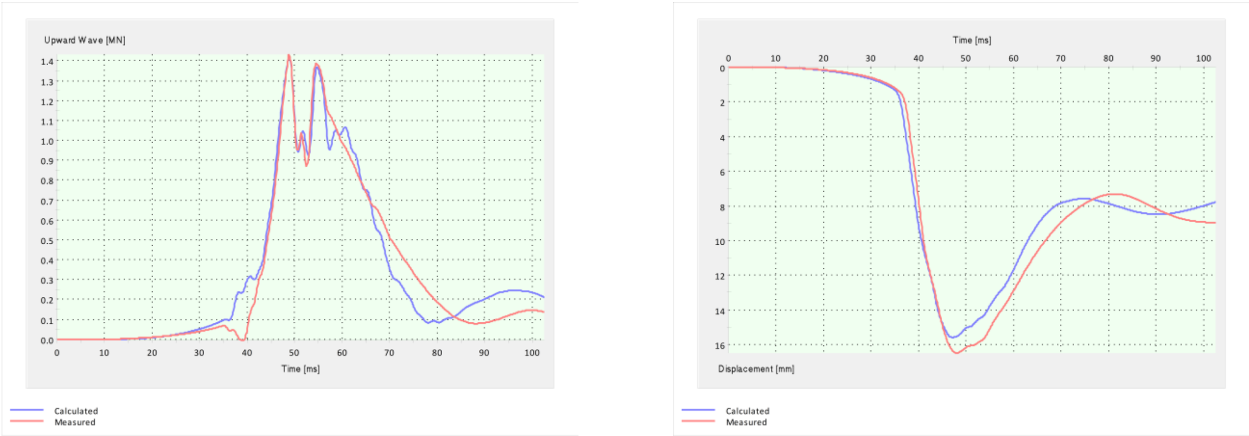

Figure 81: Signal matching results for upward wave (left) and displacement (right) for closed-ended piles

7.2.2 Signal matching results of open-ended monopiles

In addition to the results in Figure 81, a similar matching procedure has been performed on the offshore open-ended monopiles shown in Figure 82. In contrast with the closed-ended piles, each monopile has been tested two times, at end of initial driving and a couple of hours later at restrike. Figure 82 shows the best obtained signal match for each monopile on the force of the upward travelling stress wave and pile head displacement. After some filtering, the signals for monopiles are slightly more noisy because of higher degree of impedance changes along the pile due to changing wall thickness and long cable lengths between sensors and pile driving recorder (PDR) affecting electronical signal quality. A well observed soil strength gain between EOID and RS at the lower pile sections and pile base can be observed for example at pile NZ UK D15**.** At end of driving the upward travelling stress wave goes from a tensional stress wave to a compressional stress wave in a couple of hours after installation. The increase in shaft resistance can be partly explained by setup effects, but also caused by increased damping or higher soil stiffness when the results of the design methods are adhered to.

NZ NL EOID

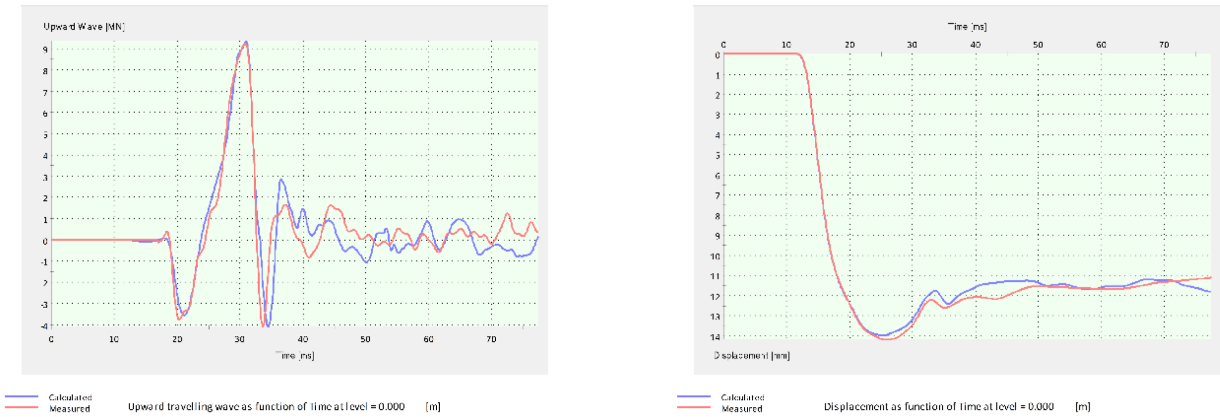

NZ NL RS

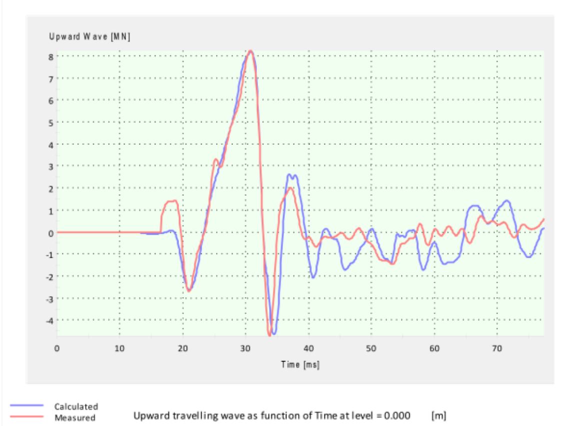

NZ GE EOID

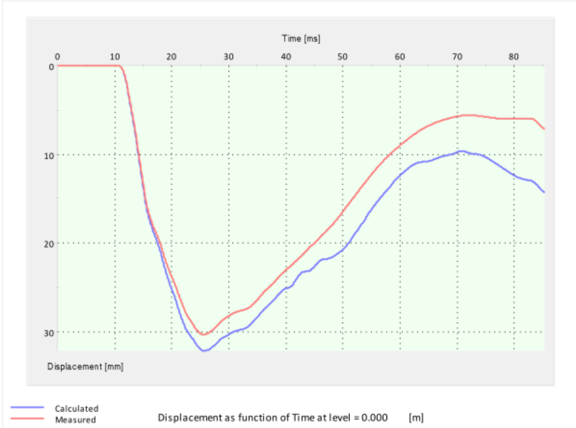

NZ GE RS

NZ UK B04 EOID

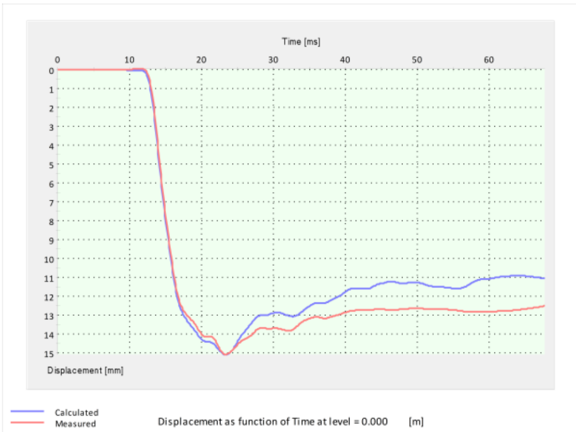

NZ UK B04 RS

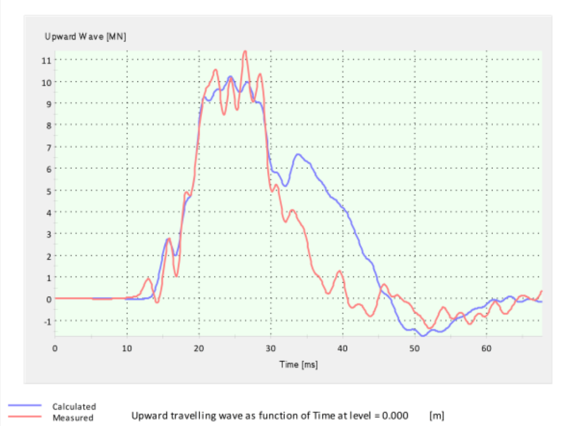

UK C01 EOID

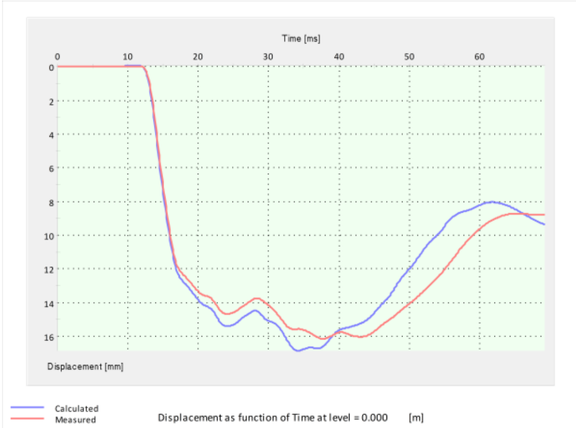

NZ UK C01 RS

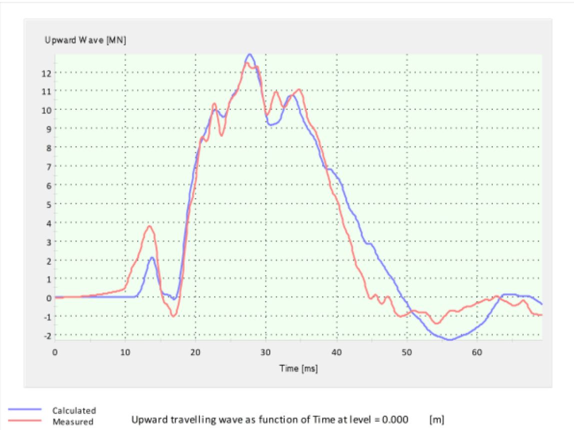

NZ UK C11 EOID

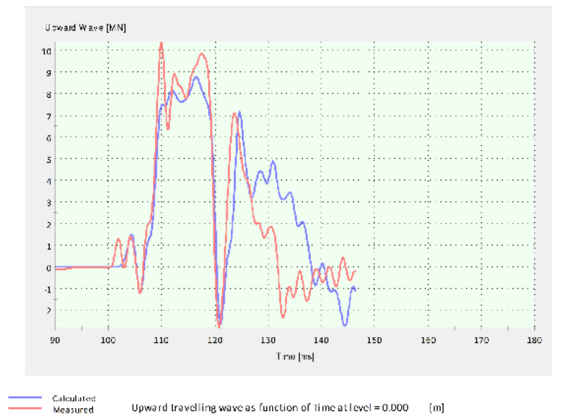

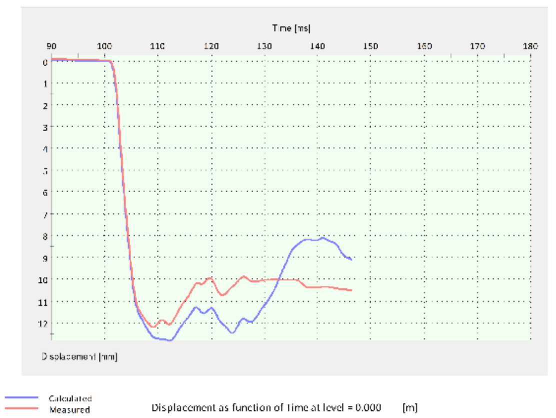

NZ UK C11 RS

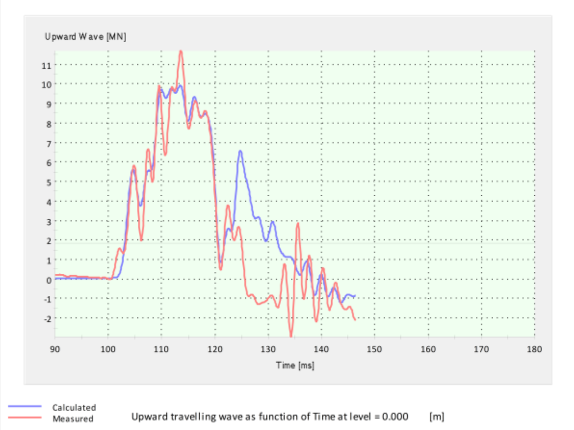

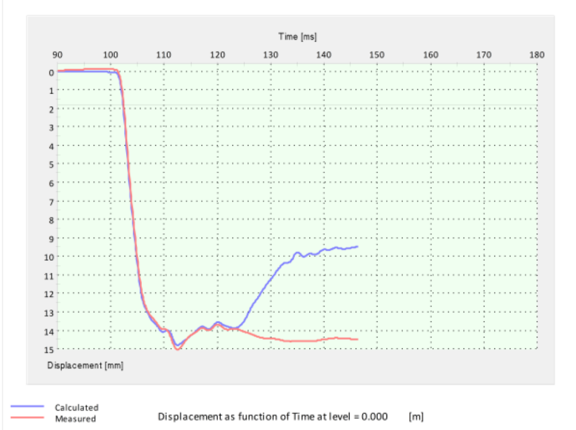

NZ UK D11 EOID

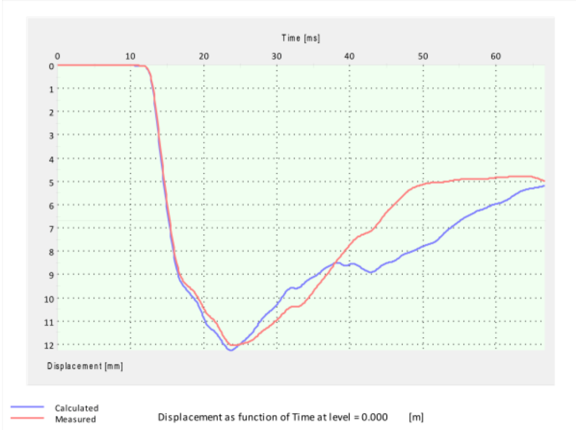

NZ UK D11 RS

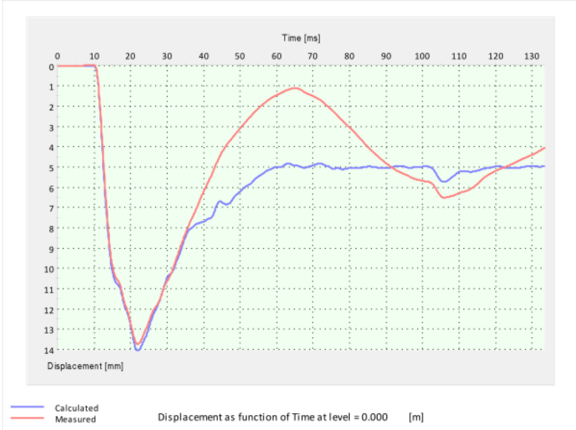

NZ UK D14 EOID

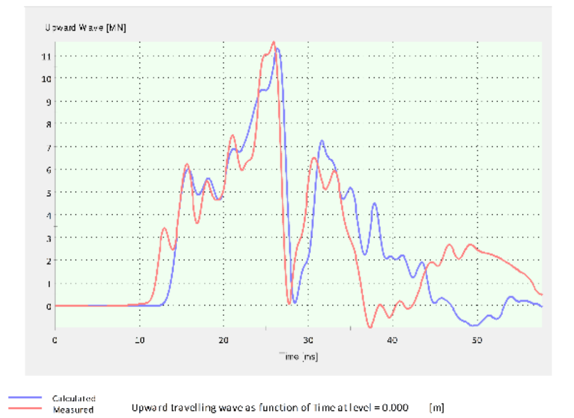

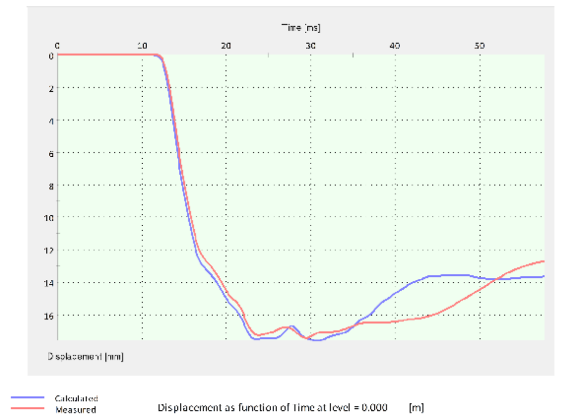

NZ UK D14 RS

Calculated
Measured
Upward travelling wave as function of Time at level = 0.000 [m]

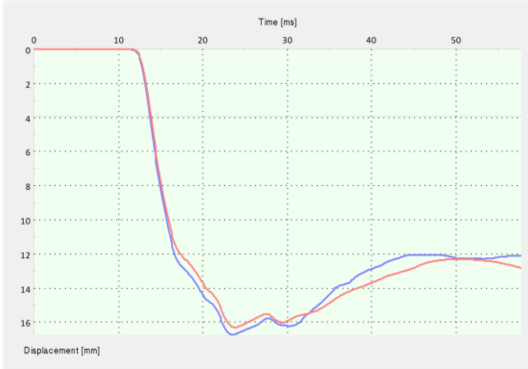

Calculated
Measured
Displacement as function of Time at level = 0.000 [m]

NZ UK D15 EOID

Calculated
Measured
Upward travelling wave as function of Time at level = 0.000 [m]

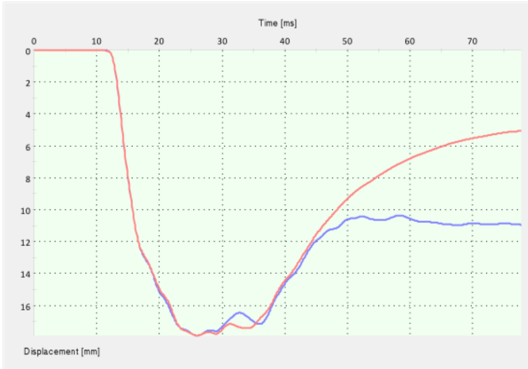

Calculated
Measured
Displacement as function of Time at level = 0.000 [m]

NZ UK D15 RS

Calculated
Measured
Upward travelling wave as function of Time at level = 0.000 [m]

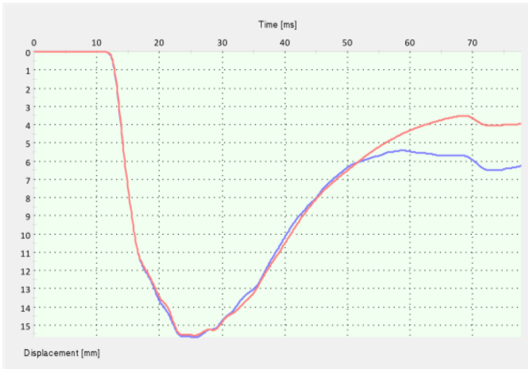

Calculated
Measured
Displacement as function of Time at level = 0.000 [m]

NZ UK F23 EOID

Calculated
Measured
Upward travelling wave as function of Time at level = 0.000 [m]

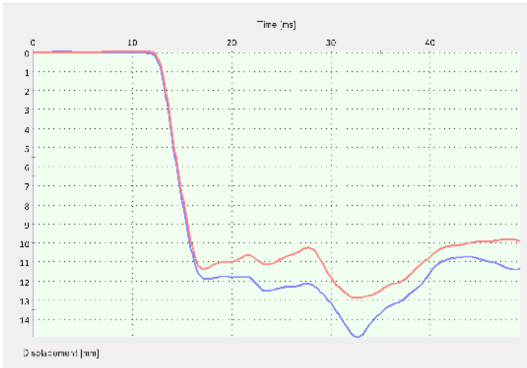

Calculated
Measured
Displacement as function of Time at level = 0.000 [m]

NZ UK F23 RS

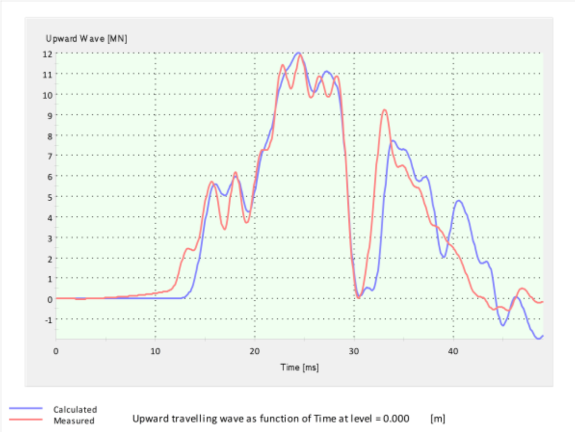

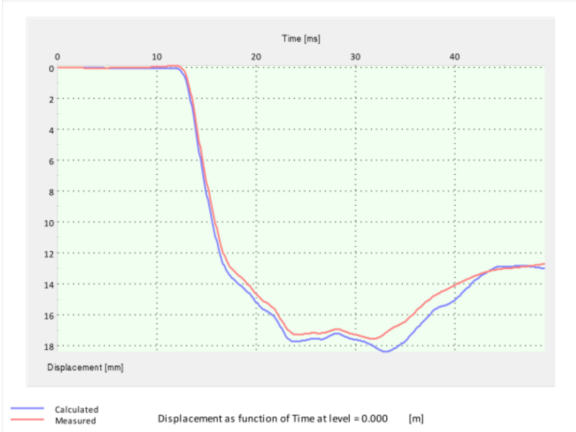

NZ UK F24 EOID

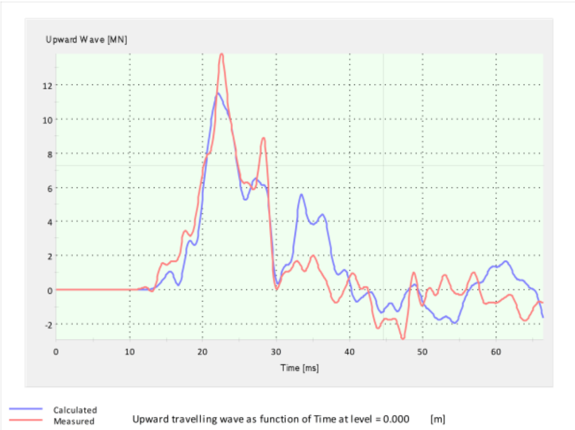

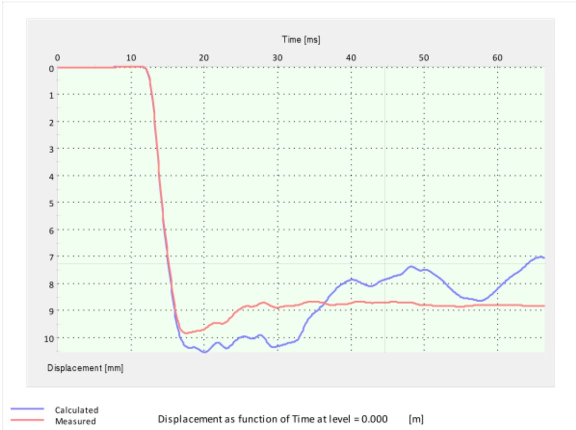

NZ UK F24 RS

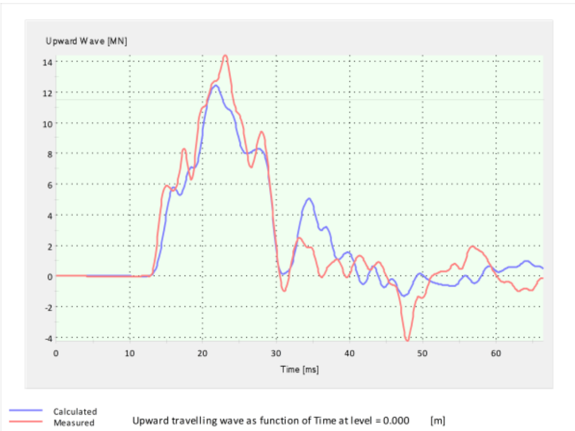

Figure 82: Signal matching results for upward wave (left) and displacement (right) for open-ended piles in the North Sea, NL, GE and UK.

7.3 Local ultimate shaft friction calculations by the unified method

As mentioned in Section 4.3, the unified method for driven piles in sand gives values for local ultimate shaft friction for setup periods of 14 days. The set-up of shaft friction is not considered explicitly in the method and the method is intended to provide an estimate of medium-term static capacity corresponding to a set-up period of 2 weeks (median set-up time for the pile load tests in the unified database). For driven piles in clay the unified method provides the local ultimate shaft friction for piles with at least 80% of consolidation. During dynamic loading of the pile, it is assumed that the yield stress by means of a plastic slider in the mechanical TNO soil model (Chapter 2 and 5) represents the calculated local ultimate shaft friction obtained from the unified CPT based axial pile capacity design methods with corrections for setup periods for sand and clay (Section 4.6). Soil investigation data for the offshore windfarms in the Dutch and German territory of the North Sea indicates merely sandy subsoils, but in the UK sector of the North Sea the presence of some very stiff clay layers are observed. Soil investigation data from the UK territory also provide information about the undrained shear strength of these clay layers. In case a plausible signal match was only possible if very high local shaft friction had to be applied and high damping constants were not sufficient to explain the high shaft resistance a decision was made to take the yield stress in the TNO soil model close to the undrained shear strength from the provided lab test results. It was observed that for the deep stiff clay layers near the pile base, local ultimate shaft friction close to the undrained shear strength increased the matching quality significantly rather than increasing the damping constant in order to increase the shaft resistance. The distribution of local ultimate shaft friction for all the piles in Figure 83 are with predefined setup periods as formulated by the authors of the unified CPT based axial pile capacity design methods for piles in sand (2 weeks) and clay (80% consolidation). In order to start the signal matching procedure in Allwave-DLT after a dynamic load test is performed at end-of-initial-driving (EOID) or restrike (RS), a setup factor is applied to correct the initially calculated local ultimate shaft friction for EOID and RS to represent the estimated in-situ soil friction properly in the TNO soil model for that short setup period. The setup factor for piles in sand at EOID ($t = 0.01$) is about 0.69 and at restrike at 1 day after driving ($t = 1$) is 0.74 in accordance with equation (93). The setup factor for the clay layers is not only a function of time but also depends on pile dimensions and plug length ratio as formulated in equation (95).

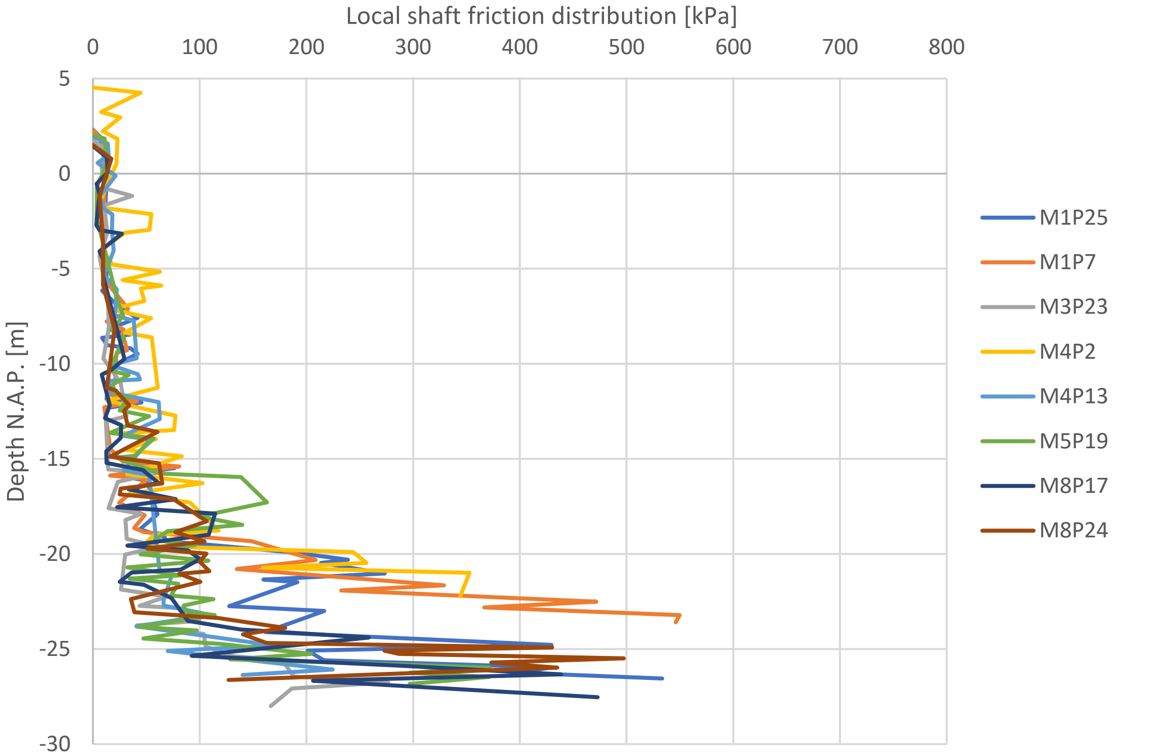

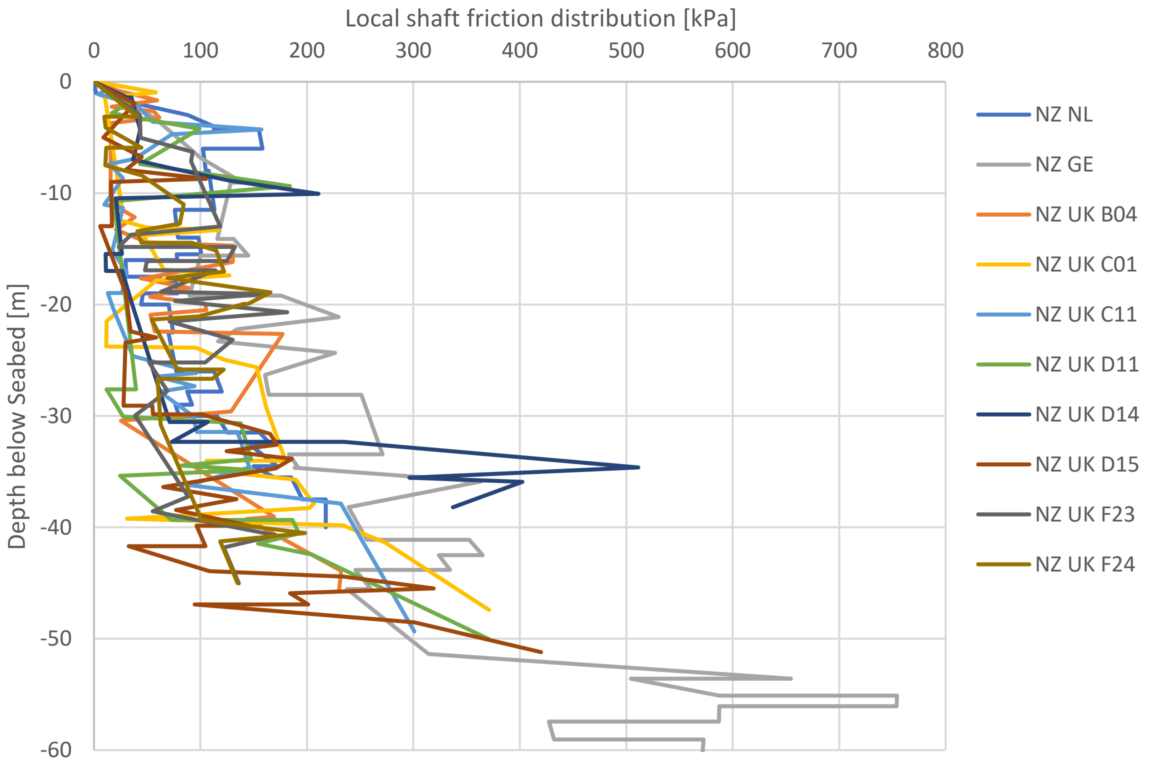

Figure 83: Local ultimate shaft friction distribution obtained from direct calculations by the unified methods for piles in sand and clay for closed- (top) and open-ended piles (bottom)

7.4 Shaft yield stress deviation from local ultimate shaft friction

As starting point for the yield stress in the TNO soil model, the local ultimate shaft friction calculated by the unified methods for piles in sand and clay has been considered. The unified methods are the latest developed CPT-based bearing capacity methods in industry in 2022. The coefficient of variation for total capacity based on the unified method is in the order of 20% to 25% (ASCE, 2020). Figure 84 shows the statistics of commonly used empirical methods for total pile capacity calculations and the recently improved unified method. The calculated values for pile capacity by the unified method is based on (average) cone resistance values $\mathrm{q_c}$, interface friction angle between pile and soil φ_{cv}, degree of soil displacement or plugging PLR, influence of relative pile base depth h, changes in radial stress during loading $\Delta\sigma_{\mathrm{rd}}$, initial radial stresses σ_{rc} and pile dimension $\mathrm{D/t}$ (Section 4.3). Pile dimensions, relative pile depth and cone resistance are fixed values, while the other parameters depends on correlation functions in relation to the cone resistance and pile dimensions. In particular, the interface friction angle between pile and soil must be estimated by correlation functions between the cone resistance. Due to method uncertainty in estimating the pile axial capacity, the applied yield stresses in the TNO soil model are allowed to vary within an acceptable range from the calculated local ultimate shaft friction obtained from the design method. The soil around the pile is subdivided into sand and clay layers and the number of layers i.e. datapoints in this research are respectively for sand and clay 486 and 92 for the closed-ended piles and for the open-ended monopiles respectively 852 and 76. The number of datapoints for clay layers are relative limited compared to the set of datapoints related to the sand layers, because monopiles are preferably constructed in stable and predictable soils in the North Sea. On top of that, the relative constant cone resistance for the clay layers resulted in thicker layers whereby the number of distinguished clay layers reduces.

Method	μ_w	σ_w	CoV_w	Range of validity
API-00	1.48	0.73	0.49	$0.5<Q_{m,t}/Q_{c,t}<2$
Fugro-05	0.93	0.31	0.33	$0.5<Q_{m,t}/Q_{c,t}<1$
ICP-05	1.25	0.56	0.45	$Q_{m,t}/Q_{c,t}<0.7$
	1.07	0.33	0.31	$Q_{m,t}/Q_{c,t}>0.7$
NGI-05	0.99	0.34	0.35	$0.5<Q_{m,t}/Q_{c,t}<1.25$
UWA-05	1.07	0.30	0.28	$0.5<Q_{m,t}/Q_{c,t}<2$
ICP-API	1.23	0.36	0.29	$0.7<Q_{m,t}/Q_{c,t}<1.5$
UWA-OS	1.30	0.41	0.32	$Q_{m,t}/Q_{c,t}<1$
	1.29	0.34	0.27	$Q_{m,t}/Q_{c,t}>1$
Unified	**1.05**	**0.24**	**0.23**	**All**

Figure 84: Method uncertainty for total capacity calculations for several empirical methods *(ASCE, 2020)*

In Figure 85, the deviations between the calculated values for local ultimate shaft friction from the unified methods (τ_{sf}) are compared with the obtained yield stresses (F_y in Chapter 3.1) after signal matching analysis with the highest matching quality for both closed- and open-ended piles for each pile-soil element. The local ultimate shaft friction is corrected by a setup factor for each pile depending on duration between installation and testing and soil type. Figure 85 shows the deviations plotted against relative pile depth $\mathrm{h/R^*}$ to compare the results at similar friction fatigue levels. The top scatter plot in Figure 85 shows the deviations for the closed-ended piles and the lower scatter plot the deviations for the open-ended piles. Figure 85 shows that for almost all closed-ended piles, the obtained yield stresses are within a range of -15% to +15% from the calculated local ultimate shaft friction regardless relative pile depth. The positive deviation for restrike at 1 day after installation for sandy layers show that the yield stress appeared to be higher than the calculated local ultimate shaft friction. After pile driving, the soil around the pile may be compacted and densified due to the dynamic loading from the hammer blows. This densification can result in increased shaft friction and end bearing capacity of the pile, leading to higher initial pile capacity than what would be predicted based on initial soil conditions. Over time, as the soil around the pile gradually returns to its natural state, the stresses and pore pressures may readjust. Opposite to that, mainly negative deviations are observed for all other restrikes days (4,5 and 57) regardless soil type. The yield stress of the clay layers mainly vary between -5% and -20% from the calculated values, but do not show any switch of sign in deviation after longer setup periods as can be seen for the sand layers at 1 day after installation. It seems that the clay layers do not recover some of their shear strength at the same pace as the setup correction suggests after installation effects diminish. In general for the pile shaft in sand, the calculated local ultimate shaft friction underestimates the yield stress at 1 day after installation, but overestimates the yield stress once the setup period is longer. Increasing or decreasing the shaft friction and decreasing or increasing the shaft radiation damping constants did not overcome the under- or overestimation of the local ultimate shaft friction and reduced the matching quality significantly once pile base reflection should be dominant (signal period 4 & 5 in Chapter 6.6). Increasing the radiation damping constants along the shaft causes a higher dissipation of stress wave energy in the surrounding. As a consequence, the energy of the downward travelling stress wave reduces significantly and mobilize less shear friction near the pile base resulting in lower permanent pile displacement. The lower scatter plot in Figure 85 shows the deviations between the TNO soil model and design method calculations for the open-ended piles in the three different regions in the North Sea. The yield stress deviations are equally distributed within a range of -10% to +10% from the calculated local ultimate shaft friction regardless soil type and time of restrike. There are a few extreme deviations visible in the scatter plot, but these outlier are mainly caused by lack of continuous CPT data over depth for the monopile in the Dutch Nort Sea. Summarized, the deviation between the yield stress in the TNO soil model and the calculated local ultimate shaft friction by the unified method are within an acceptable range of uncertainty as mentioned by the authors of unified CPT-based axial pile capacity design method for driven piles in sand and clay (Figure 84).

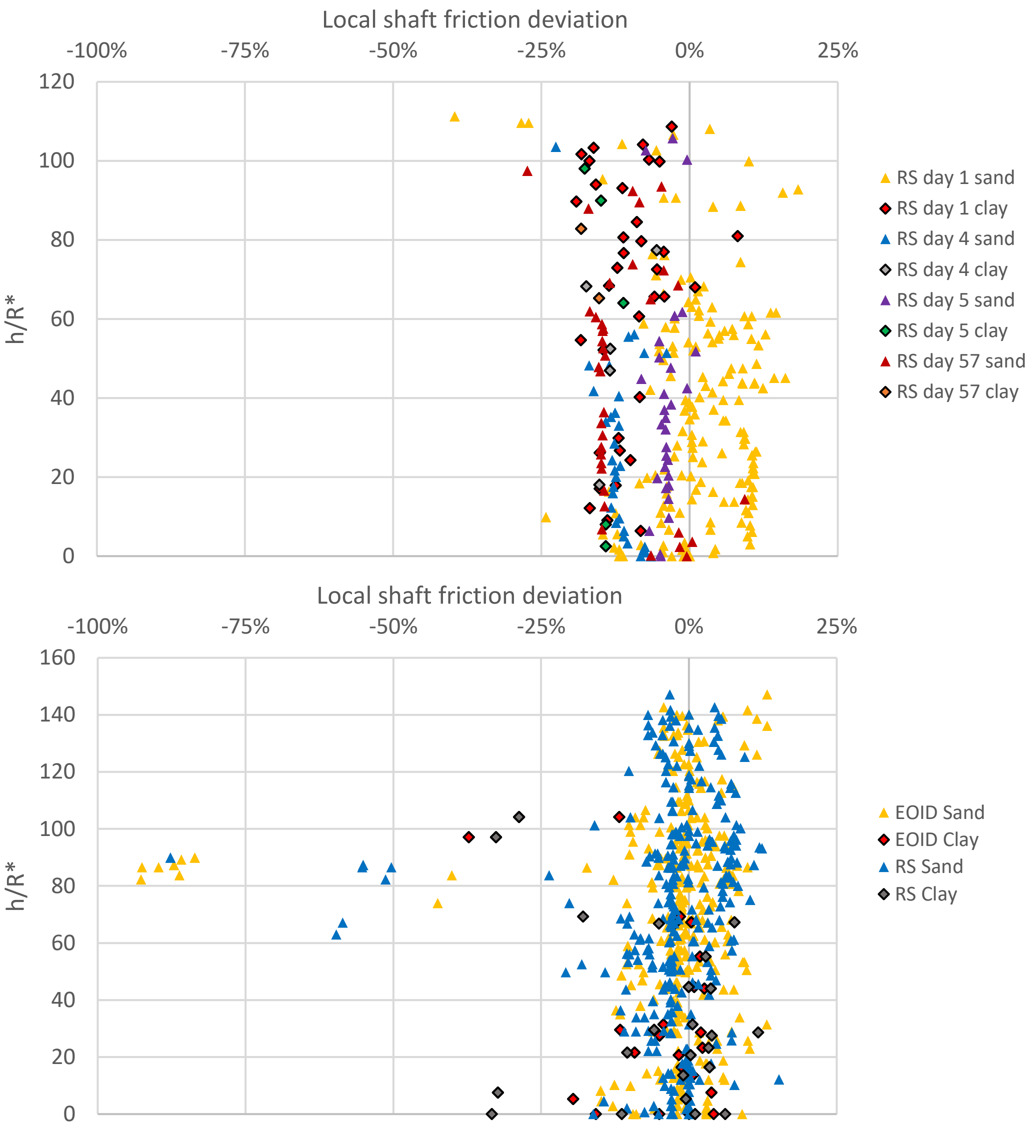

Figure 85: Local shaft friction deviations between unified method and signal matching for closed-ended (upper) and open-ended piles (lower)

7.5 Shaft quake values and shear modulus reduction

The quake value determines the elastic range of the elastoplastic springs in the TNO soil model. When the displacement between the pile and soil is larger than the quake value, all the available static resistance is activated and the yield stress in the TNO soil model has reached the maximum value. The soil changes from elastic to plastic behaviour and slippage between pile and soil results in a permanent pile displacement. In the asymmetric elastoplastic model, a loading and unloading quake must be defined. From experience a loading and unloading quake around 2 to 2.5mm is commonly used in practise for the shaft spring. In Figure 86 the obtained loading quakes after signal matching analysis are shown for the closed- and open-ended piles at end of driving and restrike. All the restrikes on the open-ended piles are performed within a couple of hours after driving and therefore clustered. The scatter plot shows that the loading quakes for both closed- and open-ended piles are close to the proposed range of 2 to 2.5mm for impact driving and are soil type independent. Slightly more spreading is observed for the open-ended piles, but still in a range from 2 to 3 mm for the pile shaft and closer to the pile base the scatter becomes larger. An explanation for the larger deviation for the open-ended piles might be caused by the high embedment of the monopiles with significant stresses acting on the lower pile shaft and base which could result in the presence of post-driving residual stresses or not a full mobilization of lower shaft resistance. Relative low quake values could be due to locking in of residual stresses after driving, where the soil close to the pile base did not fully rebound and remained in a state of incomplete unloading with compressive stresses and negative skin friction in the upper parts of the pile. Reloading a soil in compressional state during dynamic loading reduces the pile displacement that is needed to reach the yielding point and the obtained yield stress and loading quake seems to be reasonable lower for the bottom parts of the shaft. On the other hand, the soil that experience negative skin friction (upper pile shaft) needs more pile displacement to fully activate the shaft friction during a restrike and to reach the yielding point whereby a higher loading quake is expected and could be higher than usually values about 2.5 mm in the upper parts of the pile. In Section 4.8 the relation between residual stresses and the spring model are discussed in more detail. The variability of the quake values can also be the result of different soil conditions. Factors that affect the quake values are soil stiffness and density; stiff and dense soils like dense sands tend to provide more resistance to driving, resulting in reduced pile displacement or quake value. Softer soils like normal consolidated clays allow more pile displacement to achieve full resistance.

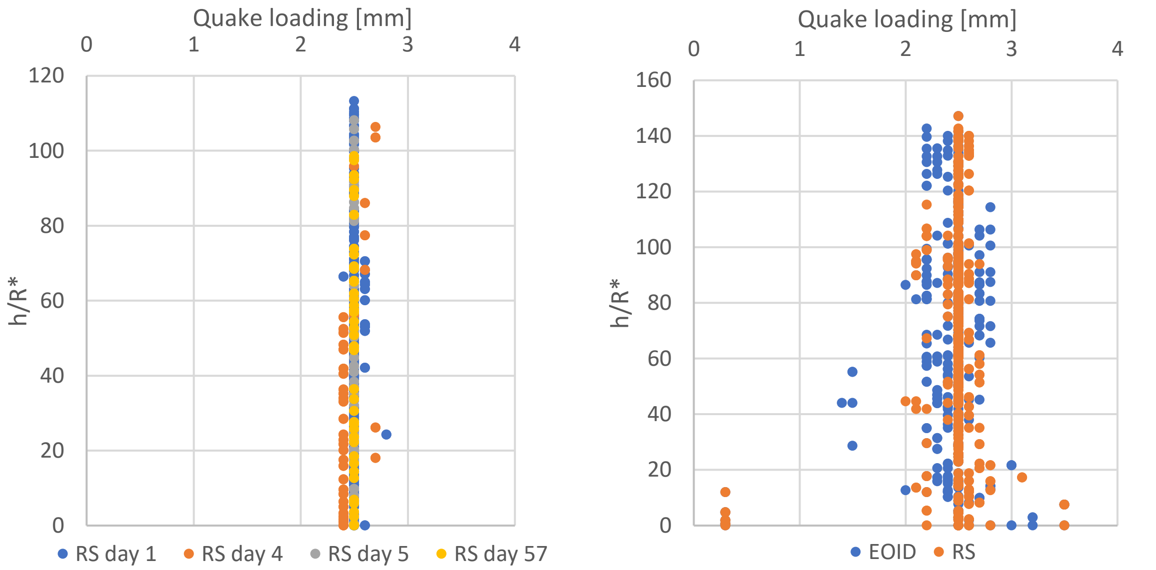

Figure 86: Loading quake values obtained after signal matching analysis for closed- (left) and open-ended piles (right)

In Figure 87, the unloading quakes for the shaft are given for the closed- and open-ended piles. The unloading quakes for the closed-ended piles show similar values as for the loading quake and remain around 2.5mm. Unloading quakes close or equal to 2.5mm could be an indication of absence of residual stresses in the soil. After each hammer blow the soil is expected to rebound completely from its elastic regime and allows the pile to recover to its original shape if no residual loads are active. In the scatter plot of the unloading quakes for the open-ended piles a large scatter is visible with most of the unloading quakes distributed between 0.1 and 3 mm. An explanation for a very low unloading quake value could be that the unloading stiffness of that particular dense soil layer is very high and the pile displacement needed to go from a state of compression to a state of tension is very small. Another explanation could be that very low values for unloading quakes at high values for h/R^* can indicate the presence of negative skin friction in the upper part of the pile shaft where a relative small pile displacement is needed to reach fully negative yield stress i.e. unloading branch in the tensional phase of the spring model. In general the closed-ended piles show quake values close to commonly used values, but for open-ended piles the quake values can vary widely and might indicate the presence of residual stresses or very stiff and dense sandy soils with complex stress distribution directly after driving.

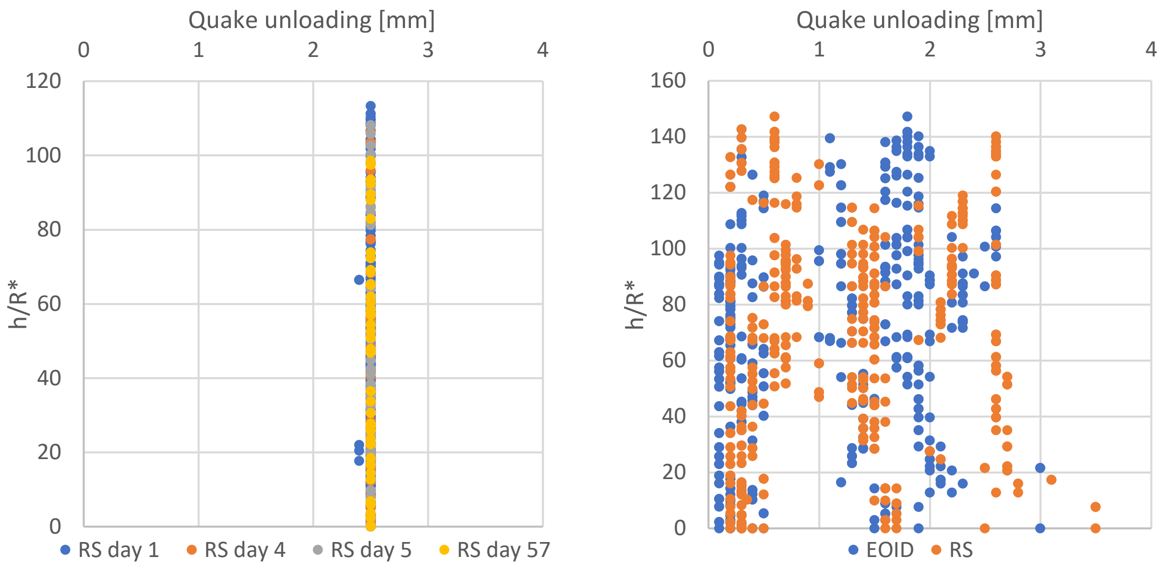

Figure 87: Unloading quake values obtained after signal matching analysis for closed- (left) and open-ended piles (right)

Simons and Randolph (1985) defined the spring parameters in the mechanical model with clear physical meaning in which the soil shear stiffness is a function of the operational shear modulus and the pile radius as mentioned in Section 5.4 by equation (131). Dividing the yield stress over the loading quake gives the local operational soil shear stiffness from the spring model and enables to back-calculate the operational shear modulus (G_s) at time of end of driving and restrike. Due to cyclic loading and installation effects on the soil during pile driving, the initial soil shear stiffness is expected to reduce and shear modulus reduction occurs. In Figure 88, shear modulus reduction is plotted against relative pile depth. The initial shear modulus, G_{max}, is calculated by CPT-based correlation functions for sand and clay (Chapter 4.5.1). The operational soil shear stiffness must be scaled with the equivalent pile diameter in order to get the derived operational shear modulus. The equivalent diameter for the closed- and open-ended piles are respectively 510mm (450x450) and around 620-720 mm, depending on wall thickness and diameter of each section of the monopile. The shear modulus reduction curve for the closed-ended piles (Figure 88, top) shows that closer to the pile base, the normalized shear modulus is higher. This in line with expectation that the soil closer to the pile base has experienced less cyclic shearing and material damping and therefore the reduction of the initial shear modulus is relatively lower than soil closer to ground level. Furthermore the restrike on the closed-ended pile with a setup time of 57 days (red triangles) show even less shear modulus reduction than the piles with lower setup period. This might indicate some soil stiffness recovery resulting in a higher operational shear modulus in the setup period after driving. A clear degradation pattern for the shear modulus for the open-ended piles is not observed (Figure 88, bottom). A few outliers show a very high operational shear modulus for the middle clay layers and the sand layers close to the pile base, but this might be respectively the consequence of undrained loading in which the yield stress is close to a very high value for the undrained shear strength of the soil or of residual stresses. In general, the normalized shear modulus reduction for the closed-ended pile is about 5% to 10% for the upper and middle part of the shaft and reaches values up to 40% very close to the pile base. The shear modulus reduction for the open-ended piles do not show any relation with relative pile depth and ranges between 5% and 15% for the entire shaft regardless soil type.

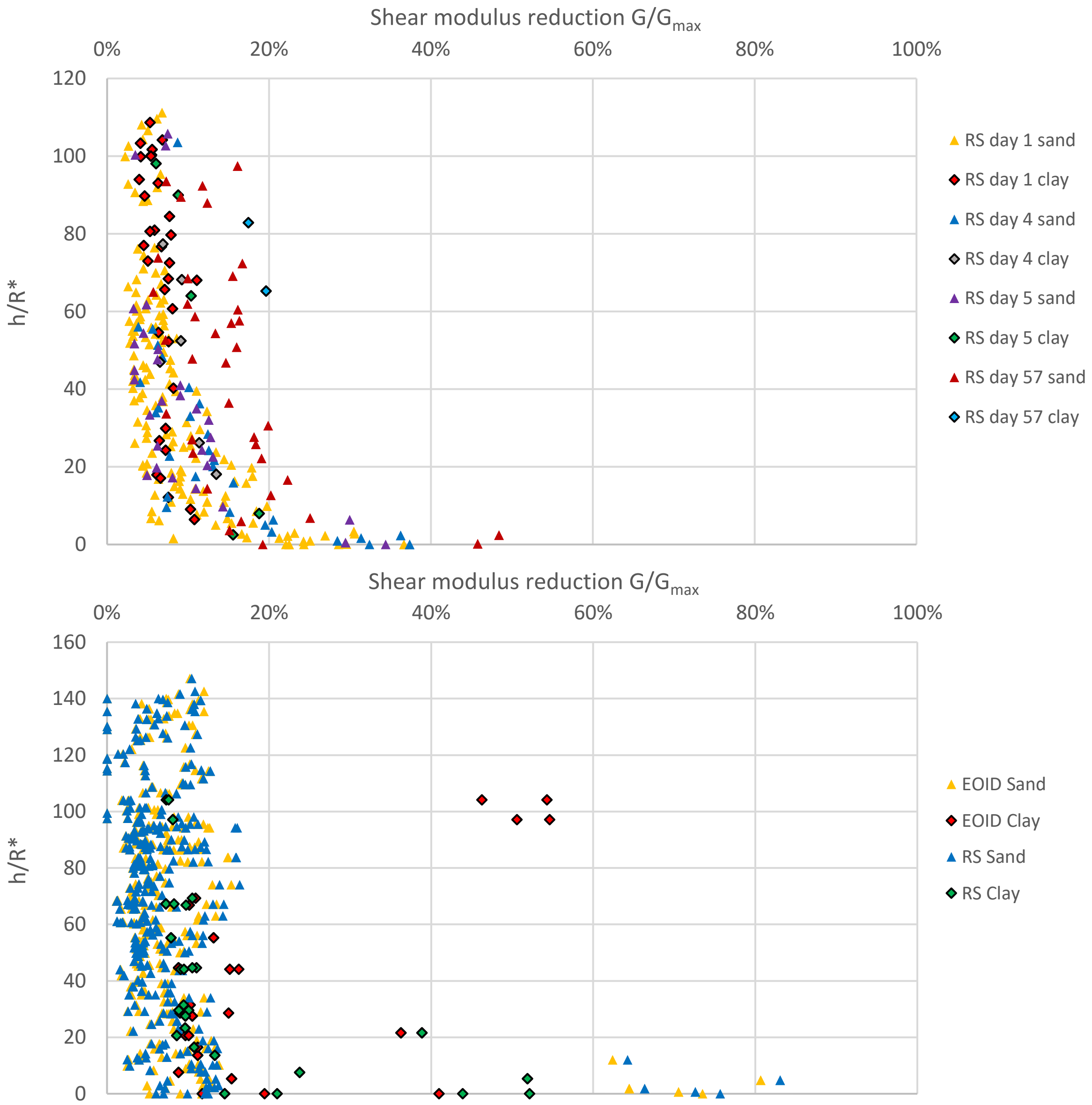

Figure 88: Back-calculated operational shear modulus for closed- (top) and open-ended piles (bottom) for during loading

7.6 Shaft radiation damping constant with geotechnical correlations

In the TNO soil model, shaft damping is defined as the shaft radiation damping in the shaft model proposed by Simons and Randolph (1985). All the damping is combined into one radiation damping constant and a contribution of viscous damping is neglected, because radiation damping is the dominant factor in controlling the dynamic resistance (Fakharian et al., 2013). The input for the shaft radiation damping constant is the shear modulus $\mathrm{G_{max}}$ and the shear wave velocity $\mathrm{V_s}$. Due to installation effects, equalisation and reloading, the actual shaft radiation damping at the pile-soil interface in the TNO soil model is different compared to the initial shaft radiation damping assumed in the outer field of the pile-soil system proposed by Simons and Randolph (1985) in a perfect elastic medium. In the TNO soil model the shaft radiation damping is a sort of lumped damping term combining the damping in all zones in the pile-soil interface. The radiation damping term in the soil model accounts for radial stress wave propagating in the soil surrounding the pile. The exponent α linked to the pile velocity in the radiation damping constant is set to 1 for both sand and clay what makes it a linear damper. Besides that, it reduces the number of variables in the signal matching analysis. The exponent had no meaningful effect on the dynamic resistance if α is between 0.6 and 1.0. Furthermore the pile velocity decreases at higher penetration depths because of energy loss by friction and damping whereby the effect of exponent on the magnitude of the damping force also reduces.

7.6.1 Shaft radiation damping and relative pile depth

On the basis of signal matching analysis, the shaft radiation damping constants for all soil sublayers along the shaft are determined by an interactive process to define the parameter in the TNO soil model such that the highest matching quality is achieved with field measurements. In general, as the pile depth increases, the shaft radiation damping constants tends to increase as well. The obtained shaft radiation damping constant ($\mathrm{C_s}$) and the normalized radiation damping constant ($\mathrm{C_s/C_i}$) plotted against relative pile depth are shown in Figure 89, respectively left and right. The shaft radiation damping constants for the closed-ended pile show a tendency to increase with depth with a clear linear trend, if the upper layers are not taken into consideration. The clay and peat layers at the upper part of the pile do not show meaningful damping and almost no driving energy is dissipated by these upper layers. The Figure show that a relative short setup period of a couple of days seems to have a limited effect on the shaft radiation damping constant at similar relative pile depth. On the other hand, a relative long setup period with a restrike at 57 days after installing show higher radiation damping constants for the sand layers surrounding the closed-ended piles closer to higher end of the range around the linear proportional trendline with damping versus depth. The clay layers do not deviate significantly from the overall trend in which the sand layers are dominant because of the number of datapoints. An slight increasing linear trend between the shaft radiation damping constant and relative pile depth can also be observed for the open-ended piles but with larger scattering at increased penetration. A large difference in magnitude of the radiation damping constants between the closed- and open-ended piles at equal levels of relative pile depth can't be concluded based on the results. A main reason for this could be that the radiation damping constants for the open-ended piles are slightly lower because of a lower setup period in comparison to the closed-ended piles. The right charts in Figure 89 show that the initial calculated radiation damping constants by equation (132) are too high when taken directly into the signal matching analysis resulting in extreme overestimation of the dynamic pile resistance. Therefore the magnitude of the initial shaft radiation damping constants have to be reduced significantly to obtain reliable matching results. The normalized damping constants have some in common with the damping ratio related to an underdamped system. Underdamping because of the fact that the actual damping of the soil is much smaller than the initial damping proposed in the Simons and Randolph (1985) shaft model. The proposed initial shaft radiation damping constant from equation (132) leads to an extremely overdamped system that is not in line with obtained field measurements i.e. upward travelling stress wave. Regarding the closed-ended piles, a linear trend between the normalized radiation damping constants and relative pile depth is also present, but for the open-ended piles this trend does not remain in place. The increase in actual radiation damping for the open-ended piles does not follow the increase in initial calculated radiation damping, probably due to the greater influence of installation effects present at moment of testing. The actual radiation damping over the initial radiation damping varies within a bandwidth over relative pile depth, without a clear linear proportional trend as observed for the closed-ended piles. The ratio of the normalized shaft radiation damping constants in relation to relative pile depth are for most sublayers within a range of 1% to 20% of the initial calculated radiation damping constants. The large scatter without a clear trend between relative pile depth and normalized radiation damping constants might also be caused by changing wall thicknesses of the steel sections what might affect the radial stress wave propagation. In absolute terms, for both types of piles, the shaft radiation damping constants shows an increase in magnitude with increasing depth, but with larger scattering for the open-ended piles. On top of that the setup periods also seems to be an important factor on the magnitude of the shaft damping constants.

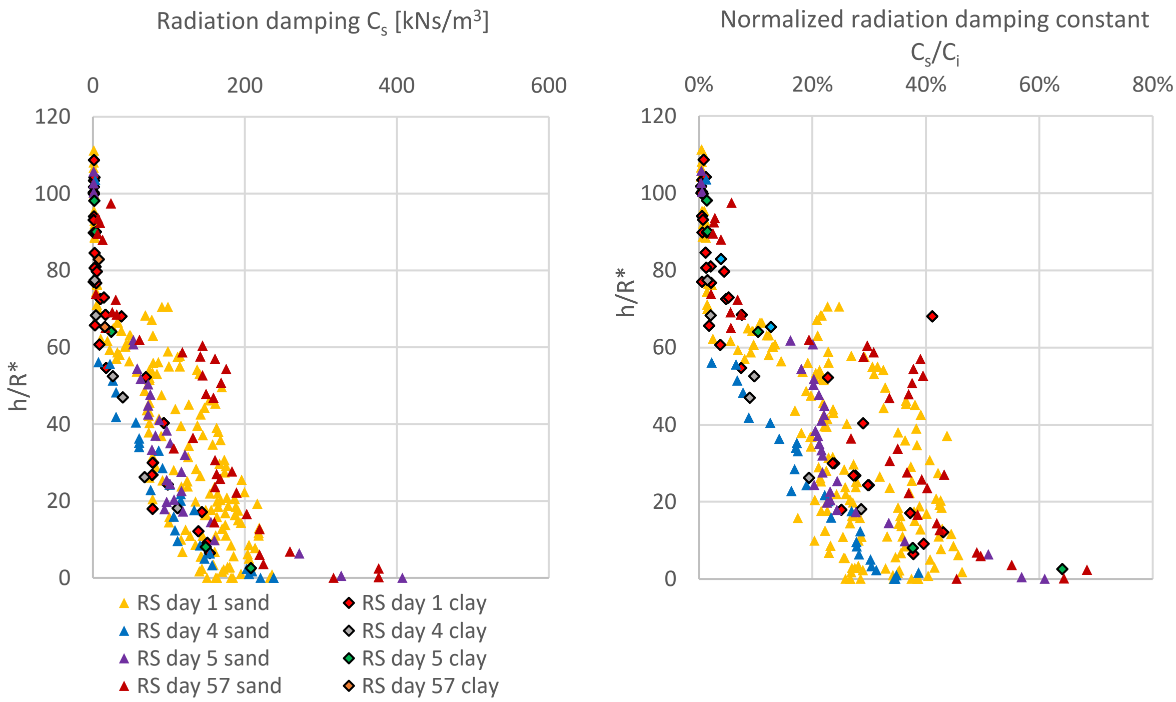

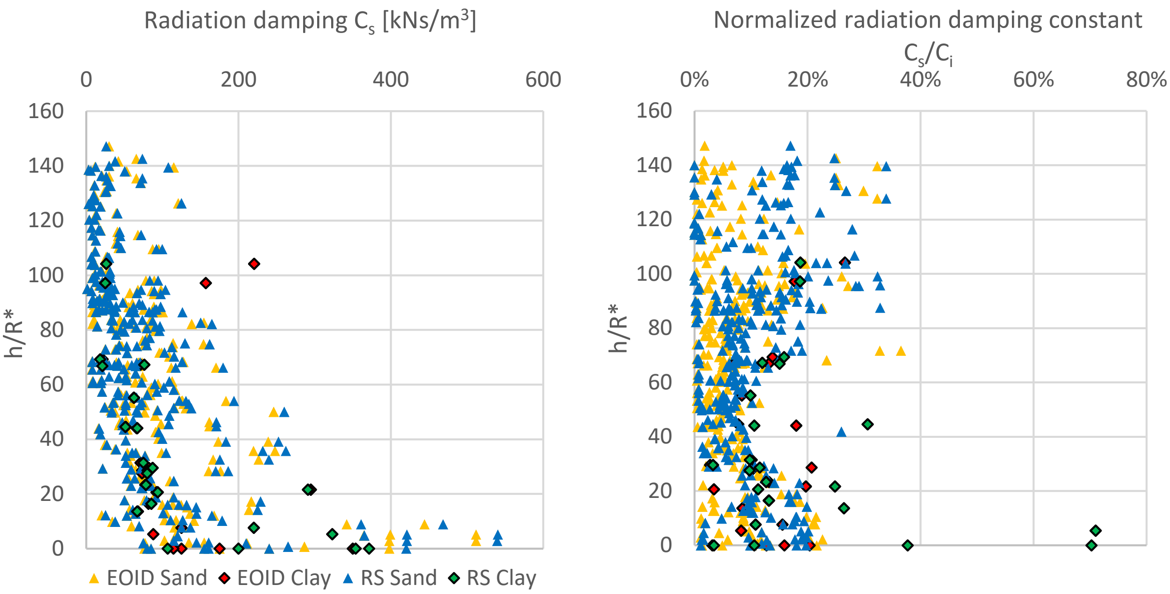

Figure 89: Shaft radiation damping constant (left) and normalized shaft radiation damping constant (right) for closed- (top) and open-ended piles (bottom) against relative pile depth

7.6.2 Shaft radiation damping and vertical effective stress

Another approach to relate the shaft radiation damping to relative pile depth is by looking at the correlation between vertical effective stress and shaft radiation damping constants. As vertical effective stresses increases, the horizontal effective stress acting on the pile shaft should increases and the soil tends to become stiffer, resulting in higher shear wave velocity and higher energy dissipation outwards from the foundation pile. The vertical effective stress influences the contact between soil particles and affects the effectiveness of energy dissipation, thus impacting the damping characteristics. Figure 90 shows the relation between vertical effective stress of the soil surrounding the pile and shaft radiation damping constants for both closed- and open-ended piles. The upper plot shows a clear trend for the closed-ended piles in which increasing vertical effective stress results in higher radiation damping constants for both sand and clay layers. The best fitted trendline between the vertical effective stress and radiation damping constants are given by a power function (Table 18).

Pile Type	Formula	Reliability
Closed-ended sand	$C_s = 0.022(\sigma_v')^{1.64}$	$R^2 = 0.75$
Closed-ended clay	$C_s = 0.0001(\sigma_v')^{2.6}$	$R^2 = 0.95$

Table 18: Equations and reliability for shaft damping for closed-ended piles in sand and clay as function of vertical effective stress

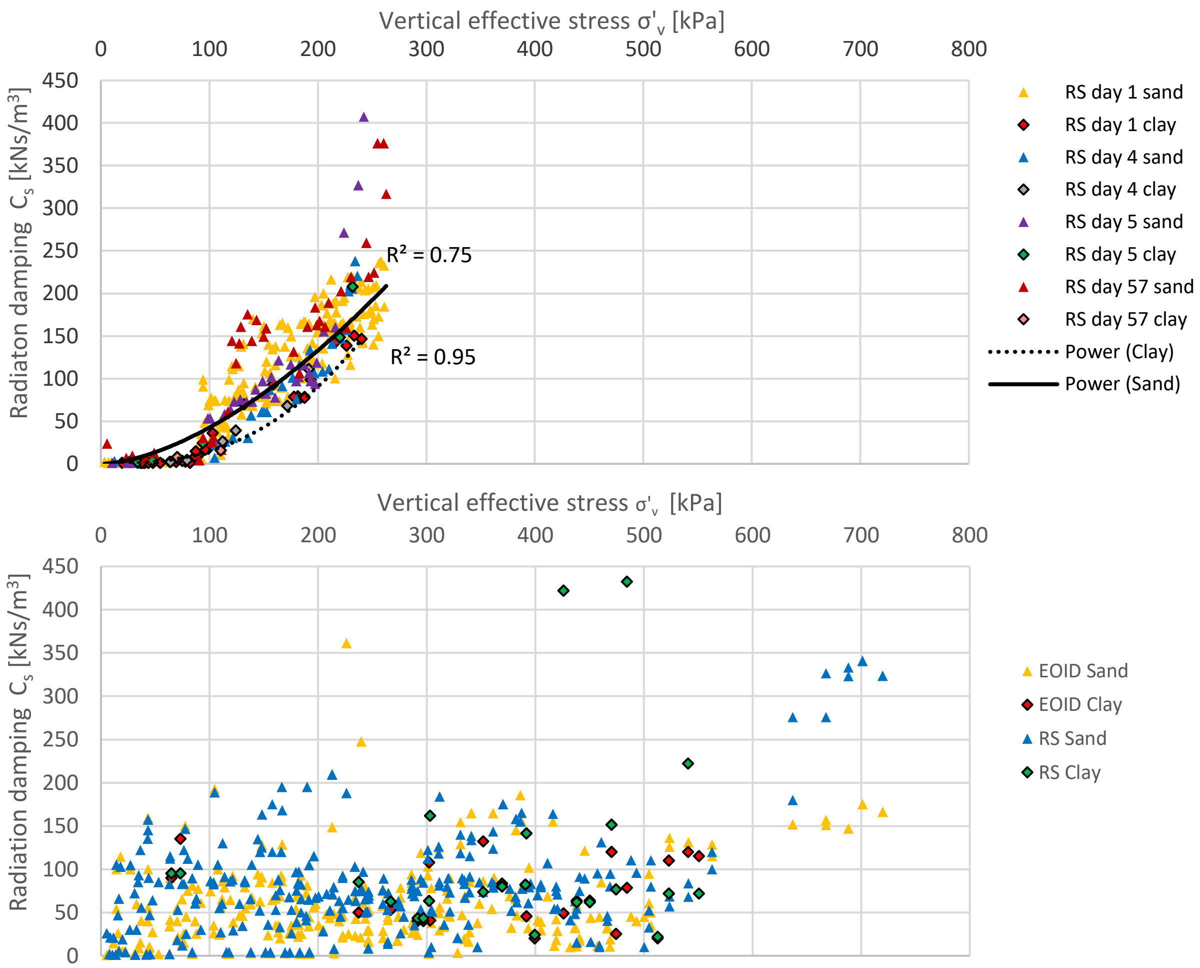

Figure 90: Relation between radiation damping constants and vertical effective stress

The equation which relates the radiation damping constants for the clay layers with the vertical effective stress for closed-ended piles show a relative high R-squared of 0.95, suggesting a strong correlation between those two variables. The goodness-of-fit of the power trendline for the sand layers surrounding the closed-ended piles is lower, but the quality of the trendline gives a R-squared value of 0.75, indicating that the higher the vertical effective stress, the higher the radiation damping constants along the shaft, but with a bit more variability. An increasing trendline between vertical effective stress and shaft radiation damping constants for open-ended piles are not visible at all in which the damping constants remain in a bandwidth independent of vertical effective stress. Comparing the radiation damping constants for closed- and open-ended piles at similar vertical effective stresses levels do not show equal magnitudes of radiation damping, indicating that the stress state after installation plays an important role. In general, the shaft radiation damping constants for the monopiles remain close to a range of about 0 to $100\ \mathrm{kNs/m^3}$ from mudline up to $500\ \mathrm{kPa}$ vertical effective stress. When the vertical effective stress is higher than $500\ \mathrm{kPa}$ the damping constants also increases. The increase in radiation damping constants in relation to vertical effectives stress appears to start at relative lower vertical effective stress for closed-ended piles than for open-ended piles. An explanation for this might be that soil layers at equal vertical effective stress have experienced more cyclic shearing and distortion for open-ended piles than for closed-ended piles. An explanation for the relative higher damping constants for the closed-ended concrete piles compared to the open-ended steel piles could also be due to the pile material whereby surface roughness is an important factor. The higher surface roughness for the prefab concrete piles could increase the resistance to pile motion and promoting the transmissibility of the stress wave energy into the surrounding soil. A kind of roughness factor can be incapsulated in the obtained shaft radiation damping constants in the TNO soil model after signal matching analysis. In addition, the dynamic load tests on the open-ended piles were directly performed after initial driving and a restrike after a couple of hours, whereby the soil damping characteristics could be much more affected by installation effects including pore pressure dissipation and soil relaxation. The closed-ended piles have larger time period between installation and testing and gradual recovery of the damping properties have led to an increase of radiation damping constants.

7.6.3 Shaft radiation damping and yield stress

As mentioned in Chapter 3.2 radiation damping in the soil models is part of the outer field of the pile-soil system. The correlation between yield stress and radiation damping is not a direct relationship. Yield stress is a mechanical property of a material that represents the stress at which it undergoes permanent deformation or yielding. On the other hand, radiation damping is a damping characteristic related to the dissipation of energy in the soil during pile driving. As mentioned in Chapter 6.5, viscous damping is decoupled from the static resistance in the TNO model, while in the shaft model proposed by Simons and Randolph (1985) viscous damping is certainly correlated with the static resistance i.e. yield stress. To examine if the derived shaft radiation damping constants show any correlation with the yield stresses, the two variables are plotted against each other in Figure 91. It seems that the best-fitted trendline between radiation damping constants and yield stresses for the sand layers around the closed-ended piles fit with a logarithmic function, while as the setup period increases, this fit to a logarithmic trendline diminished for 4 and 57 days and the damping constants show no increase as yield stress increases. A logarithmic trendline is a best-fit curved line that is most useful when the rate of change in the data decreases quickly and then levels out, what is well observed for the sand layers with a restrike of 1 day. The plot also shows that on average the setup period has an positive effect on the magnitude of the radiation damping constant at similar yield stresses and suggest some time effect on soil radiation damping properties. The clay layers show also a logarithmic trend with similar reliability as for the sand layers, but it must be noted that the number of data points for the clay layers are limited. Regarding the open-ended piles, the correlation between yield stress and shaft radiation damping constant show a more linear trend, but also with a moderate reliability as for the closed-ended piles. The clay layers around the monopile show the highest reliability and fit to the linear trendline with a R-squared of 0.75 slightly higher than the rest. As described in the soil model by Simons and Randolph (1985) in Chapter 5.4, viscous damping is the only type of damping that is coupled with the static soil resistance. Figure 91 shows a small prove of viscous damping in case the yield stresses are linked with the shaft radiation damping constants, but a moderate R-squared does not automatically mean causality. In general, the yield stress is related to the strength of the soil and not directly linked to radiation damping, but Figure 91 show some positive correlation between these two variables whereby the correlation for the closed-ended piles fits the best to a logarithmic trendline, whereas the open-ended piles fits the best to a linear trendline. In addition, setup seems to have also its influence on the damping constants, because at similar yield stress the magnitude of the shaft radiation damping constant is higher with a longer setup period.

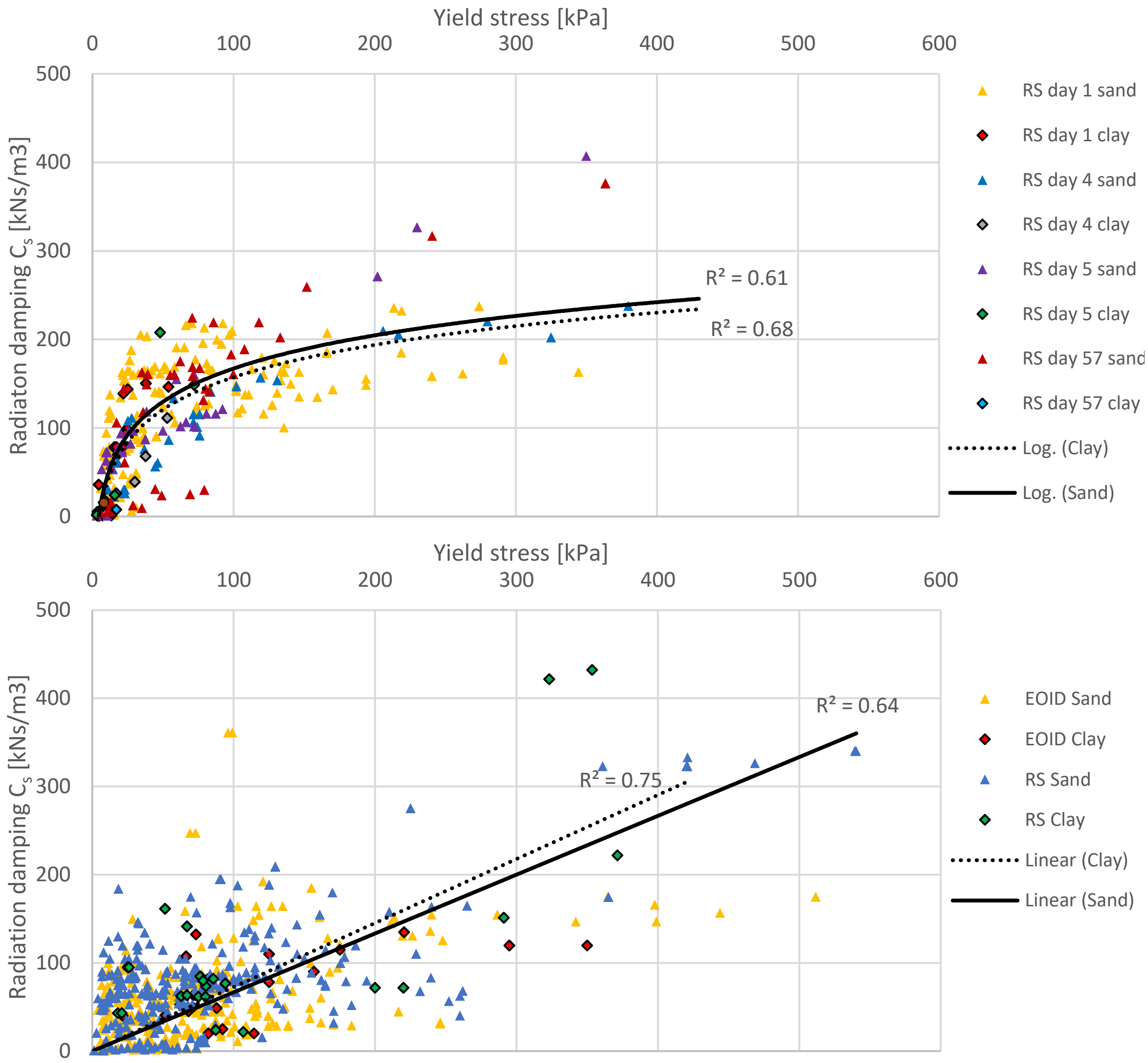

Figure 91: Shaft damping constant as function of the yield stress for closed- (top) and open-ended piles (bottom)

7.6.4 Shaft radiation damping and cone resistance

In order to improve the initial soil model parameters in the TNO soil model which are used as the starting points for performing a signal matching analysis, it makes sense to find initial model parameters that show reliable correlation with soil investigation data. The cone resistance is an important value that provides valuable information about geotechnical properties of the soil. Key insight are soil type and classification, but also soil strength. In granular soils such as sand, the cone resistance generally increases with increasing soil stiffness. Higher cone resistance values are typically associated with stiffer soils, indicating a greater resistance to deformation. Damping refers to the ability of a soil or material to dissipate energy during cyclic loading or vibration. When a soil undergoes cyclic loading, such as during an earthquake or dynamic loading from impact hammer, it experiences deformation due to the applied forces. Soil damping plays a crucial role in controlling the magnitude and rate of this deformation. A direct correlation between shaft damping by means of shaft radiation damping constants and cone resistance values is shown in Figure 92. Coloured trendlines are added for each soil type and setup period. Respectively, the black solid line and dotted line are the best-fitted trendlines for the combined datapoints of the sand and clay layers. The reliability for each soil type and setup period differs significantly, also because the number of datapoints per individual series varies. Figure 92 shows a few important things. At first, regarding the closed-ended piles in the upper chart, it appears that a longer setup period generally gives a higher shaft radiation damping constant at same cone resistance value for the sand layers, while this is not clearly visible for the clay layers. Secondly, relatively low cone resistance values resulted in a bit higher damping constants for the clay layers than for the sand layers. The steepness of all the trendlines indicate that the rate of change in damping with respect to the cone resistance is higher for the clay layers than for the sand layers. Thirdly, it is difficult to make conclusion related to the damping characteristics for very stiff over-consolidated clays with high cone resistance, because the absence of these type of clay layers. The observations in Figure 92 tend to show that soil type, sand or clay, plays a crucial role in the rate at which the shaft radiation damping constants changes in comparison to the cone resistance values and that a direct correlation between q_t and C_s is difficult to draw and only provides a reasonable direction. The lower scatter plot in Figure 92 shows the results of the shaft radiation damping constants and cone resistance for the open-ended pile at EOID and RS. The best-fitted lines are linear trendlines, but still with a low reliability regardless setup period for both sand and clay layers. The radiation damping constants show a poor correlation with CPT data and vary widely at same values for cone resistance. The scattered data shows that defining a radiation damping constant for a specific soil layers only based on the cone resistance values gives an unreliable value if testing is performed directly and after a couple of hours of monopile installation. It can be noted that defining a starting point regarding the magnitude of the radiation damping constant for the clay layers before signal matching analysis is performed is even more difficult, because of the large scatter at similar cone resistance. Similar to the sand layers surrounding the closed-ended piles, the setup period also has its effect on the magnitude of the shaft radiation damping constants for the open-ended pile considering the two linear trendlines for EOID and RS. Different setup periods ranging from a couple of hours for the open-ended piles to several days for the closed-ended piles have a meaningful effect on the magnitude of shaft radiation damping constant in relation to the cone resistance. A direct comparison between soil type and evolving radiation damping with equal setup periods for the closed- and open-ended piles was not possible due to the difference in duration time between pile installation and testing of both pile types (hours vs days). In general, a direct correlation between cone resistance and shaft radiation damping constants for both closed- and open-ended is difficult to make, because of the large difference in reliability of the trendlines within each pile type and soil type. An explanation might be that the pile shaft roughness and pile diameter have can affect the shaft damping characteristics regarding the transfer of the stress waves at the pile-soil interface. The surface roughness of a concrete pile is higher compared to a steel monopile and can affect the transferability of energy to the surrounding soil. Regardless of the weight of the number of datapoints for each soil type and setup period, rough correlation functions between the corrected cone resistance and shaft radiation damping constant are given in Table 23.

Pile Type	Formula	Reliability
Closed-ended sand	$C_s = 0.0103q_t$	$R^2 = 0.72$
Closed-ended clay	$C_s = 0.0458q_t$	$R^2 = 0.72$
Open-ended sand	$C_s = 0.0017q_t$	$R^2 = 0.61$
Open-ended clay	$C_s = 0.0182q_t$	$R^2 = 0.56$

Table 19: Equations and reliability for shaft damping for closed-ended piles in sand and clay as function of vertical effective stress

Overall, the difference in radiation damping between clay and sand is mainly influenced by their respective particle sizes, cohesion, water content, internal friction characteristics and stiffness. Clay tends to exhibit higher radiation damping due to its finer particles, higher water content, and greater energy dissipation capabilities, while sand generally exhibits lower radiation damping due to its larger particles and lower energy dissipation characteristics.

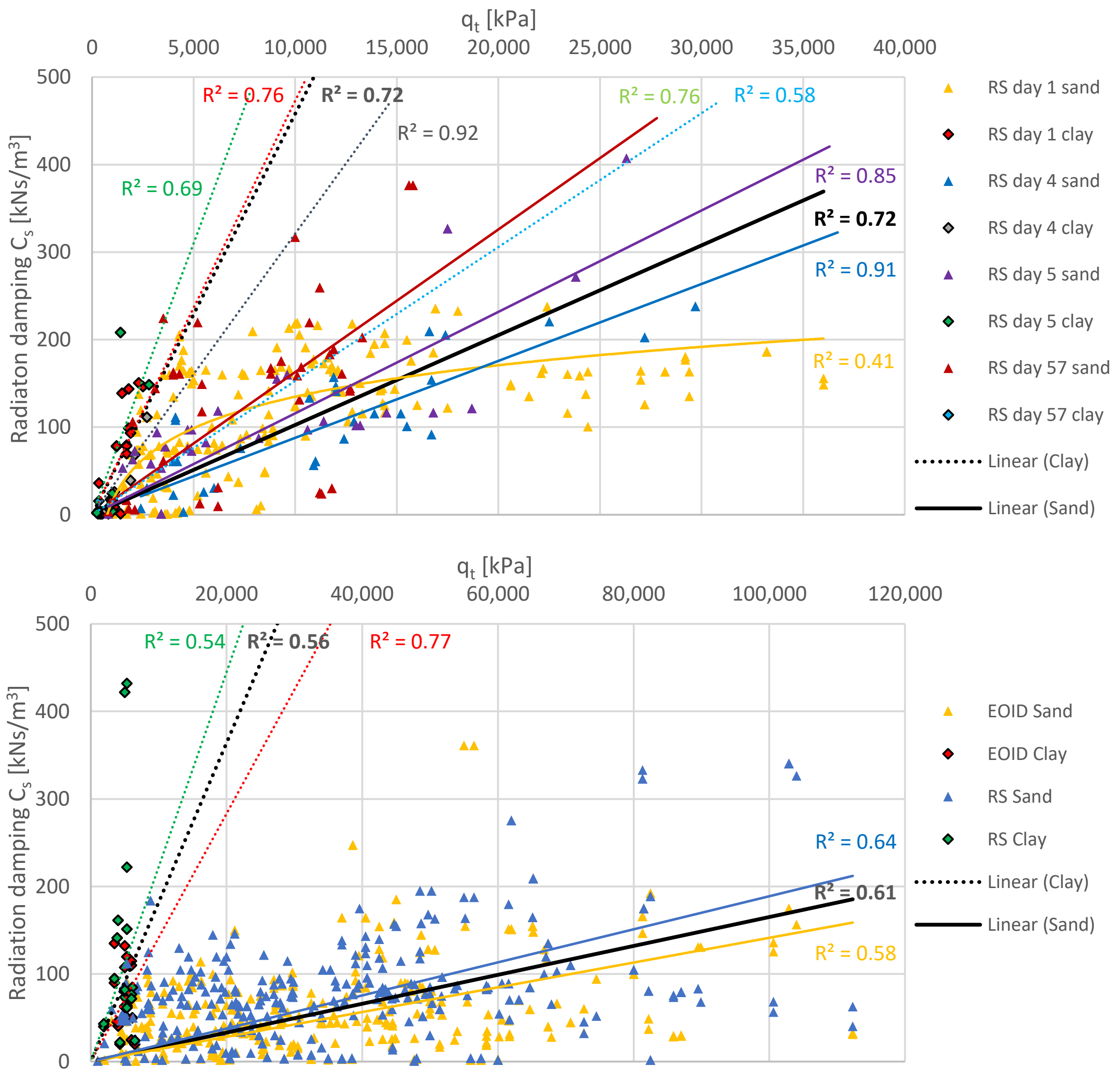

Figure 92: Relation between Cs and qt for sand and clay in case of closed- (top) and open-ended piles (bottom)

The effect of relative pile depth (h) and the degradation effect on stress wave transferability on shaft damping is ignored in Figure 92. It is expected that dissipation of driving energy into radiation damping is affected by the number of loading cycles and distortion the soil has experienced at the pile-soil interface as pile penetration proceeds. In a few soil models in Chapter 5, hysteresis damping or material damping is incorporated in the mechanical soil model by means of nonlinear springs. Actually hysteresis damping is primarily associated with dynamic soil behaviour rather than static soil properties. In Figure 93, hysteresis damping is roughly estimated by the relative pile depth and related to ratio of the obtained shaft radiation damping constants over the corrected cone resistance, C_s/q_t. The focus in Figure 93 is to find whether soil layers with the same cone resistance, generate different shaft radiation damping constants due to a difference in relative pile depth. Figure 93 has similarities to Figure 89, but the actual shaft radiation damping constants are normalized by the cone resistance to related it to CPT data and thus to initial geotechnical engineering properties of the soil layers. The relative pile depth includes till some extend also the increase in vertical stress and therefore an increase in soil density, horizontal effective stress on the pile shaft and stiffness. In Figure 93 the relative pile depth is divided by the equivalent pile diameter to compare the effect of embedment for piles with different dimensions at similar levels. The upper chart in Figure 93, showing the results for the closed-ended piles, indicate an increasing C_s/q_t ratio with very large unequal variability as relative pile depth increases depth h/R^*. Regarding the sand layers, the ratio C_s/q_t starts below 1% close ground level with very low damping and ranges from 1% up to 6% of the cone resistance value close to the pile base with increased scatter from ground level to pile base. The ratio C_s/q_t for the clay layers show less variability and more trending over relative depth and start from below 1% at ground level up to 6% to 10% at pile base with a few outliers. A more reciprocal function can be drawn through the scattered datapoints of the clay layers. In general, the results show that the ratio of shaft radiation damping constants over cone resistance for the clay and sand layers do not show a well observed setup effect in the results. On the other hand, the ratio C_s/q_t remains quite constant over relative pile depth for the open-ended piles. At mudline, the ratio in the sand layers is relatively higher with more scattering than closer to the pile base and the ratio C_s/q_t does exceed 2% along the entire shaft at EOID and RS. The clay layers show a bit higher ratio C_s/q_t between 1% and 4% along the entire pile shaft, but with higher variability at EOID and RS along entire shaft. The clay layers can be well distinguished from the sand layers. In general, the open-ended piles in Figure 93 shows a relative constant ratio of C_s/q_t on relative pile depth which could indicate that the obtained radiation damping constants and cone resistance are proportional to each other at low relative pile depth due to less soil distortion to driving.

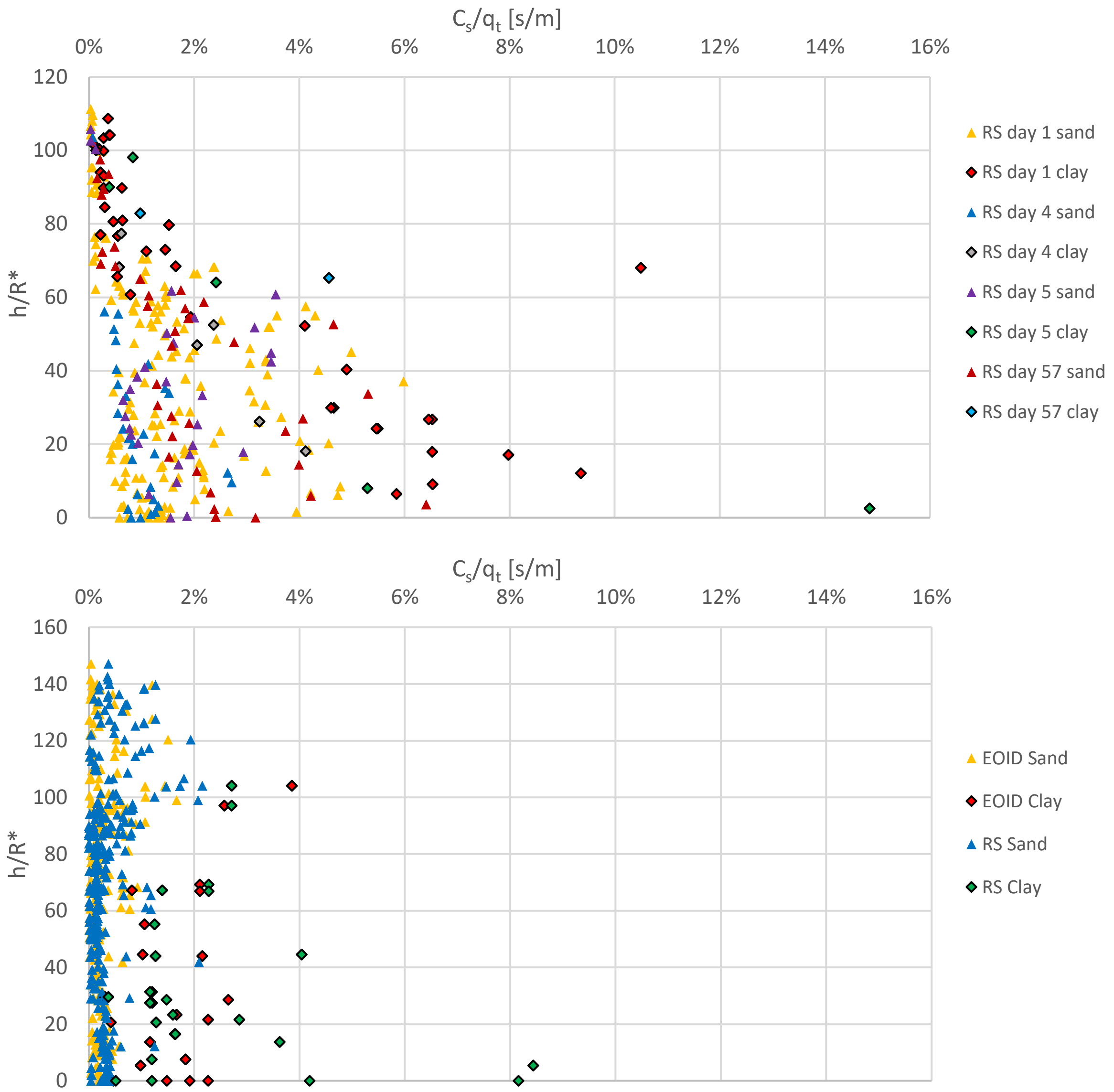

Figure 93: Shaft radiation damping constant normalized with cone resistance plotted against relative pile h/R* for closed- (top) and open-ended piles (bottom)

The shaft radiation damping constants plotted against cone resistance divided by the vertical effective stress is shown in Figure 94. Similar to the previous charts, the clay layers show neither a correlation with solely the corrected cone resistance nor q_t/σ'_v for both closed- and open-ended piles. The vertical effective stress always increases with depth, but soil strength measured by cone resistance can obvious vary over depth. Regarding the open-ended piles, a correlation with a linear trendline with moderate R-squared of 0.63 and 0.57 can be assigned to the sand layers, while the clay layers show no correlation at all. The equations in Table 20 give a rough estimate of the shaft radiation damping constant in relation to q_t/σ'_v .

Pile Type	Formula	Reliability
Closed-ended sand	$C_s = 1.77\frac{q_t}{\sigma'_v}$	$R^2 = 0.63$
Open-ended sand	$C_s = 0.47\frac{q_t}{\sigma'_v}$	$R^2 = 0.57$

Table 20: Equations and reliability for shaft damping for closed- and open-ended piles in sand as function of q_t/σ'_v

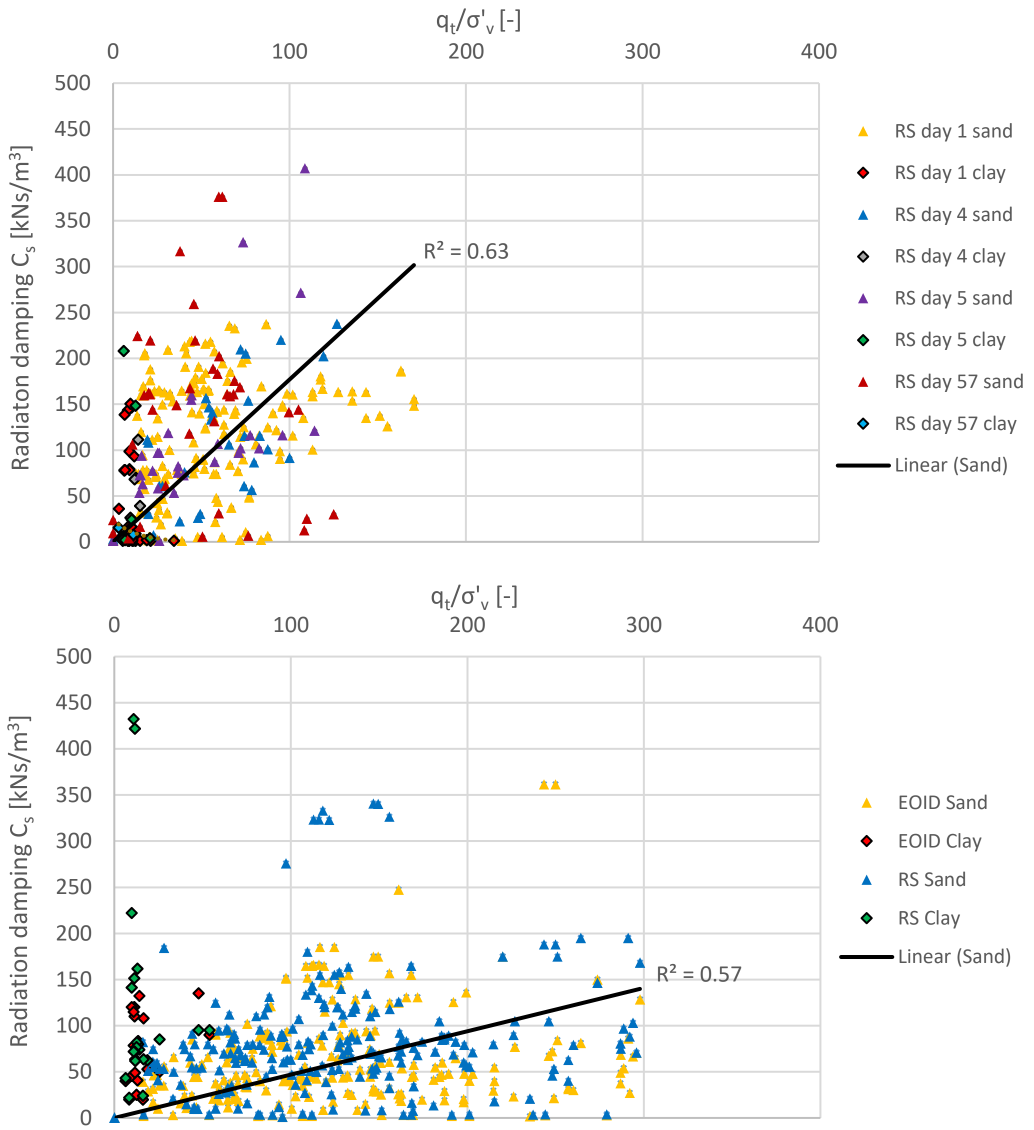

Figure 94: Shaft radiation damping constants versus ratio of cone resistance over vertical effective stress

7.7 Pile base capacity

In the unified methods for driven piles in sand and clay, the pile end bearing capacity or ultimate base resistance is defined as the maximum mobilized resistance reached at large pile base displacements. Research has shown that the bearing stress acting at the base of a closed- and open-ended driven pile is defined at ultimate conditions at a displacement of 10% of the pile (equivalent) diameter ($q_{0.1b}$) and varies in direct proportion to the average cone resistance q_c in the vicinity of the pile tip ($q_{c,avg}$). The average cone resistance is calculated by averaging the cone resistance over a distance of +1.5D above and -1.5D below the pile base, following the LCPC approach . For the closed-ended piles, the ultimate base capacity is approximated by taking 50% of the average cone resistance. All the end bearing of the closed-ended piles in Rotterdam comes from deep stiff sand layers. For the ultimate base capacity for the large offshore open-ended piles in sand, 15% of the averaging cone resistance could be taken to estimate the ultimate base capacity assuming full coring during driving. A number of piles have a target depth in stiff clay layers and the ultimate base capacity is estimated by taking 20% of the average net cone resistance based on the analysis of driven piles in clay from the Unified database. After every hammer blow during pile driving, the pile must overcome all the friction in order to penetrate into the soil. From driving recordings such as blow count numbers, it is not customary that pile penetration occurs at increments of 10% of the pile diameter as the design methods demand to define the ultimate base capacity. In the following sections the quake values with corresponding base resistance obtained after signal matching analysis is compared with the displacement criterium ($0.1D_{eq}$) and calculated end bearing capacity according to the unified methods. In reality the pile displacement before failure is nonlinear and a hyperbolic function fits well through the measurement points in a load-displacement diagram. The initial stiffness of the hyperbolic load-settlement curve at the pile base is compared with the back-calculated operational stiffness from the obtained base loading quake values according to Deeks and Randolph pile base model (1995) in Chapter 5.7. The TNO soil model aims to replicate the nonlinear load-settlement behaviour of the pile base into a simplified elastoplastic spring model with stepwise elastoplastic behaviour in which the magnitude of the pile base displacement and achieved base resistance depending on the actual stiffness at the base.

7.7.1 Pile base stress and shear modulus reduction

In Figure 95, the mobilized pile base stress (q_b) divided by the calculated ultimate base capacity ($q_{b0.1}$) is plotted against the shear modulus reduction derived by using Deeks and Randolph model (1995). On the basis of the obtained loading quake value and pile base stress after signal matching analysis, the relevant operational shear modulus (G) is back-calculated. Figure 95 shows that for piles in clay, the obtained mobilized pile base stress during the dynamic load test is relatively close to the calculated ultimate base capacity and varies within a range of -20% to +20% from the initially calculated value for end-bearing capacity. The results show that piles with their base located in clay layers, the ultimate base capacity is almost fully mobilized and with a few cases in which the mobilized base stress is exceeding the calculated ultimate base capacity probably due to higher stresses at the pile base generated by installation effects. Figure 95 also shows that when the operational shear modulus (G) approaches the initial shear modulus (G_{max}), resulting in a stiffer soil response at the base, the degree of mobilized base capacity ($q_b/q_{b0.1}$) also increases and less softening has taken place. Regarding the datapoints for pile bases in clay, a logarithmic trendline fits best and gives an equation that relates the two ratio's, without providing an explicit estimated value for q_b or G beforehand. The trendline equation does not estimate an value for the mobilized base resistance or quake value before signal matching analysis starts. The clay layers show, independent of pile type, that the ratio of mobilized pile base stress over the ultimate base stress show a logarithmic trend in relation to the shear modulus reduction with a $R^2 = 0.96$ for pile base in clay, but for limited cases. For piles in sand, at similar shear modulus reduction, the ratio of mobilized pile base stress over the ultimate shear stress is significantly lower than for piles base in clays. This suggest that when the operational stiffness at the base is equal to the initial stiffness based on G_{max} (100% horizontal axis), no stiffness reduction has occurred and the mobilized base stress approaches the ultimate base stress (100% vertical axis). A linear trendline with intercept between the points for the pile base in sandy soils fits the best and with high reliability of $R^2 = 0.84$, including some outliers with a shear modulus reduction above 100%. Figure 95 shows that the back-calculated value for operational shear modulus and achieved base resistance can be respectively larger the initial calculated shear modulus and ultimate shear stress. Stronger and stiffer soil behaviour at the pile base could be attributed to ignored viscous effects or very dense (dilative) sands at the pile base with strength increase due to negative pore pressure effects.

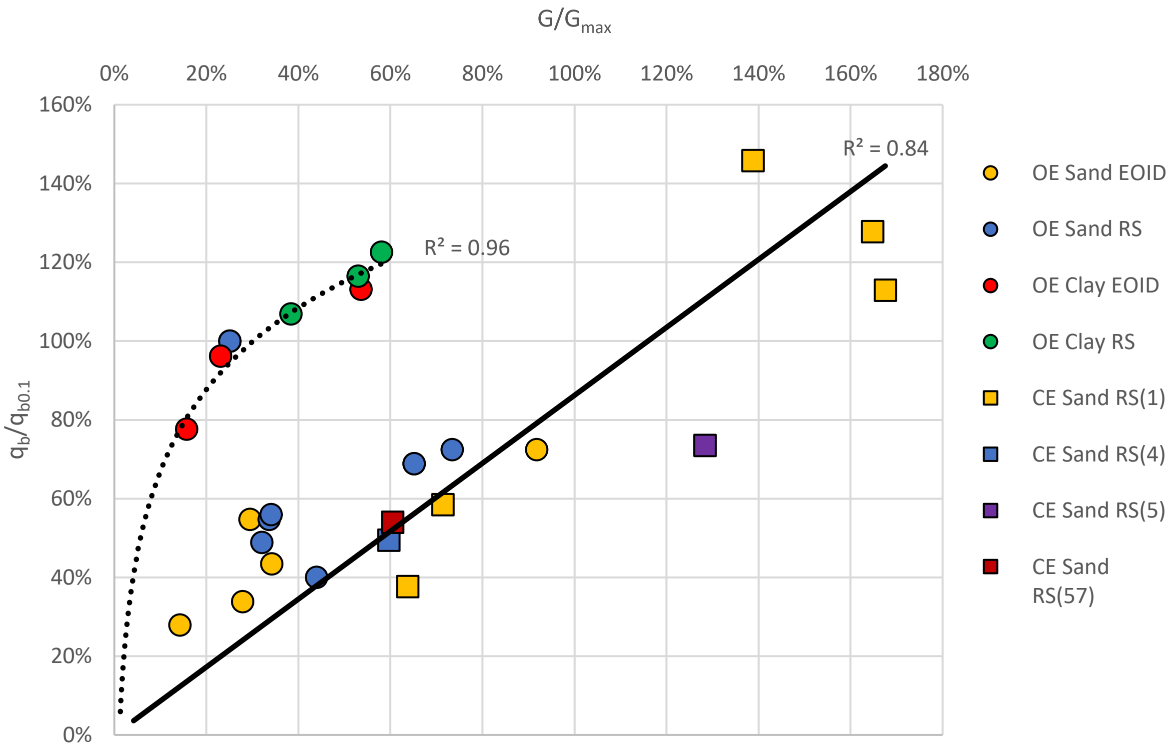

Figure 95: Ratio of the mobilized pile base stress over the calculated ultimate pile base stress in relation to stiffness reduction at the base for both the closed- and open-ended pile

Situation	Formula	Reliability
Pile base in clay	$\frac{q_b}{q_{b0.1}} = 0.3 \ln\left(\frac{G}{G_{max}}\right) + 1.36$	$R^2 = 0.96$
Pile base in sand	$\frac{q_b}{q_{b0.1}} = 0.86\left(\frac{G}{G_{max}}\right)$	$R^2 = 0.84$

Table 21: Equations relating the ratio of the mobilized base stress and ultimate base stress and shear modulus reduction at the pile base

7.7.2 Pile base stress and quake value

As mentioned in Chapter 7.5 the nonlinear load-displacement behaviour at the pile base is approached by linear elastic perfectly plastic springs in the TNO soil model. In the design methods, the ultimate base resistance is reached at a pile displacement of 10% of the equivalent pile diameter. During dynamic loading, the impact force has a short wavelength and travels via a stress wave along the pile shaft to the pile base. In comparison to static loading, the smaller duration of impact force is not able to deform the soil surrounding the pile at a similar magnitude as in static loading and therefore the pile influence radius and spherical zone is smaller during dynamic loading for respectively the pile shaft and pile base. During dynamic loading, such as pile driving, the applied load is transient and applied over a shorter duration compared to static loading. As a result, the stress distribution around the pile is more localized, with the highest stresses occurring near the pile-soil interface. In contrast, during static loading, the load is applied gradually and maintained over an extended period. This allows for stress dissipation and redistribution within the surrounding soil. The stresses spread out over a larger area, resulting in a broader and more diffuse stress distribution around the pile base. In Figure 96 the ratio of mobilized base stress obtained from signal matching analysis and calculated ultimate base stress in relation to the ratio of the permanent base displacement (U_b) over the ultimate base displacement criterium ($U_{b0.1}$) for static loading. In dynamic load testing, it is usual that the permanent pile displacement is relatively low because of the short duration of the impact force, resulting in a smaller spherical zone of mobilized stresses around the pile base. Therefore the elastoplastic behaviour in terms of pile displacement and mobilized base stress varies between dynamic and static loading. Figure 96 shows a moderate correlation between the two ratio's for a closed-ended pile base situated in sand and open-ended pile bases in sand or clay. The degree increment of mobilized base resistance in relation to 'mobilized' ultimate base displacement is lower for open-ended piles in sand and clay than for closed-ended piles. A possible explanation is that less driving energy reaches the pile base of the monopiles and therefore the mobilized base resistance and permanent pile base displacement is also lower compared to closed-ended prefab piles.

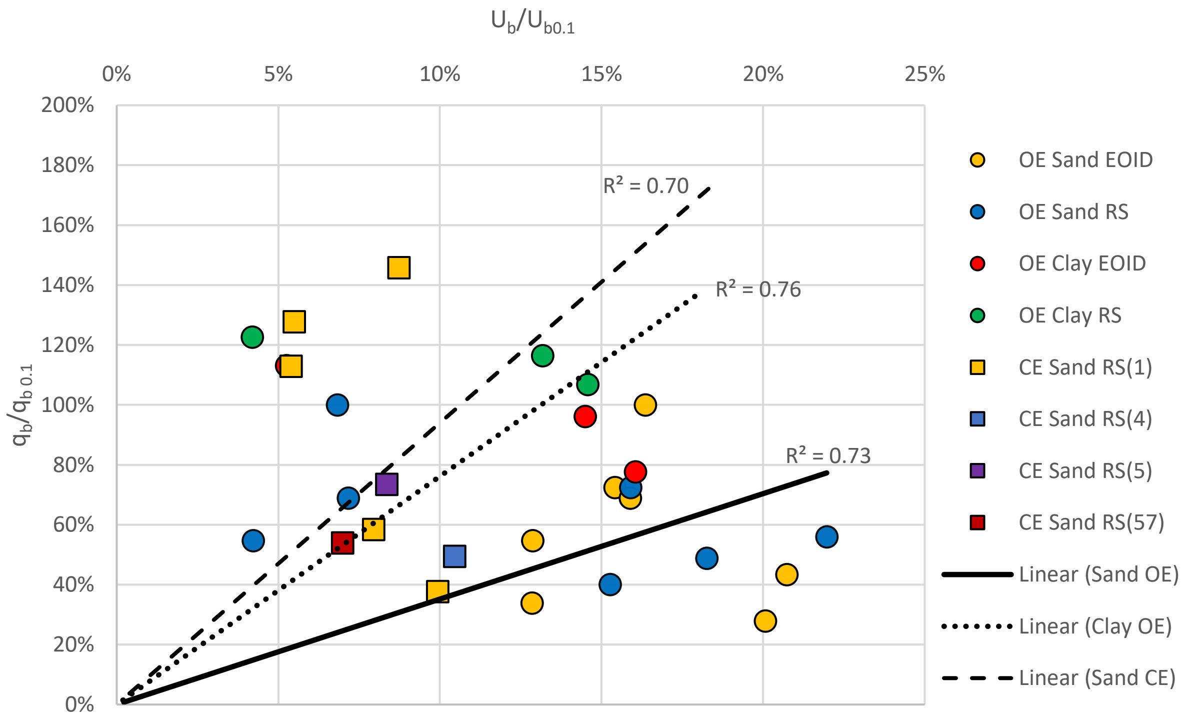

Figure 96: Ratio of the mobilized base stress and calculated ultimate base stress in relation to the derived permanent base displacement divided by the ultimate base displacement criterium

Situation	Formula	Reliability
Open-ended pile base in sand	$\frac{q_b}{q_{b0.1}} = 3.52 \frac{U_b}{U_{b0.1}}$	$R^2 = 0.73$
Open-ended pile base in clay	$\frac{q_b}{q_{b0.1}} = 7.61 \frac{U_b}{U_{b0.1}}$	$R^2 = 0.76$
Closed-ended pile base in sand	$\frac{q_b}{q_{b0.1}} = 9.40 \frac{U_b}{U_{b0.1}}$	$R^2 = 0.70$

Table 22: Equations relating ratio of mobilized base resistance and ultimate base capacity to ratio of permanent pile base displacement and ultimate pile base displacement of 0.1D after a hammer blow

From comparisons between the load-displacement curves of static loads tests and dynamic load tests, it is not always guaranteed that the pile base capacity will be completely mobilized. Although the shaft resistance is often completely mobilized due to the relative low pile shaft displacement that is needed to fully mobilized the ultimate shaft friction. In the TNO model with elastic-plastic springs at the pile base, the quake value and yield stress are not equal to the elastic regime and ultimate base stress defined in the CPT-based axial pile capacity design methods. Regarding the actual nonlinear behaviour of the load-displacement curve at the pile base, the elastic-plastic approach in the TNO model attempts to simulate the nonlinearity in a stepwise matter. In case of very soft soils and short monopiles a dynamic load test is able to fully mobilize the axial capacity , it is expected that the yield stress in the TNO model is in line with the calculated ultimate base stress. On the other hand, when piles are located in soils with relative high strength and high shaft friction, it is likely that the mobilized pile base stress obtained from signal matching analysis strongly deviates from the calculated ultimate base stress. Figure 97 shows the analysis of the quake value (U_q) and mobilized base resistance (q_b) in comparison with the ultimate pile displacement ($U_{b0.1}$) and ultimate base stress ($q_{b0.1}$). It can be observed that for an open-ended pile with a pile base in a clay layer, the ultimate base stress in a dynamic load test is easily achieved. In addition, the pile base displacement needed to reach the state of ultimate base capacity is with a quake value of about 3% to 7% of the ultimate pile displacement. As the quake value is relative large compared to the ultimate pile displacement, it seems that the mobilized pile base stress becomes lower. This might be an indication of large shear modulus reduction at the pile base making it more difficult to get a higher degree of mobilized base stress at a certain pile base displacement. On the other hand, none of the open-ended piles with a pile base in (dense) sand show a fully mobilized pile base resistance during dynamic loading. Regarding the closed-ended prefab concrete piles, there are some outliers that show a mobilized base stress based on signal matching analysis that is higher than the calculated ultimate base stress. This large deviation might be caused by averaging the cone resistance ($q_{c,avg}$) or a higher than assumed damping at the pile base. On average, a rough estimate of the mobilized base stress for both closed- and open-ended piles with the pile base in sand, is about 55% of the calculated ultimate base stress and for clays it can reach values up to 80% to 120%. The horizontal trendline indicates that there is no direct correlation between relative value of the quake compared to the ultimate pile base displacement and the ratio of the mobilized base stress over the ultimate base stress. The loading quake value relative to the ultimate base displacement varies in range of about 8% to 13% for the closed-ended piles in sand and 2% to 5% for the open-ended piles in sand and clay.

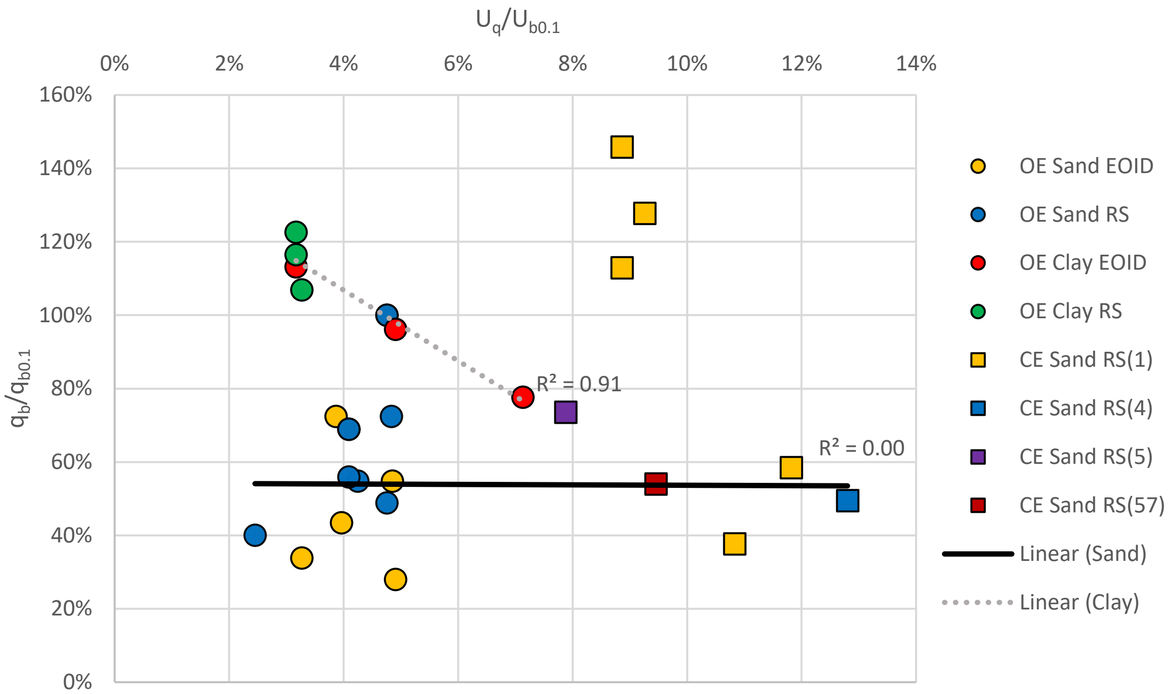

Figure 97: Ratio of mobilized pile base stress and ultimate base stress versus loading quake value divided by 0.1D pile displacement

7.8 Total pile capacity

The total pile capacity can be divided into a contribution of the shaft and base resistance. Signal matching analysis is a quick procedure to verify the total (static) pile capacity and behaviour of piles under dynamic loading conditions. It allows engineers to assess whether the actual pile capacity meets the design requirements and to validate the assumptions made during the design phase. In the design phase, the total axial bearing capacity could be calculated by using the new Unified CPT-based axial pile capacity design method for driven piles in sand and clay (2020) as described in Chapter 4.3 and 4.4. To verify the design calculations, it is possible to check the total bearing capacity with field measurements by means of a dynamic load test. In Table 23 the results for shaft and base resistance obtained from signal matching analysis on dynamically tested piles are listed and compared with outcomes from calculations from the design methods. Table 23 shows that the deviation between the calculated shaft resistance and obtained shaft resistance after signal matching analysis are relatively small. Comparable results for shaft resistance could be caused by the relative small pile displacement that is needed to mobilize the available shaft friction. The dynamic load tests were able to generate sufficient pile movement to reach the local ultimate shaft friction. Furthermore, as mentioned in Chapter 7.3, the yield stresses in the TNO soil model derived after signal matching analysis appeared to show a high degree of similarity to the calculated local ultimate shaft friction from the design methods. A noteworthy outlier is pile NZ UK D11 which has a significant part of the lower pile shaft located in an relatively thick extremely stiff clay layer with high shear strength, whereby the undrained shear strength had to be taken to increase the matching quality instead of the calculated local ultimate shaft friction from the design method for driven piles in clay. The ultimate base stress in the design methods is the base stress reached at a pile base displacement of 10% of the (equivalent) pile diameter. From driving recordings, none of the piles met this state of ultimate base capacity based on the derived pile base displacements in AllWave-DLT (Figure 42). Therefore the mobilized pile base stress during the dynamic load test had to be analysed by varying the loading quake and yield stress in the signal matching procedure.

Pile type	Pile (setup time)	Shaft [MN]	%	Base [MN]	%	Total [MN]	%
Closed-ended piles	M1P25 (1)	1.93	1%	1.11	-41%	3.04	-21%
	M1P7 (1)	1.51	-12%	0.91	-62%	2.42	-36%
	M3P23 (1)	1.40	-7%	1.62	28%	3.02	13%
	M4P2 (57)	2.22	26%	0.85	-46%	3.07	-33%
	M4P13 (1)	1.35	-12%	1.38	46%	2.72	27%
	M5P19 (1)	1.91	-18%	1.96	13%	3.88	15%
	M8P17 (5)	1.69	-6%	1.22	-26%	2.90	-11%
	M8P24 (4)	1.69	1%	1.05	-51%	2.74	-28%
Open-ended piles	NZ NL (EOID)	16.72	18%	1.85	-32%	18.57	-20%
	NZ NL (RS)	18.76	14%	1.98	-28%	20.74	-16%
	NZ GE (EOID)	69.12	2%	3.21	-45%	72.32	-5%
	NZ GE (RS)	73.33	2%	3.21	-45%	76.54	-5%
	NZ UK B04 (EOID)	16.72	-2%	1.18	-31%	17.89	-1%
	NZ UK B04 (RS)	16.81	-2%	1.18	-31%	17.99	-1%
	NZ UK C01 (EOID)	15.81	5%	0.25	-22%	16.0	-5%
	NZ UK C01 (RS)	21.38	-28%	0.38	17%	21.76	27%
	NZ UK C11 (EOID)	18.08	5%	0.27	-4%	18.35	-5%
	NZ UK C11 (RS)	18.13	6%	0.29	7%	18.43	-6%
	NZ UK D11 (EOID)	30.85	-55%	0.38	13%	31.22	55%
	NZ UK D11 (RS)	32.36	-60%	0.41	23%	32.77	59%
	NZ UK D14 (EOID)	16.73	-1%	1.25	-57%	17.98	-7%
	NZ UK D14 (RS)	16.63	2%	1.40	-52%	18.02	-9%
	NZ UK D15 (EOID)	19.69	4%	0.38	0%	20.07	-4%
	NZ UK D15 (RS)	21.40	1%	0.38	0%	21.77	-1%
	NZ UK F23 (EOID)	22.84	-33%	0.29	-85%	23.13	-21%
	NZ UK F23 (RS)	16.84	5%	0.59	-69%	17.43	-11%
	NZ UK F24 (EOID)	15.57	8%	0.32	-66%	15.89	-11%
	NZ UK F24 (RS)	16.80	2%	0.38	-60%	17.19	-5%

Table 23: Comparison between obtained shaft and base resistance compared to calculated resistances by design methods

In Figure 98 the obtained total mobilized resistance ($Q_{t,DLT}$) generated by shaft resistance ($Q_{s,DLT}$) and base resistance ($Q_{b,DLT}$) from the dynamic load test are set out against the calculated shaft, base and total pile capacity ($Q_{s,c}$, $Q_{b,c}$ and $Q_{t,c}$) derived from the unified methods. The upper chart in Figure 98 shows that on average the obtained mobilized shaft resistance of both closed- and open-ended piles based on signal matching analysis are almost equal with the calculated shaft capacity, with a trendline following the line of equality. The magnitude of mobilized shaft resistance for the closed-ended piles are much lower than for the open-ended piles, but the trendlines are in line with each other and underpinned with a high reliability to the datapoints. Using the unified method as starting point for the local ultimate shaft friction as yield stress in the TNO soil model in signal matching analysis seems to be a good approach. Regarding the correlation between the calculated and obtained values for the pile base resistance, the mobilized base resistance is about 54% of the calculated end-bearing resistance for open-ended piles and about 67% for the closed-ended piles. The two trendlines from the closed- and open-ended piles deviate slightly from each other. Also the reliability of the trendline for the closed-ended piles has slightly a lower reliability compared to the open-ended piles. It can be concluded that in most cases the hammer impact was not able to fully mobilized the calculated end-bearing capacity. Comparing the total mobilized pile resistance based on signal matching analysis with the calculated pile capacity shows that for the open-ended piles a good match can be achieved. Despite the deviation in degree of mobilisation in pile base resistance, for an open-ended pile, the majority of the shaft resistance typically comes from the side friction along the shaft rather than the base. The open-ended pile does not have a closed or pointed base to develop significant end-bearing capacity. Therefore the base resistance has a less significant effect on the total mobilized resistance than the shaft resistance. In general the mobilized total pile resistance is about 98% of the calculated total pile bearing capacity for open-ended piles. The deviation between total calculated pile capacity and the obtained mobilized pile resistance for the closed-ended piles are more significant. The deviation can be mainly explained by the difference in mobilized end-bearing resistance to the calculated end-bearing capacity. End bearing is a critical component of load-carrying capacity for closed-ended piles. Closed-ended piles, also known as bearing piles or end-bearing piles, are designed to transfer significant vertical loads to the underlying stratum through the base of the pile. Unlike open-ended piles, closed-ended piles have a solid base that can develop substantial end-bearing capacity. In general the mobilized total pile resistance is about 83% of the calculated total pile bearing capacity for closed-ended piles. The equations relating the signal matching analysis results and design method calculations are given in Table 24.

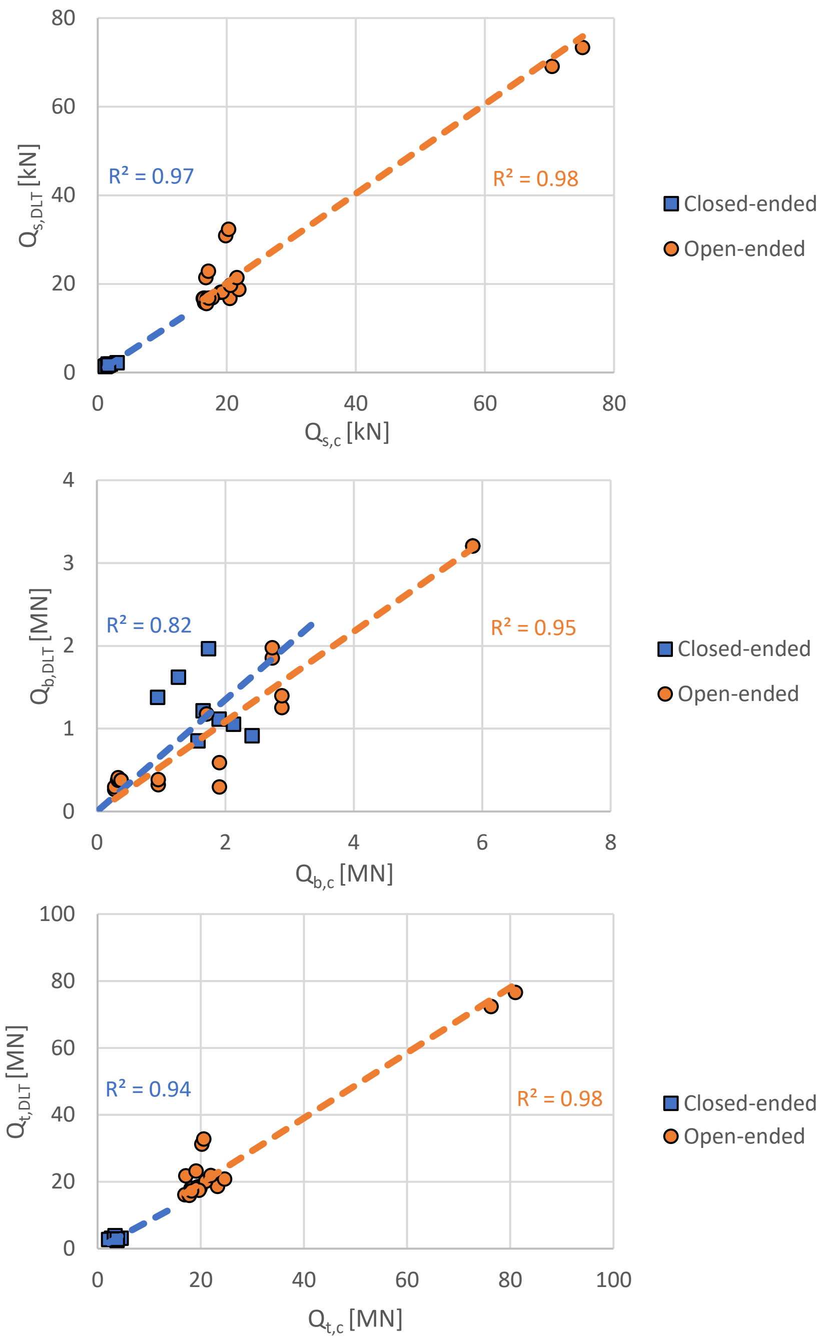

Figure 98: Obtained mobilized shaft (top), base (middle) and total resistance (bottom) based on signal matching analysis in comparison to calculated capacities by the design methods

Pile type	Formula	Reliability
Closed-ended piles	$Q_{s,DLT} = 0.95 * Q_{s,c}$ $Q_{b,DLT} = 0.67 * Q_{b,c}$ $Q_{t,DLT} = 0.83 * Q_{t,c}$	$R^2 = 0.97$ $R^2 = 0.82$ $R^2 = 0.94$
Open-ended piles	$Q_{s,DLT} = 1.00 * Q_{s,c}$ $Q_{b,DLT} = 0.54 * Q_{b,c}$ $Q_{t,DLT} = 0.98 * Q_{t,c}$	$R^2 = 0.98$ $R^2 = 0.95$ $R^2 = 0.98$

Table 24: Equations relating ratio of mobilized base resistance and ultimate base capacity to ratio of permanent pile base set after hammer impact and ultimate pile base displacement of 0.1D

8. Conclusions

The objectives of this research can be divided into two main aspects, one section focussing on the static part of the mechanical system and the other part on the dynamic component of the mechanical model under dynamic loading. The first main objective was to validate if the new Unified CPT-based axial pile capacity design methods for piles in sand and clay are applicable as the yield stresses in TNO soil model to describe the local ultimate shaft friction and end-bearing stress at ultimate conditions. The pile displacement dependent static part of the mechanical system consisting of springs and plastic sliders representing the generated static soil resistance under dynamic loading. Secondly, if the velocity dependent dynamic part of the mechanical system consisting of a linear dashpot could be related to geotechnical soil parameters obtained from site investigation data.

1. How applicable are the new Unified CPT-based axial pile capacity design methods for driven piles in sand and clay in predicting the local ultimate shaft friction and end bearing stresses in the TNO soil model in signal matching analysis?

In the analysis of a dynamic load test, the starting values from where signal matching analysis is performed can be very subjective. The distribution of shaft friction and damping can be unrealistic and arbitrary chosen even if the signal match between the measured and the generated signals seems to be in line with each other. The first objective of this research was to validate if the local ultimate shaft friction calculated from the CPT-based axial pile capacity design methods including setup effects could serve as reasonable initial values for yield stresses in the TNO soil model for signal matching analysis to make it more in line with axial pile capacity estimations from CPT-based methods. At first glance, Chapter 7.2 shows that it is feasible to obtain high quality matches if the design methods are taken into consideration in the signal matching analysis. From the results of the signal matching analysis regarding the obtained yield stresses in the TNO soil model, Chapter 7.4 shows that the deviation between the calculated local ultimate shaft friction and yield stress are within a range of -15% and +15% for closed-ended piles and -10% to +10% for the open-ended piles for the sand layers. The deviations regarding the clay layers are sometimes significant what might indicate an apparent increased undrained shear strength in the stiff clay layers due to installation effects and rate of loading. It should be noted that the calculations from the design methods also have some uncertainty due to CPT based correlation function for the input parameters (soil density and interface friction angle) in the formulations for shaft friction and end bearing as mentioned in Chapter 4. The obtained quake values for the TNO soil model presented in Chapter 7.5 show the loading quakes for closed- and open-ended piles are close to the commonly used value of about 2mm to 3mm. The unloading quakes for closed-ended piles are similar to the loading quakes, but the open-ended piles show a large spreading of the unloading quake. The unloading quake or rebound settlement of open-ended piles are more complex after unloading of the pile what might indicate the appearance of residual stresses, in which incomplete rebound leads to lower unloading quakes. Quantifying the residual stresses acting at the pile base is difficult and beyond the scope of this research. Other factors leading to large spreading of the quake values for the open-ended piles could be caused by incomplete mobilization of the local ultimate shaft friction at the lower pile parts. The loading quake values also indicate that shear modulus reduction occurs, due to cyclic loading of the soil along the pile shaft. Chapter 7.5 shows that based on the loading quake values and formulation of the shaft stiffness according to Simons and Randolph (1985) the operational shear modulus reduces to 5% to 10% of the initial shear modulus, G_{max}, for the largest portion of the shaft and closer to the pile base the operational shear modulus reduces up to 40% of its initial value for the closed-ended piles. Setup effects tend to increase the soil stiffness along the pile shaft for longer setup periods after installation which are that is closer to the higher end of this range. Regarding the open-ended piles, the shear modulus reduction is relative uniform along the pile shaft and varies within a range of 5% to 15%. The limited setup time between end of driving (EOID) and restrike (RS) do not show any signs of stiffness increase. Both for the closed- and open-ended piles, the clay layers do not show a meaningful difference in shear modulus reduction compared to the sand layers. The results from Chapter 7.7 show that the ultimate base stress at 10% (equivalent) pile diameter displacement in not often achieved, whereby the mobilized base resistance is lower than the calculated end bearing capacity. In chart show that the mobilization of the base stress tends to increase faster for the closed-ended piles than the open-ended piles. Following the trendline between the ratio of the permanent set after a hammer impact over the ultimate base displacement of 0.1D, with the degree of pile base stress mobilization, the closed-ended piles appears to reach 100% mobilization of end bearing capacity at around 11% of 0.1D, or about 1% of the equivalent diameter. The full mobilization of the end bearing resistance related to pile base displacement after a hammer impact is about 16% of 0.1D or 1.6% of equivalent diameter for the open-ended piles with a base in clay and even up to 50% of 0.1D or 5% for the a pile base in sand. An answer to the first main question comes together in Chapter 7.8, in which the total pile bearing capacities are compared between the results from the signal matching analysis and from the design methods. The deviation between the mobilized shaft resistance and calculated shaft capacity are generally in line with each other with the exceptions of piles with an large portion of the pile shaft in a thick extremely stiff clay layers. The outcomes of the signal matching analysis show that the yield stress are almost equal to the local ultimate shaft friction because the dynamic load test is able to generate sufficient pile shaft displacement to fully mobilize the shaft capacity. Regarding the pile base resistance, most of the dynamic load tests were unable to fully mobilize the end bearing capacity because the pile base displacements were not sufficient. Table 24 and Figure 98 in Chapter 7.8 shows that in general, the closed- and open-ended piles were respectively able to mobilize 95% and 100% of the total shaft capacity. The mobilized base resistance was about 67% and 54% of the calculated end bearing capacity for respectively the closed- and open- ended piles. Overall, combing the contribution of the mobilized shaft resistance and base resistance into the total mobilized pile resistance it can be concluded that during the dynamic load tests, the closed-ended piles were able to mobilize 83% of the total pile bearing capacity and the open-ended piles 98%. It must be noticed that the effect of end bearing on the closed-ended piles has a considerable effect on the total mobilized pile resistance compared to the open-ended piles in which shaft resistance is the dominant factor in the total pile resistance.

2. What is the strength of the correlations between the obtained shaft radiation damping constants in the TNO soil model based on the results from signal matching analysis with geotechnical soil parameters obtained from site investigation data?

In Chapter 7.6 the focus in on the correlations between obtained shaft radiation damping constants and geotechnical soil parameters obtained from site investigation. It is assumed that the base radiation damping constant is equal to calculated base radiation damping constant proposed by Deeks and Randolph (1995). Signal matching analysis is an iterative process in which the yield stress and damping constant in the TNO soil model are varied to obtain the optimum solution for the model parameters that gives the highest match quality compared to the measured signals during the dynamic load test. Radiation damping in soil refers to the dissipation of energy due to the radiation of elastic waves during dynamic loading or vibration. When a soil mass is subjected to dynamic forces or vibrations, it generates elastic waves that propagate through the soil medium. These waves carry energy, and as they propagate away from the source, they gradually lose energy due to various damping mechanisms. The damping mechanism considered in this research is radiation damping. Viscous and hysteric damping are neglected. The generated damping force in the TNO model is only pile velocity dependent and is decoupled from the static resistance. Chapter 7.6.1 and 7.6.2 show that the shaft radiation damping constants tend to increase with depth and vertical effective stress for the closed-ended piles with a good fit to a power trendline. Setup time has a limited effect on the strength of the correlation. The correlation between the damping constants with depth and vertical effective stress is less observed for the open-ended piles and the radiation damping constants remain in constant range along the pile shaft. An explanation for this lack of trending might be partly found in the difference in transferability of stress waves to the surrounding soil due to a difference in surface roughness between concrete and steel. Another explanation could be that the soil around the pile shaft becomes more stable over time after installation which affect the radiation damping characteristics. The dynamic load tests on the open-ended piles were performed within a couple of hours after pile installation. In Chapter 7.6 the shaft radiation damping constants some correlation with the obtained yield stresses, with a logarithmic trendline for the closed-ended piles and a linear tend for the open-ended piles, but both correlation show a high variance. In Chapter 7.6.4 the shaft radiation damping constants are compared with the measured cone resistance values for each soil layer. A direct correlation between cone resistance and shaft radiation damping constant gives a weak trend and therefore the cone resistance is not able to give a good estimate for the shaft radiation damping constant. When the cone obtained shaft radiation damping constants is normalized with the cone resistance and plotted against relative pile depth, it appears that the spreading is very large starting from 0% to 8% closer to the pile base for the closed-ended piles and this is independent of soil type. The results also show that regarding the open-ended piles the shaft radiation damping constant normalized with the cone resistance remains between 0% and 1% along the entire shaft at end of driving and restrike. The ratio varies between 1% and 4% for the clay layers. Any clear correlation between the cone resistance normalized with the vertical effective stress and shaft radiation damping constants neither visible in the charts. Based on all the signal matching analysis results for the shaft radiation damping constants in the TNO soil model, it is recommend to use the equation which relates the shaft radiation damping constants with vertical effective stress as starting point for signal matching analysis in case of closed-ended piles. Regarding signal matching analysis on open-ended piles within a couple of hours after installation, it is recommend to take the shaft radiation damping constant in the sand layers up to 1% of the cone resistance value and for clay layers a value between 1% and 4% of the cone resistance is a good first approach.

9. Discussion and recommendations

The findings from this research provide significant insights into the applicability of new Unified CPT-based axial pile capacity design methods in signal matching analysis for driven piles in sand and clay. The integration of these methods into signal matching analysis, particularly in the context of dynamic load testing, represents a notable advancement in geotechnical engineering.

Initially, this research underscores the importance of addressing the subjectivity in selecting initial values for signal matching analysis.. This research highlights the advantage of using calculated values for yields stresses in the static part of TNO soil model from the design methods as initial values for performing the signal matching analysis on the results of a dynamic load test. Using directly the raw CPT data by means of cone resistance and sleeve friction for respectively pile base and shaft values as yield stresses in the TNO models results in low quality signal matching results. This approach can lead to unrealistic distributions of shaft friction and damping and an imbalance in resistance that has been assigned to generated static resistance in comparison to the dynamic resistance The unified methods formulates a correction on the cone resistance and in combination with a correction on the theoretical damping constant the matching quality significantly increases. The use of CPT-based methods as starting points introduces a more objective and data-driven approach, enhancing the accuracy of signal matching analysis. The uncertainties inherent in the CPT-based correlation functions, used in design methods to define all the geotechnical soil parameters, must be acknowledged. The significant deviations observed in clay layers warrant further investigation. Understanding the role of undrained shear strength and loading rate effects and other (dynamic) soil properties in these layers is crucial for improving the starting points for yield stresses in the TNO model for subsequent signal matching analysis. The design method calculations for piles in clay, originally devised for piles under static loading, may yield unrealistic values for static shaft and base friction when applied to dynamically loaded piles. To more effectively validate and reinforce the application of these design methods for estimating axial pile capacity from dynamic load tests, it is essential to conduct a greater number of pile tests where both static and dynamic load tests are comprehensively performed on the same piles.

Finally, this research brings into focus the concept of radiation damping, which pertains to the loss of energy via elastic waves during dynamic loading or vibrations. This damping mechanism is unique as it solely depends on the velocity of the pile and remains unaffected i.e. decoupled by the generated static resistance in the TNO soil model. For closed-ended piles, the study identified a notable correlation between the shaft radiation damping constants and variables such as depth and vertical effective stress. Conversely, in the case of open-ended piles, the research found that the radiation damping constants were largely uniform along the length of the pile shaft, showing no significant variation with depth or stress, what might be caused by the short duration between installation and testing. This observation points to an intrinsic difference in how closed-ended and open-ended piles interact with the dynamic properties of soil. Moreover, the limited correlation observed between cone resistance and shaft radiation damping constants implies that relying on cone resistance as a sole indicator for damping behavior may be inadequate. This underscores the importance of adopting a comprehensive approach when analyzing soil parameters for their impact on pile dynamics.

References

Aasen, S., Page, A., Skau, K., & Nygaard, T. (2017). Effect of foundation modelling on the fatigue lifetime of a monopile-based offshore wind turbine. *Wind Energy Science*(2), 361-376.

Aoki, N., & Velleso, D. (1975). An Approximate Method to Estimate The Bearing Capacity Of Piles. *Proceedings, Fifth Pan-American Conference of Soil Mechanics and Foundation Engineering*, *Vol. 1*, pp. 367-376. Buenos Aires.

ASCE, G.-I. o. (Director). (2020). *ISFOG 2020 Webinar: New proposed ISO/API unified CPT-based method for axial pile capacity in sand* [Motion Picture]. Retrieved from https://www.youtube.com/watch?v=bU3y4G4kCL4

Bielefeld, M., & Courage, W. (1992). TNOWAVE automatic signal matching. *Application of stress wave theory to piles*.

Bond, A., & Jardine, R. (1991). Effects of installing displacement piles in a high OCR clay. *Geotechnique, No.3*(41), 341-363.

Brennan, A., Thusyanthan, N., & Madabhushi, S. (2005). Evaluation of Shear Modulus and Dampingin Dynamic Centrifuge Tests. *Journal of Geotechnical and Geoenvironmental Engineering, 131*.

Cetin, K., & Ozan, C. (2009). CPT-Based Probabilistic Soil Characterization and Classification. *Journal of Geotechnical and Geoenvironmental Engineering, 135*(1), 84-107.

Chow, F. (1997). *Investigation in the Behavior of Displacement Piles for Offshore Foundations. Ph.D Thesis.* Imperial College, U.K.

Chow, Y. (1986). Analysis of vertically loaded pile groups. *International journal for numerical and analytical methods in geomechanics, Vol. 10*, 59-72.

Cooke, R. (1974). The Settlement of friction Pile Foundations. *Proceeding Conference on Tall Buildings.* Kuala Lumpur.

Coop, M., Mayne, P., Springman, S., Huang, A., & Zornberg, J. (2009). SOA-1: Geomaterial behavior and testing. *In Proceeding of the 17th International Conference on Soil Mechanics and Geotechnical Engineering, vol. 4 (ICSMGE, Alexandria).* Millpress/IOS Press Rotterdam: 2777-2872.

Coyle, H., & Gibson, G. (1970). Emperical damping constants for sands and clays. *Journal of the soil mechanics and foundation division. Proceedings of the American Society of Civil Engineers*, 949-965.

Coyle, H., Bartoskewitz, R., & Berger, J. (1973). *Bearing capacity by wave equation analysis - state of art.* Texas Transportation Institute. Texas: Texas A & M University.

Cummings, A. (1940). Dynamic Pile Driving Formulas. *Journal of Boston Society of Civil Engineers*.

de Jong, J., Randolph, M., & White, D. (2003). Interface load transfer degradation during cyclic loading: a microscopic investigation. *Soils Found., 43(4)*, 81-93.

De' Nicola, A., & Randolph, M. (1993). Tensile and compressive shaft capacity of piles in sand. *Journal Geotechnical Engineering, 19(12)*, 1952-1973.

Doherty, P., Gavin, K., & Gallagher, D. (2010). Field investigation of base resistance of pipe piles in clay. *Proceedings of the institution of civil engineers - Geotechnical Engineering, Vol. 163*(No. 1), 13-22.

El Naggar, M., & Novak, M. (1994). *Nonlinear axial interaction in pile dynamics.* ASCE.

Eslami, A., & Fellenius, B. (1997). Pile capacity by direct CPT and CPTu methods applied to 102 case histories. *Canadian Geotechnical Journal, 34*(6), 880-898.

Esposito, G., Courage, W., & van Foeken, R. (1998). Application of stress wave method to automatic signal matching and to statnamic predictions. *Application of stress wave theory to piles* (pp. 575-581). Rotterdam: Balkema.

Fahey, M., & Carter, J. (1993). A finite element study of the pressuremeter test in sand using a non-linear elastic plastic model. *Canadian Geotechnical Journal*.

Fakharian, K., Masouleh, S., & Mohammadlou, A. (2013). Comparison of end-of-drive and restrike signal matching analysis for a real case using continuum numerical modelling. *Soils and foundations, 54*(2), 155-167.

Fleming, W. (1958). *The bearing capacity of pile groups.* Ph.D. Thesis Queen's University, Belfast.

Fox, E., Glanville, W., Grime, G., & Davies, W. (1938). *An Investigation of Stresses in Reinforced Concrete Piles During Driving.* Department Sci. Ind. Research. British Building Research Board Technical Paper No. 20.

Foye, K., Abou-Jaoude, G., Prezzi, M., & Salgado, R. (2006). Resistance Factors for Use in Load and Resistance Factor Design of Driven Pipe Piles in Sands. *Journal of Geotechnical and Geoenvironement Engineering*.

Gavin, K. (2020). *Axial piles in sand open-ended piles [PowerPoint slides]. Faculty of Civil Engineering and Geoscience. Delft University of Technology*. Retrieved from https://brightspace.tudelft.nl/d2l/le/content/193380/viewContent/1664297/View

Gavin, K., & Lehane, B. (2007). Base load-displacement response of piles in sand. *Canadian Geotechnical Journal, 44(9)*, 1053-1063.

Gazetas, G., Dobry, R., & Tassoulas, J. (1985). Vertical response of arbitrarily shaped embedded foundations. *Journal of geotechnical engineering, 6*(111).

Gibson, G., & Coyle, H. (1968). *Soil damping constants related to common soil properties in sands and clay.* Texas A&M University. Texas Transport Institute.

Goble, G., Likins, G., & Rausche, F. (1975). *Bearing Capacity of Piles from Dynamic Measurements, Final Report.* Case Western Reserve University, Dept of Civil Engg.

Hannigan, P., Goble, G., Thendean, G., Likins, G., & Rausche, F. (1998). *Design of construction of driven pile foundation. FHWA-HI-97-013.* US Department of Transportation. Washington, DC: Federal Highway Administration.

Hardin, B., & Drnevich, V. (1972b). Shear modulus and damping in soils, measurement and parameter effects. *J. SMFD, Proc. ASCE, Vol. 98, July*.

Herrington, K. (2018). *Integrating pile setup in the LRFD design of driven piles in Louisiana. LSU Master's Thesis.* Lousiana State University, Agricultural and Mechanical College.

Hirsch, T., Lowery, L., Coyle, H., & Samson Jr, C. (1970). *Pile-Driving Analysis by One-Dimensional Wave Theory: State of the Art.* Highway Research Record 333.

Holeyman, A. (1985). Dynamic Non-Linear Skin Friction of Piles. *Proceedings of the International Symposium on Penetrability and Drivability of Piles.* San Fransisco.

Huizinga, T. (1969). *Grondmechanica.* Argon/Elsevier.

Isaacs, D. (1931). Reinforced concrete pile formulas. *Trans. Inst. Engineers Aust*(XII).

Iwasaki, T., Tatsuoka, F., & Takagi, Y. (1978). Shear moduli of sands under cyclic torsional shear loading. *Soils and foundations, 18*(1), 39-50.

Jamiolkowski, M., Presti, D., & Manassero, M. (2001). Evaluation of relative density and shear strength of sands from CPT and DMT. *Soil behavior and soft ground construction. Geotechnical Special Publication No. 119*, pp. 201-238.

Jardine, R., Thomsen, N., Mygind, M., Liingaard, M., & Thilsted, C. (2015). Axial capacity design pratice for North European wind-turbine projects. *Frontiers in offshore geotechnics III*.

Jefferies, M., & Davies, M. (1993). Use of CTPu to estimate equivalent SPT N60. *Geotechnical Testing Journal, 16(4)*, 458-467.

Kavazanjian, E., Matasovib Jr, N., Hadj-Hamou, T., & Sabatini, P. (1997). Earthquake Engineering for Highway Volume 1 design Principle. *Geotechnical Engineering Circular NO 3 Design Guidance Geotechnical*.

Lee, J., & Salgado, R. (1999, August). Determination of pile base resistance in sands. *Journal of geotechnical and geoenvironmental engineering, Vol. 125(8)*, pp. 673-683.

Lee, J., Salgado, R., & Paik, K. (2003). Estimation of the Load Capacity of Pipe Piles in Sand Based on CPT Results. *Journal of Geotechnical and Geoenvironmental Engineering, 129*(5), 391-403.

Lee, L., Ti, K., Leong, L., Wai, Y., & Ming, J. (2019). Emperical equations for predicting pile/soil setup effects. *IOP Conference Series: Material Science and Engineering, 527*.

Lehane, B. (1992). *Experimental investigation of pile behaviour using instrumented field piles. PhD Thesis.* London: Imperial College.

Lehane, B., Bittar, E., Liu, Z., Nadim, F., Lacasse, S., Bozorgzadeh, N., . . . Morgan, N. (2022). CPT-based axial capacity design method for driven piles in clay. *Journal of Geotechnical and Geoenvironmental Engineering, 148*(9).

Lehane, B., Carotenuto, P., Lim, J., Nadim, F., Jardine, R., Dijk, B., & Lacasse, S. (2017). Characteristics of unified databases for driven piles. *OSIG 2017*, (pp. 162-191).

Lehane, B., Li, Y., & Williams, R. (2020). Shaft capacity of displacement piles in clay using the cone penetration test. *Journal of geotechnical and geoenvironmental engineering, 138*(2), 253-266.

Lehane, B., Liu, Z., Bittar, E., Nadim, F., Lacasse, S., Jardine, R., . . . Gavin, K. (2020). A new unified cpt-based axial pile capacity design method for driven piles in sand. *Proceedings fourth international symposium on frontiers in offshore geotechnics.*

Liang, Y. (2000). Correlation study of Smith damping coefficient and SPT blow count. *Application of stress wave theory to piles: assurance on land and offshore piling*, pp. 461-467.

Lim, J., & Lehane, B. (2017). *Reliability of API and CPT-based axial pile capacity design methods: Unified web database of reliable pile load tests, Confidental to JIP.* Report GEO: 1216BL, Perth.

Lopes, F., Danziger, B., & Costa, L. (2011). Prediction of residual stresses in piles. *Canadian Geotechnical Journal, 38(2)*, 410-421.

Loukidis, D., Salgado, R., & Abou-Jaoude, G. (2008). *Assessment of axially-loaded pile dynamic design methods and review of INDOT axially-loaded pile design procedure.* FHWA.

Lowery , L., Edwards, T., & Hirsch, T. (1968). *Use of The Wave Equation to Predict Soil Resistance on a Pile During Driving.* Texas Transportation Institute.

Lunne, T., & Andersen, K. (2007). Soft clay shear strength parameters for deepwater geotechnical design. . *In Proceedings of the 6th International Conference on Offshore Site Investigation and Geotechnics* (pp. 151-176). London: Society for Underwater Technology.

Lunne, T., Robertson, P., & Powell, J. (1997). *Cone Penetration Testing in Geotechnical Practice.* Blackie Academic/London. New York: Routledge.

Lysmer, J. (1965). *Vertical Motion of Rigid Footings.* University of Michigan.

Mayne, P. (2007). *Cone penetration testing: a synthesis of highway practice, NCHRP Synthesis 368.* Transportation Research Board. Washington, DC: National Academic Press.

Mayne, P. (2014). Interpretation of geotechnical parameters from seismic piezocone tests. *Proceedings, 3rd International Symposium on Cone Penetration Testing, 102*, pp. 47-73.

Mayne, P., & Peuchen, J. (2012). Unit weight trends with cone resistance in soft to firm clays. *Geotechnical and Geophysical Site Characterization 4*(Vol. 1), 903-910.

Mayne, P., Coop, M., Springman, S., Huang, S., Zornberg, J., & Bin, A. (2009). State-of-the-art paper (soa-1): Geomaterial behavior and testing. *Conference: 17th International conference on soil mechanics and geotechnical engineering*, *4.* Egypt.

Michaelides, O., Gazetas, G., Bouckovalas, G., & Chrysikou, E. (1998). Approximate non-linear dynamic axial response of piles. *Geotechnique, 48. No 1*, 33-53.

Middendorp, P., & Verbeek, G. (2006). 30 Years of Experience with the Wave Equation Solution Based on the Method of Characteristics. *2006 GeoCongress.* Atlanta.

Milewski, H., & Kennedy, J. (2019). Application of friction fatigue pile driving models in GRLWEAP. *OMAE2019.* Glasgow.

Nguyen, T. (1987). *Dynamic and static behaviour of driven piles.* Statens Geotekniska Institut, Linkoping.

Novak, M., Nogami, T., & Aboul-Ella, F. (1978). Dynamic soil reactions for plane strain case. *Journal of engineering mechanics division, 104(4)*, 953-959.

Paik, K., Salgado, R., & Lee, J. (2004). Design lessons from load tests on open- and closed-ended pipe piles. *International Conference on case histories in Geotechnical Engineering*, *8.*

Paikowsky, S., Regan, J., & McDonnell, J. (1994). *A simplified field method for capacity evaluation of driven piles.* FHWA Report No. FHWA-RD-94-042.

Pando, M., Ealy, C., Filz, G., Lesko, J., & Hoppe, E. (2006). *A laboratory and field study of composite piles for bridge substructures. FHWA-HRT-04-043.* Virginia Transportation Research Council.

Poulos, H., Small, J., & Hemsley, J. (2000). Development of design charts for concrete pavements and industrial ground slabs. In H. Poulos, *Design applications of raft foundations* (pp. 39-70). J.A. Hemsley.

Randolph, M. (2003). Science and Empiricism in Pile Foundation Design. *43rd Rankine Lecture. 54(1).* Geotechnique.

Randolph, M., & Gourvenec, S. (2011). *Offshore Geotechnical Engineering.* CRC Press.

Randolph, M., & Wroth, C. (1978). Analysis of Deformation of Vertically Loaded Piles. *Journal of the Geotechnical Engineering Division, 104(12)*, 1465-1488.

Robertson, P. (2009). Interpretation of Cone Penetration Tests - a Unified Appraoch. *Canadian Geotechnical Journal 49(11)*, 1337-1355.

Robertson, P., & Cabal, K. (2010). Estimating Soil Unit Weight from CPT. *In Proceedings of the 2nd International Symposium on Cone Penetration Testing, Vol.2 (CPT10, Huntingdon Beach, CA)*, 447-454.

Salgado, R. (2008). *The Engineering of Foundations.* McGraw-Hill.

Schnaid, F., Lehane, B., & Fahey, M. (2004). In situ test characterization of unusual geomaterials. . *In Proc. 2nd Int. Conf. on Site Characterization (ISC)* (pp. 49-74). Millpress.

Smith, E. (1960). Pile Driving Analysis by the Wave Equation. *Proceedings ASCE*.

Strozyk, J. (2017). The laboratory study of shear strength of the overconsolidated and quasi-overconsolidated fine grained soils. *World Multidisciplinary Earth Sciences Symposium (WMESS)*, *95*, pp. 2-3. Wroclaw, Poland.

Svinkin, M., & Skov, R. (2000). Set-up effect of cohesive soils in pile capacity. *Proceedings of 6th international conference on the application of stress-wave theory to piles*, (pp. 107-111). Brazil.

Togliani, G., Calzolari, L., & Menghini, A. (2015). Governolo (Italy) experimental site: in situ test comparison and mutual conversion. *Third Conference on DMT, 88*.

Uzielli, M., Mayne, P., & Cassidy, M. (2013). *Probabilistic assessment of design strength for sands from in-situ testing data.* Amsterdam: IOS Press.

van Komurka, E., Wagner, A., & Tuncer, B. (2003). *A review of pile set-up.*

Voitus van Hamme, G. (1981). *Over de werking van het dieselblok. Proefschrift ter verkrijging van de graad van doctor in de technische wetenschappen aan de T.H. Eindhoven.*

Weng, K., & Sritharan, S. (2018). Improving dynamic soil parameters and advancing the pile signal matching technique. *Computers and Geotechnics*, 166-174.

White, D., & Bolton, M. (2002). Observing friction fatigue on a jacked pile. Centrifuge and Constitutive Modelling: Two Extremes.

White, D., Schneider, J., & Lehane, B. (2005). The influence of effective area ratio on shaft friction on displacement piles in sand. *Proc. Int. Symp. Front. Offshore Geotech.*, (pp. 741-747). Perth, Australia.

Xu, X., Schneider, J., & Lehane, B. (2008). Cone penetration test (CPT) methods for end-bearing assessment of open- and closed-ended driven piles in siliceous sand. *Canadian Geotechnical Journal, 45(8)*, 1130-1141.

Appendix A

M1P25 (RS 1 day)

Layer	Depth	Thickness	q_c	q_s	q_t	q_base_1.5D	Rf	Rfn	Unit Weight	Density	u	σ_v0	σ'_v0	Q_t	Q_tn	n	I_c	a_vs	V_s	G_max	G_UWA	G_ICP	G_Uni	G_clay	Dr	φ'	ψ	φ'cv	v	m'	σ'vy	OCR=YSR	S_t	h/R	h	K_c	τ_sc_UWA13		τ_sc_Unified				Skin Friction F_τ_sf	Shaft Resistance Q_s	
Nr	[m]	[m]	[KPa]	[KPa]	kPa				[kN/m3]	kg/m3	kPa	kPa	kPa						m/s	kPa	kPa	kPa	kPa	kPa	%	degree	degree	degree									clay	F_τ_sf	σ'_rc	Δσ'_rd	τ_sf	F_τ_sf	kPa	kN	G_max
1	2.3	0.4	0	1	1		0.0%	0.0%	0.0	0.0	0.0	0.0	0.0	0.0	#DIV/0!	#VALUE!	2.0	603	2	0	#DIV/0!	#DIV/0!	0		#DIV/0!	#DIV/0!	#DIV/0!	#DIV/0!	0.35	0.9	0.0	#DIV/0!		109.6	27.8								0	1	#DIV/0!
	1.9		1700	29	1700		1.7%	1.7%	17.4	1740.8	0.0	6.6	6.6	257.4	68.1	0.5	2.2	764	114	22513	13540	16915	12134		44.9	38.0	3.6	35.1	0.35	0.7	70.9	10.8		108.1	27.4				8	2	6	5	5		22513
2	1.9	2.0	1700	29	1700		1.7%	1.7%	17.4	1740.8	0.0	6.6	6.6	257.4	68.1	0.5	2.2	764	114	22513	13540	16915	12134		44.9	38.0	3.6	35.1	0.35	0.7	70.9	10.8		108.1	27.4				8	2	6	5	5	16	22513
	0.0		500	23	500		4.6%	5.0%	16.7	1667.6	0.0	39.5	39.5	11.7	9.8	0.8	3.1	2540	108	19506				24420		30.8			0.45	1.0	148.2	3.8	1.4	100.3	25.5	1.7	13	5					5		19506
3	0.0	4.2	500	23	500		4.6%	5.0%	16.7	1667.6	0.0	39.5	39.5	11.7	9.8	0.8	3.1	2540	108	19506				24420		30.8			0.45	1.0	148.2	3.8	1.4	100.3	25.5	1.7	13	5					5	30	19506
	-4.2		300	32	342		10.5%	12.0%	16.8	1683.9	40.1	109.4	69.3	2.7	2.7	1.0	3.8	5921	127	23188				18026		28.4			0.45	1.0	62.9	1.0	0.4	83.9	21.3	1.2	9	4					4		18026
4	-4.2	0.5	300	32	342		10.5%	12.0%	16.8	1683.9	40.1	109.4	69.3	2.7	2.7	1.0	3.8	5921	127	23188				18026		28.4			0.45	1.0	62.9	1.0	0.4	83.9	21.3	1.2	9	4					4	4	18026
	-4.7		400	54	456		13.6%	12.0%	17.6	1758.8	45.1	118.3	73.2	3.8	3.8	1.0	3.7	5119	140	30403				23505		29.2			0.45	1.0	92.9	1.0	0.4	82.0	20.8	1.2	13	5					5		23505
5	-4.7	0.9	400	54	456		13.6%	12.0%	17.6	1758.8	45.1	118.3	73.2	3.8	3.8	1.0	3.7	5119	140	30403				23505		29.2			0.45	1.0	92.9	1.0	0.4	82.0	20.8	1.2	13	5					5	7	23505
	-5.6		400	48	456		12.0%	12.0%	17.4	1744.1	54.4	134.4	80.0	3.3	3.3	1.0	3.7	5454	143	30590				23156		29.0			0.45	1.0	87.6	1.0	0.4	78.3	19.9	1.2	13	5					5		23156
6	-5.6	0.3	400	48	456		12.0%	12.0%	17.4	1744.1	54.4	134.4	80.0	3.3	3.3	1.0	3.7	5454	143	30590				23156		29.0			0.45	1.0	87.6	1.0	0.4	78.3	19.9	1.2	13	5					5	3	23156
	-6.0		400	16	456		4.0%	6.2%	16.2	1616.0	57.7	139.8	82.1	3.2	3.2	1.0	3.6	4493	130	22956				21370		29.0			0.45	1.0	85.8	1.0	1.2	77.0	19.5	1.0	13	5					5		22956
7	-6.0	0.2	400	16	456		4.0%	6.2%	16.2	1616.0	57.7	139.8	82.1	3.2	3.2	1.0	3.6	4493	130	22956				21370		29.0			0.45	1.0	85.8	1.0	1.2	77.0	19.5	1.0	13	5					5	2	22956
	-6.2		1700	20	1700		1.2%	1.3%	17.0	1699.8	59.8	143.4	83.6	18.6	17.9	0.8	2.6	1269	143	33582	35120	37098	28071		10.8	33.5	-0.6	34.0	0.35	0.8	136.7	1.0		76.2	19.3				9	4	8	6	6		33582
8	-6.2	0.9	1700	20	1700		1.2%	1.3%	17.0	1699.8	59.8	143.4	83.6	18.6	17.9	0.8	2.6	1269	143	33583	35122	37099	28072		10.8	33.5	-0.6	34.0	0.35	0.8	136.7	1.0		76.2	19.3				9	4	8	6	6	12	33583
	-7.1		900	18	900		2.0%	2.5%	16.6	1662.1	69.0	158.7	89.7	8.3	8.2	0.9	3.0	2200	134	27109				39221		31.3			0.45	1.0	228.9	1.4	3.0	72.5	18.4	1.0	26	10					10		27109

1953

M1P7 (RS 1 day)

Layer	Depth	Thickness	q_c	q_s	q_t	q_base_1.5D	Rf	Rfn	Unit Weight	Density	u	σ_v0	σ'_v0	Q_t	Q_tn	n	I_c	a_vs	V_s	G_max	G_UWA	G_ICP	G_Uni	G_clay	Dr	φ'	ψ	φ'cv	v	m'	σ'vy	OCR=YSR	S_t	h/R	h	K_c	τ_sc_UWA13		τ_sc_Unified				Skin Friction F_τ_sf	Shaft Resistance Q_s	
Nr	[m]	[m]	[KPa]	[KPa]	kPa				[kN/m3]	kg/m3	kPa	kPa	kPa						m/s	kPa	kPa	kPa	kPa	kPa	%	degree	degree	degree									clay	F_τ_sf	σ'_rc	Δσ'_rd	τ_sf	F_τ_sf	kPa	kN	G_max

1343

M3P23 (RS 1 day)

Layer	Depth	Thickness	q_c	q_s	q_t	q_base_1.5D	Rf	Rfn	Unit Weight	Density	u	σ_v0	σ'_v0	Q_t	Q_tn	n	I_c	a_vs	V_s	G_max	G_UWA	G_ICP	G_Uni	G_clay	Dr	φ'	ψ	φ'cv	v	m'	σ'vy	OCR=YSR	S_t	h/R	h	K_c	τ_sc_UWA13		τ_sc_Unified				Skin Friction F_τ_sf	Shaft Resistance Q_s	
Nr	[m]	[m]	[KPa]	[KPa]	kPa				[kN/m3]	kg/m3	kPa	kPa	kPa						m/s	kPa	kPa	kPa	kPa	kPa	%	degree	degree	degree									clay	F_τ_sf	σ'_rc	Δσ'_rd	τ_sf	F_τ_sf	kPa	kN	G_max
1	1.8	0.52	0	1	1		0.0%	0.0%	0.00	0.00	0.00	0.00	0.00	0.00	#DIV/0!	#VALUE!	2.0	603	2	0	#DIV/0!	#DIV/0!	0		#DIV/0!	#DIV/0!	#DIV/0!	#DIV/0!	0.35	0.86	0.00	#DIV/0!		113.27	28.76								0	4	#DIV/0!
	1.2	-	3600	29	3600		0.8%	0.8%	17.69	1769.29	0.00	9.15	9.15	392.56	115.19	0.49	1.8	468	130	29728	18481	23292	22363		60.59	40.32	5.57	35.86	0.35	0.72	119.76	13.09		111.23	28.24				16	4	13	10	10		29728
2	1.2	0.66	3600	29	3600		0.8%	0.8%	17.69	1769.29	0.00	9.15	9.15	392.56	115.19	0.49	1.8	468	130	29728	18481	23292	22363		60.59	40.32	5.57	35.86	0.35	0.72	119.76	13.09		111.23	28.24				16	4	13	10	10	7	29728
	.6	-	300	17	300		5.5%	5.9%	16.08	1608.37	0.00	19.68	19.68	14.24	10.24	0.80	3.2	2636	86	11885				14960		30.27			0.45	1.00	90.82	4.61	1.23	108.65	27.59	1.88	8	3					3		11885
3	.6	1.35	300	17	300		5.5%	5.9%	16.08	1608.37	0.00	19.68	19.68	14.24	10.24	0.80	3.2	2636	86	11885				14960		30.27			0.45	1.00	90.82	4.61	1.23	108.65	27.59	1.88	8	3					3	8	11885
	-.8	-	400	34	400		8.4%	9.4%	17.03	1702.65	5.80	42.58	36.78	9.72	8.30	0.84	3.4	3395	111	20659				21381		30.19			0.45	1.00	117.46	2.76	0.77	103.35	26.24	1.63	10	4					4		20659
4	-.8	0.41	400	34	400		8.4%	9.4%	17.03	1702.65	5.80	42.58	36.78	9.72	8.30	0.84	3.4	3395	111	20659				21381		30.19			0.45	1.00	117.46	2.76	0.77	103.35	26.24	1.63	10	4					4	6	20659
	-1.2	-	1400	112	1400		8.0%	8.3%	18.93	1892.86	9.94	50.42	40.48	33.34	24.60	0.66	3.0	2095	169	53524				49343		34.06			0.45	0.99	403.52	8.00	0.88	101.72	25.83	2.60	37	15					15		53524
5	-1.2	0.48	1400	112	1400		8.0%	8.3%	18.93	1892.86	9.94	50.42	40.48	33.34	24.60	0.66	3.0	2095	169	53524				49343		34.06			0.45	0.99	403.52	8.00	0.88	101.72	25.83	2.60	37	15					15	7	53524
	-1.7	-	400	30	400		7.6%	8.9%	16.90	1690.17	14.76	58.57	43.81	7.79	7.01	0.87	3.4	3565	113	20575				21731		29.93			0.45	1.00	112.32	1.92	0.82	99.82	25.34	1.39	11	4					4		20575
6	-1.7	1.48	400	30	400		7.6%	8.9%	16.90	1690.17	14.76	58.57	43.81	7.79	7.01	0.87	3.4	3565	113	20575				21731		29.93			0.45	1.00	112.32	1.92	0.82	99.82	25.34	1.39	11	4					4	11	20575
	-3.1	-	500	44	500		8.8%	10.6%	17.43	1742.64	29.59	84.41	54.82	7.58	7.05	0.88	3.5	3788	130	27434				26442		30.26			0.45	1.00	136.83	1.62	0.69	93.98	23.86	1.34	13	5					5		27434
7	-3.1	1.17	500	44	500		8.8%	10.6%	17.43	1742.64	29.59	84.41	54.82	7.58	7.05	0.88	3.5	3788	130	27434				26442		30.26			0.45	1.00	136.83	1.62	0.69	93.98	23.86	1.34	13	5					5	7	27434
	-4.3	-	200	17	228		8.3%	12.0%	15.93	1592.52	41.31	103.07	61.76	1.57	1.57	1.00	4.0	7594	112	15109				11542		27.45			0.45	1.00	31.98	1.00	0.43	89.37	22.69	1.19	6	2					2		11542
8	-4.3	0.24	200	17	228		8.3%	12.0%	15.93	1592.52	41.31	103.07	61.76	1.57	1.57	1.00	4.0	7594	112	15109				11542		27.45			0.45	1.00	31.98	1.00	0.43	89.37	22.69	1.19	6	2					2	1	11542
	-4.6	-	1400	10	1400		0.7%	0.8%	16.07	1606.78	43.72	106.95	63.23	20.45	18.60	0.79	2.5	1079	120	22417	30133	31368	22479		9.37	33.30	-0.83	33.97	0.35	0.76	75.21	1.00		88.42	22.45				7	4	7	5	5		22417
9	-4.6	1.90	1400	10	1400		0.7%	0.8%	16.07	1606.78	43.72	106.95	63.23	20.45	18.60	0.79	2.5	1079	120	22417	30133	31368	22479		9.37	33.30	-0.83	33.97	0.35	0.76	75.21	1.00		88.42	22.45				7	4	7	5	5	16	22417
	-6.4	-	500	15	500		3.0%	4.1%	16.16	1615.67	62.68	137.58	74.90	4.84	4.78	0.96	3.3	3286	118	19240				24835		29.79			0.45	1.00	118.99	1.00	1.78	80.95	20.55	0.95	14	6					6		19240
10	-6.4	1.66	500	15	500		3.0%	4.1%	16.16	1615.67	62.68	137.58	74.90	4.84	4.78	0.96	3.3	3286	118	19240				24835		29.79			0.45	1.00	118.99	1.00	1.78	80.95	20.55	0.95	14	6					6	22	19240
	-8.1	-	3100	35	3100		1.1%	1.2%	17.88	1788.45	79.23	167.18	87.95	33.35	32.05	0.69	2.4	946	169	49631	41600	49213	42696		26.25	35.47	1.28	34.45	0.35	0.73	115.85	1.00		74.43	18.90				17	7	15	11	11		49631
11	-8.1	1.62	3100	35	3100		1.1%	1.2%	17.88	1788.45	79.23	167.18	87.95	33.35	32.05	0.69	2.4	946	169	49631	41600	49213	42696		26.25	35.47	1.28	34.45	0.35	0.73	115.85	1.00		74.43	18.90				17	7	15	11	11	19	49631
	-9.7	-	11800	80	342		0.7%	0.7%	19.36	1936.16	95.44	198.56	103.12	112.50	3.12	0.55	3.2	2613	79	7256				203946		40.22			0.45	1.00	3707.20	18.67	10.60	68.05	17.28	2.71	10	4					4		7256
[illegible]																																													
																																												1096	

M4P2 (RS 57 days)

Layer	Depth	Thickness	q_c	q_s	q_t	q_base_1.5D	Rf	Rfn	Unit Weight	Density	u	σ_v0	σ'_v0	Q_t	Q_tn	n	I_c	a_vs	V_s	G_max	G_UWA	G_ICP	G_Uni	G_clay	Dr	φ'	ψ	φ'cv	v	m'	σ'vy	OCR=YSR	S_t	h/R	h	K_c	τ_sc_UWA13		τ_sc_Unified				Skin Friction F_τ_sf	Shaft Resistance Q_s	
Nr	[m]	[m]	[KPa]	[KPa]	kPa				[kN/m3]	kg/m3	kPa	kPa	kPa						m/s	kPa	kPa	kPa	kPa	kPa	%	degree	degree	degree									clay	F_τ_sf	σ'_rc	Δσ'_rd	τ_sf	F_τ_sf	kPa	kN	G_max
[illegible]																																													
																																												2977	

M4P13 (RS 1 day)

Layer	Depth	Thickness	q_c	q_s	q_t	q_base_1.5D	Rf	Rfn	Unit Weight	Density	u	σ_v0	σ'_v0	Q_t	Q_tn	n	I_c	a_vs	V_s	G_max	G_UWA	G_ICP	G_Uni	G_clay	Dr	φ'	ψ	φ'cv	v	m'	σ'vy	OCR=YSR	S_t	h/R	h	K_c	τ_sc_UWA13		τ_sc_Unified				Skin Friction F_τ_sf	Shaft Resistance Q_s	
Nr	[m]	[m]	[KPa]	[KPa]	kPa				[kN/m3]	kg/m3	kPa	kPa	kPa						m/s	kPa	kPa	kPa	kPa	kPa	%	degree	degree	degree									clay	F_τ_sf	σ'_rc	Δσ'_rd	τ_sf	F_τ_sf	kPa	kN	G_max
1	2.0	0.39	0	4	1		0.0%	0.0%	0.00	0.00	0.00	0.00	0.00	0.00	#DIV/0!	#VALUE!	2.0	603	2	0	#DIV/0!	#DIV/0!	0		#DIV/0!	#DIV/0!	#DIV/0!	#DIV/0!	0.35	0.86	0.00	#DIV/0!		108.18	27.47								0	3	#DIV/0!
	1.6 -		3700	60	3700		1.6%	1.6%	18.56	1856.26	0.00	7.18	7.18	514.05	115.44	0.43	2.0	606	150	41543	16996	21464	21031		64.56	40.92	6.07	36.06	0.35	0.72	122.45	17.04		106.65	27.08				17	3	14	10	10		41543
2	1.6	0.60	3700	60	3700		1.6%	1.6%	18.56	1856.26	0.00	7.18	7.18	514.05	115.44	0.43	2.0	606	150	41543	16996	21464	21031		64.56	40.92	6.07	36.06	0.35	0.72	122.45	17.04		106.65	27.08				17	3	14	10	10	10	41543
	1.0 -		3700	67	3700		1.8%	1.8%	18.69	1869.30	0.00	18.34	18.34	200.71	83.42	0.48	2.1	719	163	49512	24156	30350	28656		52.00	39.05	4.50	35.45	0.35	0.72	123.26	6.72		104.30	26.48				17	5	15	11	11		49512
3	1.0	0.42	3700	67	3700		1.8%	1.8%	18.69	1869.30	0.00	18.34	18.34	200.71	83.42	0.48	2.1	719	163	49512	24156	30350	28656		52.00	39.05	4.50	35.45	0.35	0.72	123.26	6.72		104.30	26.48				17	5	15	11	11	5	49512
	0.6 -		1000	30	1000		3.0%	3.1%	17.24	1724.04	0.00	25.62	25.62	38.03	24.15	0.67	2.7	1453	119	24417	19742	21177	13317		12.46	33.69	-0.44	34.05	0.35	0.89	150.03	5.86		102.64	26.06				5	2	4	3	3		24417
4	0.6	0.67	1000	30	1000		3.0%	3.1%	17.24	1724.04	0.00	25.62	25.62	38.03	24.15	0.67	2.7	1453	119	24417	19742	21177	13317		12.46	33.69	-0.44	34.05	0.35	0.89	150.03	5.86		102.64	26.06				5	2	4	3	3	6	24417
	-0.1 -		800	53	800		6.6%	6.9%	17.82	1781.72	0.00	37.52	37.52	20.32	15.68	0.74	3.1	2329	133	31634				33612		32.32			0.45	0.99	240.12	6.40	1.06	100.01	25.39	2.27	21	8					8		31634
5	-0.1	1.09	800	53	800		6.6%	6.9%	17.82	1781.72	0.00	37.52	37.52	20.32	15.68	0.74	3.1	2329	133	31634				33612		32.32			0.45	0.99	240.12	6.40	1.06	100.01	25.39	2.27	21	8					8	9	31634
	-1.2 -		200	11	228		5.3%	7.2%	15.39	1538.81	10.18	54.28	44.10	3.30	3.30	1.00	3.6	4628	92	12372				12623		27.91			0.45	1.00	48.06	1.00	1.01	95.72	24.30	1.02	6	2					2		12623
6	-1.2	0.67	200	11	228		5.3%	7.2%	15.39	1538.81	10.18	54.28	44.10	3.30	3.30	1.00	3.6	4628	92	12372				12623		27.91			0.45	1.00	48.06	1.00	1.01	95.72	24.30	1.02	6	2					2	4	12623
	-1.9 -		400	11	400		2.6%	3.1%	15.66	1565.91	16.86	64.74	47.88	7.00	6.49	0.90	3.2	2631	96	13810				20432		29.79			0.45	1.00	108.54	1.68	2.33	93.09	23.63	1.10	11	4					4		13810
7	-1.9	0.28	400	11	400		2.6%	3.1%	15.66	1565.91	16.86	64.74	47.88	7.00	6.49	0.90	3.2	2631	96	13810				20432		29.79			0.45	1.00	108.54	1.68	2.33	93.09	23.63	1.10	11	4					4	4	13810
	-2.1 -		4200	30	4200		0.7%	0.7%	17.80	1780.13	19.67	69.74	50.07	82.49	62.72	0.60	2.0	595	157	43745	36335	45205	43453		41.94	37.61	3.24	35.01	0.35	0.72	132.68	1.90		91.98	23.35				21	7	18	13	13		43745
8	-2.1	0.84	4200	30	4200		0.7%	0.7%	17.80	1780.13	19.67	69.74	50.07	82.49	62.72	0.60	2.0	595	157	43745	36335	45205	43453		41.94	37.61	3.24	35.01	0.35	0.72	132.68	1.90		91.98	23.35				21	7	18	13	13	18	43745
	-3.0 -		4100	47	4100		1.2%	1.2%	18.33	1833.36	28.11	85.21	57.10	70.31	55.87	0.59	2.2	731	172	53835	37942	46996	44652		39.53	37.27	2.94	34.92	0.35	0.72	131.44	1.54		88.66	22.51				20	7	18	13	13		53835
[illegible]																																													
																																												1198	

M5P19 (RS 1 day)

Layer	Depth	Thickness	q_c	q_s	q_t	q_base_1.5D	Rf	Rfn	Unit Weight	Density	u	σ_v0	σ'_v0	Q_t	Q_tn	n	I_c	a_vs	V_s	G_max	G_UWA	G_ICP	G_Uni	G_clay	Dr	φ'	ψ	φ'cv	v	m'	σ'vy	OCR=YSR	S_t	h/R	h	K_c	τ_sc_UWA13		τ_sc_Unified				Skin Friction F_τ_sf	Shaft Resistance Q_s	
Nr	[m]	[m]	[KPa]	[KPa]	kPa				[kN/m3]	kg/m3	kPa	kPa	kPa						m/s	kPa	kPa	kPa	kPa	kPa	%	degree	degree	degree									clay	F_τ_sf	σ'_rc	Δσ'_rd	τ_sf	F_τ_sf	kPa	kN	G_max
[illegible]																																													
																																												1618	

M8P17 (RS 5 days)

Layer	Depth	Thickness	q_c	q_s	q_t	q_base_1.5D	Rf	Rfn	Unit Weight	Density	u	σ_v0	σ'_v0	Q_t	Q_tn	n	I_c	a_vs	V_s	G_max	G_UWA	G_ICP	G_Uni	G_clay	Dr	ϕ'	ψ	ϕ'cv	v	m'	σ'vy	OCR=YSR	S_t	h/R	h	K_c	τ_sc_UWA13		τ_sc_Unified				Skin Friction F_τ_sf	Shaft Resistance Q_s	
Nr	[m]	[m]	[KPa]	[KPa]	kPa				[kN/m3]	kg/m3	kPa	kPa	kPa						m/s	kPa	kPa	kPa	kPa	kPa	%	degree	degree	degree									clay	F_τ_sf	σ'_rc	Δσ'_rd	τ_sf	F_τ_sf	kPa	kN	G_max
1	1.45	0.60	100	1	1		0.0%	0.0%	0.00	0.00	0.00	0.00	0.00	0.00	#DIV/0!	#VALUE!	2.00	603	2	0	#DIV/0!	#DIV/0!	0		#DIV/0!	#DIV/0!	#DIV/0!	#DIV/0!	0.35	0.86	16.93	#DIV/0!		108.12	27.45								0	5	#DIV/0!
	0.85	-	3400	28	3400		0.8%	0.8%	17.64	1764.15	0.00	10.57	10.57	320.75	104.15	0.50	1.84	494	129	29553	19232	24210	22572		57.12	39.80	5.14	35.69	0.35	0.72	114.90	10.87		105.76	26.85				16	4	13	11	11		29553
2	0.85	0.79	3400	28	3400		0.8%	0.8%	17.64	1764.15	0.00	10.57	10.57	320.75	104.15	0.50	1.84	494	129	29553	19232	24210	22572		57.12	39.80	5.14	35.69	0.35	0.72	114.90	10.87		105.76	26.85				16	4	13	11	11	14	29553
	0.07	-	3400	24	3400		0.7%	0.7%	17.47	1746.98	0.00	24.30	24.30	138.93	75.11	0.57	1.92	546	136	32198	26281	32871	29711		45.96	38.18	3.75	35.18	0.35	0.72	114.62	4.72		102.67	26.07				16	5	14	11	11		32198
3	0.07	0.60	3400	24	3400		0.7%	0.7%	17.47	1746.98	0.00	24.30	24.30	138.93	75.11	0.57	1.92	546	136	32198	26281	32871	29711		45.96	38.18	3.75	35.18	0.35	0.72	114.62	4.72		102.67	26.07				16	5	14	11	11	7	32198
	-0.53	-	800	15	800		1.8%	1.9%	16.32	1631.65	3.53	34.07	30.54	25.08	18.21	0.73	2.67	1409	104	17611	19943	19589	12152		4.12	32.66	-1.48	33.85	0.35	0.87	109.24	3.21		100.31	25.47				4	2	4	3	3		17611
4	-0.53	0.56	800	15	800		1.8%	1.9%	16.32	1631.65	3.53	34.07	30.54	25.08	18.21	0.73	2.67	1409	104	17611	19943	19589	12152		4.12	32.66	-1.48	33.85	0.35	0.87	109.24	3.21		100.31	25.47				4	2	4	3	3	3	17611
	-1.10	-	200	13	228		6.4%	8.1%	15.61	1561.12	9.15	42.85	33.70	4.66	4.39	0.94	3.54	4229	91	12223				12381		28.29			0.45	1.00	51.81	1.21	0.90	98.10	24.91	1.12	6	4					4		12223
5	-1.10	1.61	200	13	228		6.4%	8.1%	15.61	1561.12	9.15	42.85	33.70	4.66	4.39	0.94	3.54	4229	91	12223				12381		28.29			0.45	1.00	51.81	1.21	0.90	98.10	24.91	1.12	6	4					4	7	12223
	-2.71	-	100	34	114		33.5%	12.0%	16.48	1647.76	25.25	69.37	44.12	0.69	0.69	1.00	4.30	11031	88	8112				5914		26.04			0.45	1.00	10.11	1.00	0.07	91.75	23.30	1.51	3	2					2		5914
6	-2.71	0.26	100	34	114		33.5%	12.0%	16.48	1647.76	25.25	69.37	44.12	0.69	0.69	1.00	4.30	11031	88	8112				5914		26.04			0.45	1.00	10.11	1.00	0.07	91.75	23.30	1.51	3	2					2	1	5914
	-2.97	-	200	73	228		36.6%	12.0%	17.67	1766.51	27.87	74.00	46.13	2.73	2.73	1.00	3.81	5937	104	16151				13582		27.85			0.45	1.00	41.57	1.00	0.13	90.72	23.03	1.40	6	4					4		13582
7	-2.97	0.19	200	73	228		36.6%	12.0%	17.67	1766.51	27.87	74.00	46.13	2.73	2.73	1.00	3.81	5937	104	16151				13582		27.85			0.45	1.00	41.57	1.00	0.13	90.72	23.03	1.40	6	4					4	3	13582
	-3.16	-	1000	60	1000		6.0%	6.5%	18.06	1806.10	29.75	77.40	47.65	19.36	15.94	0.74	3.05	2265	147	37738				40245		32.66			0.45	0.99	287.51	3.71	1.12	89.98	22.85	1.80	27	16					16		37738
8	-3.16	0.94	1000	60	1000		6.0%	6.5%	18.06	1806.10	29.75	77.40	47.65	19.36	15.94	0.74	3.05	2265	147	37738				40245		32.66			0.45	0.99	287.51	3.71	1.12	89.98	22.85	1.80	27	16					16	15	37738

1594

M8P24 (RS 4 days)

1698

NL NZ (EOID)

Layer	Depth	Thickness	q_c	q_s	q_t	q_base_1.5D	Rf	Rfn	Unit Weight	Density	u	σ_v0	σ'_v0	Q_t	Q_tn	n	I_c
Nr	[m]	[m]	[KPa]	[KPa]	kPa				[kN/m3]	kg/m3	kPa	kPa	kPa				
1	0.00	1.00	0	2	0		0.0%	0.0%	20.50	2050.00	0.00	0.00	0.00	0.00	#DIV/0!	#VALUE!	2.00
	-1.00	0.00	1000	2	1000		0.2%	0.2%	20.50	2050.00	10.00	20.50	10.50	93.29	50.09	0.72	1.61
2	-1.00	0.30	1000	2	1000		0.2%	0.2%	20.50	2050.00	10.00	20.50	10.50	93.29	50.09	0.72	1.61
	-1.30	0.00	5265	3	5265		0.1%	0.1%	20.50	2050.00	13.00	26.65	13.65	383.76	227.32	0.74	0.89
3	-1.30	1.70	5265	2	5265		0.0%	0.0%	20.50	2050.00	13.00	26.65	13.65	383.76	245.88	0.78	0.90
	-3.00	0.00	47650	1	47650		0.0%	0.0%	20.50	2050.00	30.00	61.50	31.50	1510.75	1510.75	1.00	1.34
4	-3.00	1.00	47650	1	47650		0.0%	0.0%	20.50	2050.00	30.00	61.50	31.50	1510.75	1510.75	1.00	1.34
	-4.00	0.00	60000	4	60000		0.0%	0.0%	20.50	2050.00	40.00	82.00	42.00	1426.62	1426.62	1.00	1.06
5	-4.00	0.30	60000	4	60000		0.0%	0.0%	20.50	2050.00	40.00	82.00	42.00	1426.62	1426.62	1.00	1.06
	-4.30	0.00	60000	4	60000		0.0%	0.0%	20.50	2050.00	43.00	88.15	45.15	1326.95	1326.95	1.00	1.02
6	-4.30	1.70	82500	4	82500		0.0%	0.0%	20.50	2050.00	43.00	88.15	45.15	1825.29	1825.29	1.00	1.11
	-6.00	0.00	82500	6	82500		0.0%	0.0%	20.50	2050.00	60.00	123.00	63.00	1307.57	1307.57	1.00	1.02
7	-6.00	2.00	56000	6	56000		0.0%	0.0%	20.50	2050.00	60.00	123.00	63.00	886.94	871.76	0.96	0.94
	-8.00	0.00	56000	14	56000		0.0%	0.0%	20.50	2050.00	80.00	164.00	84.00	664.71	645.47	0.83	0.75
8	-8.00	3.50	57500	14	57500		0.0%	0.0%	20.50	2050.00	80.00	164.00	84.00	682.57	663.16	0.83	0.74
	-11.50	0.00	57500	18	57500		0.0%	0.0%	19.00	1900.00	115.00	230.50	115.50	495.84	508.60	0.82	0.82
9	-11.50	2.50	38500	18	38500		0.0%	0.0%	19.00	1900.00	115.00	230.50	115.50	331.34	341.73	0.79	0.96
	-14.00	0.00	38500	18	38500		0.0%	0.0%	19.00	1900.00	140.00	278.00	138.00	276.97	294.15	0.81	1.03
10	-14.00	1.50	48000	18	48000		0.0%	0.0%	19.00	1900.00	140.00	278.00	138.00	345.81	365.02	0.83	0.96
	-15.50	0.00	48000	20	48000		0.0%	0.0%	19.00	1900.00	155.00	306.50	151.50	314.81	339.21	0.82	0.98
11	-15.50	0.50	37000	41	37000		0.1%	0.1%	19.00	1900.00	155.00	306.50	151.50	242.20	274.98	0.69	1.12
	-16.00	0.00	37000	43	37000		0.1%	0.1%	19.00	1900.00	160.00	316.00	156.00	235.15	269.68	0.69	1.14
12	-16.00	1.50	14000	43	14000		0.3%	0.3%	19.00	1900.00	160.00	316.00	156.00	87.72	101.49	0.67	1.69
	-17.50	0.00	14000	32	14000		0.2%	0.2%	19.00	1900.00	175.00	344.50	169.50	80.56	93.20	0.72	1.67
13	-17.50	0.50	28500	32	28500		0.1%	0.1%	19.00	1900.00	175.00	344.50	169.50	166.11	190.87	0.74	1.28
	-18.00	0.00	28500	22	28500		0.1%	0.1%	19.00	1900.00	180.00	354.00	174.00	161.76	181.40	0.79	1.27
14	-18.00	1.00	35000	22	35000		0.1%	0.1%	19.00	1900.00	180.00	354.00	174.00	199.11	221.83	0.81	1.17
	-19.00	0.00	35000	23	35000		0.1%	0.1%	19.00	1900.00	190.00	373.00	183.00	189.22	212.68	0.81	1.19
15	-19.00	1.00	20500	36	20500		0.2%	0.2%	19.00	1900.00	190.00	373.00	183.00	109.98	130.17	0.72	1.51
	-20.00	0.00	20500	39	20500		0.2%	0.2%	19.00	1900.00	200.00	392.00	192.00	104.73	125.69	0.72	1.54
16	-20.00	2.50	32500	39	32500		0.1%	0.1%	19.00	1900.00	200.00	392.00	192.00	167.23	199.08	0.73	1.28
	-22.50	0.00	32500	64	32500		0.2%	0.2%	19.00	1900.00	225.00	439.50	214.50	149.47	190.44	0.68	1.40
17	-22.50	3.50	30500	64	30500		0.2%	0.2%	19.00	1900.00	225.00	439.50	214.50	140.14	178.76	0.68	1.43
	-26.00	0.00	30500	35	30500		0.1%	0.1%	19.00	1900.00	260.00	506.00	246.00	121.93	146.58	0.80	1.41
18	-26.00	1.80	44500	35	44500		0.1%	0.1%	19.00	1900.00	260.00	506.00	246.00	178.84	211.63	0.81	1.22
	-27.80	0.00	44500	41	44500		0.1%	0.1%	20.00	2000.00	278.00	542.00	264.00	166.51	201.46	0.80	1.26
19	-27.80	1.20	32500	93	32500		0.3%	0.3%	20.00	2000.00	278.00	542.00	264.00	121.05	165.92	0.68	1.55
	-29.00	0.00	32500	106	32500		0.3%	0.3%	20.00	2000.00	290.00	566.00	276.00	115.70	161.88	0.67	1.59
20	-29.00	1.00	27000	56	27000		0.2%	0.2%	20.00	2000.00	290.00	566.00	276.00	95.78	122.89	0.75	1.59
	-30.00	0.00	27000	60	27000		0.2%	0.2%	20.00	2000.00	300.00	586.00	286.00	92.36	119.56	0.75	1.61
21	-30.00	1.50	39000	60	39000		0.2%	0.2%	20.00	2000.00	300.00	586.00	286.00	134.31	172.78	0.76	1.40
	-31.50	0.00	39000	65	39000		0.2%	0.2%	20.00	2000.00	315.00	616.00	301.00	127.52	165.82	0.76	1.44
22	-31.50	1.00	48500	65	48500		0.1%	0.1%	20.00	2000.00	315.00	616.00	301.00	159.08	205.11	0.77	1.32
	-32.50	0.00	48500	70	48500		0.1%	0.1%	20.00	2000.00	325.00	636.00	311.00	153.90	200.58	0.77	1.34
23	-32.50	2.00	42500	70	42500		0.2%	0.2%	20.00	2000.00	325.00	636.00	311.00	134.61	176.37	0.76	1.41
	-34.50	0.00	42500	175	42500		0.4%	0.4%	20.00	2000.00	345.00	676.00	331.00	126.36	192.34	0.65	1.61
24	-34.50	1.00	37000	175	37000		0.5%	0.5%	20.00	2000.00	345.00	676.00	331.00	109.74	166.72	0.65	1.69
	-35.50		37000	175	37000		0.5%	0.5%	20.00	2000.00	355.00	696.00	341.00	106.46	161.67	0.66	1.70
25	-35.50	2.00	40500	190	40500	44168	0.5%	0.5%	20.00	2000.00	355.00	696.00	341.00	116.73	179.96	0.65	1.67
	-37.50		40500	203	40500	44168	0.5%	0.5%	20.00	2000.00	375.00	736.00	361.00	110.15	171.38	0.66	1.70
26	-37.50	2.50	45000	203	45000	44168	0.5%	0.5%	20.00	2000.00	375.00	736.00	361.00	122.61	191.18	0.65	1.64
	-40.00		45000	250	45000	44168	0.6%	0.6%	20.00	2000.00	400.00	786.00	386.00	114.54	184.22	0.65	1.71
27	-40.00	1.50	42000	250	42000		0.6%	0.6%	20.00	2000.00	400.00	786.00	386.00	106.77	171.28	0.65	1.76
	-41.50		42000	250	42000		0.6%	0.6%	20.00	2000.00	415.00	816.00	401.00	102.70	163.95	0.66	1.77
28	-41.50	0.50	29000	250	29000		0.9%	0.9%	20.00	2000.00	415.00	816.00	401.00	70.28	108.99	0.68	2.00
	-42.00		29000	250	29000		0.01	0.01	20.00	2000.00	420.00	826.00	406.00	69.39	107.33	0.69	2.00

GE NZ (EOID)

Layer	Depth	Thickness	q_c	q_s	q_t	q_base_1.5D	Rf	Rfn	Unit Weight	Density	u	σ_v0	σ'_v0	Q_t	Q_tn	n	I_c
Nr	[m]	[m]	[KPa]	[KPa]	kPa				[kN/m3]	kg/m3	kPa	kPa	kPa				
1	0.00	3.29	0	111	0		0.0%	0.0%	0.00	0.00	0.00	0.00	0.00	0.00	#DIV/0!	#VALUE!	2.00
	-3.29	0.00	25500	251	25500		1.0%	1.0%	21.01	2100.50	32.89	69.09	36.20	702.60	355.33	0.33	1.36
2	-3.29	3.51	25500	251	25500		1.0%	1.0%	21.01	2100.50	32.89	69.09	36.20	702.60	355.33	0.33	1.36
	-6.80	0.00	43000	298	43000		0.7%	0.7%	21.41	2141.05	67.97	144.19	76.22	562.24	472.20	0.36	1.28
3	-6.80	2.27	43000	298	43000		0.7%	0.7%	21.41	2141.05	67.97	144.19	76.22	562.24	472.20	0.36	1.28
	-9.06	0.00	58400	517	58400		0.9%	0.9%	22.18	2217.62	90.62	194.42	103.80	560.73	575.17	0.32	1.37
4	-9.06	5.04	54000	517	54000		1.0%	1.0%	22.15	2214.56	90.62	194.42	103.80	518.35	531.71	0.32	1.42
	-14.10	0.00	47700	402	47700		0.8%	0.8%	21.80	2180.21	141.04	304.35	163.31	290.22	389.77	0.40	1.53
5	-14.10	1.50	53600	323	53600		0.6%	0.6%	21.59	2159.11	141.04	304.35	163.31	326.35	432.07	0.43	1.39
	-15.60	0.00	58300	562	58300		1.0%	1.0%	22.27	2227.34	156.04	337.76	181.72	318.97	464.22	0.37	1.55
6	-15.60	3.60	41100	446	41100		1.1%	1.1%	21.87	2186.57	156.04	337.76	181.72	224.31	320.00	0.41	1.68
	-19.20	0.00	36000	303	36000		0.8%	0.9%	21.36	2136.06	192.04	414.66	222.62	159.85	240.68	0.49	1.71
7	-19.20	1.91	67900	491	67900		0.7%	0.7%	22.17	2217.46	192.04	414.66	222.62	303.15	481.05	0.42	1.47
	-21.11	0.00	85900	621	85900		0.7%	0.7%	22.54	2254.19	211.08	457.58	246.50	346.63	588.06	0.41	1.43
8	-21.11	1.10	85900	621	85900		0.7%	0.7%	22.54	2254.19	211.08	457.58	246.50	346.63	588.06	0.41	1.43
	-22.21	0.00	51400	495	51400		1.0%	1.0%	22.08	2207.53	222.07	481.84	259.77	196.01	330.61	0.45	1.69
9	-22.21	1.10	51400	495	51400		1.0%	1.0%	22.08	2207.53	222.07	481.84	259.77	196.01	330.61	0.45	1.69
	-23.31	0.00	44400	535	44400		1.2%	1.2%	22.11	2210.92	233.06	506.14	273.08	160.74	276.43	0.46	1.82
10	-23.31	1.03	44400	535	44400		1.2%	1.2%	22.11	2210.92	233.06	506.14	273.08	160.74	276.43	0.46	1.82
	-24.33	0.00	82200	1089	82200		1.3%	1.3%	23.18	2318.34	243.32	529.92	286.60	284.96	555.27	0.37	1.69
11	-24.33	1.98	82200	1089	82200		1.3%	1.3%	23.18	2318.34	243.32	529.92	286.60	284.96	555.27	0.37	1.69
	-26.31	0.00	58300	773	58300		1.3%	1.3%	22.65	2264.72	263.10	574.72	311.62	185.24	350.81	0.44	1.81
12	-26.31	1.80	58300	773	58300		1.3%	1.3%	22.65	2264.72	263.10	574.72	311.62	185.24	350.81	0.44	1.81
	-28.11	0.00	58300	844	58300		1.4%	1.5%	22.75	2275.02	281.10	615.67	334.57	172.41	336.09	0.45	1.85
13	-28.11	5.35	87000	943	87000		1.1%	1.1%	23.04	2303.67	281.10	615.67	334.57	258.20	519.38	0.42	1.64
	-33.46	0.00	87000	1048	87000		1.2%	1.2%	23.16	2316.05	334.59	739.55	404.96	213.01	452.40	0.46	1.73
14	-33.46	1.20	60200	435	60200		0.7%	0.7%	21.99	2198.56	334.59	739.55	404.96	146.83	262.37	0.58	1.70
	-34.66	0.00	61700	817	61700		1.3%	1.3%	22.73	2273.43	346.59	766.83	420.24	144.99	289.24	0.52	1.88
15	-34.66	1.23	61700	817	61700		1.3%	1.3%	22.73	2273.43	346.59	766.83	420.24	144.99	289.24	0.52	1.88
	-35.89	0.00	112300	1083	112300		1.0%	1.0%	23.30	2329.88	358.91	795.54	436.63	255.38	549.85	0.48	1.61
16	-35.89	2.29	112300	1083	112300		1.0%	1.0%	23.30	2329.88	358.91	795.54	436.63	255.38	549.85	0.48	1.61
	-38.18	0.00	72700	963	72700		1.3%	1.3%	22.99	2299.12	381.76	848.07	466.31	154.08	318.29	0.53	1.86
17	-38.18	2.93	72700	963	72700		1.3%	1.3%	22.99	2299.12	381.76	848.07	466.31	154.08	318.29	0.53	1.86
	-41.11	0.00	74500	987	74500		1.3%	1.3%	23.03	2302.96	411.06	915.55	504.49	145.86	298.99	0.56	1.88
18	-41.11	1.39	100600	1333	100600		1.3%	1.3%	23.50	2349.94	411.06	915.55	504.49	197.59	440.56	0.50	1.79
	-42.50	0.00	100600	1454	100600		1.4%	1.5%	23.60	2360.13	424.98	948.40	523.42	190.38	429.40	0.51	1.83
19	-42.50	1.32	89900	1300	89900		1.4%	1.5%	23.43	2342.60	424.98	948.40	523.42	169.94	371.04	0.53	1.86
	-43.82	0.00	89500	1079	89500		1.2%	1.2%	23.21	2320.58	438.17	979.01	540.84	163.67	340.48	0.57	1.81
20	-43.82	1.72	66800	805	66800		1.2%	1.2%	22.75	2274.79	438.17	979.01	540.84	121.70	231.67	0.62	1.90
	-45.54	0.00	67100	728	67100		1.1%	1.1%	22.63	2263.18	455.38	1017.96	562.58	117.46	215.36	0.65	1.88
21	-45.54	5.85	61600	668	61600		1.1%	1.1%	22.50	2249.75	455.38	1017.96	562.58	107.69	192.06	0.67	1.91
	-51.38	0.00	62000	822	62000		1.3%	1.4%	22.74	2274.33	513.84	1150.92	637.08	95.51	163.86	0.71	2.01
22	-51.38	2.19	62000	822	62000		1.3%	1.4%	22.74	2274.33	513.84	1150.92	637.08	95.51	163.86	0.71	2.01
	-53.58	0.00	104000	1879	104000		1.8%	1.8%	23.91	2391.49	535.77	1203.36	667.59	153.98	330.87	0.60	1.96
23	-53.58	1.54	81300	1470	81300		1.8%	1.8%	23.53	2353.08	535.77	1203.36	667.59	119.98	234.03	0.65	2.03
	-55.11	0.00	81300	1372	81300		1.7%	1.7%	23.45	2344.99	551.12	1239.36	688.24	116.33	218.27	0.67	2.02
24	-55.11	0.95	102900	1735	102900	73015	1.7%	1.7%	23.82	2381.73	551.12	1239.36	688.24	147.71	304.48	0.63	1.95
	-56.06		102900	1611	102900	73015	1.6%	1.6%	23.73	2373.03	560.62	1261.90	701.28	144.93	289.43	0.64	1.93
25	-56.06	1.39	81300	1274	81300	73015	1.6%	1.6%	23.36	2336.30	560.62	1261.90	701.28	114.13	207.42	0.69	2.00
	-57.45		81300	1274	81300	73015	1.6%	1.6%	23.36	2336.30	574.50	1294.33	719.83	111.14	196.92	0.71	2.01
26	-57.45	1.61	60200	1015	60200	73015	1.7%	1.7%	22.98	2297.91	574.50	1294.33	719.83	81.83	129.12	0.77	2.13
	-59.06		60900	1027	60900	73015	1.7%	1.7%	23.00	2299.74	590.58	1331.31	740.73	80.42	123.34	0.79	2.14

UK B01 (EOID)

Layer	Depth	Thickness	q_c	q_s	q_t	q_base_1.5D	Rf	Rfn	Unit Weight	Density	u	σ_v0	σ'_v0	Q_t	Q_tn	n	I_c
Nr	[m]	[m]	[KPa]	[KPa]	kPa				[kN/m3]	kg/m3	kPa	kPa	kPa				
1	0	0.80	0	0	0		0.00	0.00	0.00	0.00	0.00	0.00	0.00	0.00	#DIV/0!	#VALUE!	2.00

UK C01 (EOID)

Layer	Depth	Thickness	q_c	q_s	q_t	q_base_1.5D	Rf	Rfn	Unit Weight	Density	u	σ_v0	σ'_v0	Q_t	Q_tn	n	I_c	a_vs	V_s	G_max	G_UWA	G_ICP	G_Uni	G_clay	Dr	φ'	ψ	δ_cv	v	m'	σ'vy	OCR=YSR	S_t	h/R	h	K_c	τ_sc_UWA13 clay	τ_sc_UWA13 F_τ_sf	τ_sc_Unified σ'_rc	τ_sc_Unified Δσ'_rd	τ_sc_Unified τ_sf	τ_sc_Unified F_τ_sf	Skin Friction F_τ_sf	Shaft Resistance Q_s	G_max
Nr	[m]	[m]	[KPa]	[KPa]	kPa				[kN/m3]	kg/m3	kPa	kPa	kPa						m/s	kPa	kPa	kPa	kPa	kPa	%	degree	degree	degree															kPa	kN	
1	0.04	1.00	0	0	0		0.0%	0.0%	0.00	0.00	0.00	0.00	0.00	0.00	#DIV/0!	#VALUE!	2.00	0	0	0	0	#DIV/0!	0		#DIV/0!	45.00	9.50	37.40	0.35	0.86	0.00	#DIV/0!		118.58	43.10						0	0	0	157	0
	-0.96		25300	263	25300		1.0%	1.0%	21.06	2105.67	9.63	21.01	11.38	2220.46	462.72	0.28	1.24	231	242	123025	32664	91468	0		109.91	48.47	11.74	39.07	0.35	0.72	488.09	23.23		115.83	42.10						58	40	40		123024.8
2	-0.96	0.46	25300	263	25300		1.0%	1.0%	21.06	2105.67	9.63	21.01	11.38	2220.46	462.72	0.28	1.24	231	242	123025	32664	91468	0		109.91	48.47	11.74	39.07	0.35	0.72	488.09	23.23		115.83	42.10						58	40	40	86	123024.8
	-1.42		5300	110	5300		2.1%	2.1%	19.42	1942.36	14.24	29.97	15.73	335.05	115.19	0.42	1.81	472	158	48269	24946	31486	0		63.69	40.79	5.96	36.02	0.35	0.72	157.87	5.27		114.56	41.64						11	8	8		48268.93
3	-1.42	9.65	5300	110	5300		2.1%	2.1%	19.42	1942.36	14.24	29.97	15.73	335.05	115.19	0.42	1.81	472	158	48269	24946	31486	0		63.69	40.79	5.96	36.02	0.35	0.72	157.87	5.27		125.27	41.64						10	7	7	953	48268.93
	-11.08		11900	115	11900		1.0%	1.0%	19.79	1979.19	110.75	220.98	110.23	105.95	110.95	0.53	1.89	522	247	120671	63375	79835	0		59.28	40.12	5.41	35.79	0.35	0.72	280.08	1.27		96.23	31.99						26	18	18		120670.6
4	-11.08	1.17	11900	115	11900		1.0%	1.0%	19.79	1979.19	110.75	220.98	110.23	105.95	110.95	0.53	1.89	522	247	120671	63375	79835	0		59.28	40.12	5.41	35.79	0.35	0.72	280.08	1.27		101.34	31.99						26	18	18	137	120670.6
	-12.24		8000	148	8000		1.9%	1.9%	19.93	1993.25	122.43	244.26	121.83	63.66	69.42	0.56	2.24	819	252	126605	59580	74620	0		47.29	38.37	3.91	35.24	0.35	0.72	216.53	1.00		97.64	30.82						17	12	12		126605.2
5	-12.24	0.84	8000	148	8000		1.9%	1.9%	19.93	1993.25	122.43	244.26	121.83	63.66	69.42	0.56	2.24	819	252	126605	59580	74620	0		47.29	38.37	3.91	35.24	0.35	0.72	216.53	1.00		97.64	30.82						17	12	12	152	126605.2
	-13.08		22100	115	22100		0.5%	0.5%	20.03	2003.38	130.84	261.11	130.27	167.64	190.16	0.52	1.56	346	275	151271	78766	100708	0		73.63	42.33	7.20	36.57	0.35	0.72	439.30	1.68		94.98	29.98						49	34	34		151270.7
6	-13.08	0.23	22100	115	22100		0.5%	0.5%	20.03	2003.38	130.84	261.11	130.27	167.64	190.16	0.52	1.56	346	275	151271	78766	100708	0		73.63	42.33	7.20	36.57	0.35	0.72	439.30	1.68		94.98	29.98						49	34	34	105	151270.7
	-13.32		50000	164	50000		0.3%	0.3%	20.77	2076.92	133.18	265.97	132.79	374.53	432.40	0.49	1.16	208	322	215177	97297	148615	0		95.25	45.89	9.91	37.96	0.35	0.72	794.52	2.99		94.24	29.74						117	81	81		215177.4
7	-13.32	0.47	50000	164	50000		0.3%	0.3%	20.77	2076.92	133.18	265.97	132.79	374.53	432.40	0.49	1.16	208	322	215177	97297	148615	0		95.25	45.89	9.91	37.96	0.35	0.72	794.52	2.99		94.24	29.74						117	81	81	207	215177.4
	-13.79		20800	214	20800		1.0%	1.0%	20.74	2073.84	137.85	275.65	137.80	148.94	176.58	0.47	1.79	464	308	197355	79234	100821	0		71.25	41.95	6.91	36.43	0.35	0.72	420.16	1.52		92.76	29.28						46	32	32		197354.6
8	-13.79	3.08	20800	214	20800		1.0%	1.0%	20.74	2073.84	137.85	275.65	137.80	148.94	176.58	0.47	1.79	464	308	197355	79234	100821	0		71.25	41.95	6.91	36.43	0.35	0.72	420.16	1.52		92.76	29.28						46	32	32	939	197354.6
	-16.87		27900	373	27900		1.3%	1.4%	21.50	2150.47	168.69	341.98	173.29	159.03	216.93	0.44	1.85	501	371	296635	92920	119584	0		76.05	42.71	7.51	36.71	0.35	0.72	519.58	1.52		82.99	26.19						66	45	45		296634.6
9	-16.87	0.51	27900	373	27900		1.3%	1.4%	21.50	2150.47	168.69	341.98	173.29	159.03	216.93	0.44	1.85	501	371	296635	92920	119584	0		76.05	42.71	7.51	36.71	0.35	0.72	519.58	1.52		82.99	26.19						66	45	45	269	296634.6
	-17.38		51800	504	51800		1.0%	1.0%	22.10	2209.95	173.83	353.33	179.50	286.60	410.93	0.38	1.58	353	426	401813	109909	159623	0		92.16	45.36	9.52	37.74	0.35	0.72	814.13	2.30		81.36	25.68						127	88	88		401813.1

16569

UK C11 (EOID)

19057

UK D11 (EOID)

19852

UK D14 (EOID)

16480

UK D15 (EOID)

Layer	Depth	Thickness	q_c	q_s	q_t	q_base_1.5D	Rf	Rfn	Unit Weight	Density	u	σ_v0	σ'_v0	Q_t	Q_tn	n	I_c	a_vs	V_s	G_max	G_UWA	G_ICP	G_Uni	G_clay	Dr	φ'	ψ	δ_cv	v	m'	σ'vy	OCR=YSR	S_t	h/R	h	K_c	τ_sc_UWA13		τ_sc_Unified				Skin Friction F_τ_sf	Shaft Resistance Q_s	
Nr	[m]	[m]	[KPa]	[KPa]	kPa				[kN/m3]	kg/m3	kPa	kPa	kPa						m/s	kPa	kPa	kPa	kPa	kPa	%	degree	degree	degree									clay	F_τ_sf	σ'_rc	Δσ'_rd	τ_sf	F_τ_sf	kPa	kN	G_max
1	-0.03	1.91	300	2	0		0.00	0.00	0.00	0.00	0.31	0.00	0.00	0.00	#DIV/0!	#VALUE!	2.00	0	0	0	0	#DIV/0!			#DIV/0!	45.00	9.50	37.40	0.35	0.86	43.32	#DIV/0!		140.05	50.90						0	0	0	199	0
	-1.94		18500	172	18500		0.01	0.01	20.44	2043.64	19.42	39.05	19.63	940.26	320.99	0.34	1.29	245	213	92369	37055	55569			94.22	45.71	9.78	37.89	0.35	0.72	389.24	9.97		134.79	48.99					38	27	27		92368.98
2	-1.94	3.05	18500	172	18500		0.01	0.01	20.44	2043.64	19.42	39.05	19.63	940.26	320.99	0.34	1.29	245	213	92369	37055	55569			94.22	45.71	9.78	37.89	0.35	0.72	389.24	9.97		134.79	48.99					38	27	27	391	92368.98
	-4.99		4500	42	4500		0.01	0.01	18.23	1823.07	49.94	94.69	44.75	98.43	69.40	0.57	1.90	533	153	42769	35443	44300			45.29	38.08	3.66	35.15	0.35	0.72	138.81	1.47		126.39	45.94					9	6	6		42769.28
3	-4.99	1.76	4500	42	4500		0.01	0.01	18.23	1823.07	49.94	94.69	44.75	98.43	69.40	0.57	1.90	533	153	42769	35443	44300			45.29	38.08	3.66	35.15	0.35	0.72	138.81	1.47		138.20	45.94					9	6	6	256	42769.28
	-6.75		21300	158	21300		0.01	0.01	20.39	2039.19	67.51	130.52	63.01	335.96	256.31	0.41	1.44	298	251	128638	59436	78639			82.37	43.73	8.30	37.10	0.35	0.72	429.56	3.29		132.92	44.18					45	31	31		128637.6
4	-6.75	1.14	21300	158	21300		0.01	0.01	20.39	2039.19	67.51	130.52	63.01	335.96	256.31	0.41	1.44	298	251	128638	59436	78639			82.37	43.73	8.30	37.10	0.35	0.72	429.56	3.29		139.98	44.18					45	31	31	232	128637.6
	-7.89		14400	134	14400		0.01	0.01	20.05	2004.57	78.91	153.37	74.46	191.32	163.04	0.46	1.68	404	240	115338	57378	72826			69.64	41.70	6.71	36.34	0.35	0.72	323.00	2.11		136.37	43.04					30	21	21		115338
5	-7.89	0.80	14400	134	14400		0.01	0.01	20.05	2004.57	78.91	153.37	74.46	191.32	163.04	0.46	1.68	404	240	115338	57378	72826			69.64	41.70	6.71	36.34	0.35	0.72	323.00	2.11		136.37	43.04					30	21	21	294	115338
	-8.69		47200	410	47200		0.01	0.01	21.82	2182.11	86.93	170.88	83.95	560.24	498.00	0.33	1.37	270	356	277215	80752	137115			99.85	46.68	10.48	38.30	0.35	0.72	763.16	4.47		133.83	42.24					105	73	73		277214.8
6	-8.69	0.31	47200	410	47200		0.01	0.01	21.82	2182.11	86.93	170.88	83.95	560.24	498.00	0.33	1.37	270	356	277215	80752	137115			99.85	46.68	10.48	38.30	0.35	0.72	763.16	4.47		133.83	42.24					105	73	73	102	277214.8
	-9.00		8300	57	8300		0.01	0.01	18.83	1882.80	90.01	176.67	86.66	93.73	88.22	0.58	1.84	491	200	75136	52921	66517			52.84	39.17	4.61	35.49	0.35	0.72	215.60	1.22		132.85	41.93					16	11	11		75135.92
7	-9.00	3.95	8300	57	8300		0.01	0.01	18.83	1882.80	90.01	176.67	86.66	93.73	88.22	0.58	1.84	491	200	75136	52921	66517			52.84	39.17	4.61	35.49	0.35	0.72	215.60	1.22		132.85	41.93					16	11	11	355	75135.92
	-12.95		8800	213	8800		0.02	0.02	20.40	2039.67	129.47	257.16	127.69	66.90	74.86	0.54	2.31	888	275	154727	62101	77896			49.22	38.64	4.15	35.32	0.35	0.73	241.19	1.00		120.35	37.98					17	12	12		154727.3
8	-12.95	6.01	3100	75	3100		0.02	0.03	18.76	1876.49	129.47	257.16	127.69	22.26	23.81	0.73	2.68	1431	202	76339	47843	54987			21.26	34.82	0.66	34.29	0.35	0.88	365.55	1.42		120.35	37.98					6	4	4	581	76339.31
	-18.96		14200	211	14200		0.01	0.02	20.57	2057.26	189.58	380.82	191.24	72.26	96.27	0.56	2.14	717	315	203733	81440	102503			56.63	39.73	5.08	35.66	0.35	0.72	319.87	1.00		101.30	31.97					30	21	21		203732.9
9	-18.96	3.45	14200	211	14200		0.01	0.02	20.57	2057.26	189.58	380.82	191.24	72.26	96.27	0.56	2.14	717	315	203733	81440	102503			56.63	39.73	5.08	35.66	0.35	0.72	319.87	1.00		101.30	31.97					30	21	21	601	203732.9
	-22.41		15600	203	15600		0.01	0.01	20.56	2056.41	224.11	451.83	227.72	66.52	93.28	0.59	2.13	708	328	220677	89018	112048			56.81	39.75	5.10	35.67	0.35	0.72	341.35	1.00		90.36	28.52					34	24	24		220676.6
10	-22.41	0.56	15600	203	15600		0.01	0.01	20.56	2056.41	224.11	451.83	227.72	66.52	93.28	0.59	2.13	708	328	220677	89018	112048			56.81	39.75	5.10	35.67	0.35	0.72	341.35	1.00		90.36	28.52					34	24	24	140	220676.6
	-22.97		25800	288	25800		0.01	0.01	21.17	2117.08	229.65	463.56	233.91	108.32	162.62	0.52	1.92	545	371	292160	101969	129478			69.93	41.75	6.74	36.36	0.35	0.72	489.33	1.06		88.61	27.97					58	40	40		292159.8
11	-22.97	0.46	25800	288	25800		0.01	0.01	21.17	2117.08	229.65	463.56	233.91	108.32	162.62	0.52	1.92	545	371	292160	101969	129478			69.93	41.75	6.74	36.36	0.35	0.72	489.33	1.06		88.61	27.97					58	40	40	111	292159.8
	-23.43		13400	300	13400		0.02	0.02	20.96	2096.26	234.28	473.26	238.98	54.09	77.00	0.59	2.35	941	349	254933	87264	109644			52.09	39.06	4.51	35.45	0.35	0.73	342.14	1.00		87.14	27.50					30	21	21		254933.1
12	-23.43	5.64	13400	300	13400		0.02	0.02	20.96	2096.26	234.28	473.26	238.98	54.09	77.00	0.59	2.35	941	349	254933	87264	109644			52.09	39.06	4.51	35.45	0.35	0.73	342.14	1.00		87.14	27.50					30	21	21	881	254933.1
	-29.07		11600	79	11600		0.01	0.01	19.34	1934.16	290.66	582.31	291.65	37.78	48.57	0.77	2.18	754	288	160671	90701	113397			45.55	38.12	3.69	35.16	0.35	0.72	273.56	1.00		69.28	21.86					28	19	19		160671.3
13	-29.07	0.77	1900	13	1900		0.01	0.01	16.52	1651.85	290.66	582.31	291.65	4.52	4.52	1.00	3.07	2324	175	50574				73042		31.81			0.45	0.99	413.09	1.00	7.40	69.28	21.86		55	22					22	134	50574.19
	-29.84		1900	17	1900		0.01	0.01	16.83	1683.31	298.40	595.34	296.94	4.39	4.39	1.00	3.13	2509	181	55111				74407		31.78			0.45	1.00	417.12	1.00	5.60	66.82	21.09		55	22					22		55110.65
14	-29.84	1.78	39200	365	39200		0.01	0.01	21.61	2161.21	298.40	595.34	296.94	130.01	216.94	0.53	1.81	472	427	394155	123807	160374			77.95	43.02	7.74	36.82	0.35	0.72	662.19	1.11		66.82	21.09					101	70	70	1285	394155.3
	-31.62		60600	978	60600		0.02	0.02	22.94	2293.81	316.15	636.06	319.91	187.44	369.16	0.42	1.87	509	552	700167	141962	197441			88.62	44.76	9.08	37.50	0.35	0.72	909.51	1.43		61.20	19.32					166	115	115		700167.1
15	-31.62	0.97	60600	978	60600		0.02	0.02	22.94	2293.81	316.15	636.06	319.91	187.44	369.16	0.42	1.87	509	552	700167	141962	197441			88.62	44.76	9.08	37.50	0.35	0.72	909.51	1.43		61.20	19.32					166	115	115	892	700167.1
	-32.59		61600	878	61600		0.01	0.01	22.82	2281.81	325.89	658.28	332.39	183.34	360.03	0.44	1.83	487	545	677428	144606	200962			88.55	44.75	9.07	37.50	0.35	0.72	919.99	1.40		58.11	18.34					172	119	119		677427.8
16	-32.59	0.57	61600	878	61600		0.01	0.01	22.82	2281.81	325.89	658.28	332.39	183.34	360.03	0.44	1.83	487	545	677428	144606	200962			88.55	44.75	9.07	37.50	0.35	0.72	919.99	1.40		58.11	18.34					172	119	119	461	677427.8
	-33.16		44900	473	44900		0.01	0.01	21.97	2196.91	331.62	670.87	339.25	130.37	231.43	0.53	1.84	494	467	479798	134641	175764			79.80	43.32	7.97	36.94	0.35	0.72	730.42	1.09		56.30	17.77					124	86	86		479798.1
17	-33.16	0.69	44900	473	44900		0.01	0.01	21.97	2196.91	331.62	670.87	339.25	130.37	231.43	0.53	1.84	494	467	479798	134641	175764			79.80	43.32	7.97	36.94	0.35	0.72	730.42	1.09		56.30	17.77					124	86	86	579	479798.1
	-33.85		64700	1283	64700		0.02	0.02	23.28	2328.20	338.49	686.86	348.37	183.75	384.56	0.41	1.94	560	599	834127	148993	208584			89.23	44.87	9.15	37.54	0.35	0.72	954.10	1.39		54.12	17.08					186	129	129		834126.8
18	-33.85	0.86	64700	1283	64700		0.02	0.02	23.28	2328.20	338.49	686.86	348.37	183.75	384.56	0.41	1.94	560	599	834127	148993	208584			89.23	44.87	9.15	37.54	0.35	0.72	954.10	1.39		54.12	17.08					186	129	129	832	834126.8
	-34.71		58600	1309	58600		0.02	0.02	23.27	2326.68	347.08	706.85	359.77	160.92	335.90	0.43	2.02	617	598	830958	147114	199919			86.15	44.35	8.77	37.34	0.35	0.72	889.37	1.26		51.40	16.22					171	118	118		830958.1
19	-34.71	1.66	58600	1309	58600		0.02	0.02	23.27	2326.68	347.08	706.85	359.77	160.92	335.90	0.43	2.02	617	598	830958	147114	199919			86.15	44.35	8.77	37.34	0.35	0.72	889.37	1.26		51.40	16.22					171	118	118	1064	830958.1
	-36.37		22500	250	22500		0.01	0.01	20.95	2095.14	363.69	741.65	377.96	57.57	87.54	0.68	2.14	716	395	326335	117967	148633			59.83	40.21	5.48	35.82	0.35	0.72	443.73	1.00		46.14	14.56					65	45	45		326335
20	-36.37	1.09	22500	250	22500		0.01	0.01	20.95	2095.14	363.69	741.65	377.96	57.57	87.54	0.68	2.14	716	395	326335	117967	148633			59.83	40.21	5.48	35.82	0.35	0.72	443.73	1.00		46.14	14.56					65	45	45	588	326335
	-37.46		43500	567	43500		0.01	0.01	22.17	2216.93	374.57	765.77	391.20	109.24	199.54	0.56	1.96	575	496	544604	140911	181934			77.04	42.87	7.63	36.77	0.35	0.72	713.49	1.00		42.69	13.47					134	93	93		544604.2
21	-37.46	0.97	43500	567	43500		0.01	0.01	22.17	2216.93	374.57	765.77	391.20	109.24	199.54	0.56	1.96	575	496	544604	140911	181934			77.04	42.87	7.63	36.77	0.35	0.72	713.49	1.00		42.69	13.47					134	93	93	558	544604.2
	-38.43		25000	310	25000		0.01	0.01	21.24	2124.48	384.31	786.46	402.15	60.21	94.23	0.68	2.15	728	420	374419	123966	156315			61.83	40.51	5.73	35.92	0.35	0.72	480.32	1.00		39.60	12.50					77	53	53		374419.3
22	-38.43	1.43	25000	310	25000		0.01	0.01	21.24	2124.48	384.31	786.46	402.15	60.21	94.23	0.68	2.15	728	420	374419	123966	156315			61.83	40.51	5.73	35.92	0.35	0.72	480.32	1.00		39.60	12.50					77	53	53	867	374419.3
	-39.86		43800	462	43800		0.01	0.01	21.93	2193.19	398.63	817.87	419.24	102.52	180.77	0.60	1.92	546	484	514760	144865	186581			76.30	42.75	7.54	36.72	0.35	0.72	715.99	1.00		35.07	11.07					146	101	101		514760.4
23	-39.86	1.83	29500	311	29500		0.01	0.01	21.31	2131.33	398.63	817.87	419.24	68.41	108.62	0.68	2.06	651	432	397985	131235	165867			65.71	41.10	6.21	36.13	0.35	0.72	537.43	1.00		35.07	11.07					96	67	67	1000	397985.3
	-41.70		29900	427	29900		0.01	0.01	21.69	2169.03	416.95	857.61	440.66	65.91	107.95	0.67	2.16	735	462	462831	134161	169525			65.40	41.05	6.17	36.11	0.35	0.72	548.40	1.00		29.26	9.24					105	72	72		462831.1
24	-41.70	2.23	9700	139	9700		0.01	0.02	19.93	1993.42	416.95	857.61	440.66	20.07	23.00	0.91	2.59	1271	335	224020	101252	124098			35.23	36.68	2.40	34.76	0.35	0.82	571.31	1.00		29.26	9.24					32	22	22	854	224020.1
	-43.93		27800	1034	27800		0.04	0.04	22.70	2269.88	439.29	908.31	469.02	57.34	97.92	0.65	2.49	1117	548	681857	134859	170114			62.61	40.62	5.83	35.96	0.35	0.77	830.13	1.00		22.18	7.00					108	75	75		681856.8
25	-43.93	0.49	27800	1034	27800		0.04	0.04	22.70	2269.88	439.29	908.31	469.02	57.34	97.92	0.65	2.49	1117	548	681857	134859	170114			62.61	40.62	5.83	35.96	0.35	0.77	830.13	1.00		22.18	7.00					108	75	75	286	681856.8
	-44.42		6000	258	6000		0.04	0.05	20.47	2047.17	444.16	918.28	474.12	10.72	10.72	1.00	3.11	2452	353	255083				211475		34.83			0.45	0.99	1605.55	1.75	1.44	20.64	6.51		234	94					94		255083.4
26	-44.42	1.06	6000	258	6000		0.04	0.05	20.47	2047.17	444.16	918.28	474.12	10.72	10.72	1.00	3.11	2452	353	255083				211475		34.83			0.45	0.99	1605.55	1.75	1.44	20.64	6.51		234	94					94	1838	255083.4
	-45.48		70700	1052	70700		0.01	0.02	23.08	2308.39	454.75	942.73	487.98	142.95	296.89	0.54	1.92	544	616	876198	172853	236847			87.10	44.51	8.89	37.40	0.35	0.72	1014.67	1.08		17.28	5.46					319	221	221		876198.1
27	-45.48	0.43	70700	1052	70700		0.01	0.02	23.08	2308.39	454.75	942.73	487.98	142.95	296.89	0.54	1.92	544	616	876198	172853	236847			87.10	44.51	8.89	37.40	0.35	0.72	1014.67	1.08		17.28	5.46					319	221	221	588	876198.1
	-45.91		40700	526	40700		0.01	0.01	22.06	2205.53	459.05	952.21	493.16	80.60	137.77	0.66	2.06	650	508	570212	151162	192665			72.15	42.10	7.02	36.48	0.35	0.72	679.83	1.00		15.92	5.03					184	127	127		570211.8
28	-45.91	1.00	40700	526	40700		0.01	0.01	22.06	2205.53	459.05	952.21	493.16	80.60	137.77	0.66	2.06	650	508	570212	151162	192665			72.15	42.10	7.02	36.48	0.35	0.72	679.83	1.00		15.92	5.03					184	127	127	1049	570211.8
	-46.91		40700	1263	40700		0.03	0.03	23.08	2308.24	469.07	975.34	506.27	78.46	147.48	0.61	2.33	920	605	843543	152656	194440			71.80	42.04	6.98	36.46	0.35	0.73	761.36	1.00		12.75	4.02					201	139	139		843542.8
29	-46.91	1.63	19800	612	19800		0.03	0.03	21.95	2195.12	469.07	975.34	506.27	37.18	53.48	0.78	2.57	1241	483	512959	127492	160218			52.49	39.12	4.56	35.47	0.35	0.81	950.36	1.00		12.75	4.02					95	65	65	839	512958.7
	-48.54		6000	214	6000		0.04	0.04	20.25	2025.25	485.40	1008.41	523.01	9.54	9.54	1.00	3.10	2438	349	246416				212883		34.66			0.45	0.99	1574.65	1.56	1.70	7.57	2.39		301	120					120		246416
30	-48.54	2.66	6000	214	6000	6000	0.04	0.04	20.25	2025.25	485.40	1008.41	523.01	9.54	9.54	1.00	3.10	2438	349	246416				212883		34.66			0.45	0.99	1574.65	1.56	1.70	7.57	2.39		301	120					120	2707	246416
	-51.20		6000	228	6000	6000	0.04	0.05	20.33	2032.68	512.03	1062.54	550.51	8.97	8.97	1.00	3.14	2567	356	257651				215437		34.57			0.45	1.00	1577.09	1.48	1.58	0.00	0.00		420	168					168		257650.8
																																												20564	

UK F23 (EOID)

Layer	Depth	Thickness	q_c	q_s	q_t	q_base_1.5D	Rf	Rfn	Unit Weight	Density	u	σ_v0	σ'_v0	Q_t	Q_tn	n	I_c	a_vs	V_s	G_max	G_UWA	G_ICP	G_Uni	G_clay	Dr	φ'	ψ	δ_cv	v	m'	σ'vy	OCR=YSR	S_t	h/R	h	K_c	τ_sc_UWA13		τ_sc_Unified				Skin Friction F_τ_sf	Shaft Resistance Q_s	
Nr	[m]	[m]	[KPa]	[KPa]	kPa				[kN/m3]	kg/m3	kPa	kPa	kPa						m/s	kPa	kPa	kPa	kPa	kPa	%	degree	degree	degree									clay	F_τ_sf	σ'_rc	Δσ'_rd	τ_sf	F_τ_sf	kPa	kN	G_max
1	0.00	2.95	0	0	0		0.00	0.00	0.00	0.00	0.00	0.00	0.00	0.00	#DIV/0!	#VALUE!	2.00	0	0	0	0	#DIV/0!			[illegible]	[illegible]	[illegible]	37.40	0.35	0.86	0.00	#DIV/0!		114.44	41.59						0	0	0	345	0
	-2.95		19100	174	19100		0.01	0.01	20.46	2046.24	29.47	60.30	30.83	617.52	290.85	0.36	1.36	269	226	104692	44239	61794			[illegible]	[illegible]	[illegible]	37.53	0.35	0.72	397.99	6.60		106.33	38.64						43	30	30		104692
2	-2.95	2.07	19100	174	19100		0.01	0.01	20.46	2046.24	29.47	60.30	30.83	617.52	290.85	0.36	1.36	269	226	104692	44239	61794			[illegible]	[illegible]	[illegible]	37.53	0.35	0.72	397.99	6.60		106.33	38.64						43	30	30	489	104692
	-5.02		19300	208	19300		0.01	0.01	20.68	2067.58	50.18	103.12	52.94	362.60	244.08	0.38	1.55	341	256	135336	54323	71745			[illegible]	[illegible]	[illegible]	37.08	0.35	0.72	400.35	3.88		100.63	36.57						44	30	30		135336
3	-5.02	1.27	19300	208	19300		0.01	0.01	20.68	2067.58	50.18	103.12	52.94	362.60	244.08	0.38	1.55	341	256	135336	54323	71745			[illegible]	[illegible]	[illegible]	37.08	0.35	0.72	400.35	3.88		100.63	36.57						44	30	30	337	135336
	-6.29		3500	125	3500		0.04	0.04	19.41	1941.13	62.92	127.85	64.93	51.93	43.43	0.59	2.96	2032	262	133034				[illegible]	[illegible]	[illegible]	[illegible]		0.45	0.98	972.61	7.61	1.97	97.12	35.30	2.85	93	37					250		133033.7
4	-6.29	0.88	3500	125	3500		0.04	0.04	19.41	1941.13	62.92	127.85	64.93	51.93	43.43	0.59	2.96	2032	262	133034				[illegible]	[illegible]	[illegible]	[illegible]		0.45	0.98	972.61	7.61	1.97	97.12	35.30	2.85	93	37					250	253	133033.7
	-7.17		3500	125	3500		0.04	0.04	19.41	1941.13	71.68	144.86	73.18	45.85	40.49	0.60	2.96	2032	261	132363				[illegible]	[illegible]	[illegible]	[illegible]		0.45	0.98	967.79	6.68	1.96	104.13	34.42	2.70	91	36					250		132362.9
5	-7.17	5.81	3500	125	3500		0.04	0.04	19.41	1941.13	71.68	144.86	73.18	45.85	40.49	0.60	2.96	2032	261	132363				[illegible]	[illegible]	[illegible]	[illegible]		0.45	0.98	967.79	6.68	1.96	104.13	34.42	2.70	91	36					250	2707	132362.9
	-12.98		48900	761	48900		0.02	0.02	22.56	2256.01	129.82	276.02	146.20	332.58	431.89	0.31	1.70	414	448	453707	100313	148343			[illegible]	[illegible]	[illegible]	37.83	0.35	0.72	781.75	2.83		86.54	28.61						119	82	82		453707.5
6	-12.98	0.74	48900	761	48900		0.02	0.02	22.56	2256.01	129.82	276.02	146.20	332.58	431.89	0.31	1.70	414	448	453707	100313	148343			[illegible]	[illegible]	[illegible]	37.83	0.35	0.72	781.75	2.83		86.54	28.61						119	82	82	310	453707.5
	-13.73		15800	178	15800		0.01	0.01	20.41	2041.49	137.26	291.21	153.95	100.74	123.90	0.52	1.95	563	296	178316	77109	97256			[illegible]	[illegible]	[illegible]	35.95	0.35	0.72	343.76	1.18		91.10	27.86						35	24	24		178316.3
7	-13.73	1.09	15800	178	15800		0.01	0.01	20.41	2041.49	137.26	291.21	153.95	100.74	123.90	0.52	1.95	563	296	178316	77109	97256			[illegible]	[illegible]	[illegible]	35.95	0.35	0.72	343.76	1.18		91.10	27.86						35	24	24	171	178316.3
	-14.81		10600	131	10600		0.01	0.01	19.90	1989.94	148.14	312.86	164.72	62.45	76.60	0.59	2.14	715	271	146396	71578	89873			[illegible]	[illegible]	[illegible]	35.39	0.35	0.72	258.48	1.00		87.54	26.78						23	16	16		146396.4
8	-14.81	1.27	55500	686	55500		0.01	0.01	22.49	2248.79	148.14	312.86	164.72	335.04	467.01	0.33	1.62	372	453	461492	108274	165104			[illegible]	[illegible]	[illegible]	37.95	0.35	0.72	856.33	2.74		87.54	26.78						133	92	92	888	461491.8
	-16.09		51700	521	51700		0.01	0.01	22.14	2213.76	160.85	341.00	180.15	285.09	410.50	0.38	1.59	359	430	408549	110003	159534			[illegible]	[illegible]	[illegible]	37.74	0.35	0.72	813.13	2.38		83.39	25.51						125	86	86		408548.7
9	-16.09	0.83	21600	218	21600		0.01	0.01	20.77	2077.48	160.85	341.00	180.15	118.01	157.66	0.51	1.86	506	328	223659	88439	112108			[illegible]	[illegible]	[illegible]	36.29	0.35	0.72	431.05	1.26		83.39	25.51						50	34	34	221	223658.8
	-16.92		20600	207	20600		0.01	0.01	20.70	2069.56	169.17	358.22	189.05	107.07	144.93	0.52	1.89	527	327	220675	88992	112578			[illegible]	[illegible]	[illegible]	36.18	0.35	0.72	416.18	1.16		80.67	24.67						48	33	33		220675.3
10	-16.92	1.94	46900	472	46900		0.01	0.01	21.98	2198.37	169.17	358.22	189.05	246.19	360.44	0.40	1.63	379	420	387383	109314	152324			[illegible]	[illegible]	[illegible]	37.51	0.35	0.72	757.47	2.11		80.67	24.67						114	79	79	934	387382.8
	-18.86		26000	289	26000		0.01	0.01	21.18	2117.79	188.59	399.34	210.75	121.47	176.49	0.50	1.88	518	364	281094	98250	125080			[illegible]	[illegible]	[illegible]	36.45	0.35	0.72	492.82	1.23		74.32	22.73						63	44	44		281093.8
11	-18.86	0.20	26000	289	26000		0.01	0.01	21.18	2117.79	188.59	399.34	210.75	121.47	176.49	0.50	1.88	518	364	281094	98250	125080			[illegible]	[illegible]	[illegible]	36.45	0.35	0.72	492.82	1.23		74.32	22.73						63	44	44	124	281093.8
	-19.06		63100	602	63100		0.01	0.01	22.38	2238.49	190.62	403.89	213.27	293.98	467.36	0.39	1.56	347	467	487430	123176	187752			[illegible]	[illegible]	[illegible]	37.95	0.35	0.72	938.71	2.32		73.65	22.53						161	112	112		487430.2
12	-19.06	0.61	63100	602	63100		0.01	0.01	22.38	2238.49	190.62	403.89	213.27	293.98	467.36	0.39	1.56	347	467	487430	123176	187752			[illegible]	[illegible]	[illegible]	37.95	0.35	0.72	938.71	2.32		73.65	22.53						161	112	112	396	487430.2
	-19.68		30700	488	30700		0.02	0.02	21.86	2185.72	196.76	417.31	220.55	137.31	212.42	0.45	1.95	567	414	375517	104177	133805			[illegible]	[illegible]	[illegible]	36.67	0.35	0.72	556.65	1.33		71.64	21.91						76	53	53		375517
13	-19.68	1.01	30700	488	30700		0.02	0.02	21.86	2185.72	196.76	417.31	220.55	137.31	212.42	0.45	1.95	567	414	375517	104177	133805			[illegible]	[illegible]	[illegible]	36.67	0.35	0.72	556.65	1.33		71.64	21.91						76	53	53	703	375517
	-20.68		68700	1200	68700		0.02	0.02	23.23	2322.71	206.81	440.65	233.84	291.90	520.25	0.32	1.78	454	557	719798	130244	202569			[illegible]	[illegible]	[illegible]	38.03	0.35	0.72	998.10	2.27		68.36	20.91						182	126	126		719798.4
14	-20.68	0.84	68700	1200	68700		0.02	0.02	23.23	2322.71	206.81	440.65	233.84	291.90	520.25	0.32	1.78	454	557	719798	130244	202569			[illegible]	[illegible]	[illegible]	38.03	0.35	0.72	998.10	2.27		68.36	20.91						182	126	126	573	719798.4
	-21.52		27900	415	27900		0.01	0.02	21.63	2162.98	215.16	458.71	243.55	112.67	177.16	0.49	1.99	597	405	354290	105571	134390			[illegible]	[illegible]	[illegible]	36.44	0.35	0.72	518.99	1.13		65.63	20.07						71	49	49		354290.2
15	-21.52	1.64	27900	415	27900		0.01	0.02	21.63	2162.98	215.16	458.71	243.55	112.67	177.16	0.49	1.99	597	405	354290	105571	134390			[illegible]	[illegible]	[illegible]	36.44	0.35	0.72	518.99	1.13		65.63	20.07						71	49	49	895	354290.2
	-23.15		48100	994	48100		0.02	0.02	22.87	2286.69	231.52	496.12	264.60	179.91	326.56	0.39	1.96	574	523	624590	124790	168006			[illegible]	[illegible]	[illegible]	37.26	0.35	0.72	771.12	1.55		60.28	18.44						130	90	90		624590
16	-23.15	2.04	48100	994	48100		0.02	0.02	22.87	2286.69	231.52	496.12	264.60	179.91	326.56	0.39	1.96	574	523	624590	124790	168006			[illegible]	[illegible]	[illegible]	37.26	0.35	0.72	771.12	1.55		60.28	18.44						130	90	90	1303	624590
	-25.20		37400	416	37400		0.01	0.01	21.75	2174.71	251.95	540.55	288.60	127.72	214.61	0.51	1.87	508	433	407232	121060	156319			[illegible]	[illegible]	[illegible]	36.77	0.35	0.72	640.66	1.19		53.60	16.40						104	72	72		407232.3
17	-25.20	2.56	19200	213	19200		0.01	0.01	20.70	2070.16	251.95	540.55	288.60	64.65	96.06	0.63	2.09	679	356	262240	102473	129083			[illegible]	[illegible]	[illegible]	35.79	0.35	0.72	395.25	1.00		53.60	16.40						52	36	36	840	262239.7
	-27.75		23700	201	23700		0.01	0.01	20.72	2071.59	277.51	593.50	315.99	73.12	110.52	0.64	1.98	588	369	281484	111747	141037			[illegible]	[illegible]	[illegible]	36.02	0.35	0.72	458.40	1.00		45.24	13.84						69	48	48		281484.5
18	-27.75	2.22	23700	201	23700		0.01	0.01	20.72	2071.59	277.51	593.50	315.99	73.12	110.52	0.64	1.98	588	369	281484	111747	141037			[illegible]	[illegible]	[illegible]	36.02	0.35	0.72	458.40	1.00		45.24	13.84						69	48	48	650	281484.5
	-29.97		12700	140	12700		0.01	0.01	20.05	2004.80	299.73	638.05	338.32	35.65	47.98	0.76	2.31	891	328	215340	98089	122692			[illegible]	[illegible]	[illegible]	35.18	0.35	0.73	310.67	1.00		37.98	11.62						39	27	27		215340
19	-29.97	7.26	12700	140	12700		0.01	0.01	20.05	2004.80	299.73	638.05	338.32	35.65	47.98	0.76	2.31	891	328	215340	98089	122692			[illegible]	[illegible]	[illegible]	35.18	0.35	0.73	310.67	1.00		37.98	11.62						39	27	27	2505	215340
	-37.24		19400	246	19400		0.01	0.01	20.87	2087.45	372.35	789.64	417.29	44.60	64.49	0.74	2.26	839	395	325917	117974	148381			[illegible]	[illegible]	[illegible]	35.56	0.35	0.73	412.09	1.00		14.24	4.36						88	61	61		325917.4
20	-37.24	1.33	19400	246	19400		0.01	0.01	20.87	2087.45	372.35	789.64	417.29	44.60	64.49	0.74	2.26	839	395	325917	117974	148381			[illegible]	[illegible]	[illegible]	35.56	0.35	0.73	412.09	1.00		14.24	4.36						88	61	61	516	325917.4
	-38.56		10700	406	10700		0.04	0.04	21.23	2122.95	385.60	817.77	432.17	22.87	29.16	0.83	2.80	1651	404	346429	103012	127204			[illegible]	[illegible]	[illegible]	34.86	0.35	0.94	1911.85	2.34		9.91	3.03						55	38	38		346428.6
21	-38.56	2.15	10700	406	10700		0.04	0.04	21.23	2122.95	385.60	817.77	432.17	22.87	29.16	0.83	2.80	1651	404	346429	103012	127204			[illegible]	[illegible]	[illegible]	34.86	0.35	0.94	1911.85	2.34		9.91	3.03						55	38	38	1317	346428.6
	-40.71		29500	404	29500		0.01	0.01	21.62	2162.01	407.07	864.19	457.12	62.64	100.46	0.69	2.16	740	460	458072	135562	171191			[illegible]	[illegible]	[illegible]	36.06	0.35	0.72	543.44	1.00		2.89	0.88						171	118	118		458072.3
22	-40.71	1.11	29500	404	29500	23813	0.01	0.01	21.62	2162.01	407.07	864.19	457.12	62.64	100.46	0.69	2.16	740	460	458072	135562	171191			[illegible]	[illegible]	[illegible]	36.06	0.35	0.72	543.44	1.00		2.89	0.88						171	118	118	708	458072.3
	-41.82		21400	169	21400	23813	0.01	0.01	20.47	2047.27	418.20	886.97	468.77	43.76	58.14	0.82	2.15	731	387	307130	126295	158906			[illegible]	[illegible]	[illegible]	35.62	0.35	0.72	426.43	1.00		0.00	0.00						122	84	84		307130.2
23	-41.82	3.21	21400	226	21400	23813	0.01	0.01	20.81	2081.35	418.20	886.97	468.77	43.76	60.64	0.79	2.22	798	405	340834	126295	158906			55.61	39.58	4.95	35.62	0.35	0.72	434.29	1.00									122	84			340833.6
	-45.03		23800	326	23800	23813	0.01	0.01	21.28	2128.46	450.27	955.23	504.96	45.24	64.51	0.78	2.28	855	442	415716	133364	167901			57.46	39.85	5.18	35.70	0.35	0.73	482.54	1.00									136	94			415715.8
																																												17180	

UK F24 (EOID)

Layer	Depth	Thickness	q_c	q_s	q_t	q_base_1.5D	Rf	Rfn	Unit Weight	Density	u	σ_v0	σ'_v0	Q_t	Q_tn	n	I_c	a_vs	V_s	G_max	G_UWA	G_ICP	G_Uni	G_clay	Dr	φ'	ψ	δ_cv	v	m'	σ'vy	OCR=YSR	S_t	h/R	h	K_c	τ_sc_UWA13		τ_sc_Unified				Skin Friction F_τ_sf	Shaft Resistance Q_s	
Nr	[m]	[m]	[KPa]	[KPa]	kPa				[kN/m3]	kg/m3	kPa	kPa	kPa						m/s	kPa	kPa	kPa	kPa	kPa	%	degree	degree	degree									clay	F_τ_sf	σ'_rc	Δσ'_rd	τ_sf	F_τ_sf	kPa	kN	G_max
1	0.00	3.13	0	0	0		0.00	0.00	0.00	0.00	0.00	0.00	0.00	0.00	#DIV/0!	#VALUE!	2.00	0	0	0	0	#DIV/0!			#DIV/0!	45.00	9.50	37.40	0.35	0.86	0.00	#DIV/0!		115.29	41.90						0	0	0	346	0
	-3.13		18200	262	18200		0.01	0.01	20.92	2092.35	31.26	65.41	34.15	531.08	259.60	0.33	1.57	349	251	132294	45415	61829			86.37	44.39	8.80	37.35	0.35	0.72	384.27	5.88		106.69	38.77						41	28	28		132294.2
2	-3.13	0.98	4700	68	4700		0.01	0.01	18.81	1881.27	31.26	65.41	34.15	135.73	80.07	0.51	1.93	549	159	47858	32374	40632			50.08	38.77	4.26	35.36	0.35	0.72	144.01	2.20		106.69	38.77						10	7	7	55	47858.36
	-4.10		5200	188	5200		0.04	0.04	20.04	2004.46	41.01	84.95	43.94	116.41	76.10	0.48	2.27	850	208	87103	36496	45785			49.41	38.67	4.18	35.33	0.35	0.73	162.33	1.91		104.01	37.80						11	8	8		87103.48
3	-4.10	1.81	5200	188	5200		0.04	0.04	20.04	2004.46	41.01	84.95	43.94	116.41	76.10	0.48	2.27	850	208	87103	36496	45785			49.41	38.67	4.18	35.33	0.35	0.73	162.33	1.91		104.01	37.80						11	8	8	273	87103.48
	-5.91		19600	246	19600		0.01	0.01	20.88	2087.86	59.12	122.76	63.64	306.05	230.94	0.38	1.65	386	274	156835	58430	76351			80.01	43.35	8.00	36.95	0.35	0.72	404.56	3.30		99.02	35.99						45	31	31		156834.7
4	-5.91	1.59	5400	68	5400		0.01	0.01	18.87	1886.69	59.12	122.76	63.64	82.92	67.89	0.56	2.04	637	183	63390	42332	52920			45.46	38.11	3.68	35.16	0.35	0.72	158.57	1.29		99.02	35.99						12	8	8	96	63390.07
	-7.50		5200	210	5200		0.04	0.04	20.17	2017.44	75.01	154.82	79.81	63.22	57.07	0.55	2.48	1112	237	113181	45650	56744			41.42	37.54	3.18	34.99	0.35	0.77	226.98	1.47		104.06	34.40						11	7	7		113181
5	-7.50	0.90	5200	210	5200		0.04	0.04	20.17	2017.44	75.01	154.82	79.81	63.22	57.07	0.55	2.48	1112	237	113181	45650	56744			41.42	37.54	3.18	34.99	0.35	0.77	226.98	1.47		104.06	34.40						11	7	7	134	113181
	-8.40		20300	226	20300		0.01	0.01	20.79	2079.28	83.97	173.45	89.48	224.93	210.73	0.41	1.69	408	287	170765	66979	86291			76.38	42.77	7.55	36.73	0.35	0.72	414.23	2.39		101.35	33.50						45	31	31		170765
6	-8.40	2.60	20300	226	20300		0.01	0.01	20.79	2079.28	83.97	173.45	89.48	224.93	210.73	0.41	1.69	408	287	170765	66979	86291			76.38	42.77	7.55	36.73	0.35	0.72	414.23	2.39		101.35	33.50						45	31	31	909	170765
	-11.00		36200	320	36200		0.01	0.01	21.43	2142.67	109.97	229.16	119.19	301.80	335.95	0.39	1.53	333	346	256818	86186	119164			88.04	44.67	9.01	37.46	0.35	0.72	629.22	2.75		93.49	30.90						84	58	58		256818.3
7	-11.00	1.72	36200	320	36200		0.01	0.01	21.43	2142.67	109.97	229.16	119.19	301.80	335.95	0.39	1.53	333	346	256818	86186	119164			88.04	44.67	9.01	37.46	0.35	0.72	629.22	2.75		93.49	30.90						84	58	58	769	256818.3
	-12.72		34200	350	34200		0.01	0.01	21.51	2150.96	127.16	266.13	138.97	244.18	297.55	0.40	1.64	382	360	279120	90007	120723			84.46	44.08	8.56	37.23	0.35	0.72	603.36	2.27		88.29	29.18						81	56	56		279119.8
8	-12.72	0.70	34200	350	34200		0.01	0.01	21.51	2150.96	127.16	266.13	138.97	244.18	297.55	0.40	1.64	382	360	279120	90007	120723			84.46	44.08	8.56	37.23	0.35	0.72	603.36	2.27		88.29	29.18						81	56	56	230	279119.8
	-13.41		18500	241	18500		0.01	0.01	20.83	2083.19	134.12	280.63	146.51	124.35	151.93	0.48	1.92	545	315	206986	78735	99653			67.29	41.34	6.41	36.21	0.35	0.72	385.91	1.38		93.14	28.49						41	28	28		206986.1
9	-13.41	1.05	18500	241	18500		0.01	0.01	20.83	2083.19	134.12	280.63	146.51	124.35	151.93	0.48	1.92	545	315	206986	78735	99653			67.29	41.34	6.41	36.21	0.35	0.72	385.91	1.38		93.14	28.49						41	28	28	242	206986.1
	-14.46		20000	224	20000		0.01	0.01	20.78	2077.66	144.57	302.34	157.77	124.85	157.69	0.49	1.87	514	318	210420	82545	104601			68.38	41.51	6.55	36.27	0.35	0.72	408.04	1.35		89.72	27.44						45	31	31		210419.7
10	-14.46	0.72	39600	442	39600		0.01	0.01	21.84	2184.06	144.57	302.34	157.77	249.08	329.47	0.39	1.66	394	393	337862	97917	133684			86.69	44.44	8.84	37.37	0.35	0.72	670.61	2.22		89.72	27.44						92	64	64	404	337862.3
	-15.18		48500	564	48500		0.01	0.01	22.21	2220.56	151.76	318.31	166.55	289.29	400.70	0.36	1.64	380	428	406716	105120	151079			91.40	45.23	9.42	37.69	0.35	0.72	776.60	2.44		87.37	26.72						115	79	79		406716
11	-15.18	1.87	48500	564	48500		0.01	0.01	22.21	2220.56	151.76	318.31	166.55	289.29	400.70	0.36	1.64	380	428	406716	105120	151079			91.40	45.23	9.42	37.69	0.35	0.72	776.60	2.44		87.37	26.72						115	79	79	1206	406716
	-17.05		50200	724	50200		0.01	0.01	22.51	2251.19	170.48	360.45	189.97	262.35	397.52	0.35	1.74	432	464	484204	111393	158378			90.56	45.09	9.32	37.63	0.35	0.72	795.79	2.21		81.25	24.85						122	85	85		484204.3
12	-17.05	0.56	50200	724	50200		0.01	0.01	22.51	2251.19	170.48	360.45	189.97	262.35	397.52	0.35	1.74	432	464	484204	111393	158378			90.56	45.09	9.32	37.63	0.35	0.72	795.79	2.21		81.25	24.85						122	85	85	288	484204.3
	-17.60		29000	256	29000		0.01	0.01	21.08	2107.84	176.03	372.15	196.12	145.97	205.60	0.49	1.75	441	355	266342	98281	126249			75.43	42.61	7.43	36.67	0.35	0.72	533.88	1.43		79.44	24.30						69	48	48		266342.3
13	-17.60	1.32	29000	256	29000		0.01	0.01	21.08	2107.84	176.03	372.15	196.12	145.97	205.60	0.49	1.75	441	355	266342	98281	126249			75.43	42.61	7.43	36.67	0.35	0.72	533.88	1.43		79.44	24.30						69	48	48	839	266342.3
	-18.92		65200	827	65200		0.01	0.01	22.77	2277.01	189.17	402.07	212.90	304.36	498.24	0.35	1.65	388	502	572705	124108	192468			96.04	46.02	10.00	38.02	0.35	0.72	961.28	2.39		75.14	22.98						166	115	115		572705.1
14	-18.92	1.04	65200	827	65200		0.01	0.01	22.77	2277.01	189.17	402.07	212.90	304.36	498.24	0.35	1.65	388	502	572705	124108	192468			96.04	46.02	10.00	38.02	0.35	0.72	961.28	2.39		75.14	22.98						166	115	115	875	572705.1
	-19.95		56500	747	56500		0.01	0.01	22.59	2259.48	199.54	425.50	225.96	248.16	413.46	0.37	1.72	424	487	536629	122447	175990			91.40	45.23	9.43	37.69	0.35	0.72	866.27	2.04		71.75	21.95						145	100	100		536628.9
15	-19.95	1.11	55000	501	55000		0.01	0.01	22.12	2211.59	199.54	425.50	225.96	241.52	386.87	0.42	1.61	366	447	441836	121626	173191			90.68	45.11	9.34	37.64	0.35	0.72	849.48	2.00		71.75	21.95						141	97	97	719	441835.9
	-21.06		38600	747	38600		0.02	0.02	22.45	2244.59	210.60	450.33	239.73	159.14	266.61	0.41	1.97	583	471	498837	113818	149004			80.40	43.41	8.05	36.97	0.35	0.72	657.65	1.46		68.13	20.84						99	68	68		498836.6
16	-21.06	0.30	38600	747	38600		0.02	0.02	22.45	2244.59	210.60	450.33	239.73	159.14	266.61	0.41	1.97	583	471	498837	113818	149004			80.40	43.41	8.05	36.97	0.35	0.72	657.65	1.46		68.13	20.84						99	68	68	124	498836.6
	-21.36		21700	501	21700		0.02	0.02	21.75	2175.24	213.59	456.83	243.24	87.33	135.54	0.51	2.21	784	408	362187	99095	125158			64.77	40.95	6.10	36.08	0.35	0.72	443.18	1.00		67.16	20.54						54	37	37		362187
17	-21.36	4.48	21700	501	21700		0.02	0.02	21.75	2175.24	213.59	456.83	243.24	87.33	135.54	0.51	2.21	784	408	362187	99095	125158			64.77	40.95	6.10	36.08	0.35	0.72	443.18	1.00		67.16	20.54						54	37	37	1610	362187
	-25.84		28200	345	28200		0.01	0.01	21.42	2141.73	258.38	552.76	294.38	93.92	151.94	0.55	1.99	598	406	353872	113651	144171			69.24	41.64	6.65	36.32	0.35	0.72	521.81	1.00		52.51	16.06						78	54	54		353871.6
18	-25.84	0.83	43000	560	43000		0.01	0.01	22.15	2215.02	258.38	552.76	294.38	144.19	253.98	0.48	1.87	514	467	483550	126293	165450			80.54	43.44	8.07	36.98	0.35	0.72	709.24	1.28		52.51	16.06						122	84	84	527	483550.1
	-26.67		38700	432	38700		0.01	0.01	21.80	2180.47	266.70	570.90	304.20	125.34	214.28	0.52	1.87	513	442	426198	124533	160921			77.28	42.91	7.66	36.78	0.35	0.72	656.50	1.15		49.79	15.23						111	77	77		426198.2
19	-26.67	4.12	21300	238	21300		0.01	0.01	20.87	2087.23	266.70	570.90	304.20	68.14	103.73	0.62	2.08	665	371	287659	107263	135222			61.27	40.42	5.66	35.89	0.35	0.72	425.80	1.00		49.79	15.23						60	41	41	1366	287659.3
	-30.79		19900	152	19900		0.01	0.01	20.32	2031.99	307.85	654.52	346.67	55.52	79.38	0.71	2.06	647	353	252908	110752	139444			57.70	39.89	5.21	35.72	0.35	0.72	403.02	1.00		36.34	11.12						63	43	43		252908.4
20	-30.79	8.59	19900	152	19900		0.01	0.01	20.32	2031.99	307.85	654.52	346.67	55.52	79.38	0.71	2.06	647	353	252908	110752	139444			57.70	39.89	5.21	35.72	0.35	0.72	403.02	1.00		36.34	11.12						63	43	43	3818	252908.4
	-39.37		17900	205	17900		0.01	0.01	20.63	2062.93	393.73	831.68	437.95	38.97	53.33	0.79	2.28	864	384	304316	117739	147908			51.73	39.01	4.47	35.43	0.35	0.73	392.73	1.00		8.26	2.53						101	70	70		304315.9
21	-39.37	1.13	17900	205	17900		0.01	0.01	20.63	2062.93	393.73	831.68	437.95	38.97	53.33	0.79	2.28	864	384	304316	117739	147908			51.73	39.01	4.47	35.43	0.35	0.73	392.73	1.00		8.26	2.53						101	70	70	922	304315.9
	-40.51		34000	379	34000		0.01	0.01	21.60	2160.07	405.08	856.20	451.12	73.47	119.96	0.67	2.05	643	462	460135	139766	177140			68.53	41.53	6.57	36.28	0.35	0.72	596.06	1.00		4.55	1.39						198	137	137		460134.8
22	-40.51	0.76	34000	379	34000	21617	0.01	0.01	21.60	2160.07	405.08	856.20	451.12	73.47	119.96	0.67	2.05	643	462	460135	139766	177140			68.53	41.53	6.57	36.28	0.35	0.72	596.06	1.00		4.55	1.39						198	137	137	657	460134.8
	-41.27		20800	145	20800	21617	0.01	0.01	20.28	2028.20	412.72	871.69	458.97	43.42	56.74	0.82	2.13	708	376	286362	124411	156510			55.13	39.51	4.89	35.59	0.35	0.72	416.01	1.00		2.05	0.63						118	82	82		286362.5
23	-41.27	3.73	20800	145	20800	21617	0.01	0.01	20.28	2028.20	412.72	871.69	458.97	43.42	56.74	0.82	2.13	708	376	286362	124411	156510			55.13	39.51	4.89	35.59	0.35	0.72	416.01	1.00		2.05	0.63						118	82	82	432	286362.5
	-45.00		23600	274	23600	21617	0.01	0.01	21.08	2107.75	449.98	950.23	500.25	45.28	63.31	0.79	2.23	810	428	386588	132616	166954			57.36	39.84	5.17	35.70	0.35	0.72	468.68	1.00		0.00	0.00						135	93	93		386588
																																												16843	